Characterization of a glycated gelatin model to explore the therapeutic properties of macrofungi in diabetic wound healing: an *in vitro* study

Nadine Pringle

212418181

Submitted in partial fulfilment of requirements for the degree of *Magister Scientiae* (MSc) in the Department of Biochemistry and Microbiology in the Faculty of Science at the Nelson Mandela Metropolitan University.

January 2017

Supervisor: Prof. M. van de Venter

Co-supervisor: Dr. T. Koekemoer

TABLE OF CONTENTS

Nelson Mandela Metropolitan University

for tomorrow

DECLARATION BY CANDIDATE

NAME: Nadine Pringle

STUDENT NUMBER: 212418181
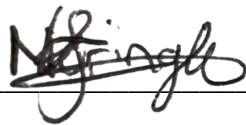
QUALIFICATION: *Magister Scientiae* in Biochemistry

TITLE OF PROJECT: Characterization of a glycated gelatin model to explore the therapeutic properties of macrofungi in diabetic wound healing: an *in vitro* study

DECLARATION

In accordance with rule G5.6.3, I hereby declare that the above-mentioned treatise/ dissertation/ thesis is my own work and that it has not previously been submitted for assessment to another University or for another qualification.

SIGNATURE: _____

DATE: _____20 March 2017_____

ACKNOWLEDGEMENTS

ABSTRACT

Diabetic wounds frequently undergo impaired and prolonged wound healing due to a multitude of factors including hypoxia, impaired angiogenesis, hyperglycaemia, formation of ROS and AGEs, and infection - all of which may lead to cellular dysfunction. To date, however, treatment options for individuals suffering from impaired diabetic wound healing are limited, non-specific, and generally unsuccessful. The search for new and effective treatment strategies is severely hampered by the availability of adequately characterized screening models which comprehensively mimic the complexity of the diabetic wound healing process. In order to explore natural products as potential therapeutics to treat diabetic wounds and to encourage more research on this topic, this study sought out to develop and characterize a more convenient and cost effective *in vitro* screening assay which mimics the effects of protein glycation on the healing process of diabetic wounds. As proof of principal, this model was subsequently used to screen the potential of five wild mushroom species (*P. tinctorius*, *R. capensis*, *B. badius*, *P. ostreatus* and *G. lucidum)* as suitable diabetic wound healing therapies.

The glycated gelatin model developed during this study was found to suitably mimic the diabetic state as it successfully simulated the major cellular dysfunctions in macrophages (NO production, phagocytosis, macrophage polarization, NF-κB translocation and COX-2 expression) and fibroblasts (proliferation and migration) documented during diabetic wound healing. Together these findings provide confidence that the model may serve as a valuable tool to study the poorly understood mechanisms which characterize cellular dysfunction in response to AGE accumulation and also to aid the identification of novel therapeutic agents to treat this pathology. Screening a number of mushroom extracts revealed that the ethanol extracts of *R. capensis* and *P. ostreatus* had the greatest potential for attenuating chronic inflammation due to their ability to promote macrophage phagocytosis, increased M2 activation (*R. capensis*) and decreased M1 activation (*P. ostreatus*) as well as reduced COX-2 expression while the water extract of *G. lucidum* proved to be the most promising candidate for stimulating fibroplasia as it was the most successful at promoting both fibroblast proliferation and migration. Different mushroom species were thus shown to promote different stages of the wound

healing process providing sufficient evidence to support further studies related to the use of macrofungi as therapeutic agents in the search for more cost-effective and efficient treatment strategies for impaired diabetic wound healing.

Keywords: diabetic wound healing; macrofungi; AGEs

LIST OF FIGURES

LIST OF TABLES

LIST OF APPENDICES

LIST OF ABBREVIATIONS

ADP	Adenosine diphosphate
AGE	Advanced glycation end product
ASL	Arginosuccinate lyase
ASS	Arginosuccinate synthetase
BAFF	B-cell activating factor
Bcl-3	B-cell lymphoma 3-encoded protein
BH4	Tetrahydrobiopterin
Ca^{2+}	Calcium ion
CaM	Calmodulin
CD14	Cluster of differentiation 14
COX	Cyclooxygenase
Cu-Zn-SOD	Copper-zinc superoxide dismutase
DC	Dendritic cell
DMEM	Dulbecco's Modified Eagle Medium
DMSO	Dimethyl sulfoxide
DPPH	2,2-diphenyl-1-picrylhydrazyl
ECM	Extracellular matrix
EGF	Epidermal growth factor
eNOS	Endothelial nitric oxide synthase
EPC	Endothelial Progenitor Cell
Erg-1	Early growth response protein 1
FAD	Flavin adenine dinucleotide
FBS	Foetal bovine serum
Fe^{2+}	Ferrous ion

Fe^{3+}	Ferric ion
$FeSO_4$	Ferrous sulfate
FGF	Fibroblast growth factor
Fizz1	Resistin-like α
FMN	Flavin mononucleotide
FOXO1	Forkhead box protein O1
FRAP	Ferric-Reducing/ Anti-oxidant Power
HCS	High content screening
HNO_2	Nitrous acid
IC_{50}	Half maximal inhibitory concentration
IFN	Interferon
IgG	Immunoglobulin G
IκB	Inhibitor of NF-κB
IKK	IκB kinase
IL	Interleukin
iNOS	Inducible nitric oxide synthase
IRF-1	Interferon regulating factor 1
ITAM	Immunoreceptor tyrosine-based activation motif
JAK	Janus kinase
L-NIL	Nω-imino ethyl L-lysine
LPB	LPS binding protein
LPS	Lipopolysaccharide
LT	Lymphotoxin-B receptor
LTR	LysoTracker Red
M1	Classically activated macrophages

M2	Alternately activated macrophages
MAPK	Mitogen-activated protein kinase
Mgl 1	Macrophage galactose-type lectin-1
MHC	Major histocompatibility complex
MMP	Metalloproteinase
MSC	Mesenchymal Stem Cell
N_2O_3	Dinitrogen trioxide
NADPH	Nicotinamide adenine dinucleotide phosphate
NED	N-1-napthylethylenediamine dihydrochloride
NEMO	NF-κB essential modulator
NF	Nuclear factor
NIK	NF-κB inducing kinase
NKT	Natural killer T-cell
nNOS	Neuronal nitric oxide synthase
NO	Nitric oxide
NOS	Nitric oxide synthase
NOX	NADPH-oxidase
O_2	Oxygen
OAT	Ornithine aminotransferase
ODC	Ornithine decarboxylase
PAMP	Pattern associated molecular pattern
pDC	Plasmacytoid dendritic cell
PDGF	Platelet derived growth factor
PD-L2	Programmed death ligand 2
PG	Prostaglandin

PGHS	Prostaglandin-endoperoxide synthase
PI	Propidium iodide
PI3K	Phosphoinositide-3 kinase
PKC	Protein kinase C
PRR	Pattern recognition receptor
RAGE	Receptor for AGEs
RANKL	Receptor activator of NF-κB ligand
ROS	Reactive oxygen species
STAT	Signal transducer and activator of transcription
TE	Trollox equivalent
TGF	Transforming growth factor
Th	T-helper cell
TIMP	Tissue inhibitor of metalloproteinases
TLR	Toll-like receptor
TNF	Tumour necrosis factor
TPTZ	2,3,5-triphenyl-1,3,4-triaza-2-azoniacyclopenta-1,4-diene chloride
TSLP	Thymic stromal lymphopoeitan
T_xA_2	Thromboxane A2
VEGF	Vascular endothelial growth factor
Ym-1	Chitinase 3-like 3

CHAPTER 1: LITERATURE REVIEW

1.1.   THE INCIDENCE OF DIABETES IN AFRICA

Diabetes was estimated to affect approximately 415 million people globally in 2015 and resulted in 5 million cases of mortality. As seen in figure 1.1, this figure is predicted to increase by fifty-five percent within the next two decades and diabetes is thus fast becoming one of the largest epidemics of the 21st century (International Diabetes Federation, 2015).
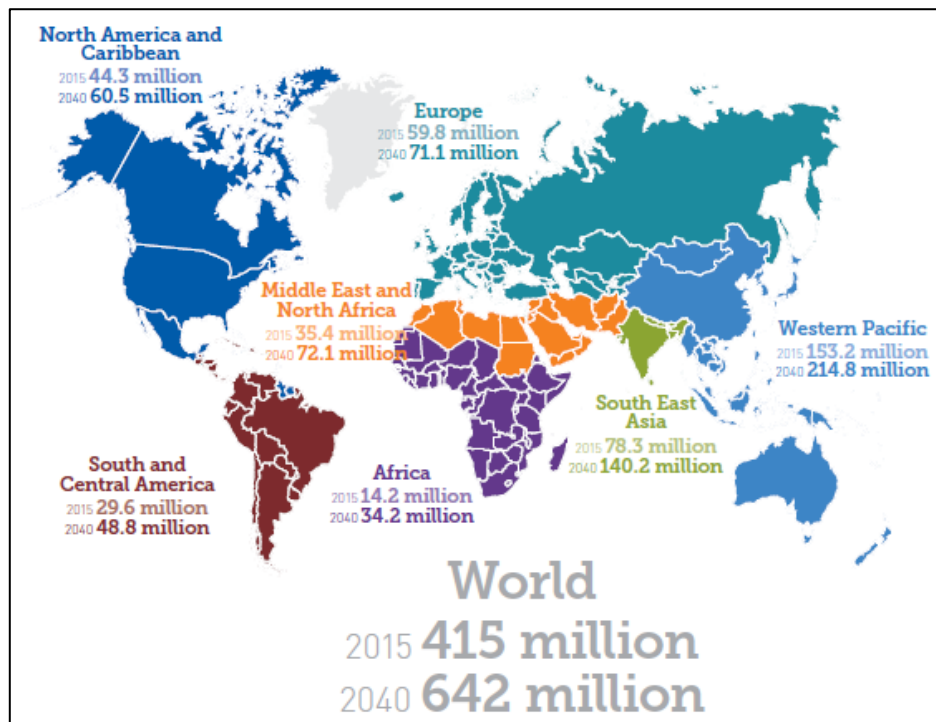
Figure 1.1: <u>Global projections of the prevalence of diabetes between the years 2015 and 2040 in people aged 20-79 years (International Diabetes Federation, 2015).</u>

While the prevalence of diabetes in Africa may not rank amongst the highest globally, the African continent is predicted to experience the largest increase in the incidence of diabetes (140 %) over the next 25 years. Currently, 14.2 million adults in Africa between the ages of 20 and 79 have diabetes thus representing a regional incidence of 3.2 %. According to recent statistics, the highest number of diabetic cases was reported for North Africa with Egypt (7.8 million diabetics), Algeria (1.7 million diabetics) and Sudan (1.7 million diabetics) taking the lead. South Africa (2.3 million diabetics) recorded the highest prevalence of diabetes in Southern Africa while Ethiopia (1.3 million diabetics) was the leading country from East Africa. From West Africa, Nigeria (1.6 million diabetics) reported the highest incidence of diabetes

while the Democratic Republic of Congo (1.8 million diabetics) recorded the highest figure from the central region of Africa (International Diabetes Federation, 2015).

1.2. THE ANATOMY OF THE SKIN

Being the largest organ of the human body, the skin forms a protective barrier and acts as the primary defence mechanism preventing the invasion of pathogens from the external environment (Nestle *et al.*, 2009; Kurahashi & Fujii, 2015). As shown in figure 1.2, the skin is composed of two layers, namely, the epidermis and the dermis.
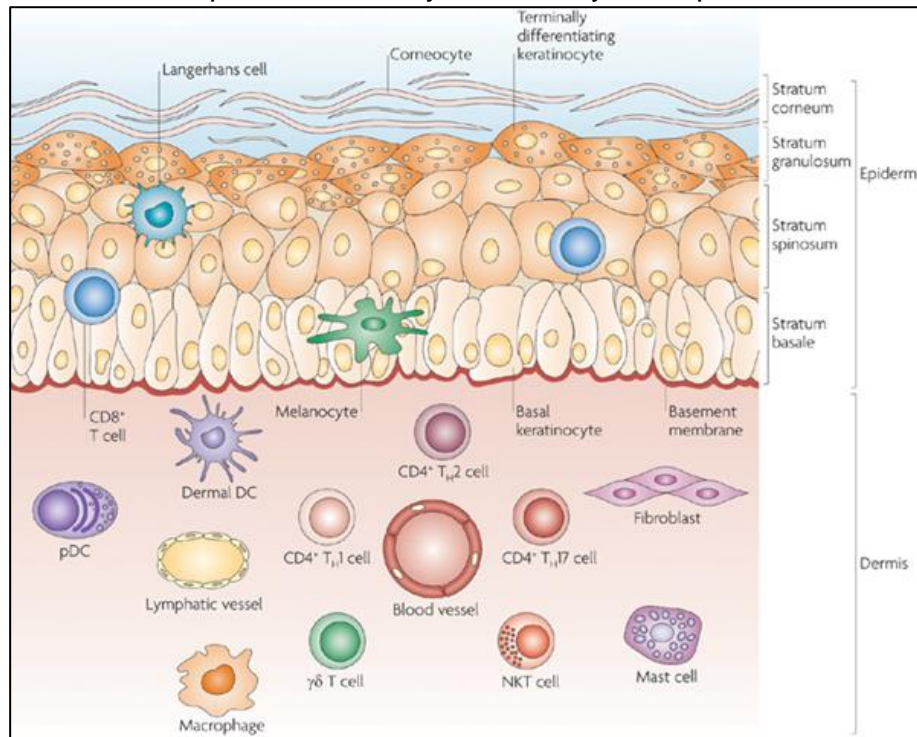
Figure 1.2: Skin anatomy and cellular components. The epidermis is largely composed of keratinocytes but also contains specialised melanocytes, Langerhans cells and CD8^{+} cytotoxic T-cells. The dermis consists of macrophages, mast cells, fibroblasts and specialised immune cells including dendritic cell (DC) subsets such as dermal DCs and plasmacytoid DCs (pDCs), T cell subsets such as CD4^{+} helper 1 (Th1), Th2 and Th17 cells, γδ T cells as well as natural killer T (NKT) cells. Blood vessels, lymphatic vessels and nerves can also be found throughout the dermis (Nestle *et al.*, 2009).

1.2.1. The epidermis

The epidermis forms the outermost layer and can be divided into four strata based on the types of cells that are present. The bottom layer, the stratum basale, contains a single row of undifferentiated epidermal cells called keratinocytes and is responsible for the constant renewal of the cells of the epidermis. As these basal keratinocytes differentiate, they will move upwards to the next layer, the stratum spinosum, where they will either mature or divide in order to replenish the basal

2

layer. The third layer, the stratum granulosum, contains keratinocytes which actively produce various keratin proteins and lipids while the cells in the final layer, the stratum corneum, are primarily responsible for the skin's barrier function. The epidermis also contains specialised cells including melanocytes, Langerhans cells and T-cells (Nestle *et al.,* 2009).

1.2.2. The dermis

The dermis consists of a dense network of cells called fibroblasts which are responsible for producing the extra-cellular matrix rich in collagen. Unlike the epidermis, the dermis is not divided into functional layers but consists instead of several specialised immune cells including dendritic cells, helper T-cells and natural killer T-cells, as well as macrophages, mast cells and fibroblasts. The dermis also contains adnexal structures such as hair follicles, sebaceous glands and sweat glands (Brodell & Rosenthal, 2008; Nestle *et al.*, 2009).

Any form of skin damage may expose the body to harmful infections; however, the importance of the skin's ability to promptly heal after a wound has been sustained is often neglected. Chronic wounds thus represent a silent epidemic affecting a rather large portion of the global population and with the predicted rise in the prevalence of diabetes, it poses a growing danger to public health (Kurahashi & Fujii, 2015).

1.3.   ACUTE VERSUS CHRONIC WOUNDS

Any event which compromises the integrity of the epithelial lining forming the skin will lead to the development of a wound. Wounds result in tissue damage, an event that sets into motion a series of complex cellular events in an attempt to restore some, if not all, of the affected tissues anatomical and functional capacity (Enoch & Leaper, 2005). Acute wounds refer to those that progress through all the relevant stages of the wound healing process in a timeous and coordinated manner whereas chronic wounds display prolonged healing up to 12 weeks following the initial insult. This is due to the failure of cells to progress through the normal phases of wound healing as they enter, instead, into a state of pathological inflammation (Menke *et al.*, 2007; Young & McNaught, 2011).

1.3.1. The economic burden of chronic wounds

Several challenges exist with regards to measuring the costs associated with chronic wounds. To date, no research related to the economic burden of chronic wounds on the South African healthcare system has been carried out. Costs associated with chronic wounds appear to be poorly documented, hidden under general cost categories or centred around direct clinical care costs without considering any of the indirect or non-monetary repercussions of the wound on the wellbeing of the patient, however, the global wound care market is estimated to exceed $22 billion USD by the year 2020 (Hurd, 2013; Tricco *et al.*, 2015).

1.3.2. Current wound healing therapies

Chronic wounds can be categorised as i) resulting from chronic diseases such as diabetes or venous insufficiency, ii) pressure ulcers, or iii) non-healing surgical wounds. Chronic wounds thus possess different etiologies with treatment strategies being targeted to the type of wound (Tricco *et al.*, 2015). Conventional wound management involves debridement in order to remove debris and necrotized tissue. This is followed by the topical application of a selection of wound dressings that ensure adequate tissue perfusion while reducing the wound pressure as well as the chances of infection (Borena *et al.*, 2015). Advances in both technology and the understanding of the cellular and biochemical mechanisms involved in impaired wound healing have led to the development of more advanced wound healing therapies. Some of these include negative pressure wound therapy, hyperbaric oxygen therapy, bioengineered skin and tissue equivalents, growth factors and stem cell therapies (Wu *et al.*, 2010; Frykberg & Banks, 2015).

1.3.3. Current wound healing models

Currently, there is a substantial lack of both *in vitro* and *in vivo* models that successfully mimic the diabetic state while simultaneously being considered reliable and optimal wound repair models. This makes the development of effective treatment approaches with regards to impaired wound healing particularly problematic and challenging (Mendes *et al.*, 2012). In order to fully understand both the function and dysfunction of the skin during wound healing, it is necessary to establish pure cell cultures of various cellular components of the skin. The results can then be reincorporated back into the context of the skin as a whole (Abdel-Naser

et al., 2005). While several *in vitro* and *in vivo* models have been designed and used to study wound repair as well as the underlying mechanisms involved, none of the models developed to date have been able to fully mimic wound healing as it occurs in humans. Each model thus has its own distinct set of advantages and disadvantages that must be carefully considered when selecting an appropriate model, however, valuable information can still be gained from each model (Ansell *et al.*, 2012; Nunan *et al.*, 2014).

1.3.3.1. *The importance of in vitro models*

Over the last two decades major developments in cell culture techniques, chemically-defined media, and the ease of access to commercially available mammalian cells, have transformed *in vitro* studies into an invaluable research asset. The utilization of *in vitro* test methods has many applications in research and avoids many of the ethical and moral dilemmas associated with animal testing (Freshney, 2005). *In vitro* models for wound healing generally involve monolayers of skin cells such as keratinocytes, fibroblasts or macrophages and are particularly useful for dose-response assays, anti-microbial studies and assessing the effect of various agents on the function of individual cell types. For studies related to chronic wound healing, the *in vitro* models can be adapted so that they incorporate at least one of the underlying etiologies of the disease of interest. More recent advances in wound healing models have led to the development of more complex 3-dimensional cell cultures as well as organ cultures such as skin explants (Perez & Davis, 2008).

To have any relevance in the field of scientific research, experimental models must suitably imitate both the physiologic and pathogenic circumstances of a clinical condition. *In vitro* models form an integral part of research pertaining to wound healing experiments due to the coordinated manner in which multiple cells interact with various systems within the human body during this process. *In vitro* modelling thus provides an essential tool which can be used to elucidate various mechanistic and functional details of particular components involved specifically in wound healing. It frequently provides an easier, more rapid and cost effective method for analyzing molecular and cellular events; however, *in vitro* tests frequently reveal short-comings regarding adequate replication of the complex interactions occurring within organisms and during pathological disorders or illnesses. As a result, *in vitro*

modelling will never be able to replace *in vivo* testing; however, it can provide essential additional information that cannot be gained from complex *in vivo* models alone and can thus prove to be a powerful research tool, particularly when it is used in conjunction with *in vivo* models (Scherer *et al.*, 2008; Stacey, 2012).

1.3.3.2. Animal models

Once sufficient evidence with regards to a possible wound healing therapy has been obtained through *in vitro* studies, more complex animal models can be used. The use of rodents and small mammals such as rabbits have emerged as fairly popular wound healing models due to their low cost and maintenance as well as their ability to produce several offspring over relatively short time periods (Perez & Davis, 2008). The rabbit ear ulcer model has been used to generate ischemic wounds; however, this model does not fully mimic hypoxic wounds in humans and is not genetically tractable. Rat magnet ischemia-reperfusion models have been generated to study pressure ulcers while diabetic mice have been used to study diabetic ulcers, however, anatomical differences between the skin of rodents and humans as well as the fact that diabetes in mice does not fully reflect diabetic complications as they occur in humans have raised some concerns with regards to the clinical relevance of these particular animal models (Nunan *et al.*, 2014).

Porcine wound healing models have emerged as the most clinically relevant wound healing models due to the structural similarities shared with human skin. These include epidermal thickness, the ratios of dermal-epidermal thickness, similar patterns of blood vessels and hair follicles, the presence of dermal collagen, dermal elasticity, and comparable physical and molecular responses to several growth factors (Perez & Davis, 2008). Pig flap ischemia has been used to study ischemic ulcers while pig wound infections have been used to study infected ulcers. Porcine models are, however, more expensive than the other animal models mentioned due to their size and are not genetically tractable (Nunan *et al.*, 2014).

1.4. ACUTE WOUND HEALING OVERVIEW

The wound healing process is considered to be one of the body's principle survival mechanisms and commences directly after an injury has been sustained (Beldon, 2010). A healed wound is defined to be one in which complete repairing of the affected and surrounding connective tissues has been accomplished and where

regeneration has allowed for the complete re-epithelialization of the wound area. Furthermore, a healed wound is one where the previously damaged area has regained at least some, if not all, of its earlier anatomical and functional capability (Enoch & Leaper, 2005).

The process of wound healing is governed by the four discrete yet overlapping phases of hemostasis, inflammation, proliferation and tissue remodelling. As can be seen in figure 1.3, this healing cascade requires the careful and precise regulation of several cellular activities where each phase is categorised according to the cell types that are present at the wound at any particular time (Enoch & Leaper, 2005; Young & McNaught, 2011).
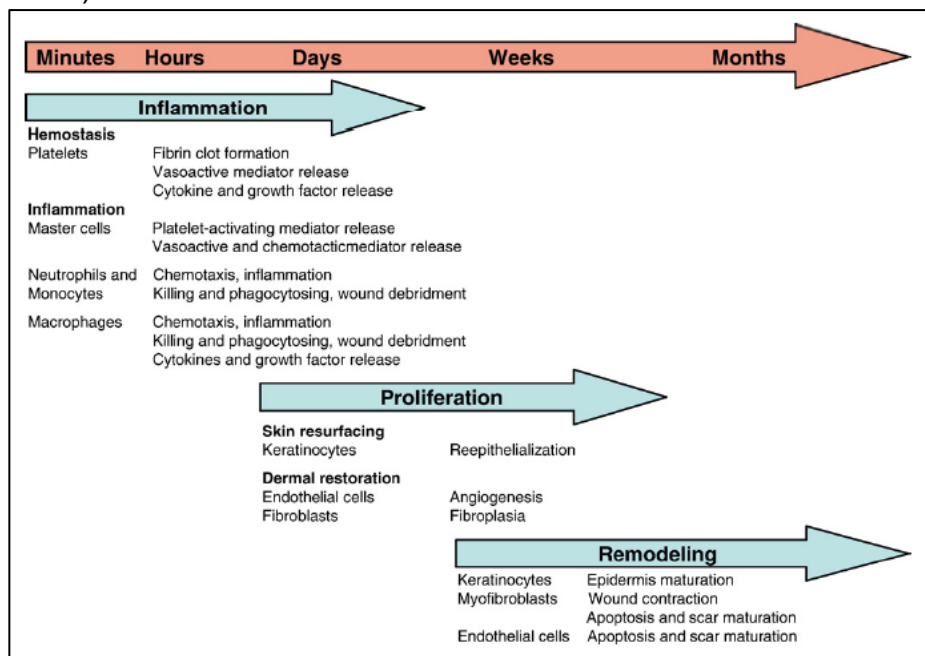
Figure 1.3: <u>A schematic representation of the normal phases of wound healing and the functions of the major cells responsible for each phase (Li *et al.,* 2007).</u>

1.4.1. Hemostasis

Hemostasis refers to the series of events that occur directly after an injury has been sustained in an attempt to prevent excessive blood loss. For this phase of wound healing to be considered successful it must: commence rapidly directly after the injury has occurred; be localised to the damaged area; and must be precisely controlled in order to ensure that the least amount of blood possible is lost. Medical intervention is required in cases where more than ten percent of the body's total blood volume is lost (Tortora & Derrickson, 2012; Silverthorn, 2014).

1.4.1.1. Vascular spasm

When vascular damage is sustained, whether micro- or macro- vascular, the blood vessels will constrict in order to reduce the blood flow to the damaged region. Rapid constriction of the affected arterial vessel is achieved through smooth muscle contraction as a direct response to the trauma sustained (Young & McNaught, 2011). The smooth muscle is positioned in the circular layer of blood vessel walls and contractions are a consequence of several factors including local muscle spasm, the presence of local autacoids that are released from damaged tissue and platelets, and nervous reflexes generated from pain receptor activation. This contraction process appears to be regulated by the increasing levels of calcium (Ca^{2+}) within the cytoplasm where the strength of the spasm is proportional to the extent of the damage (Guyton & Hall, 2006).

1.4.1.2. Platelet plug formation

Inactivated platelets appear small and disc-shaped, storing vast quantities of several growth factors such as platelet-derived growth factor (PDGF), transforming growth factor (TGF)-β, vascular endothelial growth factor (VEGF) and epidermal growth factor (EGF), as well as cytokines, chemokines, lysosomal enzymes, coagulation factors and pro-inflammatory mediators. These chemicals are stored in intracellular granules, each performing an important function during the process of hemostasis. Once cells become damaged, collagen fibres forming part of the connective tissue layer beneath the cells become exposed. Blood platelets adhere to these exposed fibres and consequently enter into an activated state (Tortora & Derrickson, 2012).

Platelet activation is mediated by several factors including adenosine diphosphate (ADP), thromboxane and thrombin. Once platelets become activated, they will undergo morphological changes involving the extension of multiple projections which enables platelet aggregation. Furthermore, the vesicular contents of the alpha and dense granules will be liberated where ADP will function with thromboxane A_2 during the activation of neighbouring platelets and serotonin will function with thromboxane A_2 in vasoconstriction in order to ensure that a reduced blood flow to the damaged vessel is maintained through continued smooth muscle contraction. Once the initial platelet plug has been formed and has successfully arrested the bleeding, it is strengthened and reinforced by the presence of both fibrin and von Willebrand factor

together with the actin and myosin filaments present in the platelet (Young & McNaught, 2011; Tortora & Derrickson, 2012).

1.4.1.3. Blood coagulation

Once the platelet plug has been successfully established, a blood clot is formed in an attempt to restrict any further blood loss. Blood clot formation can occur via the intrinsic and/ or the extrinsic pathways. The extrinsic pathway occurs rapidly in response to the leakage of tissue factor from damaged cells surrounding the affected blood vessel. This sets into motion a series of Ca^{2+}-dependent reactions resulting in the formation of prothrombinase. Activation of the slower intrinsic pathway does not require tissue damage as it is triggered by the presence of negatively charged surfaces and substances within the blood or in direct contact with the blood. Via a different series of Ca^{2+}-dependent reactions, activated clotting factor XIII will ultimately lead to the formation of prothrombinase (Guyton & Hall, 2006; Tortora & Derrickson, 2012).

The intrinsic and extrinsic pathways converge to form the final common pathway during which a strong and stable blood clot is formed. This is achieved through the production of thrombin which leads to the formation of insoluble fibrin threads as well as the activation of fibrin stabilising factor. Finally, the blood clot will retract through contraction of the fibrin threads, consequently drawing the edges of the damaged vessel towards each other in an effort to prevent further damage (Tortora & Derrickson, 2012).

1.4.2. Inflammation

Inflammation proceeds at the same time as hemostasis with the primary aim being to prevent infection of the wound area as well as to remove any dead and damaged tissue which might otherwise delay the normal healing process (Young & McNaught, 2011; Kurahashi & Fujii, 2015). Once the blood vessels have been successfully constricted, a decreased blood flow to the affected tissues results in hypoxia and consequent acidosis. This will lead to the production of nitric oxide (NO), adenosine and a multitude of various vasoactive metabolites which cause the constricted arterial blood vessels to now dilate and relax. Furthermore, mast cells will release histamine which consequently increases vasodilation as well as vascular

permeability. The result is that numerous pro-inflammatory cells are able to leave the blood stream and enter the extracellular space surrounding the injury, explaining why early wounds appear red, swollen and warm to the touch (Young & McNaught, 2011).

Inflammation is frequently categorised into the early and late phase depending on the types of cells that are present at the wound area as well as the timing and duration of the response. The inflammatory response is stimulated not only by the pro-inflammatory components housed and released by platelets but also by the conversion of arachidonic acid, from membrane glycerophospholipids in the plasma membrane of the damaged cells, into potent pro-inflammatory signalling molecules including leukotrienes, thromboxanes and prostaglandins (Li *et al.*, 2007; Young & McNaught, 2011).

1.4.2.1.   *Early phase*

Complement activation occurs via the classical and alternative pathways as summarised in figure 1.4. Both pathways converge at the activation step of complement proteins C3 and C5, ultimately forming the membrane attack complex. Complement proteins C3a and C5a form potent chemotactic signals, resulting in the infiltration of leukocytes to the wound area (Sinno & Prakash, 2013). The first leukocytes that will arrive at the site of the injury within the first 24 to 48 hours are the neutrophils. Several chemo-attractants including ECM protein fragments, TGF-β, constituents of the complement cascade, cytokines, products secreted from mast cells and formyl-methionyl peptide components produced by bacteria will attract neutrophils to the wound bed via the process of chemotaxis (Enoch & Leaper, 2005; de Mendonça & Coutinho-Netto, 2009). Furthermore, various chemotactic factors will also up-regulate the expression of specific intercellular adhesion proteins that are involved in leukocyte-homing at the wound area (Li *et al.*, 2007).

As the neutrophils arrive at the wound area, they will leave the bloodstream and enter the wound area via the process of diapedesis. During this process, the neutrophils will adhere to the endothelial cells of the affected and adjacent blood vessels through specific cell surface receptors, including selectins and integrins, after which they squeeze between the endothelial cells in order to enter the affected tissues (Enoch & Leaper, 2005; Tortora & Derrickson, 2012). Here they will be able

to phagocytose and remove bacteria and any foreign materials by releasing several enzymes and free oxygen radicals (Li *et al.*, 2007). Upon completion of their task, neutrophils will spontaneously apoptose and be removed by macrophages present in the wounded tissue (Williamson & Harding, 2004).
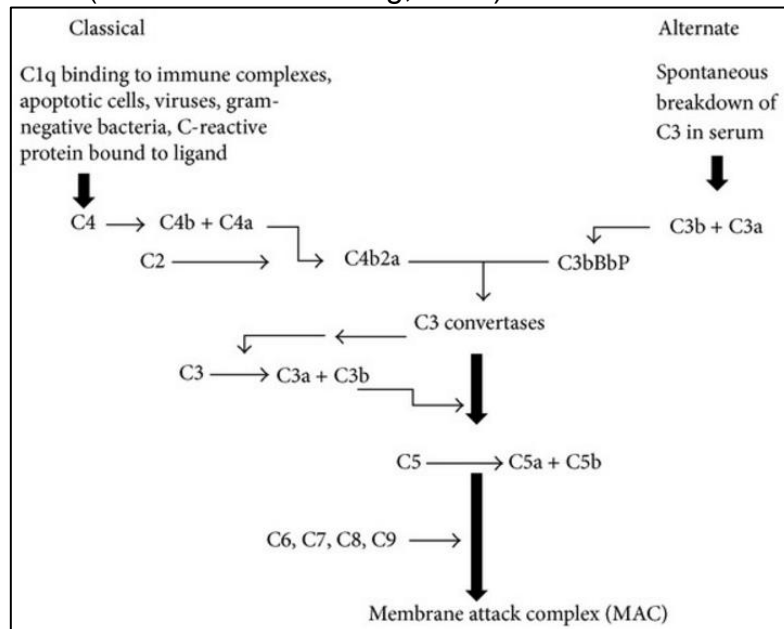
Figure 1.4: <u>A summary of the classical and alternative pathways of complement activation. Complement proteins C3a and C5a are involved in chemotaxis while the membrane attack complex formed is responsible for lysing foreign microbes (Sinno & Prakash, 2013).</u>

1.4.2.2. *Late phase*

Within 48 to 72 hours of sustaining an injury, the second type of leukocytes known as monocytes will arrive at the wounded area via the process of chemotaxis. Monocytes are attracted to similar chemo-attractants as the neutrophils with the addition of clotting factors, immunoglobulin G (IgG) fragments, growth factors and degradation products of collagen and elastin (Enoch & Leaper, 2005). Entry into the damaged tissue area is achieved via the same process of margination and diapedesis described for the neutrophils after which monocytes will be transformed into phagocytic macrophages (Li *et al.*, 2007).

1.4.2.3. *A closer look at macrophage function*

Macrophages carry out several responsibilities during inflammation including phagocytosis and removal of infectious agents, cellular debris and neutrophils via the release of various proteolytic enzymes and reactive oxygen species (ROS) (Li *et al.*,

2007). Some of the more complex pathways through which macrophages carry out their functions are described below.

1.4.2.3.1. <u>Classical and alternative macrophage activation</u>

Macrophage activation or polarization has been categorised into two main pathways based on several phenotypic and metabolic differences. Classically activated (M1) macrophages are involved in defending the host from pathogens such as bacteria, viruses and protozoa while alternatively activated (M2) macrophages perform anti-inflammatory and tissue repair functions. A useful approach to studying macrophage polarization *in vitro* has been to stimulate cells with either microbial agonists or cytokines and measuring the resultant cytokine production and alterations in gene expression, however, it is important to realise that *in vivo* macrophage responsiveness differs as macrophages represent a spectrum of polarization phenotypes rather than distinct subpopulations. Thus, while results obtained *in vitro* can provide important information with regards to macrophage polarization, they should be interpreted with great caution as M1 and M2 macrophages represent two extremes of the macrophage phenotype spectrum (Murray & Wynn, 2011).

M1 macrophages are stimulated by interferon (IFN) γ secreted by T-helper (Th) 1 cells as well as microbial products such as lipopolysaccharide (LPS) which activate Toll-like receptor (TLR) signalling. These macrophages respond by producing pro-inflammatory cytokines such as tumor necrosis factor (TNF)-α, interleukin (IL)-6 and IL-12 as well as reactive oxygen and nitrogen intermediates which are generated during the respiratory burst in order to destroy invading pathogens. While M1 macrophages are essential in preventing and eliminating infections, chronic and irregular expression has been associated with the pathogenesis of various metabolic, autoimmune and inflammatory diseases. M1 macrophage activation thus needs to undergo very tight regulation in order to prevent extensive tissue damage. M2 macrophage polarization is stimulated by IL-4, IL-10 and IL-13 produced by Th2 cells and these macrophages are largely involved in producing anti-inflammatory cytokines and tissue repair (Chawla, 2010; Murray & Wynn, 2011). M1 and M2 macrophage polarization triggers and responses are summarised in figure 1.5.
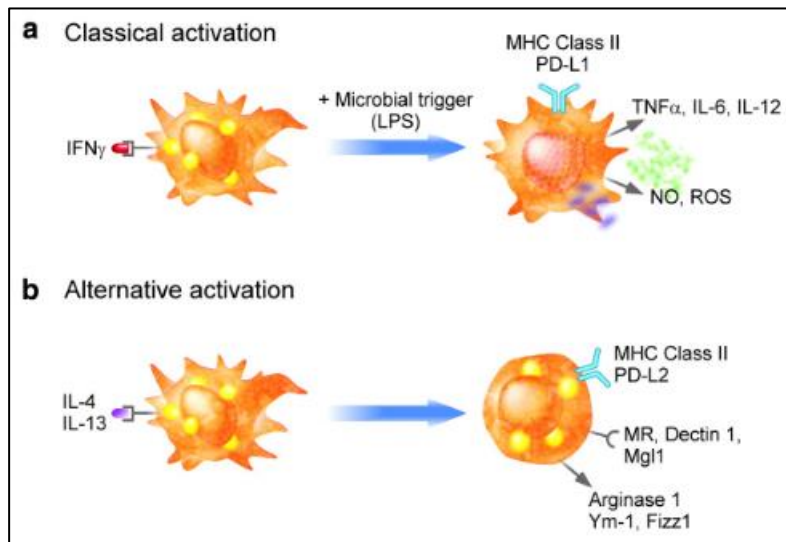
Figure 1.5: <u>Triggers and responses for classical and alternative macrophage activation. (a) M1 macrophages are stimulated by IFNγ and LPS to produce pro-inflammatory cytokines to promote cell-mediated immunity as well as NO and ROS to destroy microbes. (b) M2 macrophages are stimulated by IL-4 and IL-13 and respond by upregulating the expression of major histocompatibility complex (MHC) class II proteins and costimulatory molecules (PD-L2) as well as arginase 1 expression. Further markers for M2 macrophages include lectins (mannose receptor, dectin-1 and MgI1), chemokines, cytokines and secreted products (Ym-1 and Fizz1) (Chawla, 2010).</u>

The best studied gene induced by M2 macrophage activation is arginase 1 which is consequently acknowledged as the most reliable marker of alternative macrophage polarization. Arginine metabolism can occur via either arginase or nitric oxide synthase (NOS) activities as shown in figure 1.6. M1 macrophages express inducible-NOS (iNOS) and are consequently able to metabolise arginine to form NO and citrulline. NO can be further metabolised to form reactive nitrogen species such as peroxynitrite while citrulline is recycled for efficient NO synthesis through the action of the enzymes arginosuccinate synthetase (ASS) and arginosuccinate lyase (ASL). M2 macrophages express arginase which is responsible for hydrolysing arginine to ornithine and urea. As the arginase pathway limits the availability of arginine for NO synthesis, ornithine is further broken down into polyamines and proline by the enzymes ornithine decarboxylase (ODC) and ornithine aminotransferase (OAT), respectively (Rath *et al.*, 2014).

Additional metabolic differences that exist between M1 and M2 macrophages relate to glucose and iron metabolism. M1 macrophages undergo anaerobic glycolysis while M2 macrophages utilise oxidative glucose metabolism (fatty acid oxidation) to sustain their tissue remodelling and repair functions over long periods of time. With

regards to iron metabolism, M1 macrophages produce high levels of ferritin to store iron while M2 macrophages express increased levels of the iron exporter, ferroportin (Chazaud, 2013).
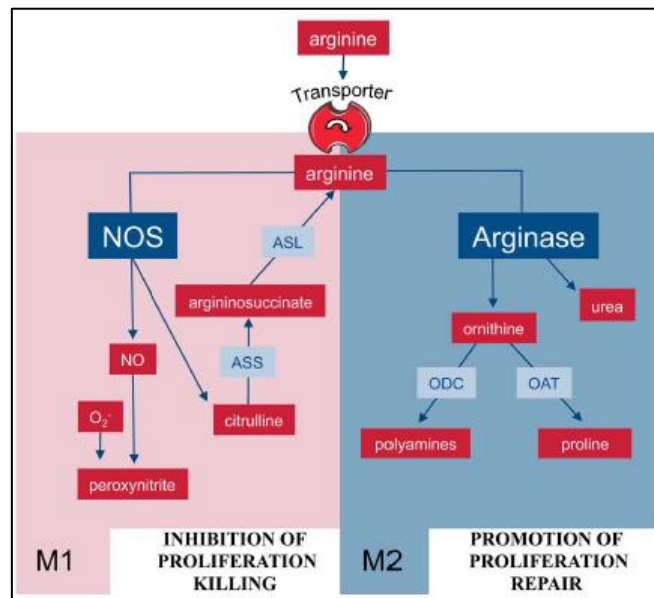
Figure 1.6: Arginine metabolism in M1 and M2 macrophages. Arginine is transported into the cytoplasm of macrophages where it will undergo degradation to either nitric oxide (NO) and citrulline through the action of nitric oxide synthase (NOS) in M1 macrophages or ornithine and urea through the action of arginase in M2 macrophages (Rath *et al*., 2014).

During the wound healing process, both M1 and M2 macrophages perform critical functions as summarised in figure 1.7. M1 macrophages destroy invading pathogens by generating NO and ROS, recruit neutrophils and helper T-cells by secreting various pro-inflammatory cytokines and aid in the degradation of the extracellular matrix (ECM) by secreting metalloproteinases (MMPs). M2 macrophages are essential for the transition from inflammation to the tissue repair process, secreting various growth factors including PDGF which stimulates myofibroblast proliferation and TGF-β1 which promotes the differentiation of fibroblasts into myofibroblasts, enhances the expression of tissue inhibitors of metalloproteinases (TIMPs) and promotes the interstitial production of fibrillar collagens within myofibroblasts (Murray & Wynn, 2011).
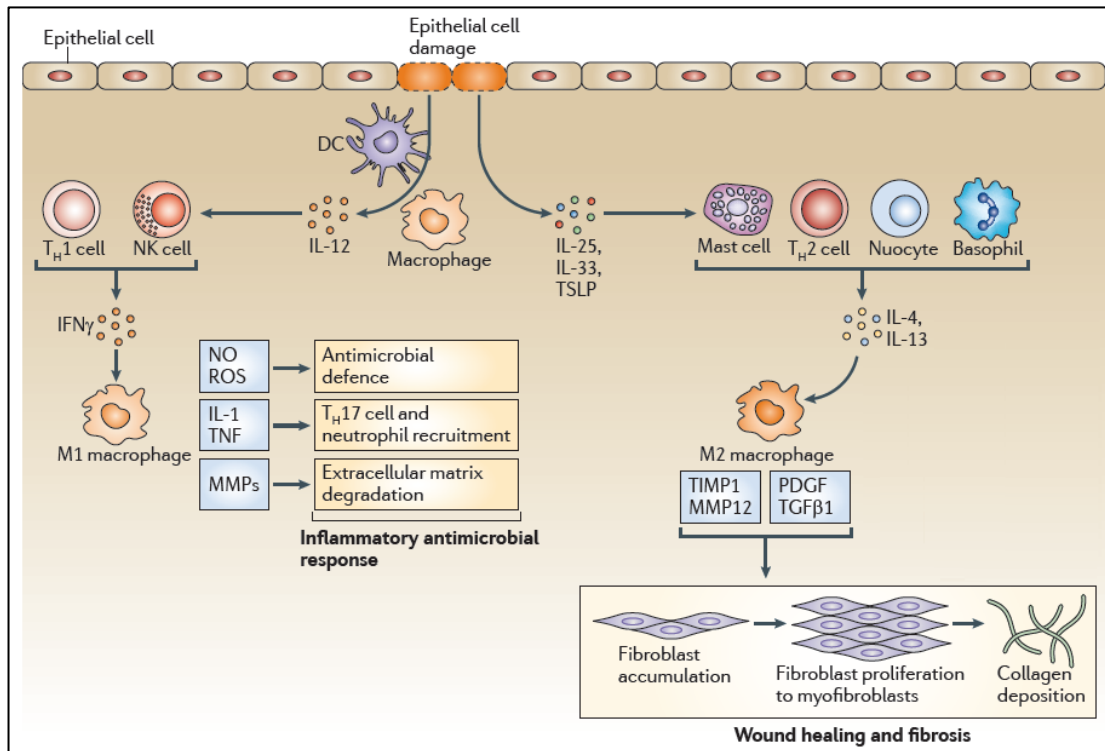
Figure 1.7: <u>The role of M1 and M2 macrophages in cutaneous wound healing. M1 macrophages produce antimicrobial agents including NO, ROS, IL-1 and TNF and regulate ECM degradation through the action of MMPs. Damaged epithelial cells release alarmins such as IL-25, IL-33 and thymic stromal lymphopoietin (TSLP) which cause the subsequent release of IL-4 and IL-13 by various innate and adaptive immune cells. Once all infectious agents have been eliminated, M2 macrophage activation will dominate thus promoting tissue regeneration and fibrosis through the production of TIMP-1, growth factors and cytokines (Murray & Wynn, 2011).</u>

1.4.2.3.2. <u>NO biosynthesis</u>

NO is a diffusible free radical acting as an intercellular signalling molecule which performs a wide range of biological functions. NO biosynthesis occurs through the action of NOS enzymes. Three NOS isozymes exist differing in structure, regulation as well as distribution and are encoded by different chromosomes. Neuronal NOS (nNOS) is synthesised by certain neuronal cells, inducible NOS (iNOS) is synthesised by macrophages and endothelial NOS (eNOS) is synthesised in endothelial tissue, however, the expression of all three isoforms in the skin tissue has been reported. Keratinocytes and melanocytes have been found to express nNOS while eNOS has been detected in keratinocytes forming part of the basal epidermal layer, dermal fibroblasts, eccrine glands as well as endothelial capillaries. iNOS induction has been reported in fibroblasts, endothelial cells, keratinocytes and Langerhans cells. NO thus forms part of important functions necessary for regulating skin homeostasis (Luo & Chen, 2005; Rath *et al.*, 2014).

While eNOS and nNOS are both constitutively expressed, iNOS is the only inducible isoform. The NOS isoforms all exist as active homodimers consisting of a C-terminal reductase domain as well as an N-terminal oxygenase domain. Within the reductase domain, one binding site for each of nicotinamide adenine dinucleotide phosphate (NADPH), flavin mononucleotide (FMN), as well as flavin dinucleotide (FAD) can be found. The oxygenase domain contains heme binding sites as well as binding sites for the tetrahydrobiopterin (BH4) cofactor and the substrate, *L*-arginine. A calmodulin (CaM) binding site can be found between the N- and the C-terminal domains and performs an important role with regards to the structure and function of the NOS enzymes. Due to their constitutive nature, eNOS and nNOS are permanently active and continuously generate very low concentrations of NO with their enzyme function being modulated by intracellular calcium fluxes as well as exogenous CaM. iNOS transcription, expression and function, however, is induced by a wide range of inflammatory stimuli, cytokines and growth factors on target cells. The consequent generation of NO thus occurs at much higher concentrations than is seen for the other two isoforms and forms part of the host immune response (Luo & Chen, 2005).

Regardless of the isoform, all NOS enzymes catalyse the same two-step reaction shown in figure 1.8 where *L*-arginine is oxidised to citrulline and NO through the formation of a N-Hydroxyarginine intermediate. NADPH serves as an electron donor during this reaction while heme, FMN, FAD and BH4 are important cofactors (Aktan, 2004).
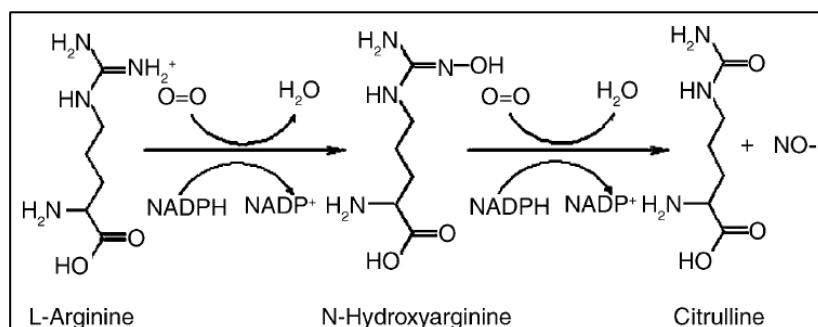
Figure 1.8: NO biosynthesis from L-arginine. This reaction is regulated by NOS enzymes which oxidise L-arginine in the presence of NADPH and O_2 to citrulline and NO via a N-Hydroxyarginine intermediate (Guix *et al.*, 2005).

iNOS is regulated at the transcriptional level through the binding of various signalling molecules, such as nuclear factor (NF)-κB and signal transducer and activator of transcription (STAT) proteins, to the promoter region of the iNOS gene. The

activation of several cellular receptor molecules regulate iNOS expression through various signalling pathways, some of which are shown in figure 1.9.
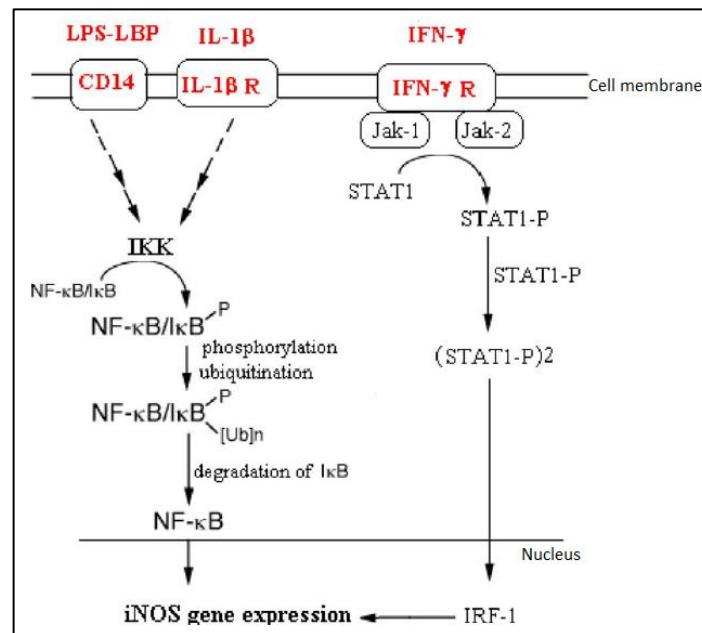
Figure 1.9: <u>Regulators of iNOS gene expression and consequent NO production. Through the action of the LPS binding protein (LBP), LPS is transferred to the CD14 cell membrane receptor which activates a signalling cascade that causes the activation and translocation of NF-κB to the nucleus where it regulates iNOS expression. Another signalling pathway involved in iNOS regulation is the JAK-STAT pathway activated by the binding of IFNγ to its cell membrane receptor (Aktan, 2004).</u>

Receptors such as cluster of differentiation 14 (CD14) and TLRs (activated by LPS) together with the IL-1β receptor (activated by the binding of IL-1β) are able to regulate iNOS expression through the activation and consequent nuclear translocation of NF-κB. NF-κB exists in the cytoplasm in an inactive form bound to its inhibitor. Once phosphorylated in response to various pro-inflammatory stimuli, NF-κB is released and undergoes subsequent translocation to the nucleus were it binds to the iNOS gene and promotes iNOS expression (Aktan, 2004; Giux *et al.*, 2005).

Another activator of iNOS expression is IFNγ which binds to the IFNγ cell-membrane receptor thus promoting iNOS induction and consequent NO production through the Janus kinase (JAK)-STAT signalling pathway. Once activated, the soluble tyrosine-kinase receptor JAK phosphorylates several tyrosine residues on the STAT1 protein which is subsequently activated and translocated to the nucleus where it promotes iNOS expression by inducing the expression of interferon regulating factor 1 (IRF-1) (Aktan, 2004). Just as several pro-inflammatory cytokines, microbial products and

hypoxia can induce iNOS expression, there are numerous cytokines including IL-4, IL-10 and TGF-β which suppress iNOS transcription. There are thus multiple levels of regulation for iNOS expression and resultant NO production with additive or synergistic combinations of effectors being the most effective (Rath *et al*, 2014).

NO performs several key functions during the normal wound healing process where it has been shown to promote angiogenesis by regulating the activity of several pro-angiogenic cytokines such as VEGF. Studies have shown that NO directly increases angiogenesis in ischemic murine tissues while NOS inhibitors were found to impair angiogenesis as it occurs in granulation tissue during gastric ulcer healing and also suppressed capillary organisation during *in vitro* studies. Additionally, NO influences several cellular processes including proliferation, differentiation and apoptosis of various cells involved in the wound healing process. A NO donor, sodium nitroprusside, was shown to promote the fetal bovine serum (FBS)-induced incorporation of thymidine into the DNA of human skin fibroblasts as well as stimulating DNA synthesis induced by fibroblast growth factor (FGF) or PDGF. Conversely, an iNOS inhibitor, N^{ω}-imino ethyl *L*-lysine (L-NIL), was shown to decrease keratinocyte proliferation at the wound edges thus causing a delay in the re-epithelialisation process. Reduced levels of NO were also found to promote *in vitro* keratinocyte proliferation. Furthermore, NO has been shown to regulate apoptosis in irradiated keratinocytes as the addition of a NOS inhibitor resulted in an increase in keratinocyte apoptosis (Luo & Chen, 2005).

Luo and Chen (2005) further explained that NO was also shown to play an important role in collagen deposition during the final stage of wound healing. Studies showed that collagen production was increased in fibroblasts derived from both normal skin and skin wounds in response to treatment with a NO donor and that this phenomenon was reversed by treatment with a NOS inhibitor. It has been suggested that this effect is not due to an increase in the *de novo* transcription of the genes encoding for collagen but rather as a result of the posttranslational enhancement of collagen production.

1.4.2.3.3.   Phagocytosis

The mechanisms by which cells are able to internalise particles and solutes include pinocytosis, receptor-mediated endocytosis as well as phagocytosis. Fluids and

solutes are generally incorporated into cells via pinocytosis while receptor-mediated endocytosis refers to the process through which macromolecules, small particles and viruses are taken up by cells. Both of these mechanisms are clathrin-based and generally proceed independently of actin filament polymerisation. Conversely, phagocytosis refers to the ingestion of particles larger than 0.5 µm in diameter through a mechanism that is actin dependent but does not rely on clathrin. Phagocytosis thus exists for the removal of infectious agents as well as dead and damaged cells with several other important roles in tissue remodelling, inflammation and other immune responses (Alem & Underhill, 1999; May & Machesky, 2001).

The process of phagocytosis is a highly complex, energy-dependent process involving several signalling pathways determined by the particles being internalised as well as the receptors involved. While no single model is fully capable of describing exactly what occurs *in vivo* during phagocytosis, there are several common features that are shared as seen in figure 1.10 (Aderem & Underhill, 1999). Briefly, cell surface receptors will recognise a pathogen and bind to it after which various signalling pathways that mediate actin polymerisation under the cell membrane at the contact site are induced. As a result, membrane extensions rich in actin called pseudopodia will extend around the particle on either side. Once the membranes of the pseudopodia fuse behind the particle to form a phagosome, it is pulled in towards the centre of the cell as the pseudopodia regress. Via a series of various membrane fusion and fission events with lysosomes, the final vesicle called a phagolysosome is formed where the pathogen will ultimately be destroyed through various proteolytic enzymes, ROS and nitrogen species (Aderem, 2003).

Both neutrophils and macrophages are capable of phagocytosis and consequently express several receptors including pattern recognition receptors (PRRs) such as TLRs, scavenger receptors and C-type lectins. PRRs recognise pathogen-associated molecular patterns (PAMPs) which include LPS and lipoteichoic acids on the surface of gram-positive and gram-negative bacteria as well as formylated peptides in bacteria and mannans in yeast cell walls. Furthermore, several high-affinity receptors for various opsonins including antibodies, plasma lectins and complement proteins exist (Aderem, 2003; Abbas *et al.*, 2012).
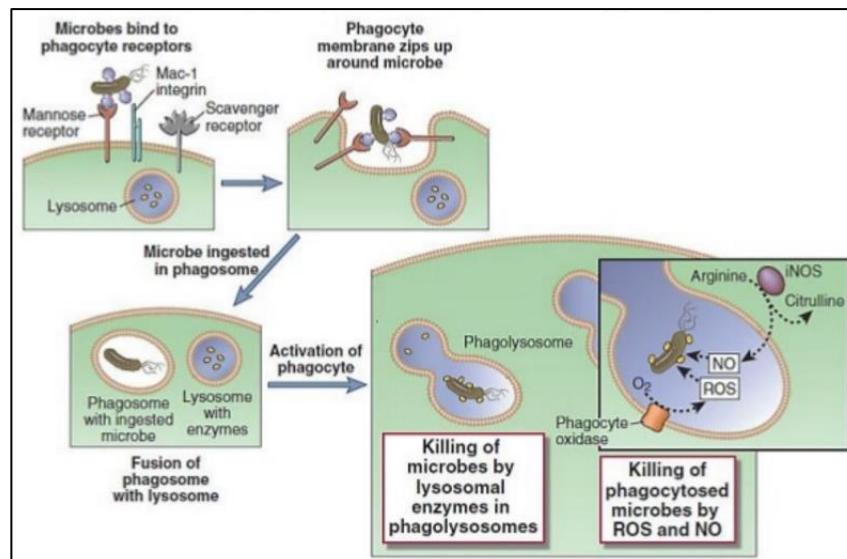
Figure 1.10: The intracellular destruction of microbes through phagocytosis. Various membrane receptors exist which are able to bind directly to microbes as well opsonised microbes. Once internalised by pseudopodia into the phagosome, it fuses with a lysosome to form a phagolysosome where the microbes will be destroyed through the action of various proteolytic enzymes as well as ROS and nitrogen species (Abbas *et al.*, 2012).

Several mechanisms of phagocytosis have been defined including Fc-receptor mediated phagocytosis, complement-receptor mediated phagocytosis and efferocytosis (phagocytosis of apoptotic cells). Different cytoskeletal elements are assembled at the site of particle internalisation during Fc-receptor mediated phagocytosis and complement-receptor mediated phagocytosis and as a result, the membrane protrusions seen during the former method of phagocytosis are not seen in the latter where the internalised particles appear to sink into the cell with no significant pseudopodia formation. Furthermore, phagocytosis mediated by the Fc-receptor is pro-inflammatory while complement-receptor mediated phagocytosis is non-inflammatory and efferocytosis is anti-inflammatory (May & Machesky, 2001; Aderem, 2003). For the purpose of this study, only Fc-receptor mediated phagocytosis will be discussed in more detail.

Most of the knowledge regarding the signalling pathways involved in phagocytosis has been obtained through studies related to Fc-receptor mediated phagocytosis. Antibodies or immunoglobulins (Igs) are produced by B-cells as part of the humoral immune response and act as opsonins. The binding of Igs to microbes thus makes them more susceptible to phagocytic engulfment. Igs contain a conserved Fc domain as shown in figure 1.11 which is recognised by the Fc- receptors on phagocytic cells. Once the ligand has bound to the Fc-receptor, receptor cross-linking occurs together

with tyrosine phosphorylation of immunoreceptor tyrosine-based activation motifs (ITAMs) thus activating various downstream signalling pathways some of which involve phosphoinositide-3 kinase (PI3K) and phospholipase C (PLC), Rho guanine triphosphate GTPases, protein kinase C (PKC) and several motor proteins (Aderem & Underhill, 1999; May & Machesky, 2001).
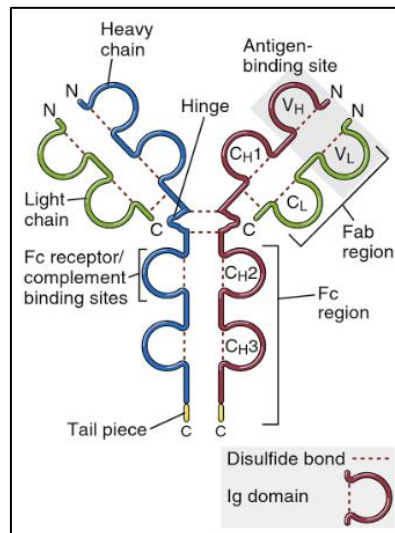
Figure 1.11: Schematic diagram of the basic antibody structure. Immunoglobulins consist of two heavy and two light polypeptide chains held together in a Y-shape by disulphide bonds. Four domains are found on the heavy chains and two domains on the light chains. One variable domain from each of the heavy and light chains form the variable region which mediates antigen specificity while the remaining domains form the constant region which determines the immunoglobulins ability to bind to the complement and Fc-receptors on phagocytic cells (Abbas *et al.*, 2012).

1.4.2.3.4. The role of NF-κB and COX-2 in inflammation

NF-κB refers to a family of transcription factors that are present in all cell types, performing an important role in cellular responses to various signals or stimuli including cytokines, stress, free radicals and bacterial or viral antigens. The transcription factors belonging to the NF-κB family are evolutionarily conserved proteins sharing several structural similarities and are classified as part of the Rel family. These members include p65/RelA, c-Rel and RelB which contain transcriptional activation domains as well as the p50 and p52 proteins which do not contain any transcriptional activation domains and are formed through the controlled proteolytic processing of the large p105 and p100 precursors, respectively. These proteins consist of homo- or heterodimers formed from at least five subunits and are translocated from the cytoplasm to the nucleus of the cell in response to certain stimuli where they are then capable of regulating the transcription of target genes by

binding to the regulatory regions of consensus DNA sequences (Patel & Santani, 2009; Wullaert et al., 2011).

When cells are in their resting state, NF-κB dimers remain sequestered in the cytoplasm in an inactive state due to the association of inhibitory proteins belonging to the inhibitors of NF-κB (IκB) family. Included in this family are IκBα, IκBβ, IκBε, the precursor proteins p100 and p105, as well as B-cell lymphoma 3-encoded protein (Bcl-3), IκBγ and IκBNS which are atypical members (Chen et al., 2002; Wullaert et al., 2011). Originally it was thought that IκB proteins were able to mask the nuclear localisation sequences of the NF-κB dimers thus retaining them in the cytoplasm, however, recent evidence has shown that IκBα and IκBγ are able to travel between the nucleus and the cytoplasm within NF-κB-IκB complexes, consequently displacing NF-κB from the target DNA sequences and transporting it back to the cytoplasm (Patel & Santani, 2009).

Once a stimulatory signal is received, IκB kinase (IKK) will phosphorylate IκB proteins at certain serine residues, ultimately triggering the ubiquitination and consequent proteasomal degradation of the IκB proteins. The C-termini of the p100 and p105 precursors also undergo partial degradation. As a result, NF-κB dimers are able to accumulate in the nucleus where they can then bind to enhancer or promoter regions thus regulating the transcription of target genes. The NF-κB consensus binding site consists of the GGGRNNYYCC sequence where R is a purine, N is any base and Y is a pyrimidine (Chen et al., 2002; Wullaert et al., 2011).

Two catalytic subunits, namely, IKK1/IKKα and IKK2/IKKβ are found on the IKK together with the NF-κB essential modulator (NEMO)/IKKγ regulatory protein. NF-κB activation is tightly regulated through a negative feedback inhibition loop via IκBα expression that is NF-κB dependent as well as the action of deubiquitinating enzymes which negatively control the activation of IKK. NF-κB activation can occur via two major signalling pathways shown in figure 1.12 to be the classical or canonical and the alternative pathways (Wullaert et al., 2011).

The classical pathway of NF-κB activation is primarily induced by pro-inflammatory cytokine receptors as well as pattern recognition receptors. During this pathway, IκBα undergoes degradation and dimers containing p50, p65 and c-Rel are

translocated to the nucleus where they will activate transcription factors of various pro-inflammatory as well as pro-survival genes. Activation of this signalling pathway requires NEMO and is mainly regulated by IKKβ, however, cells which do not contain IKKβ are able to partially compensate by using IKKα to induce IκBα phosphorylation and consequent degradation (Lawrence, 2009; Wullaert *et al.*, 2011).
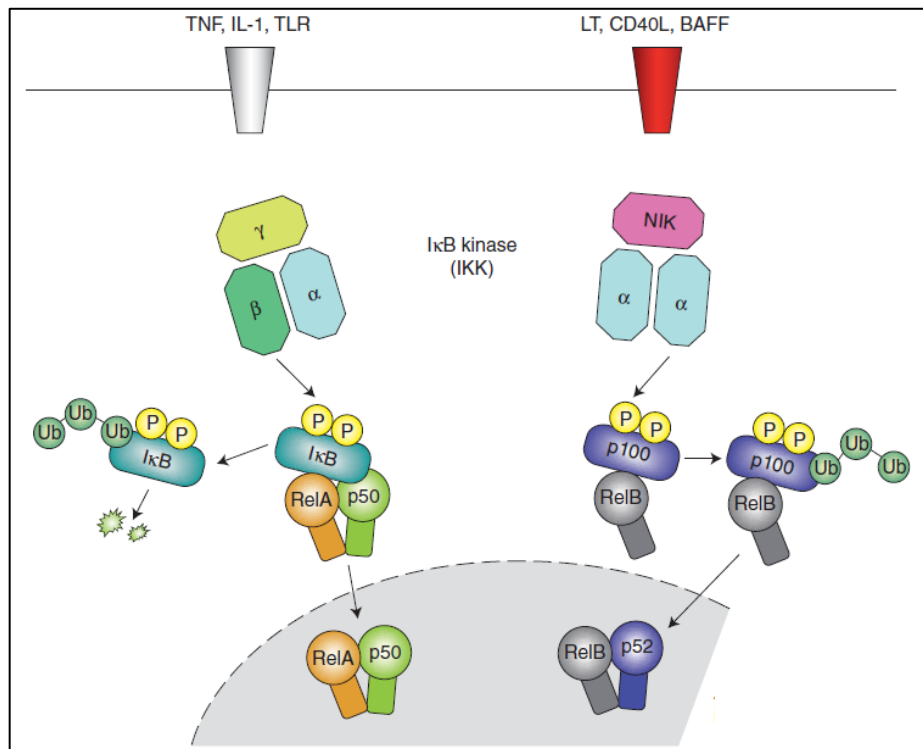
Figure 1.12: Classical and alternative pathways of NF-κB activation. The classical pathway (left) is triggered by Toll-like Receptors (TLRs) and pro-inflammatory cytokines (IL-1 and TNFα) and is mediated by IKKβ. The alternative pathway (right) is stimulated by Lymphotoxin-B receptor (LT), CD40 ligand, B cell activating factor (BAFF) and receptor activator of NF-κB ligand (RANKL not shown) and is mediated by NF-κB inducing kinase (NIK) activated IKKα (Lawrence, 2009).

Activation of the alternative NF-κB pathway is achieved mainly by receptors which regulate lymphoid organogenesis as well as lymphocyte development. This pathway is characterized by the IKKα-dependent phosphorylation of p100 into p52 coupled to the accumulation of the p52/RelB dimers in the nucleus. The upstream kinase responsible for IKKα activation has been identified as NF-κB inducing kinase (NIK) (Lawrence, 2009).

A large quantity of genes playing vital roles in regulating immune and inflammatory responses are induced by the classical pathway of NF-κB activation, some of which include chemokines, cytokines, immunoregulatory proteins as well as adhesion molecules. Furthermore, this pathway mediates the expression of several proteins

with proliferative, anti-apoptotic and antioxidant activities. This signalling pathway thus not only induces the inflammatory response but also shelters cells from the potentially harmful effects of the inflammatory response and has consequently been implicated in the pathogenesis of several inflammatory diseases (Wullaert *et al.*, 2011).

Cyclooxygenase (COX)-1 and 2, also known as prostaglandin-endoperoxide synthase (PGHS) 1 and 2, perform key functions during the inflammatory process by converting arachidonic acid to prostaglandin (PG) H_2 which undergoes subsequent conversion into prostanoids through the action of certain terminal synthases as shown in figure 1.13. Prostaglandins play critical roles in mediating the inflammatory process. COX-1 is classified as a constitutive COX while COX-2 expression is rapidly induced in most mammalian cells by various pro-inflammatory stimuli including bacterial components, cytokines and growth factors (Na *et al.*, 2015).
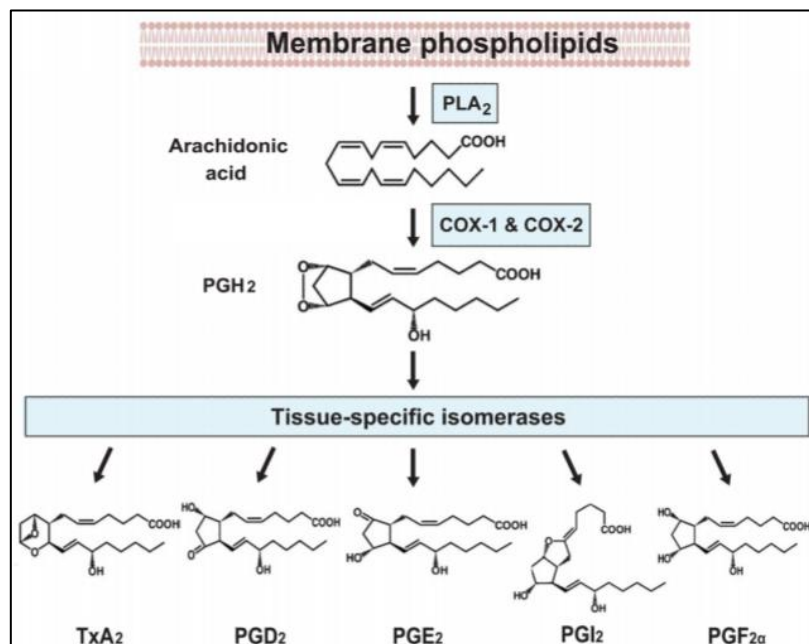
Figure 1.13: The biosynthetic pathway of prostanoids. Arachidonic acid is converted to prostaglandin H_2 (PGH$_2$) by the COX enzymes. PGH$_2$ is, in turn, converted to several prostanoids including thromboxane A_2 (TxA$_2$) and the prostaglandins D_2, E_2, I_2 and $F_{2\alpha}$ (Ricciotti & FitzGerald, 2012).

The role of COX in inflammation remains controversial due to the highly complex signalling cascades involved. While it is still believed that COX-2 synthesises mostly pro-inflammatory prostaglandins, some anti-inflammatory properties have also been revealed. It would thus appear that due to the wide diversity of effects of prostanoids on several cellular processes, the overall effect, whether pro- or anti-inflammatory, is

dependent on the balance of prostanoids as well as the timing of their synthesis within a tissue or throughout a physiological reaction (Poligone & Baldwin, 2001). In addition to its important role in the inflammatory cascade, COX-2 expression has also been linked to the function of monocytes and macrophages during wound healing (Na *et al.*, 2015).

As previously mentioned, the activation of NF-κB is frequently associated with the inflammatory response. NF-κB has been shown to upregulate the expression of COX-2 with two NF-κB binding sites having been found in the human COX-2 promoter and one in the mouse. Furthermore, a rapid increase in COX-2 expression following LPS treatment in macrophages or macrophage cell lines has been observed and has been associated with NF-κB nuclear translocation and one or both of the NF-κB consensus sequences (Ramsay *et al.*, 2003). A complex model of COX-2 expression induced by NF-κB during inflammation is shown in figure 1.14.
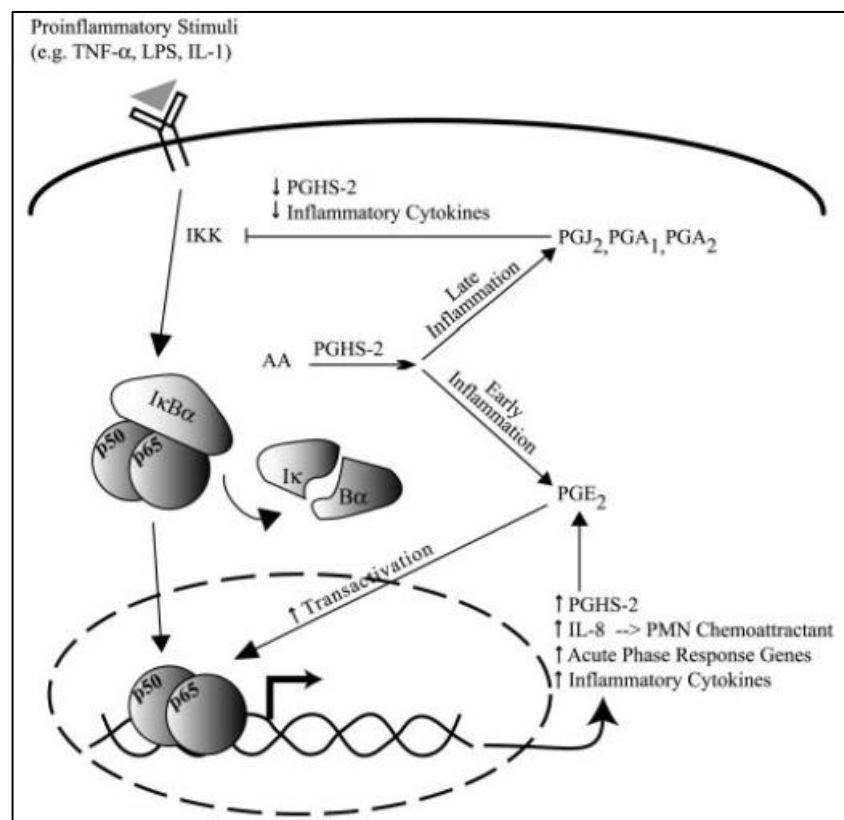
Figure 1.14: Proposed model for NF-κB in inflammation. Once NF-κB undergoes nuclear translocation, it induces the increased expression of COX-2 (PGHS-2). Initially, a positive feedback loop occurs during which the expression of NF-κB-dependent inflammatory genes are enhanced, however, eventually a shift occurs during which cyclopentenone prostaglandins become more abundant resulting in a negative feedback loop that inhibits NF-κB and resultant COX-2 expression (Poligone & Baldwin, 2001).

In the model for the role of NF-κB during inflammation as proposed by Poligone and Baldwin (2001), inflammatory stimuli will initiate the classical pathway of NF-κB activation to stimulate the nuclear translocation of NF-κB and resultant induction of COX-2. As COX-2 expression is increased, there is an increase in the rate of PGE_2 formation during the early inflammatory phase as COX-2 converts arachidonic acid to various prostaglandins of which PGE_2 is most abundant. PGE_2 has been shown to increase the transactivation function of NF-κB which further enhances the expression of the inflammatory genes induced by NF-κB. During the late inflammatory phase, however, a shift in prostaglandin production occurs during which cyclopentenone prostaglandins become the most abundant. The cyclopentenone prostaglandins are thought to partially inhibit the activity of NF-κB through the inhibition of IKK thus sequestering NF-κB in the cytoplasm and consequently down-regulating NF-κB dependent expression of several inflammatory genes as the inflammatory process is resolved.

1.4.3. Proliferation

While the important function of macrophages in regulating and mediating inflammation is obvious, they also perform crucial functions in the resolution of inflammation and the resultant transition to the proliferation and repair stages of the wound healing process (Williamson & Harding, 2004). Following the removal of foreign particles and debris, macrophages will secrete several chemotactic and growth factors required for the stimulation of angiogenesis, the construction of granulation tissue as well as cell migration, proliferation and ECM synthesis. Fibronectin is an example of an important chemotactic factor which recruits fibroblasts to the wound area while examples of growth factors produced by macrophages during wound healing include PDGF, VEGF, FGF, TGF-α, TGF-β and TNF. The process of angiogenesis is induced by the gradient of angiogenesis factors that are secreted by macrophages under the hypoxic conditions that prevail in the wound area (Li *et al.*, 2007).

In addition to cytokines and growth factors, macrophages also synthesise numerous extracellular molecules that are able to combine with the products released by degranulated platelets in order to produce a temporary scaffold rich in proteoglycans, fibronectins and glycosaminoglycans which are essential for determining the success

of the re-epithelialisation, migration and proliferation processes (Williamson & Harding, 2004).

1.4.3.1.   Re-epithelialisation

In order to re-establish an intact epidermis, various processes such as keratinocyte migration and proliferation, the formation of a stratified epidermis following neoepithelium differentiation as well as basement membrane zone reconstitution must ensue. The process of keratinocyte migration from the wound edge is initiated within the first 24 hours following an injury and it involves multiple events including structural modifications which prevent these cells from proliferating while they are migrating. Integrin receptors located on the surface of keratinocytes regulate this process as they interact with the fibronectin-rich provisional matrix as well as the collagen fibres that are produced within the wound bed. Migration is thus enabled through the association and disassociation of the interactions between the keratinocytes and the matrix fibres together with the activities of MMPs that ultimately determine the direction of migration (Falanga, 2005; Li *et al.*, 2007).

As the re-epithelialisation process continues, the keratinocytes present at the migrating front tongue will revert back to a structural form that enables proliferation, thus ensuring that there is a sufficient supply of cells to close the entire wound. Once keratinocytes from opposite edges of the wound come into contact with one another, contact inhibition causes the cessation of the migration process and the keratinocytes will re-establish their interactions with the under-lying stratum in an attempt to repair the basement membrane (Lerman *et al.*, 2003; Li *et al.*, 2007).

1.4.3.2.   Fibroplasia

Fibroblasts present at the wound edge start proliferating and begin the process of migration into the provisional matrix that has been formed in the wound bed by day four of the wound healing process. Here they produce collagen, elastin and proteoglycans necessary to re-establish an intact ECM after which they undergo gradual phenotypic changes where their primary function switches to protein synthesis (Enoch & Leaper, 2005; Li *et al.*, 2007).

1.4.3.3. Angiogenesis

In response to tissue injury, quiescent vessels surrounding the wound area will be stimulated to produce new blood vessels which branch from pre-existing vessels in close proximity to the wound. This response is triggered by a multitude of different factors produced in the wound environment, some of which include cytokine secretion by macrophages, tissue hypoxia, elevated lactic acid levels and biogenic amines. The angiogenic response is categorised by several different processes with the ultimate goal being to provide the tissue with enough oxygen and nutrients to support the tissue remodelling and repair processes. Once the provisional matrix has been completed, the blood vessels will once again regress due to changes in the growth factors within the wound environment (Williamson & Harding, 2004; Li *et al.*, 2007).

1.4.3.4. Wound contraction

Wound contraction is initiated fairly early on in the wound healing process; however, it only peaks approximately two weeks after the initial injury with the degree of contraction depending on the depth of the wound. Myofibroblasts are unique in their ability to lengthen and retract and it is for this reason that they are the primary mediators of the wound contraction process. As they align themselves along the lines of contraction within the wound, they extend pseudopodia which bind to collagen fibres and subsequently retract to draw the collagen fibres closer to them. As a result, the wound decreases in size incrementally until the wound edges are reunited. A unified response is essential for wound contraction to be successful and involves both cell-cell and cell-matrix interactions as it proceeds in the direction of skin tension lines (Li *et al.*, 2007; Tortora & Derrickson, 2012).

1.4.4. Tissue remodelling

ECM synthesis and remodelling is initiated simultaneously with granulation tissue formation and may persist for weeks to years, depending on the severity of the injury, and is characterized by the action of MMPs which regulate the synthesis and degradation of collagen. MMPs are produced by neutrophils, fibroblasts and macrophages at the wound area and can be classified into three classes based on their function. Interstitial collagenases are responsible for the cleavage of fibrillar collagen while gelatinases break down amorphous collagen as well as fibrin and

stromelysins catabolise various components of the ECM. The activity of MMPs is very tightly regulated through the action of various cytokines, growth factors and phagocytic stimuli in an effort to prevent excess collagen degradation and consequent impairment of the wound healing process (Enoch & Leaper, 2005; Gill & Parks, 2008).

There are at least sixteen different forms of collagen that are found in the human body with type I collagen being the most abundant. During the early stages of granulation tissue formation, however, type III collagen synthesis in fibroblasts becomes far more abundant than type I collagen. Maximal secretion of type III collagen occurs within the first five to seven days after sustaining a cutaneous injury and once the wound begins to close, type III collagen is once again degraded and replaced with type I collagen. While very little is known about the role of type III collagen in wound healing, this conversion is thought to be due to stimuli produced in response to the biomechanical strain and tension that is exerted over the wound area (Li *et al.*, 2007).

During the tissue remodelling process several factors result in a decline in MMP activity. Some of these include an increase in the production of TIMPs, a decline in macrophage and fibroblast activity, the termination of angiogenesis, a reduction in both blood flow and metabolic activity as well as the merging of the wound edges through the contraction of the underlying connective tissue. The granulation tissue scaffold consequently progresses towards the formation of an avascular scar which consists of dense collagen networks, inactive fibroblasts and several ECM components. An increase in the diameter of the collagen bundles occurs through the action of fibronectin and hyaluronan, resulting in an increase in the tensile strength of the wound area; however, the same degree of tensile strength that was present before the injury was sustained cannot be achieved (Enoch & Leaper, 2005; de Mendonça & Coutinho-Netto, 2009).

A summary of the roles of the cytokines and complements involved in the wound healing process is provided in table 1.1.

Table 1.1: <u>A summary of the cytokines and complements involved during each phase of the wound healing process (Sinno & Prakash, 2013).</u>

Time	Phase	Compound / Growth factor	Source	Target/effect	Vascular response	Cellular response	Event
Injury	Inflammatory	Clotting cascade	Tissue injury	Platelet, hemostatic plug, vasoconstriction	Vasoconstriction	Platelet	Clot formation
		Thromboxane A2	Tissue injury	Vasoconstriction			
		Prostaglandin F2α	Tissue injury	Vasoconstriction			
		Complement C3	Spontaneous, foreign tissue	Vasoactive and spasmogenic, activation of complement cascade, mast cell degranulation			
3 days		Complement C5	C3, platelet	Mast cell degranulation, chemotaxis of monocytes and neutrophil, vasoactive and spasmogenic, bacterial lysis		Neutrophil	
		EGF	Platelet	Reepithelialization, pleiotropic cell proliferation			Growth factor elaboration
	Proliferative	TGF-β1 and β2	Platelet, macrophage, and keratinocyte	Chemotaxis of macrophages and fibroblasts, matrix formation and remodeling		Macrophage	
		PDGF	Platelet, macrophage, and epidermal cell	Platelet, macrophages, epidermal cells, fibroblast			
		IL-i and IL-6	Neutrophil, macrophage	Inflammation, reepithelialization			
		TNF	Neutrophil, macrophage	Inflammation, reepithelialization			
7 days		VEGF	Platelet, neutrophil, macrophage, epidermal cells, and fibroblast	Angiogenesis, granulation tissue formation, increased vascular permeability			
		FGF	Macrophage, endothelial cell	Granulation tissue formation, angiogenesis, fibroblast		Fibroblast	Collagen deposition
		IGF	Epidermal cell, fibroblast	Reepithelialization, granulation tissue formation			
Weeks	Remodeling						Collagen cross-linking

1.5. DIABETIC WOUND HEALING

The normal wound healing process consists of multiple levels of complex regulation involving several cellular activities, the release of numerous cytokines, activation of various growth factors, and connective tissue formation. While acute wounds undergo a linear and coordinated progression through the different stages of wound healing, various regions of diabetic wounds appear to be in different phases and thus the synchronisation of the overlapping phases responsible for rapid healing is lost (Falanga, 2005; Li *et al.*, 2007). While the exact mechanisms responsible for the disruption of the normal wound healing process in the diabetic state have not yet been conclusively established, several contributing factors have been identified as summarised below and in figure 1.15 (McCulloch & Kloth, 2010).
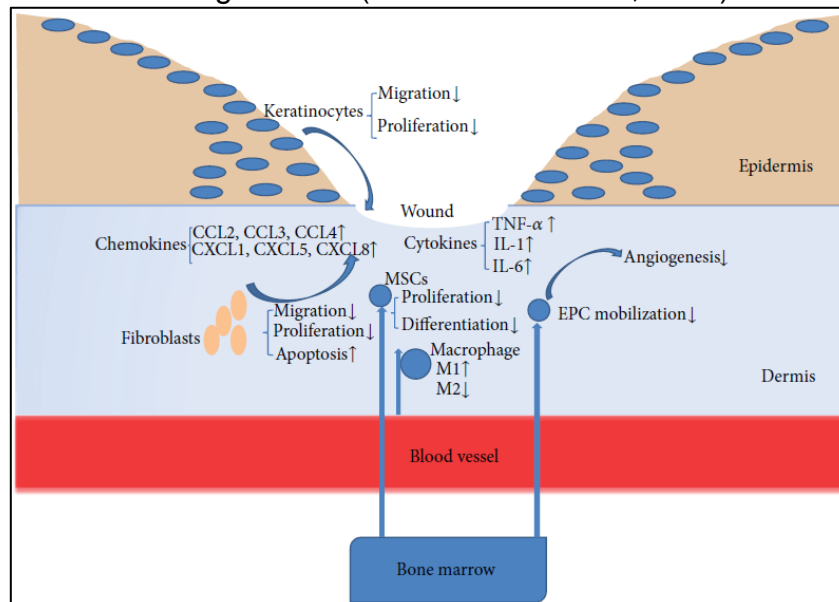
Figure 1.15: A diagrammatic illustration of some of the mechanisms responsible for impaired wound healing in diabetes. Levels of inflammatory cytokines and chemokines are increased and cellular processes such as the migration and proliferation of keratinocytes and fibroblasts, macrophage polarization as well as mesenchymal stem cell (MSCs) and endothelial progenitor cell (EPC) recruitment become impaired (Xu *et al.*, 2013).

1.5.1. Hypoxia

Oxygen is vital for most wound healing processes and the oxygenation state of a wound is thus crucial in determining its healing outcome. Prolonged hypoxia is frequently observed in chronic wounds and may be a consequence of inadequate perfusion as well as unsatisfactory angiogenesis, both of which are associated with chronic hyperglycaemia. The ensuing hypoxia is incompatible with tissue repair as it amplifies the early inflammatory phase, consequently promoting the production of

oxygen radicals at the wound area and ultimately delaying the healing process (Sen, 2009; Guo & Dipietro, 2010).

1.5.2. Infections

Diabetic wounds are frequently compromised by various microorganisms due to factors such as tissue hypoxia and persistent hyperglycaemia. In an effort to remove the pathogens, the inflammatory response is prolonged and the wound healing process is delayed. In addition to the abnormal inflammatory profile of diabetic wounds, unwarranted MMP activation leads to the impairment of cellular migration processes while simultaneously causing the degradation of essential ECM components and growth factors (Falanga, 2005; Guo & Dipietro, 2010). Furthermore, a reduced occurrence of MMP inhibitors results in an imbalance between the breakdown and synthesis of the affected tissues. The rate of tissue degradation thus exceeds that of tissue synthesis which prevents the wound from closing and may even cause wound enlargement (Menke *et al.*, 2007).

1.5.3. AGEs

Chronic hyperglycaemia results in the non-enzymatic glycation of various macromolecules, such as proteins, via the Maillard reaction as shown in figure 1.16. During this process, spontaneous reactions occur between free amino groups of proteins and the carbonyl groups of reducing sugars in order to form a reversible Schiff base. Further rearrangements lead to the formation of stable ketoamines known as Amadori products which are ultimately converted to irreversible advanced glycation end products (AGEs) (Gould *et al.*, 2011; Singh *et al.*, 2014). As glucose is the slowest reacting intracellular sugar it was originally though that AGEs only accumulated in long-lived extracellular proteins, however, several glycolytic intermediates including glyceraldehyde-3-phosphate, dihydroxyacetone-phosphate as well as the dicarbonyl compounds glyoxal, methylglyoxal and 3-deoxyglucosone have been shown to contribute to intracellular glycation (Alexandrescu *et al.*, 2016).

The glycation process is often incorrectly referred to as non-enzymatic glycosylation. Protein glycosylation refers to the post-translational modification of proteins that is essential for normal protein function. This process is mediated by several enzymes and is defined by the addition of a carbohydrate molecule to a predetermined region of the protein. While protein glycation and glycosylation thus both involve reactions

between proteins and carbohydrates, different reaction mechanisms have been established with very different intermediates and end products. Glycosylation is thus a highly controlled process whereas glycation is random and uncontrolled, impairing both protein function and stability. Furthermore, different amino acids are involved during each process where glycosylation requires asparagine for N-glycosylation and serine or threonine for O-glycosylation, glycation generally involves arginine and lysine residues (Xue *et al.*, 2011; Thermo Fisher Scientific, 2017).
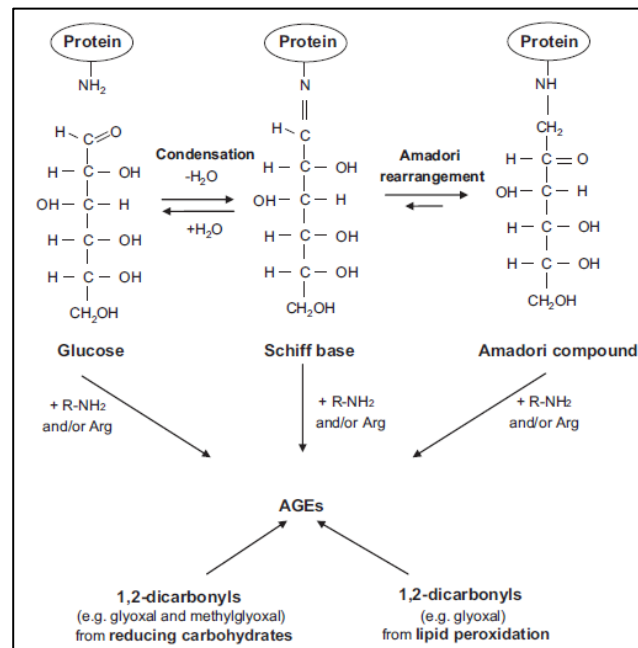
Figure 1.16: Reactions leading to the formation of AGEs. The carbonyl groups necessary for AGE formation are usually generated through carbohydrate metabolism, however, they may also be formed during either lipid or protein degradation (Stirban *et al.*, 2014).

AGEs can contribute to the development of impaired wound healing in diabetic patients by interfering with the normal structure of several proteins through the formation of cross-links, thus altering normal protein function. AGE-modified proteins may also, however, cause cellular dysfunction by binding to cell-surface receptors such as receptors for AGEs (RAGE) which creates a cascade of inappropriate cellular signals that further impair the wound healing process (McCulloch & Kloth, 2010). While several other receptors for AGEs have been identified, RAGE remains the best characterized of these receptors and has been linked to several of the complications observed during diabetic wound healing (Oliveira *et al.*, 2013).

RAGE has been characterized as a type 1 transmembrane protein forming part of the cell surface immunoglobulin superfamily. It consists of an extracellular domain

which binds to extracellular ligand, a hydrophobic transmembrane section as well as a highly charged intracellular cytoplasmic domain which is responsible for inducing intracellular signals. In diabetes, RAGE is overexpressed where its activation by AGEs and consequent up-regulation has been shown to induce inflammation and oxidative stress. This induces further AGE formation and accumulation, creating a positive feedback loop. RAGE has been identified in several cell types including macrophages, fibroblasts, keratinocytes and dendritic cells (Oliveira *et al.*, 2013; Alexandrescu *et al.*, 2016).

1.5.4. Oxidative stress

ROS have been shown to play an important role in both the removal of pathogens from the wound area as well as the regulation and stimulation of the normal wound healing process by acting as a mediator of intracellular signalling. Oxidative stress is characteristic of diabetes as the hyperglycaemic environment increases mitochondrial activity, favouring increased ROS production. When this happens, the anti-oxidative capability of the cell is surpassed, leading to further tissue damage, protein modification and subsequent impairment of the wound healing process (Schafer & Werner, 2008; Kolluru *et al.*, 2012).

1.5.5. Cellular dysfunction

A summary of the effects of diabetes on cell function during wound healing is provided in table 1.2. The process of wound healing is essentially regulated by fibroblasts, keratinocytes and macrophages. Several studies have revealed that both fibroblasts and keratinocytes demonstrate impaired proliferation, migration and collagen producing abilities in the diabetic state (McCulloch & Kloth, 2010; Xu *et al.*, 2013). It has also been shown that the efferocytic activity of macrophages in diabetic wounds becomes impaired. This results in an increased apoptotic cell burden at the wound area, ultimately prolonging and amplifying the inflammatory phase.

Also contributing to impaired wound healing is the fact that diabetic macrophages produce larger amounts of pro-inflammatory cytokines than their non-diabetic counterparts and diabetic wounds are thus characterized by a larger infiltration of inflammatory M1 macrophages than the M2 macrophages required for the generation of new tissue. Furthermore, the stage of M1 macrophage polarization which is usually relatively short-lived in the normal wound healing process is

extended in the diabetic state and consequently the wound healing process is hindered (Khanna *et al.*, 2010; Xu *et al.*, 2013).

Table 1.2: <u>Summary of the cells and their associated functions that are impaired in diabetic wound healing (McCulloch & Kloth, 2010).</u>

Phase	Cells involved	Impairment with diabetes	Outcome with diabetes
Hemostasis	Platelets	- Delayed fibrin plug formation - Delay/decrease in release of growth factors and cytokines - Impairment of microvascular hemodynamics - Abnormal vascular autoregulatory capacity	- Platelet irregularity - Delayed fibrin plug formation leaving wound open for longer - Decreased local growth factor and cytokine production - Delayed recruitment of inflammatory cells
Inflammation	Neutrophils and macrophages	- Decreased release of growth factors and cytokines - Impaired migration, adherence and phagocytosis - Thickened arterial basement membrane	- Delayed inflammatory response - Poor endogenous debridement - Chronic inflammatory state - Increased bioburden and risk of infection
Proliferation	Fibroblasts, myofibroblasts and keratinocytes	- Poor cellular response to growth factors and chemokines - Impaired fibroblast and keratinocyte proliferation, migration and function - Excessive activation of proteases - Impaired contraction of myofibroblasts	- Reduced angiogenesis - Impaired granulation tissue formation - Diminished wound contraction - Friable and poorly functioning granulation tissue - Wound stuck in cycle of chronic inflammation
Tissue remodelling	Fibroblasts and keratinocytes	- Ineffective matrix turnover	- Collagen matrix cross-linked - Reduced ultimate strength of repair tissue

1.6. MACROFUNGI AND DIABETIC WOUND HEALING

Approximately 1.5 million species of fungi are thought to exist globally, 140 000 of which can be classified as mushrooms. Of these, it is estimated that only 200 species have been traditionally gathered as food or medicine. It is well known that fungi have been poorly collected and studied and as a result, only 10% of

mushroom-forming species have been identified thus making them a valuable unexplored resource of potentially useful substances (Crous *et al.*, 2006; Erjavec *et al.*, 2012).

Mushrooms are defined as macrofungi whose fruiting bodies are visible to the naked eye and may grow above (epigeous) or below (hypogeous) the ground. Mushrooms are classified as functional foods and have thus become attractive as a source of medicine that demonstrates strong physiological benefits. There are several advantages of using mushrooms as a source of bioactive compounds over plants due to the fact that their fruiting bodies are produced over greatly reduced time periods, their mycelia and fruiting bodies can be produced fairly rapidly in liquid culture and finally, the medium in which they are cultured can be manipulated in order to produce the desired concentrations of the active compounds (Ferreira *et al.*, 2009).

Currently, several synthetic drugs are used during the treatment of diabetes; however, many of these drugs are associated with unwanted side-effects while simultaneously failing to significantly alter the progression of complications associated with diabetes. As a result, natural bioactive compounds isolated from medicinal plants as alternative treatment strategies have gained increasing popularity amongst the scientific community. The potential of medicinal mushrooms in treating several diseases have been exploited by traditional folk medicines for centuries. In addition to having a favourable ratio of macronutrients, it has also been shown that mushrooms contain several essential micronutrients and phenolic compounds which provide a high source of anti-oxidants. Today, many of the health-promoting benefits of mushrooms are attributed to the bioactive metabolites such as polysaccharides, peptides, enzymes, terpenoids, as well as various other small molecules (De Silva *et al.*, 2012).

As previously summarised, diabetic wounds frequently enter a state of pathological inflammation and are characterized by the increased occurrence of infection as well as the production of excess ROS and AGEs (McCulloch & Kloth, 2010). A literature search revealed very limited information regarding the wound healing properties of mushrooms, however, any mushroom species that displays strong anti-inflammatory, anti-oxidative or general antidiabetic properties could be useful in promoting

functional wound healing. The five mushrooms selected for this study are shown in figure 1.17 and were chosen based on their reported bioactivities pertaining to wound healing as summarised below.
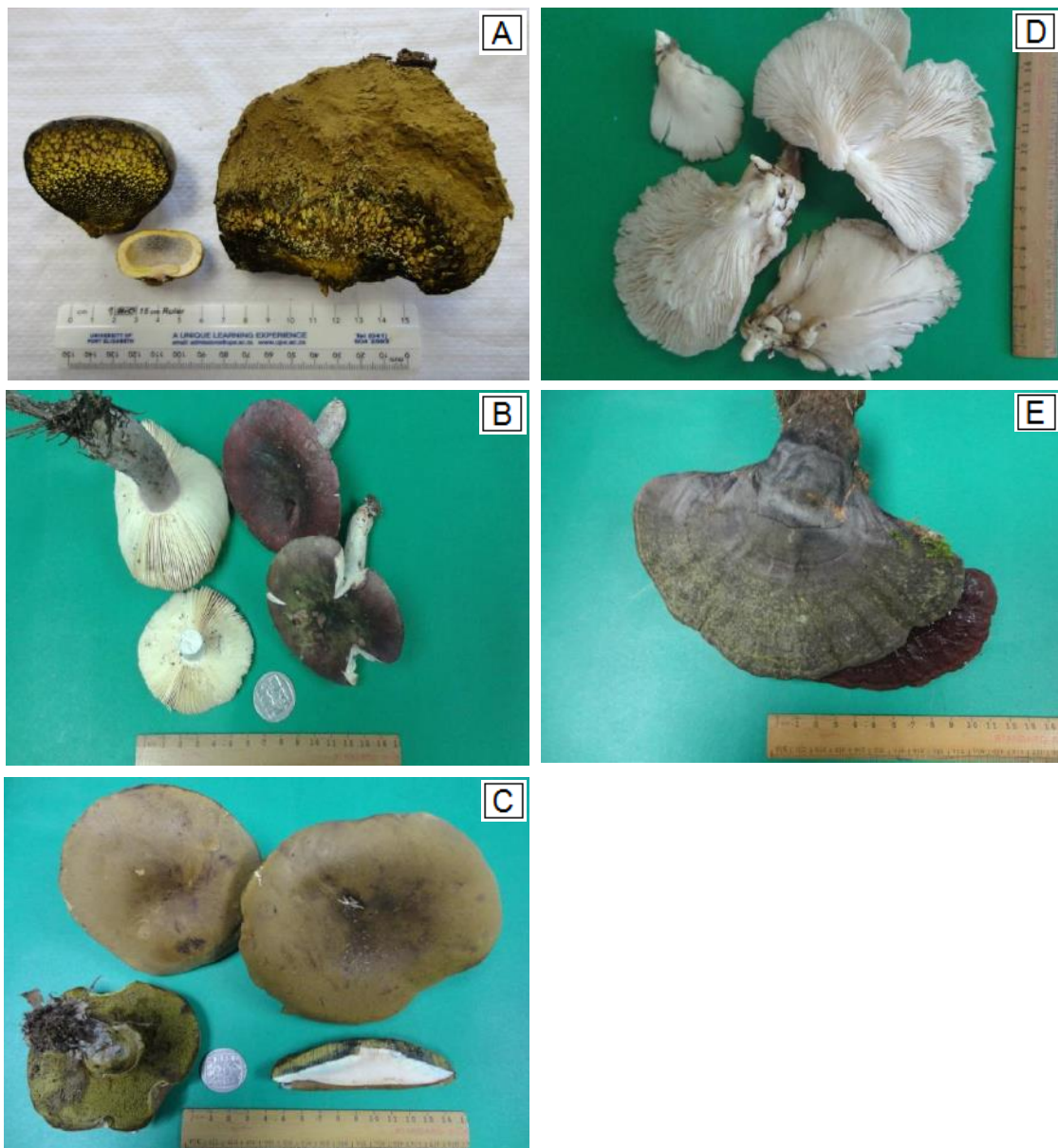
Figure 1.17: <u>Photographs of the mushroom species collected for this study. (A) *P. tinctorius*, (B) *R. capensis*, (C) *B. badius*, (D) *P. ostreatus* and (E) *G. lucidum* (Photo credit: Gerhardt Boukes).</u>

1.5.1. *Boletus badius* (Bay Bolete)

B. badius, also known as *Xerocomus badius*, is classified as part of the *Boletaceae* family. It is found growing under conifers in pine needles or under deciduous trees and is identified by its shiny brown cap which starts out convex and then flattens as well as its white to lemon-yellow flesh. The pores on the underside of the cap turn blue or green when touched (*The Great Encyclopedia of Mushrooms*, 1998:26;

Gryzenhout, 2010). While knowledge regarding the composition and properties of this mushroom species is lacking, it has been shown to contain several anti-oxidant substances including polyphenols, flavonoids, vitamins C and E, β-carotene, tocopherols and lycopene (Jaworska *et al.*, 2015) as well as several micronutrients such as zinc, iron and copper that are essential for wound healing. Zinc is a co-enzyme for several enzymatic reactions and promotes cell proliferation while copper and iron are involved in collagen synthesis and these three minerals could thus play crucial roles in promoting wound healing (Guo & Dipietro, 2010; Reczynski *et al.*, 2013).

1.5.2. *Ganoderma lucidum* (Reishi)

G. lucidum is classified as part of the *Ganodermataceae* family and is widely sought-after due to its wide range of medicinal properties. It can be found growing on the rotting stumps of several broad-leaved trees, on tree trunks or on the ground emerging from roots. It is recognised by its circular to bracket, often kidney-shaped fruiting body which grows singly or in groups where it can fuse with others or grow in tiers. It has a cork-like texture which turns woody as it ages and is covered with a thin, shiny, varnished crust that ranges in colour from yellow to red to chestnut, often with a white margin (*The Great Encyclopedia of Mushrooms*, 1998:215; Gryzenhout, 2010). The principal bioactive compounds that have been isolated from this mushroom species are considered to be mainly polysaccharides, triterpenes, sterols and some proteins such as lectin (Saltarelli *et al.*, 2015). Some of the biological activities that have been identified for *G. lucidum* include anti-oxidative and free radical scavenging, anti-inflammatory and antidiabetic effects. Studies have also shown that the polysaccharides isolated from *G. lucidum* were able to reduce the levels of AGEs, promote the activities of anti-oxidant enzymes and accelerate wound closure as well as wound angiogenesis in streptozotocin-induced diabetic mice (De Silva *et al.*, 2012; Cheng *et al.*, 2013).

1.5.3. *Pisolithus tinctorius* (Puffball mushroom)

P. tinctorius belongs to the *Sclerodermataceae* family of fungi with the most frequent and traditional uses reported for the puffball mushroom as a wound dressing as well as for the treatment of burns and itches (Burk, 1983; Gill & Watling, 1986). It is identified by its large fruiting body which occurs as an irregularly lobed ball, tapering

into a root-like base on the ground near eucalyptus or black wattle trees. The outer skin is shiny, ranging from ocre to bright yellow which darkens to a rust colour with mottled black markings. The flesh is divided into different compartments in which the spores develop as can be seen from figure 1.17 (Branch, 2001). While information regarding the properties and bioactive molecules of *P. tinctorius* are severely lacking, the traditional uses of puffballs provides sufficient evidence that this mushroom species might promote wound healing (Burk, 1983; Gill & Watling, 1986).

1.5.4. *Pleorotus ostreatus* (Oyster mushroom)

P. ostreatus has been identified as a member of the *Pleurotaceae* family of gilled mushrooms (Opletal, 1993). It is typically found growing on the dead wood of broad-leaved trees, tree stumps and logs in large, compact tufts. It is recognised by its large cap which has a definitive semi-circular to elongate fan-shape, the colour of which can vary from black to white, violet grey or yellowish (*The Great Encyclopedia of Mushrooms*, 1998:68; Gryzenhout, 2010). The presence of numerous nutritional components and active ingredients in *P. ostreatus* has led to reported antidiabetic, antibacterial, anti-inflammatory and anti-oxidant activities. Most of these activities are attributed to the presence of β-glucans and lectin. Combining these activities with the high content of several essential micronutrients presents strong evidence that this mushroom species could overcome some of the negative influences of diabetes on wound healing (Patel *et al.*, 2012).

1.5.5. *Russula capensis* (Cape Russula)

R. capensis belongs to the *Russulaceae* family, consisting of a crumbly flesh and an often bright fruiting body, ranging from pink-purple to a deep purple-red, with white gills that extend to the straight, cylindrical stem (*The Great Encyclopedia of Mushrooms*, 1998:46; Laessoe, 2013). As with most other mushroom species, the *Russula* species contain β-glucans and lectins and thus display anti-oxidative properties. Traditional uses of *Russula* species as a wound healing agent have also been reported (Jaengklang *et al.*, 2015).

CHAPTER 2: RESEARCH AIMS AND OVERVIEW OF CHAPTERS

2.1.   PROBLEM IDENTIFICATION

Impaired wound healing has been recognised as a complication of diabetes for almost three decades and is associated with high rates of amputation and mortality. There is, however, a highly intricate and multi-faceted pathophysiological relationship between diabetes and chronic wound healing which is not yet fully understood (McCulloch & Kloth, 2010). Current treatment strategies for chronic wounds are mainly based on the optimisation of healing factors that can be regulated such as the removal of infection and the provision of mechanical protection as well as nutritional support. To date, very few targeted approaches have been developed with the topical application of growth factors demonstrating very limited clinical efficacy. Due to the dearth of knowledge with regards to the molecular mechanisms behind the pathology of diabetes as well as the absence of suitable chronic wound models, current treatment regimens are limited and non-specific thus emphasising the need to identify new therapeutic targets and develop more efficient treatment approaches (McLennan *et al.*, 2006; Landén *et al.*, 2016).

In an attempt to discover a treatment modality that will address the pain, poor quality of life and excessive healthcare costs that diabetic patients suffering from impaired wound healing are burdened with, natural substances from plants and mushrooms are under current investigation. Several mushroom species have demonstrated various anti-oxidant, anti-inflammatory and blood glucose regulating activities which suggests that mushrooms could prove to be very useful in the search for safe and efficacious wound healing agents that could potentially serve as alternative treatment strategies for chronic diabetic wounds (Brem & Tomic-Canic, 2007; Cheng *et al.*, 2013).

2.2.   AIMS AND OBJECTIVES

The aim of this study was to characterize a low-cost, more convenient and more comprehensive *in vitro* diabetic wound healing model using glycated gelatin in order to explore the potential of five wild mushroom species commonly found in South Africa to promote wound healing by restoring the correct functioning back to fibroblasts and macrophages.

In order to achieve this aim, the following objectives were met:

- To derive a suitable method for glycating the gelatin and confirming the presence of AGEs.
- To assess the cytological effects of the glycated gelatin model on fibroblast and macrophage functions.
- To explore the fundamental biochemical mechanisms through which AGEs impair wound healing in diabetes using high content screening.
- To establish a more comprehensive wound healing screening platform which incorporates other potential therapeutic benefits such as antioxidant capacity, collagen turnover, glycation inhibition as well as cytotoxicity amongst others.
- To screen and prioritise five wild mushroom species for potential wound healing properties.
- To provide enough scientific evidence to support further studies related to the use of macrofungi as a potential diabetic wound healing therapy.

2.3. OVERVIEW OF CHAPTERS

Chapter 3 provides a brief overview of the methodology used throughout this study including the principles and protocols of all techniques used, cell culture conditions and background information related to some of the more complex methods.

Chapter 4 presents the results that were obtained from this study. Section 4.1 focuses on the characterization of the glycated gelatin model as a suitable diabetic wound healing model by exploring its cytotoxicity and cytological effects on fibroblasts and macrophages. These include alterations in the phagocytic capability, the activity of various inflammatory markers and the phenotype (M1/M2) of macrophages as well as changes in fibroblast proliferation and migration.

Section 4.2 presents the screening results of the selected mushroom species in terms of their cytotoxicity, anti-oxidant capacity and any other characteristics which could highlight their potential therapeutic benefits in wound healing such as glycation and collagenase inhibitory activities.

As diabetic wounds frequently enter a state of pathological inflammation, section 4.3 deals with the inflammatory phase of wound healing and provides more detailed

information regarding the cellular dysfunction observed in macrophages. The ability of each of the selected mushroom species to restore some or all of the correct macrophage functioning is assessed here in detail.

Section 4.4 focuses on the dysfunction of fibroblasts in diabetic wound healing. As fibroblasts play a crucial role during the last two phases of wound healing (proliferation and tissue remodelling), correct fibroblast functioning is essential to ensure the completion of the wound healing process. The ability of the selected mushroom species to promote the correct fibroblast function in the diabetic state is investigated here in more detail.

In chapter 5, an in-depth discussion of all the results obtained throughout this experiment is provided which summarises the most significant findings of this study and suggests some considerations for its improvement. Suggestions regarding future studies are also addressed.

A comprehensive list of materials can be found in Appendix A and procedures for reagent preparation are listed in Appendix B.

3.1.   CELL CULTURE CONDITIONS AND MAINTENANCE

Human Dermal Fibroblasts (MRHF) and RAW 264.7 macrophage-like cells were obtained from the Cellonex and the American Type Culture Collection, respectively. The MRHF cell line is an adherent cell line that was selected because of the important role that fibroblasts play in wound healing (Enoch & Leaper, 2005). The RAW 264.7 cell line is an immortal cell line derived from Balb/c mice and was selected for its relevance in wound healing assays as well as its maintenance of macrophage properties including NO production and phagocytosis (Venter *et al.*, 2015).

Both cell lines were maintained in 10 cm cell culture treated polystyrene petri dishes in complete Dulbecco's Modified Eagle Medium (DMEM) supplemented with 10% foetal bovine serum (FBS) and 1% (v/v) penicillin/ streptomycin. Cells were incubated at 37 °C in a humidified incubator with 5% $CO_{2\,(g)}$ and monitored daily for contamination using an Axiovert 40C inverted microscope (Carl Zeiss, Germany). Cells were sub-cultured using the technique described by Freshney (1986) when they reached approximately 80% confluence and the culture medium was replaced every fourth day to ensure optimal growth conditions.

Cell viability and numbers were routinely monitored using a manual haemocytometer slide and the trypan blue exclusion assay. Trypan blue is an acidic dye with a molecular weight of approximately 873 g/mol. It is a large, hydrophilic, tetra-sulphonated molecule and contains two azo chromophores as shown in figure 3.1. Due to its negative charge, trypan blue is unable to enter the cytoplasm of viable cells whose membranes are intact. Non-viable cells, however, have compromised cell membranes and trypan blue is thus able to enter these cells where it can bind to intracellular proteins within the cytoplasm of the cell effectively staining the cytoplasm blue. The blue colour is readily observed under a brightfield microscope thus allowing the easy and rapid differentiation between live (clear cytoplasm) and

non-viable (blue cytoplasm) cells (Melzer *et al.*, 2016; Santa Cruz Biotechnology, 2016).
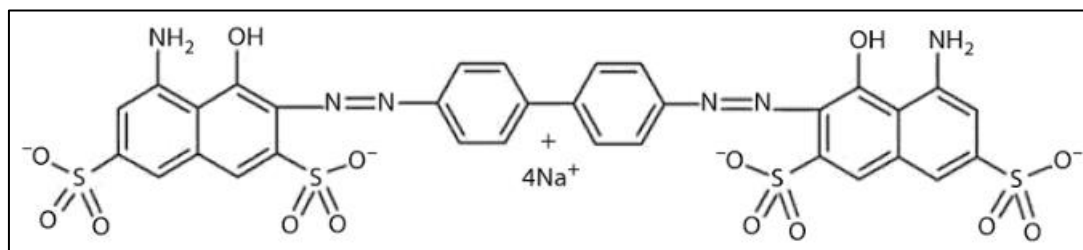
Figure 3.1: <u>Chemical structure of trypan blue. Trypan blue is frequently used to assess cell viability as this cell membrane impermeable dye is only able to stain dead cells (Dumitriu & Popa, 2013).</u>

All cells were seeded during their log phase of growth to ensure accurate and reproducible results. Cells were left overnight to attach to the appropriate culture plates prior to exposure to the relevant treatments. Seeding densities and incubation periods are specified under each protocol.

3.2.   GLYCATED GELATIN MODEL

3.2.1   Preparation of gelatin

Gelatin was dissolved in distilled water at a concentration of 20 % (w/v) with 1 M glucose in a 37 °C water bath for 30 minutes. Once dissolved, the mixture was autoclaved for 60 minutes and stored in working aliquots at 4 °C until required. Unglycated gelatin was prepared in the same way in the absence of glucose as a reference standard. Prior to use, the gelatin was heated in a 37 °C water bath for 30 minutes and added to the culture medium at the required concentration.

3.2.2   AGE autofluorescence

The intrinsic fluorescence of AGEs such as pentosidine allowed for the easy measurement of AGE formation with the use of a Fluoroskan Ascent FL fluorometer (ThermoLabsystems, Finland). The glycated and unglycated gelatin as well as the glucose stocks were thus diluted to the specified concentrations in distilled water after autoclaving (see section 3.2.1) and the fluorescence was measured using the AGE excitation wavelength of 370 nm and an emission wavelength of 440 nm (Nomoto *et al.*, 2013).

3.3.   SAMPLE COLLECTION AND EXTRACT PREPARATION

Wild mushroom samples were collected from the Eastern and Western Cape provinces of South Africa by Dr. Gerhardt Boukes, a former post-doctoral researcher

at NMMU, and identified by a mycologist, Dr. Marieka Gryzenhout, from the University of the Free State. Once collected, samples were dried at 30 °C in a drying oven for 48 to 72 hours. The dried material was cleaned with paper towelling before being briefly submersed in liquid nitrogen and crushed into a fine powder using a mortar and pestle.

Both ethanol and cold water extracts were prepared for each sample. Ethanol extracts were prepared by adding 80% ethanol (diluted with deionised distilled water) to the dried material using a 1:15 (w/v) ratio while the water extract was prepared by adding deionised distilled water at room temperature using a 1:10 (w/v) ratio. Samples were extracted for 24 hours at room temperature with continuous stirring after which the extracts were centrifuged for 5 minutes at 3000 rpm. The pellets were discarded and the supernatants were collected and filtered twice through Whatman™ filter paper (no. 1) using a vacuum. The water extracts were frozen immediately at -80 °C while the ethanol first had to be evaporated from the ethanol extracts using a rotary vacuum prior to freezing at -80 °C. Once frozen, samples were freeze-dried and stored in a desiccator at 4 °C protected from light prior to use.

Ethanolic extracts were solubilised in dimethyl sulfoxide (DMSO) at a concentration of 50 mg/ml while water extracts were solubilised in distilled water at 50 mg/ml and then filter sterilised using a 0.2 µm Acrodisc® syringe filter. Samples were refrigerated at 4 °C and prepared fresh every week.

3.4. SCREENING ASSAYS FOR POTENTIAL WOUND HEALING PROPERTIES

3.4.1. Cytotoxicity screening

Cytotoxicity screening was performed using Hoechst 33342 and propidium iodide (PI) dual staining in combination with Molecular Devices ImageXpress Micro XLS Widefield microscope for high content analysis. This microscope is Africa's first high content analysis system and thus the accuracy and sensitivity was compared to the crystal violet assay, a more traditional method of quantifying cell density.

3.4.1.1. Hoechst/ PI

Hoechst 33342 is a bisbenzimidazole derivative commonly used as a cell permeable nucleic acid dye, the structure of which can be seen in figure 3.2. This dye

intercalates DNA at A-T rich double-stranded regions with low cytotoxicity and emits blue fluorescence upon binding to DNA with an excitation/emission spectra of 346 nm and 460 nm, respectively. While Hoechst 33342 is useful for staining the nuclei of live or dead cells, it does not stain chromosomes that are dividing or replicating (Sigma-Aldrich, 2016a). Any mushroom extract that is found to be cytotoxic will be excluded from further experimentation.
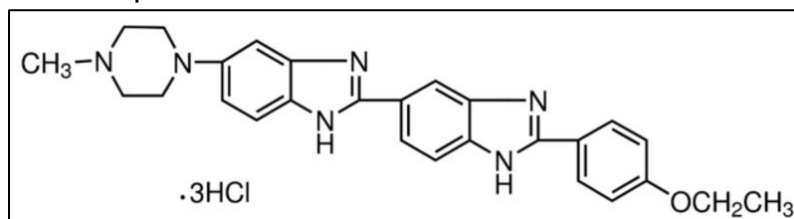
Figure 3.2: Chemical structure of Hoechst 33342. Hoechst is a membrane-permeable dye that emits blue fluorescence when bound to DNA and is used to stain the nuclei of living or fixed cells (Sigma-Aldrich, 2016a).

PI, the structure of which is shown in figure 3.3, is a membrane impermeable dye that emits red fluorescence when bound to nucleic acids. It binds to DNA in an indiscriminate manner with little to no sequence preference intercalating into every 4th or 5th base pair. When bound to nucleic acids, PI has excitation/emission maxima of 535 nm/617 nm. Non-viable and early apoptotic cells exclude PI from their cytoplasm due to the integrity of their cell membrane, however, when the integrity of the cell membrane is disrupted as in late apoptotic or dead cells PI is able to pass freely into the cell and bind to the nucleic acids (Sigma-Aldrich, 2016b; Thermo-Fisher Scientific, 2016).
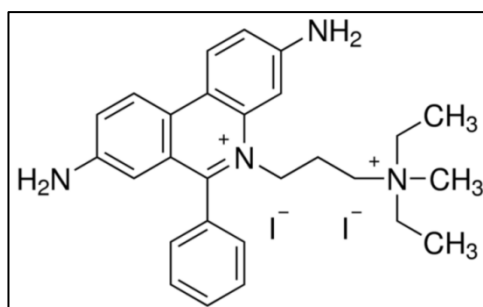
Figure 3.3: Chemical structure of propidium iodide. Since PI cannot cross the cell membrane of living cells, it is often used to detect dead cells in a population (Sigma-Aldrich, 2016b).

For all cytotoxicity experiments, RAW 264.7 macrophage-like cells and MRHF fibroblasts were seeded into a 96-well microtitre plate at a density of 20 000 and 4 000 cells per well, respectively. Treatment periods were 48 hours for the macrophages and 72 hours for the fibroblasts. The number of cells per well was determined using Hoechst 33342 and PI dual staining in combination with Molecular

Devices ImageXpress Micro XLS Widefield microscope for high content analysis. Briefly, the medium was gently removed and the cells were incubated in 50 µl of Hoechst 33342 (5 µg/ml in PBS + Ca^{2+}/Mg^{2+}) for 10 minutes at room temperature protected from light. Immediately before image acquisition, 50 µl of PI (100 µg/ml in PBS + Ca^{2+}/Mg^{2+}) was added. Nine image sites per well, covering approximately 80 % of the well, were acquired as shown in figure 3.4 using a 10 X magnification. The average cell number was calculated using MetaXpress[®] software.
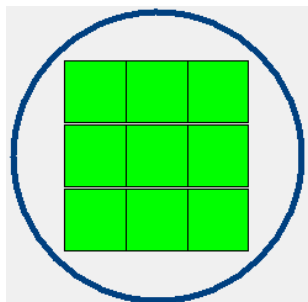
Figure 3.4: Spatial distribution of image sites acquired during the cytotoxicity screening assay. The area covered by each of the nine image sites in a single well of a 96-well microtitre plate is shown in green and was obtained using Molecular Devices ImageXpress Micro XLS Widefield microscope for high content analysis.

3.4.1.2. *Crystal violet*

Crystal violet is a cationic dye consisting of a chromophore and an auxochrome group, the structure of which can be seen in figure 3.5. The chromophore group is made up of three benzene rings and is responsible for the purple colour of the dye which readily absorbs light, while the auxochrome group aids in the binding of the dye to the target nuclear DNA and solubilisation of the resultant crystals that form (Appusamy *et al.*, 2014).
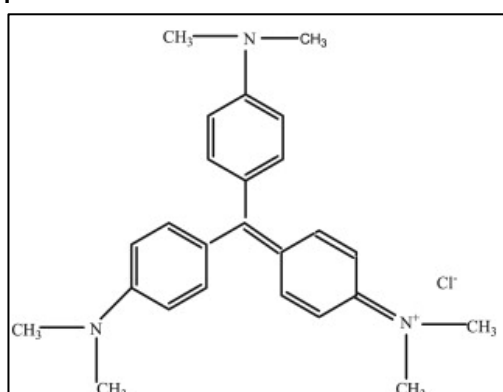
Figure 3.5: The chemical structure of crystal violet. Crystal violet binds to nuclear DNA and proteins to form crystals that can be solubilised and used to measure cell density (Appusamy *et al.*, 2014).

The crystal violet assay was chosen to measure cell density due to its apparent sensitivity and reproducibility as demonstrated by Elengoe and Hamdan (2014). Furthermore, the crystal violet assay demonstrates a higher sensitivity than the trypan-blue assay and has been proven to be particularly effective for adherent cell lines. Several mushroom species have been shown to contain large quantities of anti-oxidants and the crystal violet assay was thus chosen over the MTT assay as anti-oxidants have been shown to readily reduce MTT to formazan crystals regardless of the viability of the cells that are present (Natarajan *et al.*, 2000).

A stock solution of crystal violet was prepared at 0.01% (w/v) in distilled water and stored at room temperature. The staining procedure was carried out according to Elengoe and Hamdan (2014) with a few modifications. Briefly, the medium was gently aspirated and the cells were washed with 100 µl of PBS (+ Ca^{2+}/Mg^{2+}). Cells were fixed with 100 µl of 10% (v/v in PBS + Ca^{2+}/Mg^{2+}) formalin for 30 minutes in order to increase the permeability of the viable cells thus enabling the dye to bind to the genetic material inside the cell nucleus. The fixative was removed and the cells were stained with 100 µl of crystal violet for 1 hour after which the cells were washed three times with distilled water to remove the excess dye. The plates were left to air-dry overnight at room temperature. Once dry, 100 µl of 10% (v/v) acetic acid was added to each well and left for 20 minutes at room temperature to solubilise the crystals. The absorbance was the measured at 570 nm using a BioTek® PowerWave XS spectrophotometer (Winooski, VT, USA). The mean absorbance of the untreated cells represent 100% cell density and the percentage cell density of the cells exposed to different treatments was calculated using the following equation:

$$\% \, cell \, density = \frac{A570 \, nm \, of \, treated \, cells}{A570 \, nm \, of \, untreated \, cells} \, x \, 100.$$

3.4.2. Anti-oxidant assays

In diabetes, chronically elevated blood glucose levels result in oxidative stress which has been implicated as an important factor contributing to impaired wound healing (Kolluru *et al.*, 2012). Several anti-oxidants have been isolated from wild mushrooms including phenolic compounds, ascorbic acid, tocopherols and carotenoids. Ascorbic acid and phenolic compounds are classified as hydrophilic anti-oxidants while

carotenoids are examples of lipophilic antioxidants (Thaipong *et al.*, 2006; Preeti *et al.*, 2012).

3.4.2.1. FRAP assay

The Ferric-Reducing/ Anti-oxidant Power (FRAP) assay is a measure of the ability of antioxidants to reduce ferric iron (Fe^{3+}). As shown in figure 3.6, the FRAP assay is based on the reaction where the complex formed during the interaction of Fe^{3+} with 2,3,5-triphenyl-1,3,4-triaza-2-azoniacyclopenta-1,4-diene chloride (TPTZ) is reduced to the ferrous (Fe^{2+}) form under acidic conditions. During this reaction, an intense blue colour develops with an absorption maximum of 593 nm where the intensity of the colour is proportional to the antioxidant capacity of the sample being tested (Moon & Shibamoto, 2009; Alam *et al.*, 2013).
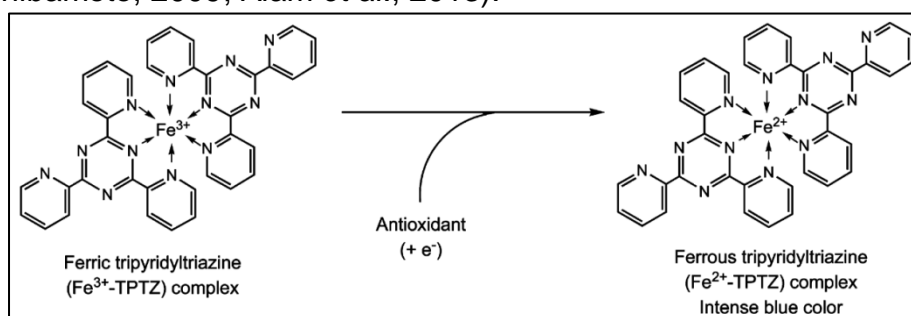
Figure 3.6: Reaction occurring during the FRAP assay. During this reaction the Fe^{3+}-TPTZ complex is reduced to form a Fe^{2+}-TPTZ complex resulting in the development of an intense blue colour (Moon & Shibamoto, 2009).

The FRAP assay is a convenient, reproducible, cost-effective, simple and rapid method of determining the antioxidant capacity of a sample, however, this reaction is not specific and thus any compound with a suitable redox potential is capable of driving this reaction. Furthermore, this method is not suitable for detecting polyphenolic compounds and thiols that react slowly or that act by radical quenching and has a poor correlation with other antioxidant capacity assays. The greatest disadvantage of the FRAP assay is that it is not mechanistically or physiologically relevant to antioxidant activity as it is based only upon the measurement of the reducing capability with regards to the ferric ion and is thus frequently coupled to other antioxidant assays (Prior *et al.*, 2005).

Briefly, samples (50 µl) were transferred into a 96-well plate and 200 µl of the FRAP reagent was added. After 30 minutes of incubation at 37°C, the absorbance was measured at 593 nm using a BioTek® PowerWave XS spectrophotometer (Winooski,

VT, USA). A stock solution of Catechin (25 mg/ml) was prepared in absolute ethanol and served as a positive control. Using a ferrous sulfate ($FeSO_4$) standard curve, the absorbance readings obtained were extrapolated and the results were thus presented as a concentration of $FeSO_4$ (µmol/l).

3.4.2.2. DPPH assay

The 2,2-diphenyl-1-picrylhydrazyl (DPPH) radical scavenging capacity assay is a decolouration assay that utilises the fact that DPPH, a stable free radical, contains an unpaired electron that is delocalised over the entire surface of the molecule (Alam *et al.*, 2013). There appears to be some controversy as to whether this reaction occurs via an electron transfer reaction or hydrogen atom abstraction. According to Prior *et al.* (2005) and MacDonald-Wicks *et al.* (2006) it is classified as an electron transfer reaction that occurs very rapidly followed by the slower transfer of a hydrogen atom which is subsequently considered to be a marginal reaction pathway. It is thus assumed that the reaction mechanism is based on both a single electron transfer and a hydrogen atom transfer reaction as shown in figure 3.7. As the DPPH free radical (violet) is converted to DPPH, the loss of colour is proportional to the antioxidant capacity of the sample being tested and can be measured using a spectrophotometer (Moon & Shibamoto, 2009).
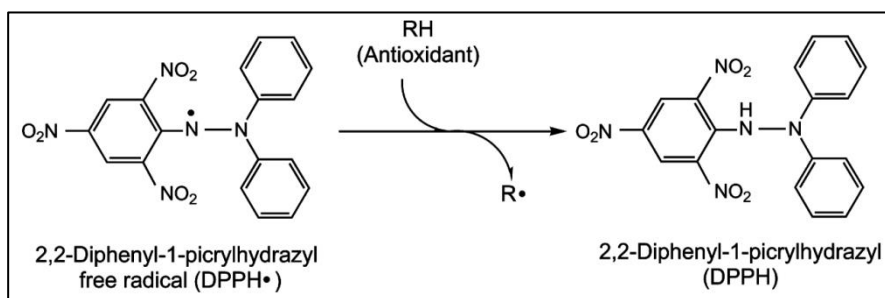
Figure 3.7: <u>Reaction occurring during the DPPH assay. As the antioxidant donates a hydrogen atom to the DPPH free radical, DPPH is formed and the reaction colour changes from violet to clear (Moon & Shibamoto, 2009).</u>

During the hydrogen atom transfer reaction, a proton and an electron are transferred from one molecule to another in one kinetic step and thus the DPPH radical will remove a proton from the antioxidant and the antioxidant will subsequently become a radical. Here, the most important parameter that determines the antioxidant capacity of a sample is the bond dissociation enthalpy and thus the lower the bond dissociation enthalpy of the proton-donating group, the faster this reaction will proceed. During the single electron transfer reaction, an electron is transferred from

the antioxidant to the DPPH free radical where the antioxidant will then become a radical cation. The most important factor to consider during this reaction is the ionisation potential of the antioxidant and thus the lower the ionisation potential, the faster this reaction will proceed. The reaction mechanism will ultimately depend on the structure and solubility of the antioxidants present in the test sample as well the partition coefficient and the polarity of the solvent (Liang & Kitts, 2014).

The advantage of the DPPH assay lies in its technical simplicity, low cost, high sensitivity and reproducibility. The greatest limitations of this assay include the physiological irrelevance of the DPPH free radical as well as the fact that DPPH is a lipophilic radical thus having limited accessibility to the hydrophilic compounds present in the test samples. As a result, an alcohol must be used to solubilise DPPH, however, ethanol has been shown to add background interference with regards to the antioxidant activity (Liang & Kitts, 2014).

Using a 96-well plate, 5 µl of sample was transferred into the relevant wells after which 120 µl of Tris-HCl buffer (50 mM, pH 7.4) and 120 µl of DPPH (0.1 mM) were added. Following incubation for 20 minutes at room temperature protected from light, the absorbance was measured at 513 nm using a BioTek$^®$ PowerWave XS spectrophotometer (Winooski, VT, USA) and the percentage radical scavenging activity was calculated using the following formula:

$$\% \, DPPH \, scavenging = \frac{A - B}{A} \, X \, 100$$

where A is the absorbance value of the reference sample and B is the absorbance value of the test sample.

3.4.2.3. *Nitric oxide scavenging assay*

The NO scavenging assay is frequently used as a measure of anti-oxidant activity and is based on the principle that when sodium nitroprusside is placed in an aqueous solution at physiological pH, it spontaneously generates NO. The NO produced reacts with oxygen to form stable products (nitrite and nitrate) which can then be measured using the Griess reaction described in section 3.5.1. NO scavengers will compete with the oxygen and there will be a subsequent decrease in the quantity of nitrite ions (Alam et al., 2013).

51

NO is an important signalling molecule that has demonstrated several important functions during the wound healing process, however, diabetic wounds have been characterized by altered macrophage function and consequent changes in NO production. NO has thus been implicated in impaired diabetic wound healing. Because NO has also been identified as an inflammatory marker, this assay also serves to establish the nature of any anti-inflammatory responses during the NO production assay performed using RAW 264.7 cells described in section 3.5.1 (Luo & Chen, 2005).

After transferring 50 µl of test sample (100 and 200 µg/ml) into a 96-well microtitre plate, 50 µl of sodium nitroprusside (10 mM) was added and incubated at room temperature under direct light for 150 minutes. This was followed by the addition of 100 µl of Griess reagent. The reaction was protected from light and incubated for 10 minutes at room temperature after which the absorbance was measured at 540 nm using a BioTek$^{®}$ PowerWave XS spectrophotometer (Winooski, VT, USA). Amino-guanidine (200 µg/ml) was added as a positive control. The percentage of NO scavenged was calculated using the following formula:

$$\% \; NO \; scavenging = \frac{A - B}{A} \; X \; 100$$

where A is the absorbance value of the reference sample and B is the absorbance value of the test sample.

3.4.3 Glycation inhibition

It is common knowledge that protein glycation generates AGEs through the Maillard reaction and that these AGEs have been implicated in the pathogenesis of diabetic complications including chronic wound healing. Identifying a natural product with sufficient protein glycation inhibitory potential could thus be greatly beneficial in inhibiting diabetic complications with very few adverse effects (Wijetunge & Perera, 2014). While glucose together with the products of glucose metabolism have been identified as the main culprits of protein glycation in diabetes, glucose forms a hemiacetal ring structure in solution which makes it poorly reactive as a glycation catalyst (Boonkaew *et al.*, 2014). Consequently, glyceraldehyde was used as a particularly effective and reactive glycating agent during the glycation inhibition assay as it does not form any hemiacetal ring structures in solution. The AGEs that

are produced from glyceraldeyde include argpyrimidine, triosidines and pentosidine. Several triosidines formed from reactions between lysine, arginine and glyceraldehyde such as the arginine-lysine cross-link arg-hydroxy-triosidine and the lysine-lysine cross-link lys-hydroxy-triosidine have been shown to be fluorescent (Schalkwijk *et al.*, 2004).

After transferring 50 µl of protein sample (20 mg/ml) into the relevant wells of a fluorescent 96-well microtitre plate, 40 µl of sample and 10 µl of glyceraldehyde solution (500 mM) was added. The plate was sealed and incubated at 37 °C for 24 hours after which the fluorescence was measured using a Fluoroskan Ascent FL fluorometer (ThermoLabsystems, Finland) with an excitation wavelength of 370 nm and an emission wavelength of 440 nm. Amino-guanidine (20 mM) was used as a positive control and the percentage of glycation inhibition was calculated using the following formula:

$$\% \, glycation \, inhibition = \frac{A - B}{A} \, X \, 100$$

where A is the relative fluorescence of the reference sample and B is the relative fluorescence of the test sample.

In order to identify false positives due to quenching, the intrinsic fluorescence of glycated gelatin was exploited by transferring 50 µl of pre-glycated gelatin (20 mg/ml) into a fluorescent 96-well microtitre plate. Next, 40 µl of sample (mushroom extract) and 10 µl of water were added and the fluorescence was measured as before. When added to pre-glycated gelatin, a decrease in the relative fluorescence in response to treatment with a particular mushroom extract was taken as a potential signal for quenching and the percentage quenching was calculated using the same formula as above.

3.4.4. Collagenase inhibition

Collagenases are endopeptidase enzymes responsible for digesting insoluble collagen fibres in their triple-helical conformation with the following sequence speicificity:

–R–Pro–X–Gly–Pro–R–

Cleavage site
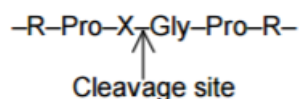
where X is typically a neutral amino acid (Sigma-Aldrich, 2016c). Chronic diabetic wounds are characterized by a persistent inflammatory state that leads to a disruption in the balance of proteases and their inhibitors that are required to maintain equilibrium between ECM deposition and degradation. As a result, wound healing is delayed and the wounds become characterized by excessive levels of proteases and reduced levels of protease inhibitors (McCarty & Percival, 2013). Natural products which are able to inhibit proteases such as collagenase could thus prove to be useful therapeutic agents in the treatment of chronic diabetic wounds.

Briefly, 10 µl of enzyme (40 µg/ml) was added to each well in a 96-well microtitre plate. Sample (10 µl) followed by 10 µl gelatin (2 mg/ml) and 10 µl assay buffer (200 mM) was added and the plate was incubated for 1 hour at 37 °C after which 20 µl of Coomasie Brilliant Blue was added. Following 5 minutes of incubation at room temperature with gentle shaking, the plate was centrifuged at 500 rcf for 5 minutes and the supernatant was gently removed. The pellet was then washed in 50 µl of 40 % methanol/ 10 % acetic acid (v/v) to remove the excess dye. Finally, the pellet was dissolved in 50 µl of DMSO and the absorbance was measured at 600 nm using a BioTek® PowerWave XS spectrophotometer (Winooski, VT, USA). Catechin (0.5 mM) was included as a positive control. The percentage collagenase inhibition was calculated using the following formula:

$$\% \, collagenase \, inhibition = \frac{A600 \, nm \, of \, test \, sample}{A600 \, nm \, of \, reference \, sample} \, x \, 100.$$

3.5. MACROPHAGE FUNCTION

3.5.1. Nitric oxide production

LPS is one of the chief components of the outer membrane of Gram-negative bacteria and induces the inflammatory phase of the immune response. One of the ways in which LPS activates macrophages is through binding to their TLRs. Following activation, the synthesis of multiple inflammatory mediators such as NO is induced. The quantity of NO produced by the macrophages can then be determined using the Griess reaction (Amura *et al.*, 1998; Mosser & Zhang, 2008). The Griess reaction measures the quantity of nitrite (NO_2^-) which is one of the two major breakdown products of NO (Bryan & Grisham, 2007).

The Griess reaction is a colorimetric method during which dinitrogen trioxide (N_2O_3) generated from the acid-catalysed formation of nitrous acid (HNO_2) from NO_2^- undergoes a reaction with sulphanilamide, thus resulting in the formation of a diazonium ion. The diazonium ion gets coupled to N-1-napthylethylenediamine dihydrochloride (NED) resulting in the production of an azo chromophore which absorbs strongly at 540 nm (Bryan & Grisham, 2007). The reaction during which sulphanilamide and NED are used in an acidic environment in the presence of phosphoric acid is demonstrated in figure 3.8.
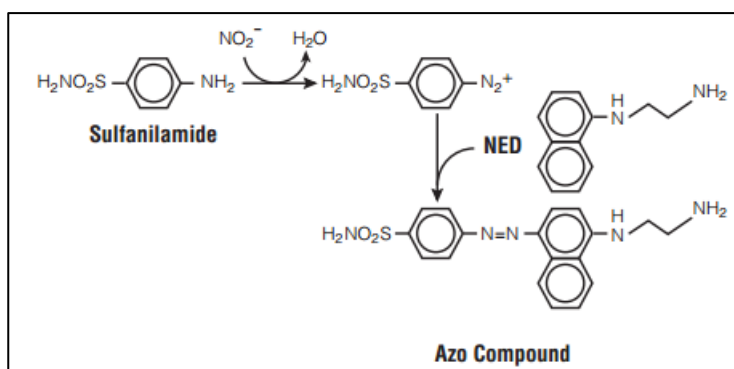
Figure 3.8: Chemical reactions occurring during the quantification of NO_2^- using the Griess reagent for nitrite (Promega, 2009).

Briefly, 100 μl of RAW 264.7 cells were seeded at a density of 100 000 cells per well into a 96-well microtitre plate and left to attach overnight at 37 °C. The medium was gently aspirated and cells were treated with 100 μl of the indicated treatment as well as 200 ng/ml LPS and incubated for a further 24 hours at 37 °C after which the Griess reaction was carried out. During this reaction, 50 μl of the culture medium from each well was transferred into corresponding wells of a new 96-well plate and 50 μl of Griess reagent for nitrite was added to each well. The reaction was protected from light and incubated for 10 minutes at room temperature after which the absorbance was measured at 540 nm using a BioTek® PowerWave XS spectrophotometer (Winooski, VT, USA). Amino-guanidine (100 μg/ml) was included as a positive control for NO inhibition.

The presence of endotoxins in the mushroom extracts was assessed using Polymyxin B sulfate. Polymyxins are a group of polypeptide antibiotics isolated from various strains of *Bacillus polymyxa*. They are capable of penetrating bacterial cell membranes thus disrupting their structure and ultimately exerting their bactericidal properties by causing permeability changes and subsequent death. They are basic

surface-active cationic detergents and consequently interact with cell membrane phospholipids. Polymyxin B, the structure of which is shown in figure 3.9, acts as a chelating agent thus binding to the lipid A component of endotoxin in a 1:1 ratio, effectively neutralising LPS (Papich, 2016).
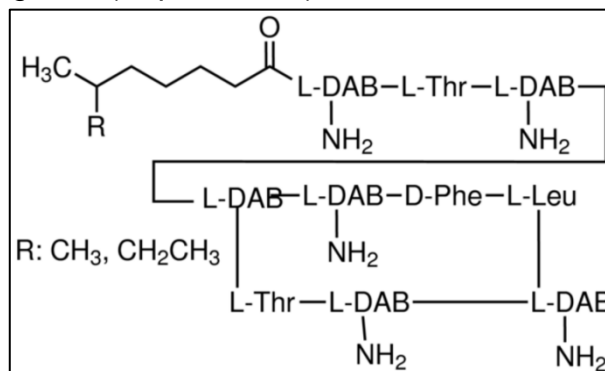
Figure 3.9: <u>Chemical structure of Polymyxin B sulfate. Polymyxin B sulfate a mixture of polymyxins B1 and B2 and contains a cyclic heptapeptide unit together with a tripeptide side chain that is *N-acetylated* by a fatty acyl residue (Sigma-Aldrich, 2016d).</u>

RAW 264.7 cells were seeded into a 96-well plate at 100 000 cells per well and left to attach overnight. Cells were then treated with the mushroom extracts (100 and 200 µg/ml) together with Polymyxin B sulfate at a concentration of 10 µg/ml for 24 hours after which the griess reaction was carried out as described above.

3.5.2. Phagocytosis

It has previously been shown that the function of macrophages at wound-sites in diabetic patients is compromised such that their phagocytic capability is impaired. Furthermore, AGEs resulting from hyperglycaemia have been shown to directly suppress the phagocytic activity of macrophages. The removal of dead cells by macrophages is an essential step in the normal wound healing process as it protects the surrounding tissues from being exposed to the toxic contents of the dead and damaged cells while simultaneously producing anti-inflammatory cytokines and chemokines in an effort to prevent further tissue damage. Furthermore, phagocytosis of microbes is essential in preventing wound infections and thus once the phagocytic capability of the macrophage becomes impaired, the wound enters a state of chronic inflammation (Khanna *et al.*, 2010).

To assess the phagocytic capability of RAW 264.7 macrophage-like cells, pHrodo™ Green BioParticles® Conjugate (Thermo Fisher Scientific) was utilised. This is a highly sensitive system consisting of unopsonised *Escherichia coli* particles

conjugated to pHrodo™ Green. The pHrodo™-dye is a fluorogenic dye whose fluorescence intensity is determined by the surrounding pH as shown in figure 3.10. The pHrodo™ Green conjugate thus does not fluoresce outside the cell due to the neutral pH, however, as the conjugates are ingested and phagolysosomes are formed, the surrounding environment becomes more acidic and the fluorescence intensity of the BioParticles® increases thus allowing for the quantitative measurement of phagocytosis. The advantage of this is that the washing and quenching steps required when nonfluorogenic indicators of bacterial uptake are used can be eliminated (Life Technologies, 2013a).
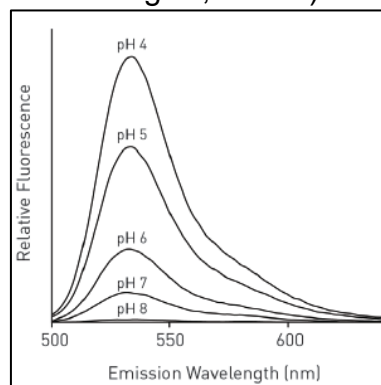
Figure 3.10: Fluorescence emission spectrum of the pHrodo™ Green conjugate utilised in the pHrodo™ Green BioParticles® Conjugate system for measuring phagocytosis (Life Technologies, 2013a).

In addition to measuring phagocytosis, acidic vacuole formation was assessed using LysoTracker® Red (Thermo Fisher Scientific). LysoTracker® Red is highly sensitive red fluorescent dye that is used to track and label acidic organelles in live cells and is based on the principle that weakly basic amines accumulate in selective manner inside cellular compartments with a low pH such as lysosomes. LysoTracker® probes consist of a fluorophore attached to a weak base that becomes only partially protonated at neutral pH. The probes are thus able to freely cross cell membranes and effectively label living cells. These probes have a high specificity for acidic organelles and do not require any secondary antibodies for detection purposes.

To measure phagocytosis and acidic vacuole formation, 100 μl of RAW 264.7 macrophage-like cells were seeded into a 96-well plate at 30 000 cells per well in DMEM without phenol red supplemented with 10 % FBS. Cells were left to attach overnight after which 50 μl of the mushroom extracts (100 μg/ml) and the specified controls were added and incubated for 24 hours at 37 °C. After 23 hours of incubation, the relevant wells were treated with Cytochalasin B (3 μg/ml) and LPS

(200 ng/ml) for 1 hour which served as positive controls for the inhibition and stimulation of phagocytosis, respectively. Next, 20 µl of pHrodo™ Green BioParticles® were added at a concentration of 20 µg/ml and incubated at 37 °C for 2 hours followed by the addition of LysoTracker® Red at 50 nM (Life Technologies, 2013b).

Fluorescent micrographs were captured using Molecular Devices ImageXpress Micro XLS Widefield microscope for high content analysis. Nine image sites per well were acquired as shown in figure 3.11 using a 20 X magnification. The mean cell integrated intensity of LysoTracker® Red and the mean stain area of the pHrodo™ Green BioParticles® was calculated using MetaXpress® software.
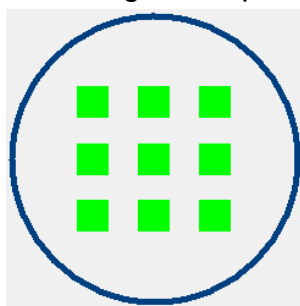
Figure 3.11: Spatial distribution of image sites acquired during the phagocytosis assay. The area covered by each of the nine image sites in a single well of a 96-well microtitre plate is shown in green and was obtained using Molecular Devices ImageXpress Micro XLS Widefield microscope for high content analysis.

3.5.3. M1/M2 macrophage polarization

Macrophages have been shown to display extraordinary plasticity with different macrophage populations exhibiting distinct physiologies depending on the stimuli that they receive. As different biochemical methods of identifying these macrophage populations have been developed, our understanding of macrophage function has also progressed together with the potential to target specific populations of activated macrophages for therapeutic intervention (Mosser & Zhang, 2008).

M1 and M2 macrophage activation was assessed using the Alexa-Fluor® anti-mouse CD86 and the APC anti-mouse CD206 antibodies from BioLegend®, respectively. Briefly, RAW 264.7 macrophages were seeded into 12-well plates at a seeding density of 200 000 cells per well and left to attach overnight at 37 °C. The cells were then treated with the specified treatments and incubated for 24 hours. LPS (200 ng/ml) and curcumin (20 µg/ml) were included as positive controls for CD86 and CD206, respectively.

The cells were scraped from the wells and transferred into Eppendorf tubes where they were washed twice with 500 µl PBS (+ Ca^{2+}/Mg^{2+}) by centrifugation at 500 rcf for 5 minutes. Cells were blocked with 500 µl of 1 % BSA for 15 minutes at room temperature after which they were washed once. The antibodies were prepared using 1 % BSA in PBS using a 1:300 dilution for CD86 and a 1:400 dilution for CD206. Samples were stained with 100 µl of antibody for 30 minutes at 37 °C protected from light. An isotype control for each fluorophore was included using a 1:400 dilution for the APC-conjugate and a 1:300 dilution for the Alexa-Fluor® conjugate. The cells were washed twice as before and resuspended in 350 µl of PBS (+ Ca^{2+}/Mg^{2+}). Samples were then transferred into a 96-well microtitre plate (175 µl per well) and stained with Hoechst 33342 (5 µg/ml in PBS + Ca^{2+}/Mg^{2+}).

After allowing the cells 1 hour to settle at the bottom of the plate, fluorescent micrographs were captured using Molecular Devices ImageXpress Micro XLS Widefield microscope for high content analysis. Nine image sites per well were acquired using a 10 X magnification as in section 3.4.1. The percentage of cells stained positive for CD86 and CD206 was calculated using MetaXpress® software.

3.5.4. NF-κB and COX-2 antibody staining

NF-κB refers to a family of transcription factors that play an important role in inflammation, immune responses, apoptosis and cell cycle progression. NF-κB proteins are able to bind to consensus DNA sequences that can be found in the regulatory regions of target genes thus regulating their transcription and enabling NF-κB to regulate the expression of numerous cytokines, iNOS and COX-2 amongst others (Chen *et al.*, 2011; Wullaert *et al.*, 2011). Inflammatory stimuli have been shown to induce high levels of COX-2 expression and COX-2 has thus been identified as a suitable target for anti-inflammatory drugs (Na *et al.*, 2015).

3.5.4.1. *NF-κB*

RAW 264.7 macrophages were seeded into a 96-well mictrotitre plate at 30 000 cells/well and left to attach overnight at 37 °C. Cells were then treated with the specified treatments and incubated for a further 24 hours. After 23 hours of incubation, LPS (200 ng/ml) was added as a positive control for one hour. Samples were fixed with 37 % formaldehyde by adding it directly to the culture medium to make up a final concentration of 4 % and incubated for 15 minutes at room

temperature. The fixative was aspirated and the cells were washed twice with 100 µl PBS (+ Ca^{2+}/Mg^{2+}) after which they were permeabilised with 100 µl of cold methanol for 10 minutes at - 20 °C. The methanol was removed and 100 µl of PBS was added for five minutes at room temperature. Cells were then washed twice with 100 µl of 1 % BSA in PBS and blocked for 45 minutes at room temperature with a 3 % BSA solution prepared in PBS and containing 0.2 % Triton-X 100.

Next, 50 µl of a 1:800 dilution of phospho-NF-κB p65 (Ser536) (93H1) Rabbit mAb in 1 % BSA/PBS was added and the cells were incubated for 1 hour at 37 °C. After removing the primary antibody and washing the cells twice with 100 µl of 1 % BSA in PBS, 50 µl of a 1:1000 dilution of Anti-Mouse IgG (H+L), F(ab')$_2$ Fragment (Alexa Fluor$^®$ 488 Conjugate) prepared in 1 % BSA in PBS was added and the cells were incubated for 1 hour at 37°C protected from light. Cells were washed three times in PBS (+ Ca^{2+}/Mg^{2+}) after which the nuclei were stained with 50 µl of Hoechst 33342 (5 µg/ml in PBS + Ca^{2+}/Mg^{2+}) for 10 minutes at room temperature.

Fluorescent micrographs were captured using Molecular Devices ImageXpress Micro XLS Widefield microscope for high content analysis. Nine image sites per well were acquired as shown in figure 3.12 using a 40 X magnification. The mean nuclear integrated intensity was calculated using MetaXpress$^®$ software.
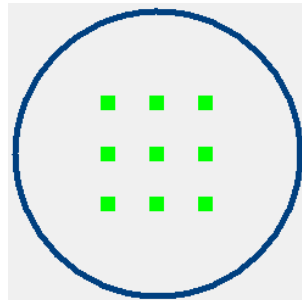
Figure 3.12: Spatial distribution of image sites acquired during the NF-κB assay. The area covered by each of the nine image sites in a single well of a 96-well microtitre plate is shown in green and was obtained using Molecular Devices ImageXpress Micro XLS Widefield microscope for high content analysis.

3.5.4.2. COX-2

RAW 264.7 macrophages were seeded into a 96-well microtitre plate at 30 000 cells/well and left to attach overnight at 37°C after which they were treated with the specified treatments for 24 hours. LPS (200 ng/ml) was included as a positive control and added together with the treatments as indicated. After 24 hours, samples were fixed, permeabilised and blocked as in section 3.5.4.1. Next, cells were incubated in

50 µl of a 1:800 dilution of Cox2 (D5H5) XP$^®$ Rabbit mAb (Alexa Fluor$^®$ 488 Conjugate) prepared in 1 % BSA/ PBS for 1 hour at 37 °C protected from light. Cells were then washed twice with 100 µl of PBS and stained with 50 µl of Hoechst 33342 (5 µg/ml in PBS + Ca^{2+}/Mg^{2+}) for 10 minutes at room temperature.

Fluorescent micrographs were captured using Molecular Devices ImageXpress Micro XLS Widefield microscope for high content analysis. Four image sites per well were acquired as shown in figure 3.13 using a 20 X magnification. The percentage of cells that were stained positive for COX-2 was calculated using MetaXpress$^®$ software.
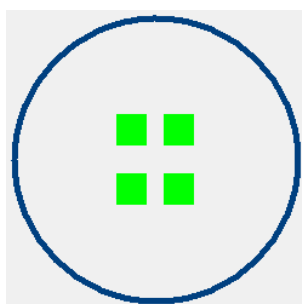
Figure 3.13: Spatial distribution of image sites acquired during the COX-2 assay. The area covered by each of the four image sites in a single well of a 96-well microtitre plate is shown in green and was obtained using Molecular Devices ImageXpress Micro XLS Widefield microscope for high content analysis.

3.6.   FIBROBLAST FUNCTION

3.6.1. Proliferation

MRHF fibroblast proliferation was measured using the same protocol as for cytotoxicity screening (section 3.4.1) with the only modification being that low-glucose DMEM was supplemented with only 1 % FBS instead of 10 %.

3.6.2. Migration

MRHF fibroblast migration was measured using the Enzo$^®$ Cell Migration Assay kit. This kit provides a sensitive, reproducible and flexible way of measuring cell migration and does not result in any ECM or cellular damage which would interfere with the findings (Hulkower & Herber, 2011; Enzo, 2015). As shown in figure 3.14, this assay utilises Cell Seeding Stoppers produced from a medical grade silicone which restricts the cells that are seeded into the plate to the outer annular regions of each well. Once the stoppers are removed, an unseeded region of 2 mm referred to as the detection zone is revealed. Cells are allowed to migrate into the detection zone over

a certain time period after which they can be analysed using either a Microplate Reader or image analysis (Enzo, 2016).
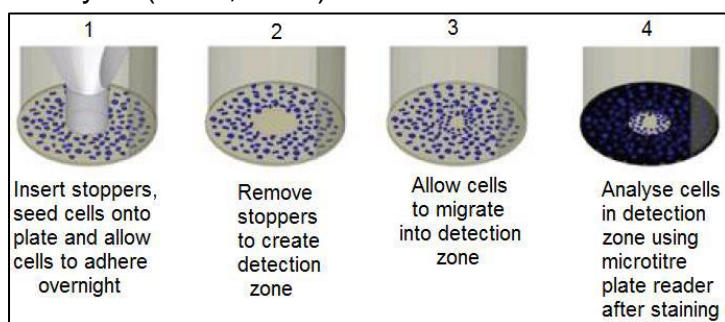
Figure 3.14: Schematic of the Cell Migration Assay adapted from Enzo® (2016).

Briefly, MRHF fibroblasts were seeded around the Cell Seeding Stoppers at a density of approximately 15 000 cells/well and left to attach overnight at 37 °C. The stoppers were then carefully removed using the Stopper Tool and the cells were washed twice with 100 µl of PBS (+ Ca^{2+}/Mg^{2+}) to remove any detached cells. The cells were then treated with 100 µl of the indicated treatments for 48 hours at 37 °C. Mitomycin C, a DNA synthesis inhibitor, was included in the culture medium at a concentration of 10 µg/ml in order to inhibit any cell proliferation (Sigma-Aldrich, 2016e).

Images were obtained using Molecular Devices ImageXpress Micro XLS Widefield microscope for high content analysis. Nine image sites per well were acquired as shown in figure 3.4 using a 10 X magnification. The micrographs were then analysed using TScratch software. TScratch is a freely available image analysis technique which utilises the fast discrete curvelet transform in order to automate the process by which the area occupied by cells in an image is calculated (Gebäck *et al.*, 2009).

3.7.   DATA- AND STATISTICAL ANALYSIS

3.7.1.   Data analysis for High Content Screening

All images obtained from Molecular Devices ImageXpress Micro XLS Widefield microscope for high content analysis were analysed using MetaXpress® 6.1 High Content Image Acquisition and Analysis Software in combination with the Multi-Wavelength Cell Scoring application module. Using this module, one is able to obtain a number of different multi-parameter measurements including cell counts, the percentage of positive and negative cells, the area of the nuclei as well as wavelength-specific intensities based on the segmentation parameters defined for each wavelength. The segmentation parameters are based on simple measurements

62

such as the approximate minimum and maximum widths of the nucleus or cell, the intensity above local background and the minimum stained area (Molecular Devices, 2017). An example of a segmentation overlay and the filter sets that were used are shown in figure 3.15.

B Filter set	Fluorescent dyes and conjugates
DAPI	Hoechst 33342
Texas Red	PI
	LysoTracker® Red
FITC	Alexa Fluor® 488
	pHrodo™ Green BioParticles®
Cy5	APC
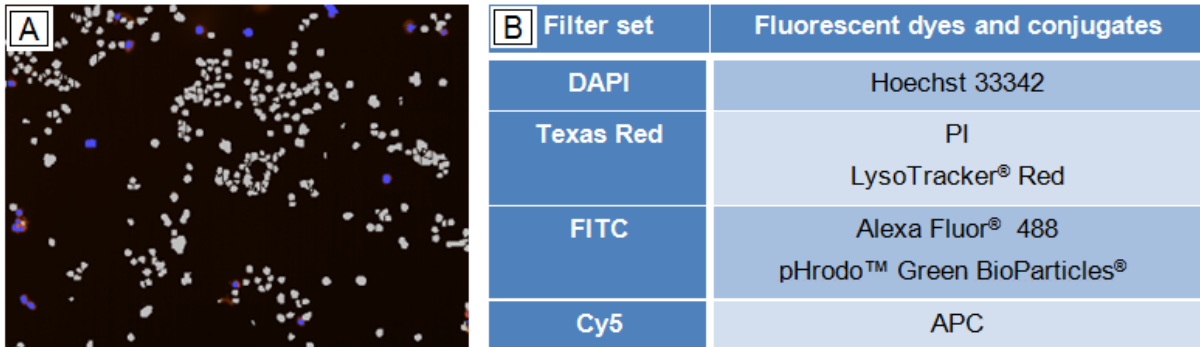
Figure 3.15: Diagram illustrating a segmentation overlay and the filter sets used during this study. (A) An example of a segmentation overlay of cells stained with Hoechst 33342 and PI obtained using MetaXpress® software where cells that stained positive for only Hoechst 33342 are shown in grey while those that stained positive for Hoechst 33342 and PI are shown in blue and (B) the filter sets used for each fluorescent dye and conjugate.

3.7.2. Data analysis for fibroblast migration

The images acquired during the migration assay were analysed using TScratch software. This software is freely available and utilises the fast discrete curvelet transform as a means of automating the process by which the area occupied by cells in a particular image is calculated. The results are reported as percentage values which correspond to the size of the wound area relative to the size of the image. A larger wound area is thus associated with a larger percentage value and vice versa. A summary of the workflow of the software is demonstrated in figure 3.16.
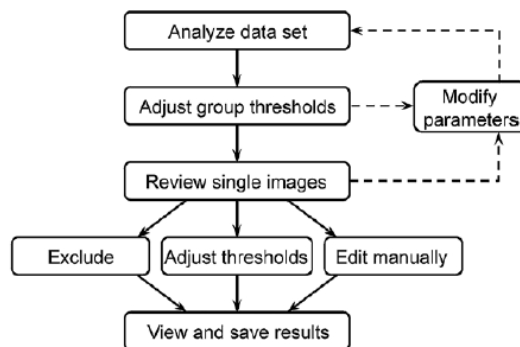
Figure 3.16: The workflow of the TScratch software. Initially the images will be segmented and grouped automatically by the software using default parameters. Group thresholds of multiple images can be manually adjusted in cases where the algorithm did not successfully determine them automatically. Individual images can then be reviewed and the analysis can be modified by excluding certain images, adjusting individual thresholds or manually editing the results using drawing tools (Gebäck et al., 2009).

3.7.3. Statistical analysis

Except where otherwise stated, all experiments were performed three times, each in triplicate for statistical analysis. Both the ANOVA and Student's t-tests were performed to compare the means of the data sets using the data analysis package from Microsoft Excel. In cases where $p < 0.05$ the data was considered statistically significant (McKillup, 2012).

4.1.   CHARACTERIZATION OF THE GLYCATED GELATIN MODEL

Diabetic individuals demonstrate enhanced protein glycation due to chronically elevated blood glucose levels. The resultant AGEs have been shown to perform important functions in the pathogeneses of various diabetic complications including impaired wound healing as protein glycation not only interferes with the function of the affected protein, but also influences several cell signalling pathways (Liao *et al.*, 2009; Singh *et al.*, 2014). The validation of an *in vitro* screening model forms an important part of the research process as it is crucial in determining the possibilities and limitations of the model across various cell lines.

4.1.1.   The autofluorescence of advanced glycation end products

AGEs are known to autofluoresce at excitation/emission wavelengths between 370 and 440 nm, respectively; this property is widely used as a means to quantify AGEs. AGE autofluorescence was measured in order to confirm the success of the glycation process (figure 4.1). The unglycated gelatin (gelatin autoclaved in the absence of glucose) served as the control in this experiment with all other treatments calculated as a percentage of this control. Although statistically significant, the fluorescence contribution of the autoclaved glucose solution was minimal and is not considered relevant.
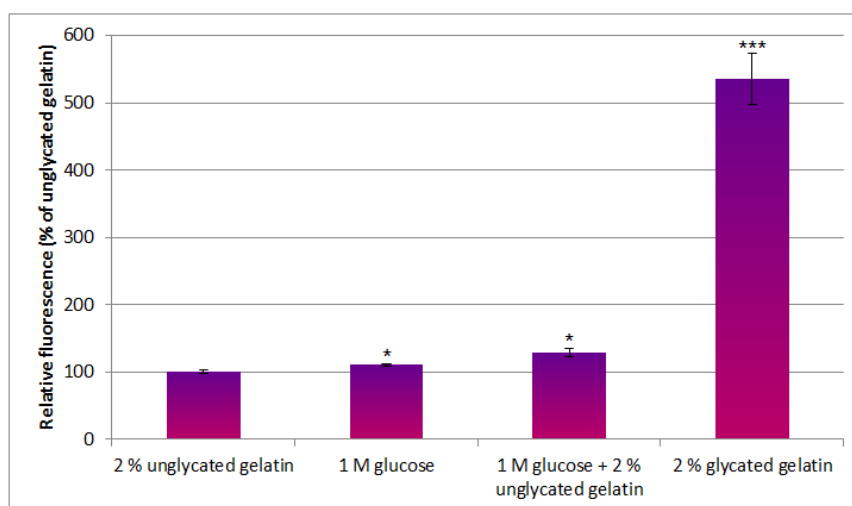
Figure 4.1: <u>A comparison of the relative fluorescence of unglycated gelatin and glucose stocks used to produce glycated gelatin after being autoclaved for 1 hour; results are reported as means ± SD where each experiment was performed three times, each in triplicate (*p<0.05; **p<0.01; ***p<0.005 compared to unglycated gelatin).</u>

Figure 4.1 shows a robust increase in the relative fluorescence of glycated gelatin (p<0.005) when compared to the unglycated gelatin, glucose and the combination of glucose with unglycated gelatin stocks, thus confirming an effective glycation process.

4.1.2. Cytotoxicity screening

The cytotoxicity of gelatin on both RAW 264.7 macrophage-like cells and MRHF fibroblasts was explored in order to define the practical concentration limits suitable for *in vitro* studies and to determine an optimal concentration of gelatin that should be used to mimic the diabetic state. Cell numbers were determined using Hoechst 33342 and propidium iodide staining while the crystal violet assay was performed to assess cell density in an attempt to confirm the accuracy of both methods.

Figure 4.2 shows examples of the fluorescent micrographs that were captured during this experiment and analysed using MetaXpress$^{®}$ software as descried in section 3.7.1 while figure 4.3 compares the results of the cytotoxicity screening assays on the macrophages and fibroblasts for both the unglycated and glycated gelatin stocks. The untreated sample contains no gelatin and consisted of DMEM supplemented with 10 % FBS and represents 100 % cell density. All treatments were calculated as a percentage of this control.
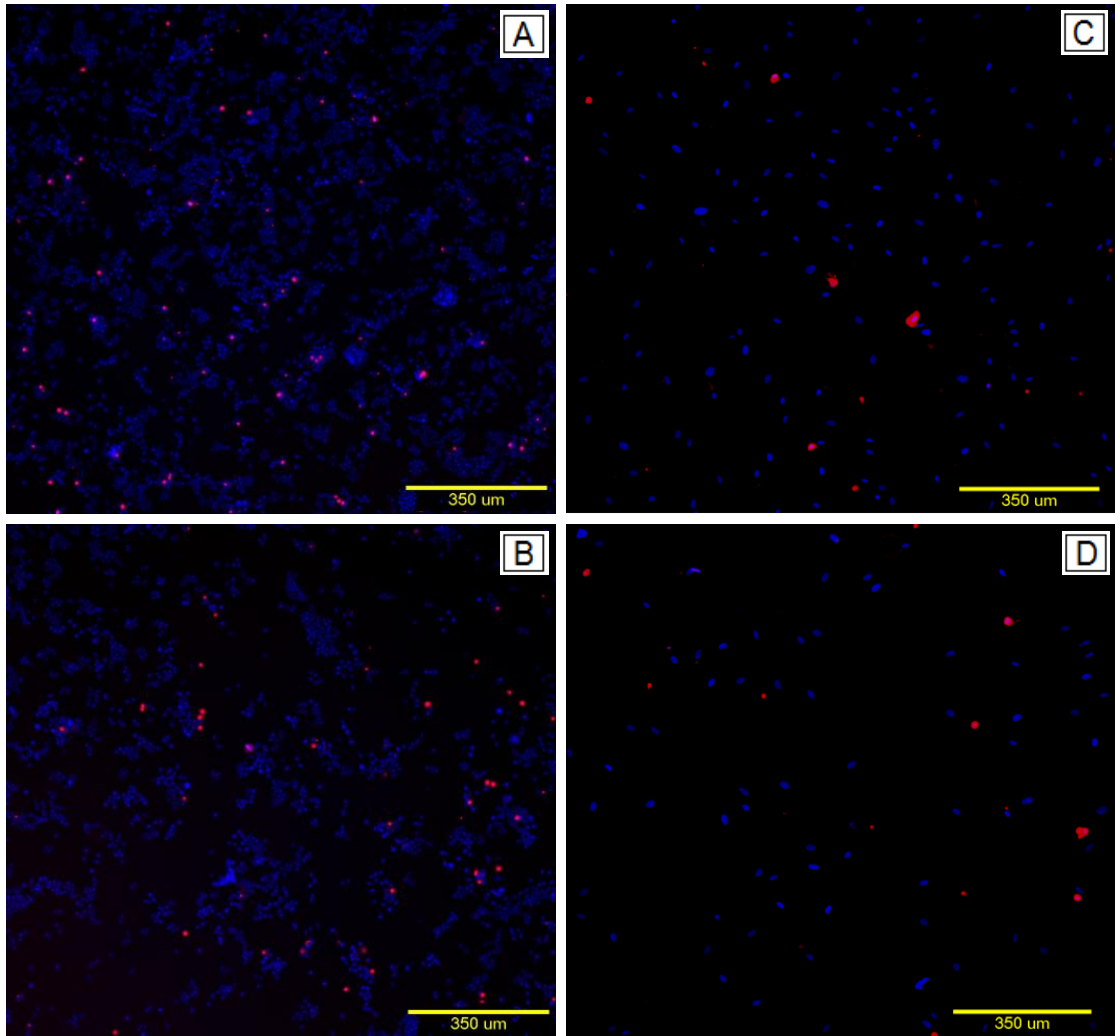
Figure 4.2: <u>Fluorescent micrographs captured during the gelatin cytotoxicity screening assay comparing (A) 1 % unglycated gelatin with (B) 1 % glycated gelatin for RAW 264.7 cells and (C) 1 % unglycated gelatin with (D) 1 % glycated gelatin for the MRHF fibroblasts using Hoechst 33342 (blue) and propidium iodide (red).</u>

From the fluorescent micrographs shown in figure 4.2 it can be seen that there are much fewer cells present in the wells that were treated with glycated gelatin when compared to treatment with unglycated gelatin for both the RAW 264.7 macrophages and the MRHF fibroblasts.
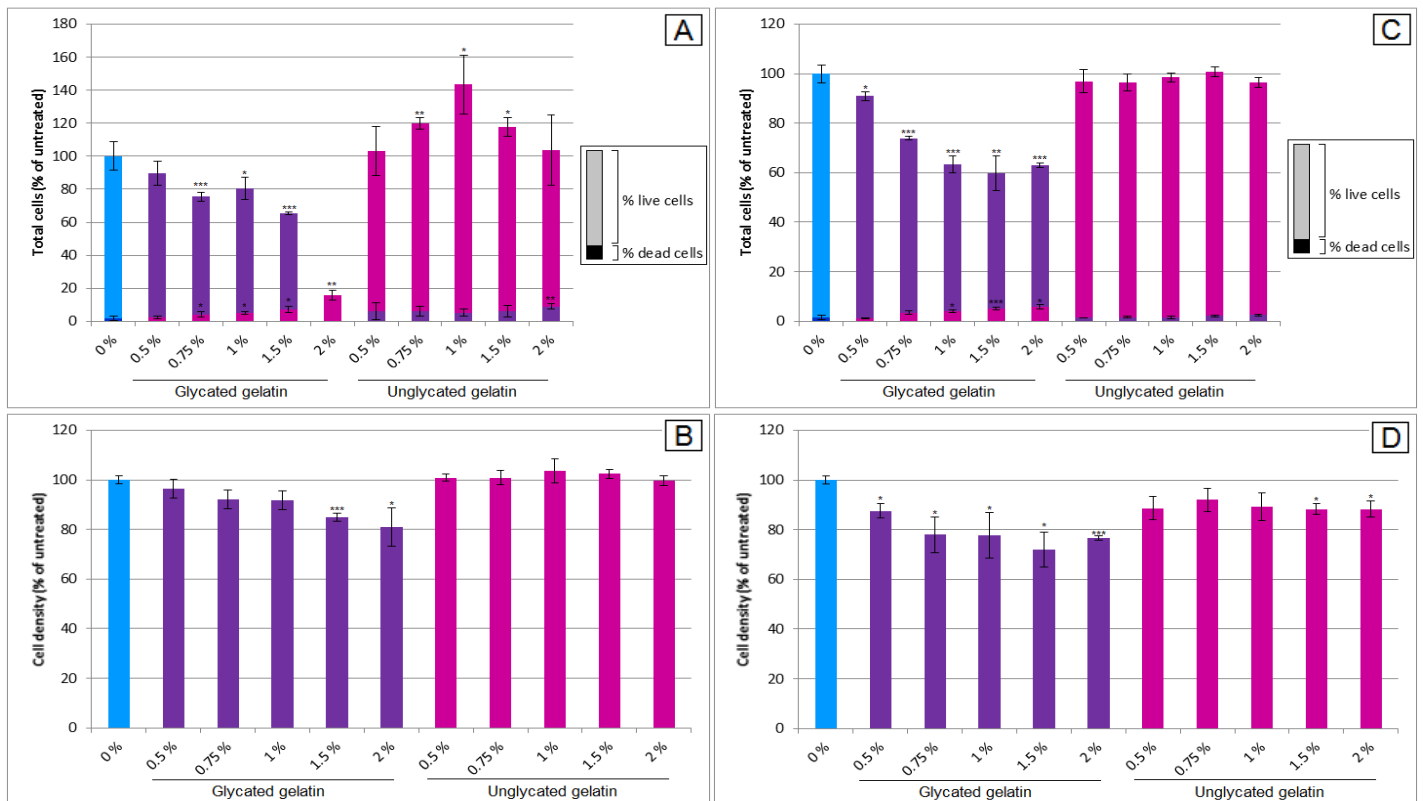
Figure 4.3: Cytotoxicity screening of gelatin comparing (A) cell number with (B) cell density for RAW 264.7 cells and (C) cell number with (D) cell density for MRHF cells; live- and dead cell numbers were obtained from Hoechst 33342 and PI staining, respectively and cell density from crystal violet staining. Results are reported as means ± SD where each experiment was performed three times, each in triplicate (*p<0.05; **p<0.01; ***p<0.005 compared to the untreated sample).

Figures 4.3 A and C show a dose-dependent decrease in cell number accompanied by a dose-dependent increase in cell death for both the RAW 264.7 cells as well as for the MRHF fibroblasts in response to glycated gelatin. The unglycated gelatin did not show any substantial cytotoxicity for either cell line, however, there was a significant increase in cell death at 2 % unglycated gelatin for the RAW 264.7 cells. Figure 4.3 D shows the same dose-dependent decrease in cell density in response to an increased concentration of glycated gelatin for the MRHF fibroblasts, however, significant decreases in RAW 263.7 cell density were only observed at concentrations of 1.5 and 2 % for the glycated gelatin as seen in figure 4.3 B. No significant differences in cell density were observed for the RAW 264.7 cells in response to the unglycated gelatin, however, a significant decrease in MRHF fibroblast cell density was observed at concentrations of 1.5 and 2 % for the unglycated gelatin.

4.1.3. Nitric oxide production in activated macrophages

The effect of both glycated and unglycated gelatin on the nitric oxide production in LPS activated RAW 264.7 cells was assessed using the Griess reaction and the results are shown in figure 4.4. LPS (200 ng/ml) was used to induce the pro-inflammatory phenotype which is associated with increased iNOS expression and concomitant NO production. All other treatments were calculated as a percentage of this control and statistical differences were calculated relative to LPS stimulated cells. Amino-guanidine, an inhibitor of iNOS activity and expression, was used to confirm that the model is responsive to anti-inflammatory signals showing complete inhibition of nitric oxide production at a concentration of 100 µg/ml.
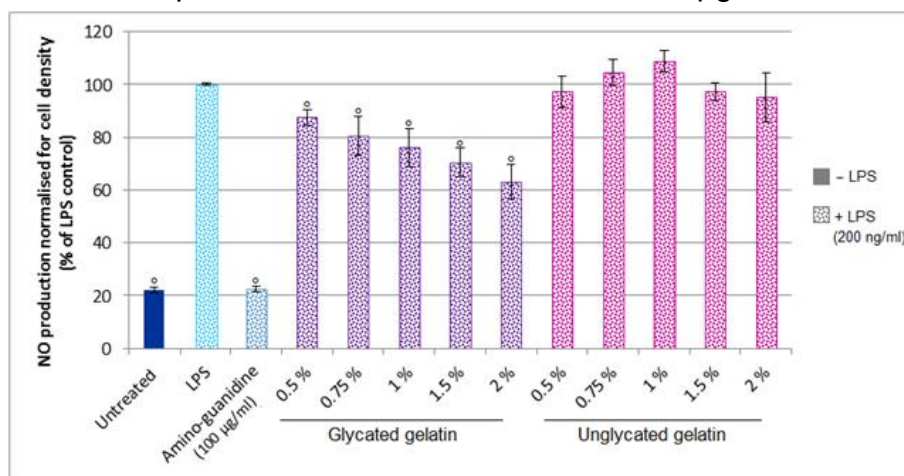
Figure 4.4: NO production of RAW 264.7 cells in response to glycated and unglycated gelatin; results are reported as means ± SD where each experiment was performed three times, each in triplicate (°p<0.05; °°p<0.01; °°°p<0.005 compared to LPS stimulated cells).

From figure 4.4 it can be seen that there is a seemingly dose-dependent inhibition of LPS induced NO production as the concentration of the glycated gelatin increases and the glycated gelatin is thus altering the normal response observed for the LPS treated cells. No significant differences in NO production were observed for the unglycated gelatin, indicating that this is dependent on glycation.

4.1.4. Nitric oxide scavenging activity

Considering that an attenuation in NO levels may be the result of direct scavenging of NO, the nitric oxide scavenging ability of the glycated and unglycated gelatin stocks was assessed and the results presented in figure 4.5. Amino-guanidine, known to function as a direct NO scavenger, was used as a positive control in this

experiment and statistical analysis was performed relative to the sodium nitroprusside control.
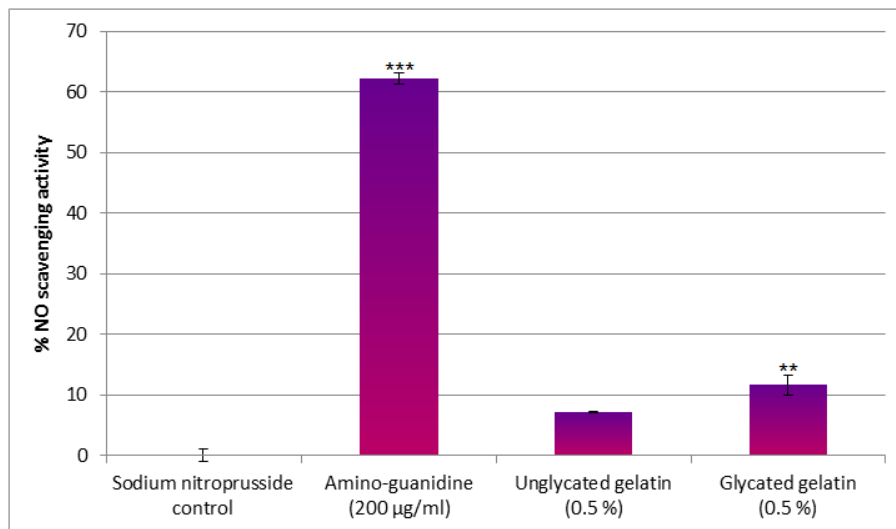
Figure 4.5: <u>NO scavenging activity of glycated and unglycated gelatin; results are reported as means ± SD where each experiment was performed three times, each in triplicate (*p<0.05; **p<0.01;***p<0.005 compared to sodium nitroprusside control).</u>

Compared to the sodium nitroprusside control, glycated gelatin revealed significant NO scavenging capabilities (p<0.01) (figure 4.5) while no scavenging effects were reported for the unglycated gelatin. These results suggest that the effect of glycated gelatin on the NO production of LPS induced cells (figure 4.4) might be due to NO scavenging rather than anti-inflammatory activity. Relative to amino-guanidine, however, both the 0.5 % unglycated and glycated gelatin possess minimal NO scavenging capabilities.

4.1.5. Phagocytosis

The phagocytic capability of RAW 264.7 macrophage-like cells was assessed using the pHrodo® Green *E. coli* BioParticles® Conjugate together with LysoTracker Red® (LTR). Examples of the fluorescent micrographs that were captured are shown in figure 4.6. Using the MetaXpress® software, the mean stain area of the pHrodo® Bioparticles® inside the RAW 264.7 cells was calculated and thus an increase in the mean stain area suggests an increase in the number of particles phagocytosed. The untreated sample consisted of high-glucose DMEM supplemented with 10 % FBS and all samples were calculated as a percentage of this control (figure 4.7). Cytochalasin B, a microtubule inhibitor, was used to inhibit phagocytosis while LPS was included as a positive control to promote phagocytosis.
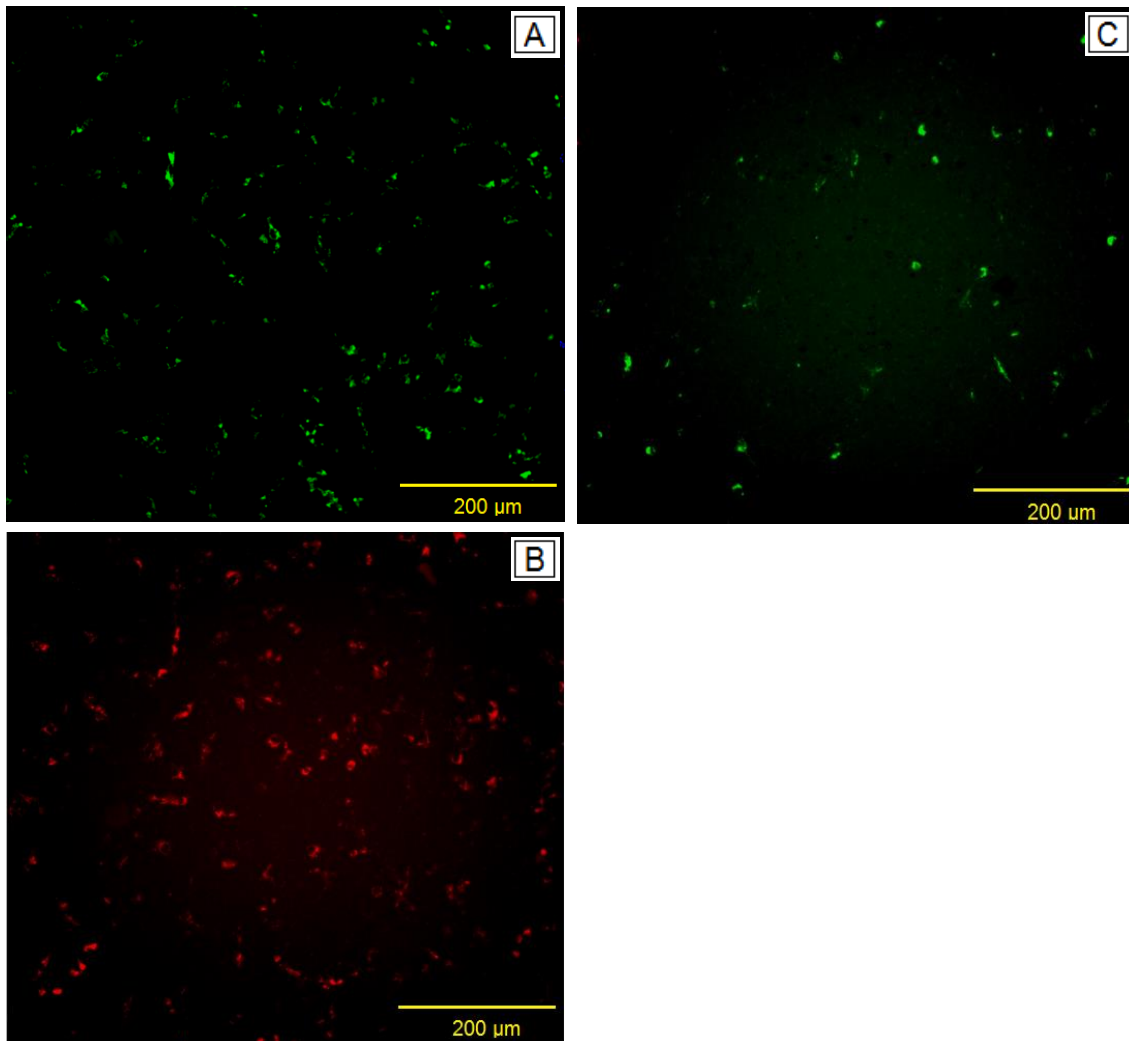
Figure 4.6: Fluorescent micrographs captured during the phagocytosis assay comparing the (A) untreated sample stained with pHrodo$^{®}$ Bioparticles$^{®}$ with (B) untreated sample stained with LTR and (C) 0.5 % glycated gelatin sample stained with pHrodo$^{®}$ Bioparticles$^{®}$ after a 2 hour incubation period.

From figure 4.6 it is clear that there were much fewer pHrodo$^{®}$ Bioparticles$^{®}$ phagocytosed by the cells that were treated with 0.5 % glycated gelatin. While a decrease in macrophage cell number in response to treatment with 0.5 % glycated gelatin was observed in figure 4.3 after a 48 hour treatment period, it is not likely that the same effect would be observed here due to a much shorter incubation period of only 24 hours. The decrease in the number of pHrodo$^{®}$ Bioparticles$^{®}$ phagocytosed between figures A and B are thus due to an impairment in the phagocytic capability of the macrophages in response to treatment with glycated gelatin rather than a decrease in cell number.
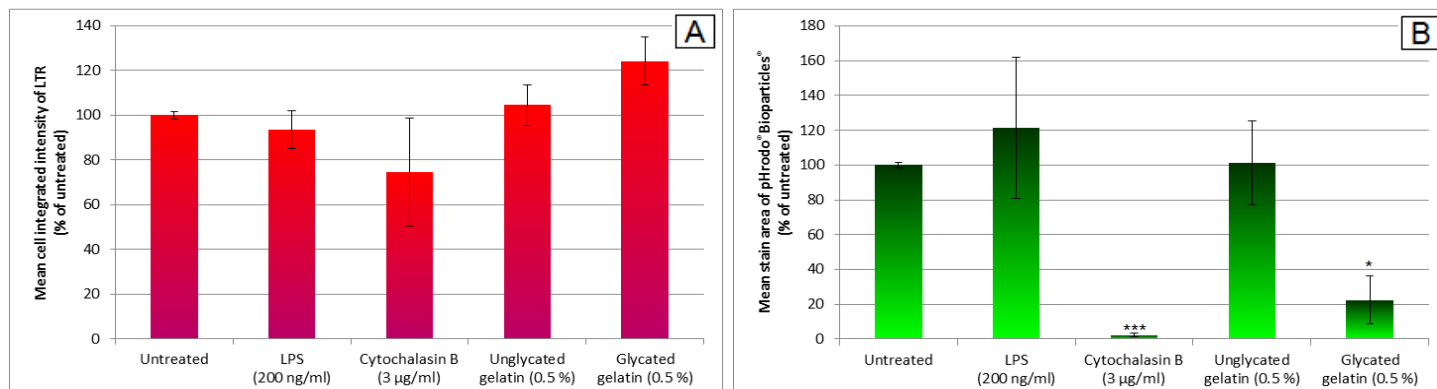
Figure 4.7: Effect of gelatin on RAW 264.7 cell phagocytosis measuring (A) acidic vacuole formation using LysoTracker Red® and (B) phagocytosis using pHrodo® Bioparticles®; results are reported as means ± SD where each experiment was performed three times, each in triplicate (*p<0.05; **p<0.01; ***p<0.005 compared to the untreated sample).

Figure 4.7 shows that while there were no significant differences in acidic vacuole content of the RAW 264.7 cells amongst the different treatments, there was significantly less phagocytosis in the cells treated with Cytochalasin B and glycated gelatin. The standard deviations were fairly large when the results for all three independent experiments were combined, however, individual experiments shown in appendix C show that standard deviations were much smaller. In all three individual experiments, the 0.5 % glycated gelatin resulted in a significant increase in acidic vacuole formation with varying trends for the remaining treatments.

4.1.6. Classical (M1) and alternative (M2) macrophage polarization

M1 and M2 macrophage polarization using RAW 264.7 macrophages was assessed using antibodies for the CD86 and CD206 cell-surface markers, respectively. Examples of the micrographs that were captured are shown in figure 4.8 while the experimental results are shown in figure 4.9. The untreated sample consisted of high-glucose DMEM supplemented with 10 % FBS and all samples were calculated as a percentage of this control. LPS was used as a positive control for M1 activation while curcumin was used as a positive control for M2 activation (Gao *et al.*, 2015).
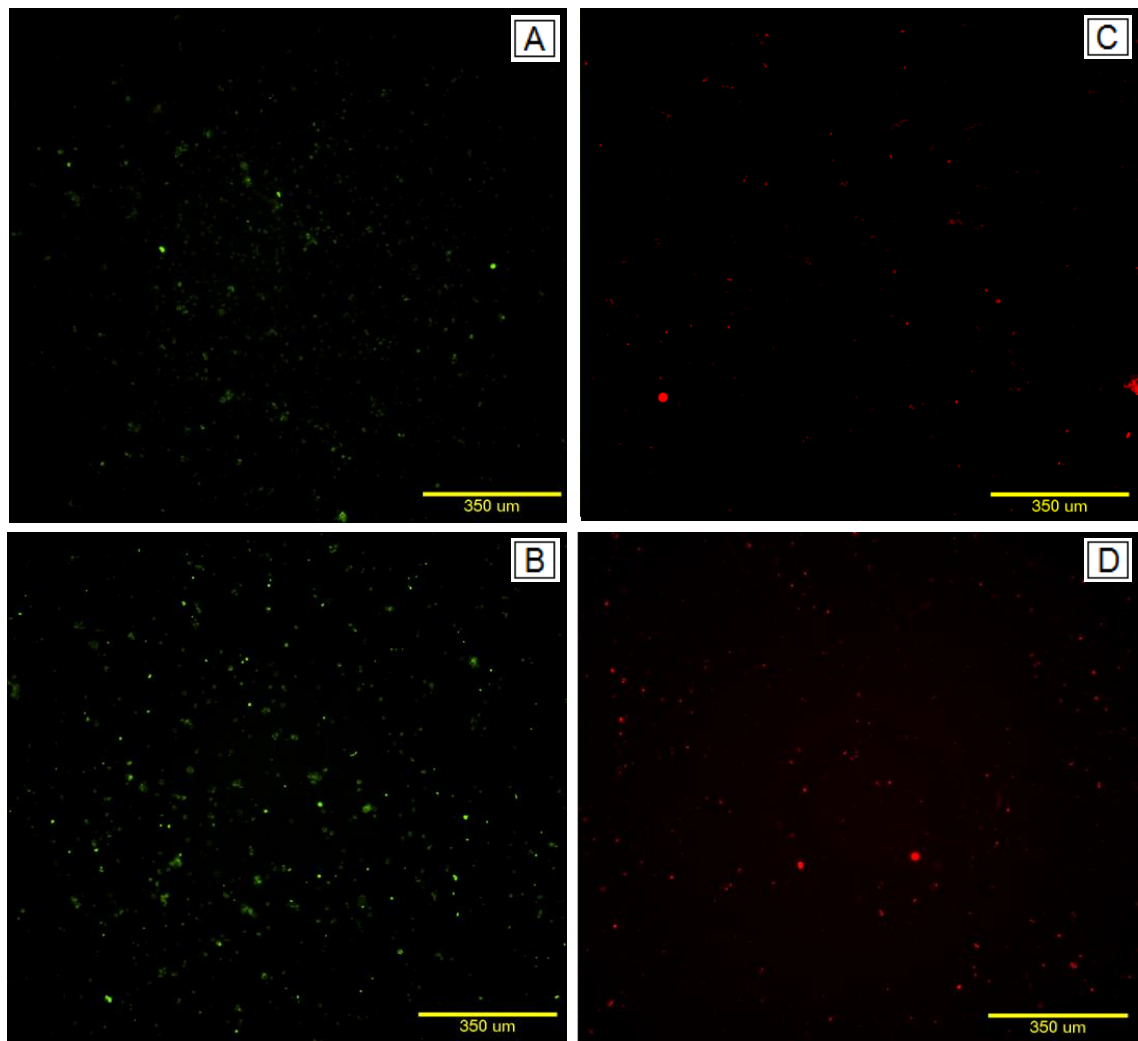
Figure 4.8: <u>Fluorescent micrographs captured during the macrophage polarization assay comparing (A) untreated sample stained with CD86 (M1) with (B) LPS stained with CD86 (M1) and (C) untreated sample stained with CD206 (M2) with (D) curcumin stained with CD206 (M2).</u>

From figure 4.8 it is evident that there was an increase in the number of cells that were stained positive for both the M1 and M2 cell surface markers in the presence of LPS and curcumin, respectively, when compared to the corresponding untreated samples.
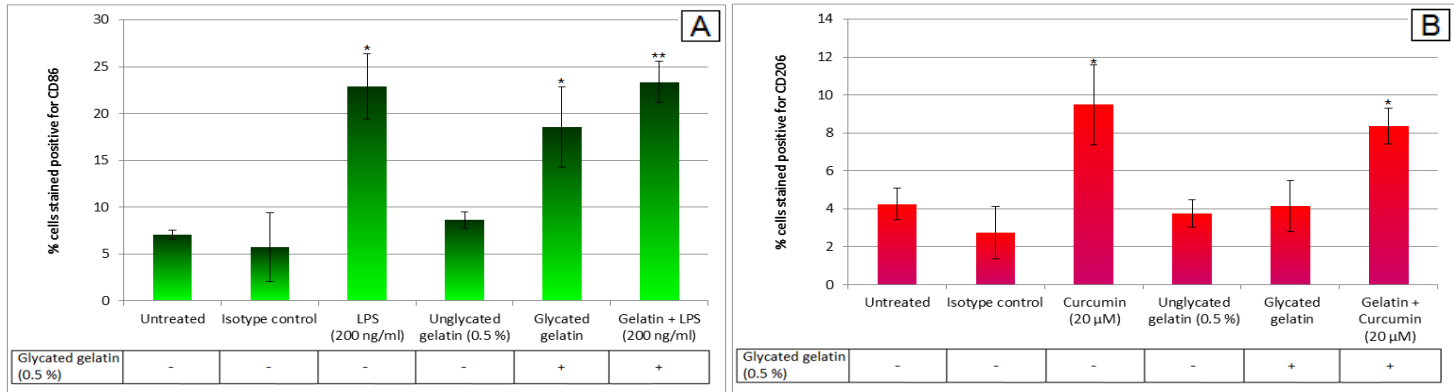
Figure 4.9: Macrophage polarization following treatment with gelatin using (A) CD86 for M1 macrophages and (B) CD206 for M2 macrophages; results are reported as means ± SD where each experiment was performed three times, each in triplicate (*$p<0.05$; **$p<0.01$; ***$p<0.005$ compared to the untreated sample).

Figure 4.9 A shows that there was a 16 % increase in the expression of CD86 for the cells treated with LPS and a 12 % increase for the cells treated with 0.5 % glycated gelatin. The expression of CD206 was more than double that of the untreated sample for the cells treated with curcumin as seen in figure 4.9 B. While the glycated gelatin alone did not increase the percentage of cells that stained positive for CD206, the addition of curcumin resulted in a two-fold increase. A slight decrease in CD206 expression was observed in the macrophages treated with both curcumin and glycated gelatin compared to cells treated with only curcumin, however, this difference was not found to be significant in any of the individual experiments (not shown) and thus glycated gelatin was not found to impair the cells' ability to become M1 or M2 macrophages.

4.1.7. NF-κB antibody staining

The nuclear translocation of phospho-p65 NF-κB in RAW 264.7 macrophages was assessed in order to confirm the effect of the glycated gelatin model on macrophage function. Examples of the micrographs captured during this experiment are shown in figure 4.10 with the experimental results depicted in figure 4.11. The untreated sample consisted of high-glucose DMEM supplemented with 10 % FBS and all samples were calculated as a percentage of this control. LPS was used as a positive control to promote NF-κB nuclear translocation.
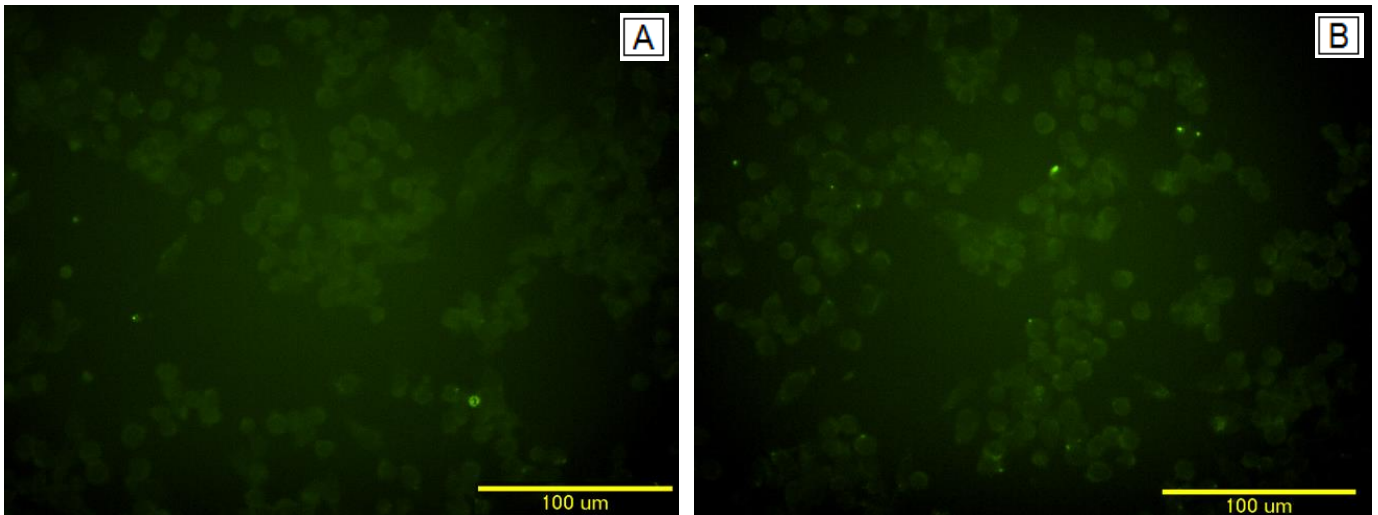
Figure 4.10: Fluorescent micrographs captured during the phospho-p65 NF-κB nuclear translocation assay comparing (A) untreated sample with (B) LPS treated sample.

While only a very small increase in the fluorescence intensity of cells treated with LPS (figure B) compared to the untreated sample (figure A) can be seen from the micrographs in figure 4.10, the MetaXpress® analysis software is sensitive enough to measure these small differences with great accuracy. The increase in fluorescence intensity in the LPS treated cells indicates that there was increased phosphorylation of the p65 subunit of NF-κB and consequent nuclear translocation.
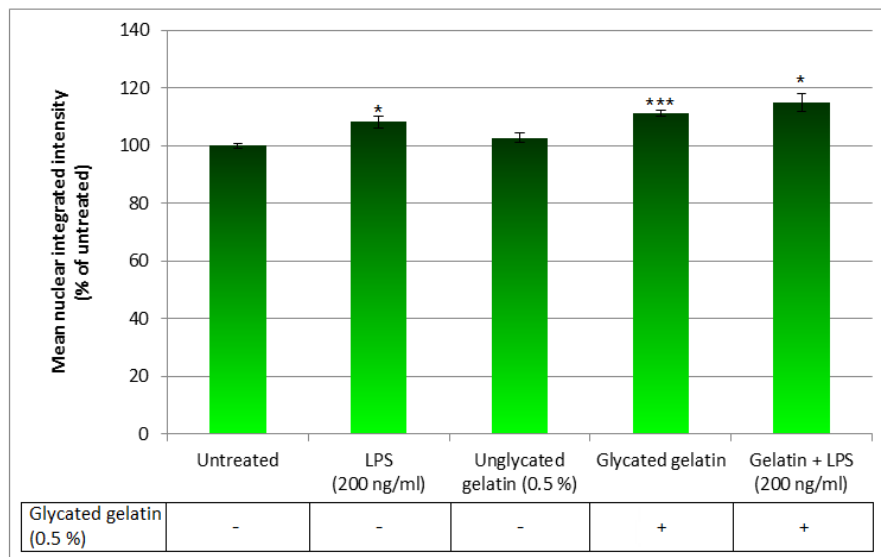
Figure 4.11: NF-κB nuclear translocation following treatment with gelatin; results are reported as means ± SD where each experiment was performed three times, each in triplicate (*p<0.05; **p<0.01; ***p<0.005 compared to the untreated sample).

The nuclear translocation of phospho-p65 NF-κB was significantly higher in cells treated with LPS than those from the untreated sample. The 0.5 % glycated gelatin also resulted in a significant increase in NF-κB nuclear translocation while the cells

75

treated with both LPS and glycated gelatin showed the highest increase of 15 % in phosph-p65 NF-κB nuclear translocation. No significant differences were reported between the samples treated with LPS and glycated gelatin or between LPS and the sample treated with both LPS and glycated gelatin.

4.1.8. COX-2 antibody staining

The ability of RAW 264.7 macrophages to express COX-2 was assessed in order to further evaluate the inflammatory status of these cells in response to different treatments. Some of the micrographs captured during this experiment are provided in figure 4.12 while the experimental results that were obtained can be found in figure 4.13. The untreated sample consisted of high-glucose DMEM supplemented with 10 % FBS while LPS was used as a positive control.
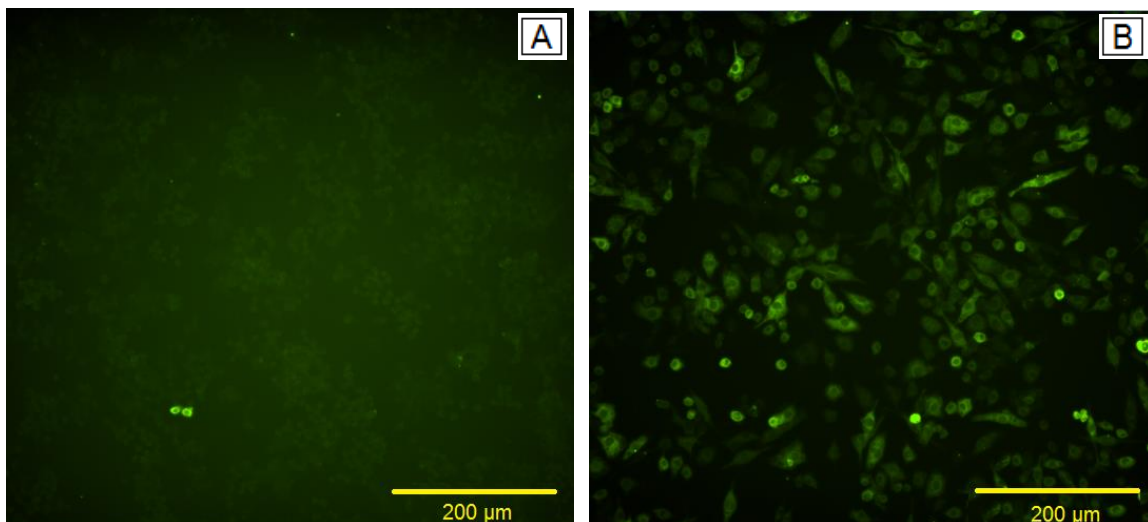
Figure 4.12: <u>Fluorescent micrographs captured during the COX-2 assay comparing (A) untreated sample with (B) 200 ng/ml LPS treated sample.</u>

Figure 4.12 shows that there is a robust increase in the expression and consequent synthesis of COX-2 in RAW 264.7 macrophages treated with 200 ng/ml LPS for 24 hours.
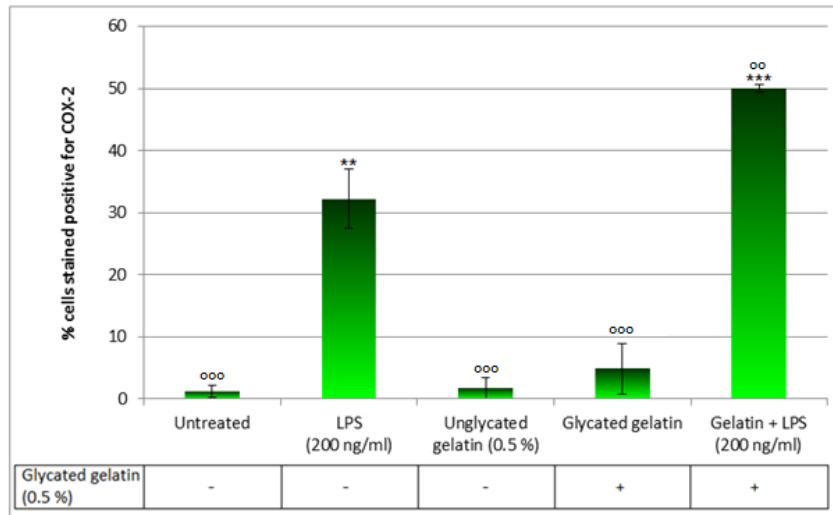
Figure 4.13: <u>COX-2 antibody staining following treatment with gelatin; results are reported as means ± SD where each experiment was performed three times, each in triplicate (*/°p<0.05; **/°°p<0.01; ***/°°°p<0.005 where *compared to the untreated sample and ° compared to LPS).</u>

Cells treated with LPS showed a 31 % increase in the expression of COX-2 as seen in figure 4.13. While neither the unglycated nor the glycated gelatin samples alone resulted in any significant changes with regards to the percentage of cells stained positive for COX-2, cells treated with both 200 ng/ml and 0.5 % glycated gelatin resulted in a robust increase in COX-2 expression of 49 %, a value significantly higher ($P<0.01$) than treatment with LPS alone.

4.1.9. Fibroblast proliferation

The effect of both glycated and unglycated gelatin on MRHF fibroblast proliferation was assessed in order to gain a better understanding of the possibilities and limitations of the glycated gelatin model with regards to adequately mimicking the diabetic state. Hoechst 33342 and PI staining was used as in section 4.1.2 and the images captured were analysed using MetaXpress® software. The untreated sample consisted of low-glucose DMEM supplemented with 1 % FBS and represented 100 % proliferation with all the other samples calculated as a percentage of this control as demonstrated in figure 4.14. The 10 % FBS sample was used as a positive control.
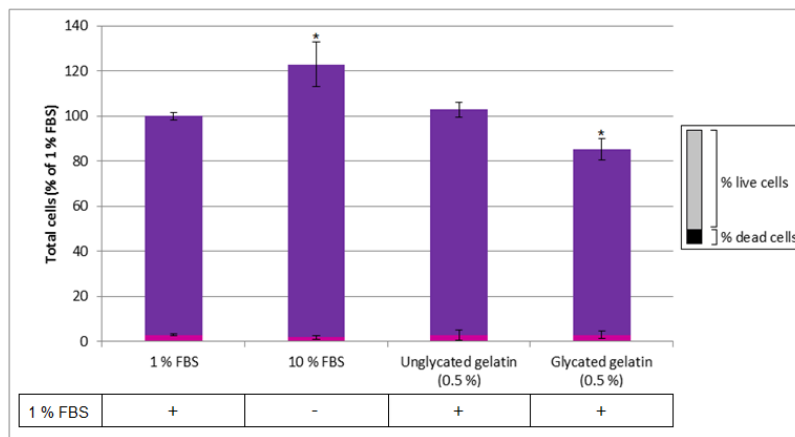
Figure 4.14: MRHF fibroblast proliferation in response to gelatin; results are reported as means ± SD where each experiment was performed three times, each in triplicate (*$p<0.05$; **$p<0.01$; ***$p<0.005$ compared to 1 % FBS).

From figure 4.14 it can be seen that there was a significant increase in fibroblast proliferation in the presence of 10 % FBS. Treatment with unglyated gelatin did not appear to influence fibroblast proliferation, however, the 0.5 % glycated gelatin significantly impaired fibroblast proliferation when compared to the 1 % FBS control.

4.1.10. Fibroblast migration

MRHF fibroblast migration was assessed using the Enzo® Cell Migration Assay kit and the experimental results are reported in figure 4.15. After the fibroblasts were treated with both mitomycin-C and the specified treatments, they were allowed to migrate for 48 hours. The untreated control consisted of low-glucose DMEM supplemented with 10 % FBS. The images that were captured were analysed using TScratch software and the values obtained were used to calculate the percentage wound closure.
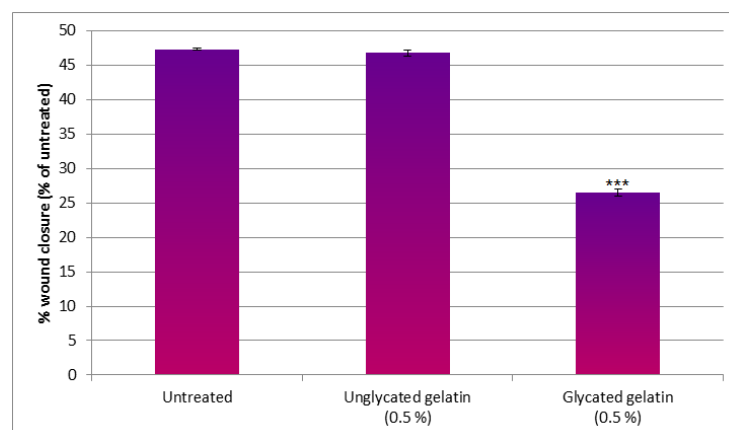
Figure 4.15: MRHF fibroblast migration in response to gelatin after 48 hours; results are reported as means ± SD where each experiment was performed three times, each in triplicate (*$p<0.05$; **$p<0.01$; ***$p<0.005$ compared to untreated sample).

78

It is evident from figure 4.16 that while the unglycated gelatin did not result in any significant changes in migration when compared to the untreated control, the 0.5 % glycated gelatin significantly impaired fibroblast migration (P<0.005).

4.2. SCREENING OF EXTRACTS FOR POTENTIAL WOUND HEALING PROPERTIES

Basal cytotoxicity screening was performed in order to ensure that the selected concentrations of each mushroom extract did not induce significant cell death. Additionally, the anti-oxidant, glycation inhibition and collagenase inhibition potential of each extract was assessed to investigate the potential benefits of each extract in combating the oxidative stress, formation of AGEs and elevated levels of MMPs in diabetes.

4.2.1 Cytotoxicity screening

Basal cytotoxicity screening was performed on both RAW 264.7 macrophages and MRHF fibroblasts. Cell numbers were determined using Hoechst 33342/ PI staining while the crystal violet assay was performed to assess cell density in an attempt to compare the accuracy of both methods.

Figure 4.16 shows examples of the fluorescent micrographs that were captured during this experiment while figures 4.17 to 4.21 compare the results of the cytotoxicity screening assays on the macrophages and fibroblasts for each of the five mushroom species used throughout thus study. The untreated sample consisted of DMEM supplemented with 10 % FBS and represents 100 % cell density. All treatments were calculated as a percentage of this control.
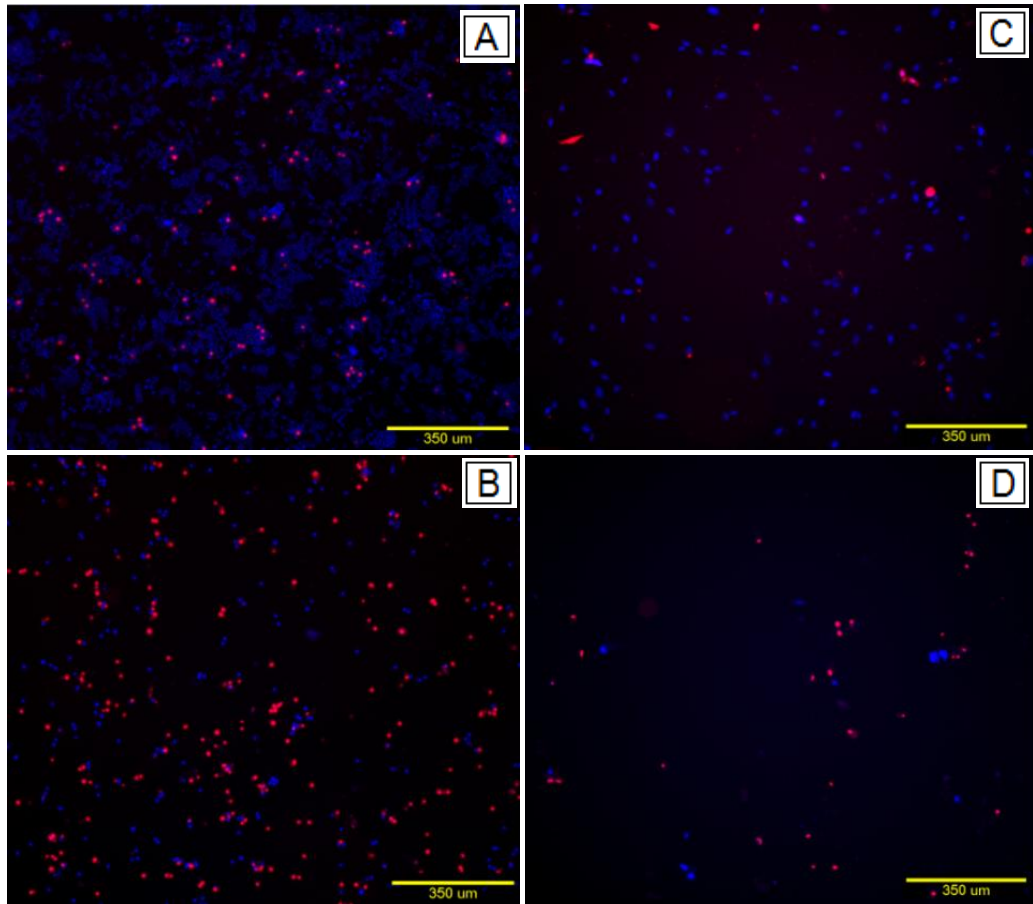
Figure 4.16: <u>Fluorescent micrographs captured during the cytotoxicity screening assay comparing (A) untreated sample with (B) 100 µg/ml ethanol extract of *G. lucidum* for RAW 264.7 cells and (C) untreated sample with (D) 100 µg/ml ethanol extract of G*. lucidum* for the MRHF fibroblasts using Hoechst 33342 (blue) and propidium iodide (red).</u>

Figure 4.16 provides an example of a cytotoxic extract where the cell numbers are greatly reduced and the number of dead cells stained positive for PI is increased.
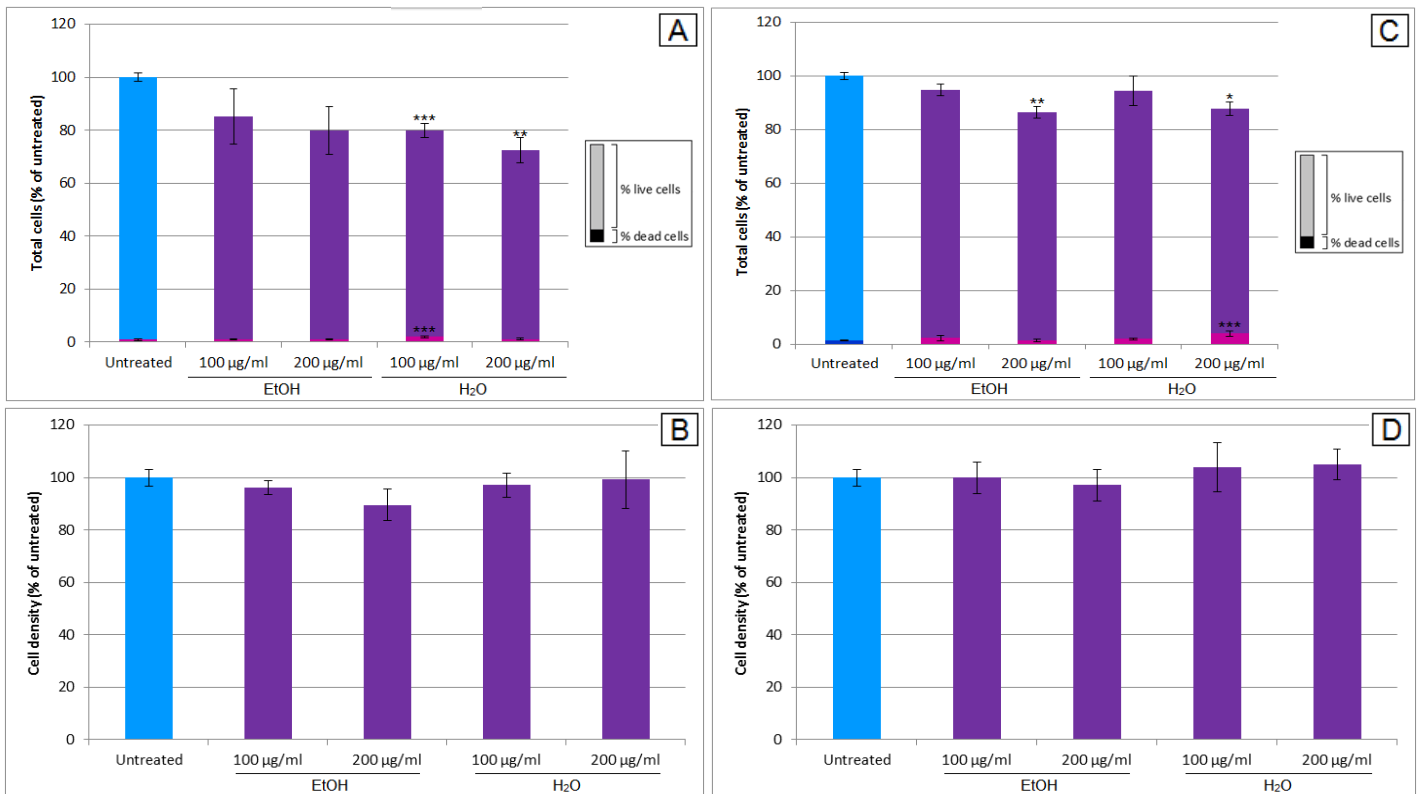
Figure 4.17: <u>Cytotoxicity screening of *P. tinctorius* comparing (A) cell number with (B) cell density for RAW 264.7 cells and (C) cell number with (D) cell density for MRHF cells; live- and dead cell numbers were obtained from Hoechst 33342 and PI staining, respectively and cell density from crystal violet staining. Results are reported as means ± SD where each experiment was performed three times, each in triplicate (*$p<0.05$; **$p<0.01$; ***$p<0.005$ compared to untreated sample).</u>

Figure 4.17 shows that there was a significant decrease in RAW 264.7 cell number for both concentrations of the water extract of *P. tinctorius* with a significant increase in cell death ($p<0.005$) at 100 µg/ml. A significant decrease in MRHF cell number was observed at 200 µg/ml for both the water and ethanol extracts with a significant increase ($p<0.005$) in cell death at 200 µg/ml for the water extract. No decrease in cell density was observed for either the water or the ethanol extracts in the crystal violet assay for either cell line.
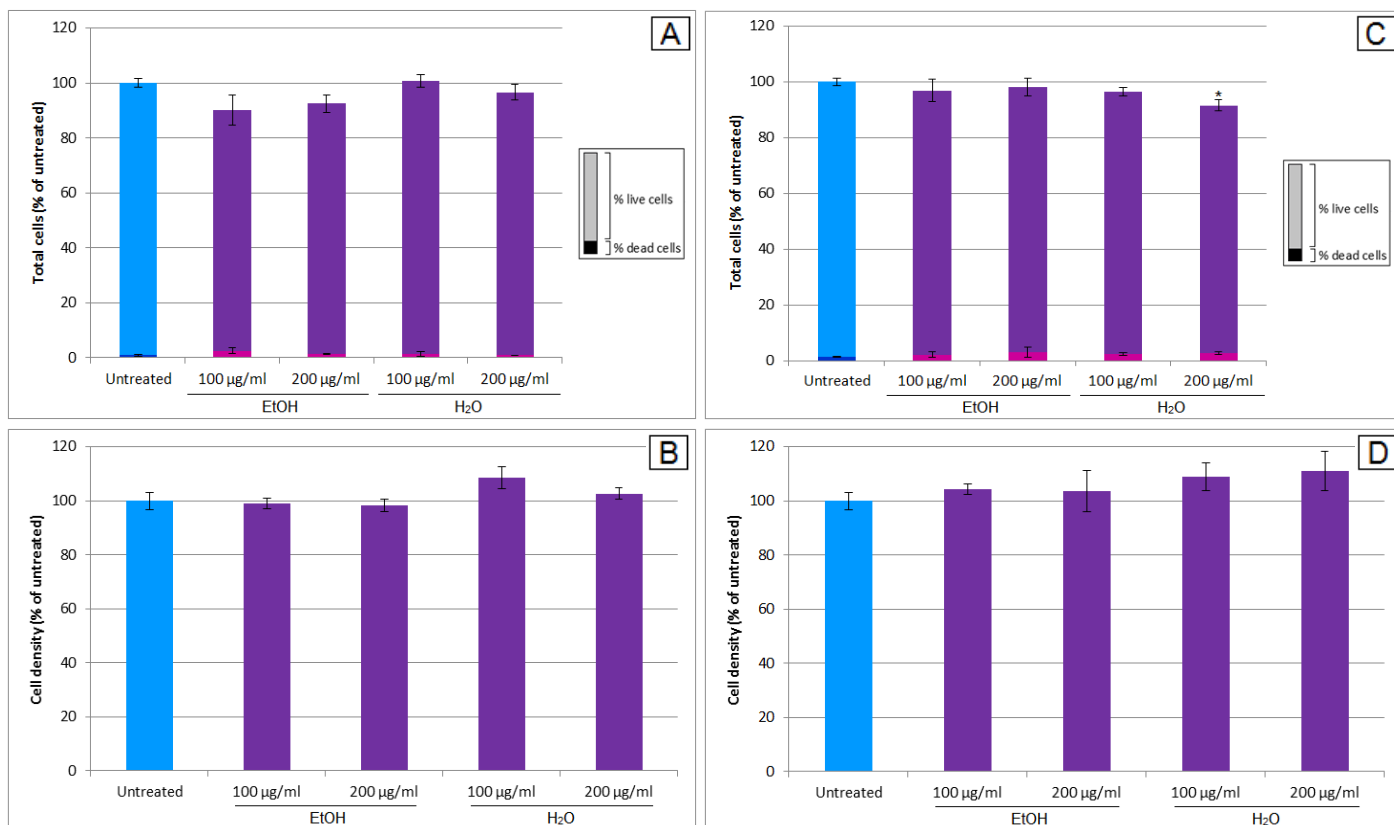
Figure 4.18: <u>Cytotoxicity screening of *R. capensis* comparing (A) cell number with (B) cell density for RAW 264.7 cells and (C) cell number with (D) cell density for MRHF cells; live- and dead cell numbers were obtained from Hoechst 33342 and PI staining, respectively and cell density from crystal violet staining. Results are reported as means ± SD where each experiment was performed three times, each in triplicate (*p<0.05; **p<0.01; ***p<0.005 compared to untreated sample).</u>

No significant cytotoxicity was observed for either the ethanol or the water extract of *R. capensis* up to a concentration of 200 µg/ml for the RAW 264.7 cells (figure 4.18). A significant decrease (p<0.05) in MRHF cell number was observed for the 200 µg/ml water extract of *R. capensis* while no significant alterations to cell density were observed for either cell line.
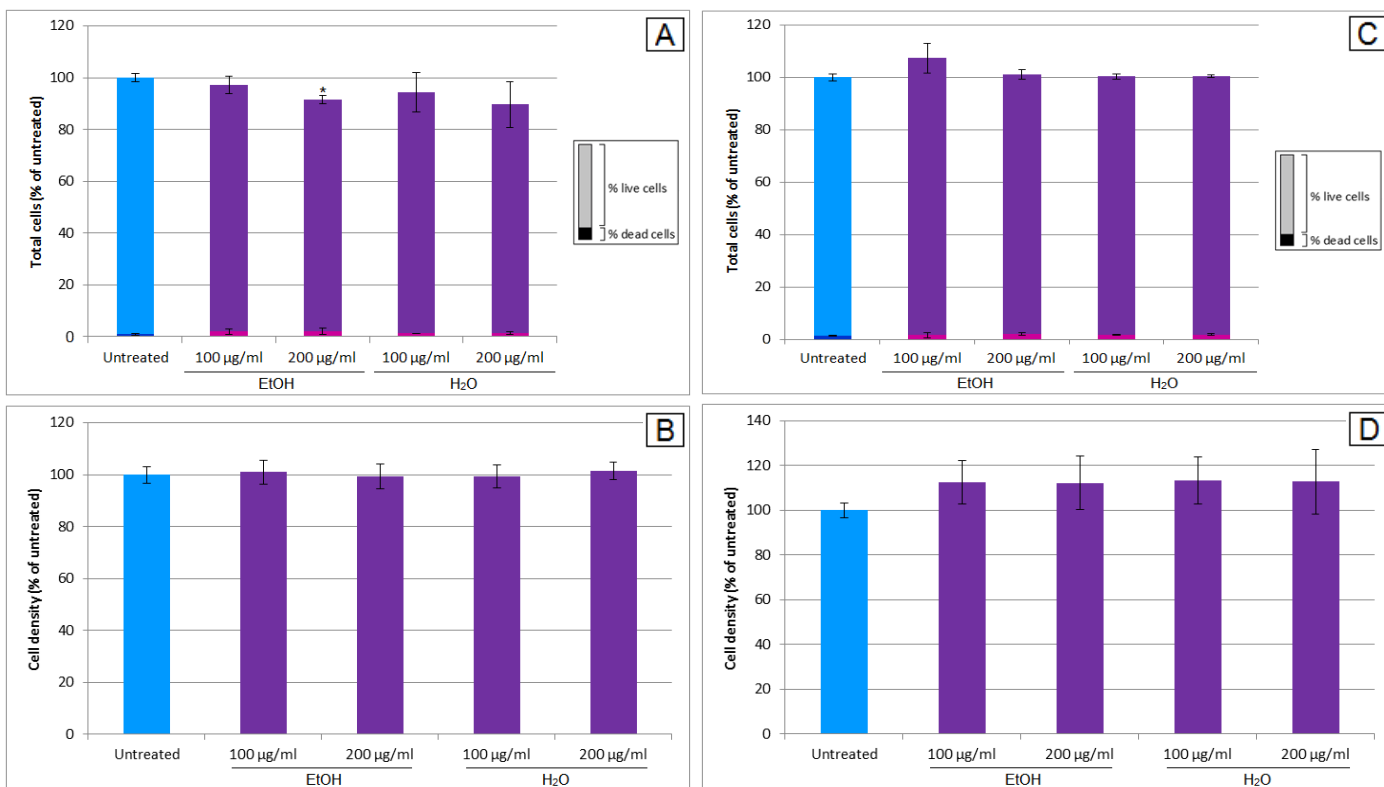
Figure 4.19: Cytotoxicity screening of *B. badius* comparing (A) cell number with (B) cell density for RAW 264.7 cells and (C) cell number with (D) cell density for MRHF cells; live- and dead cell numbers were obtained from Hoechst 33342 and PI staining, respectively and cell density from crystal violet staining. Results are reported as means ± SD where each experiment was performed three times, each in triplicate (*p<0.05; **p<0.01; ***p<0.005 compared to untreated sample).

It is evident form figure 4.19 that there is a significant decrease (p<0.05) in RAW 264.7 cell number for the 200 µg/ml ethanol extract of *B. badius*. No cytotoxicity was observed for the MRHF cells and there were no significant changes in cell death or cell density for either cell line.
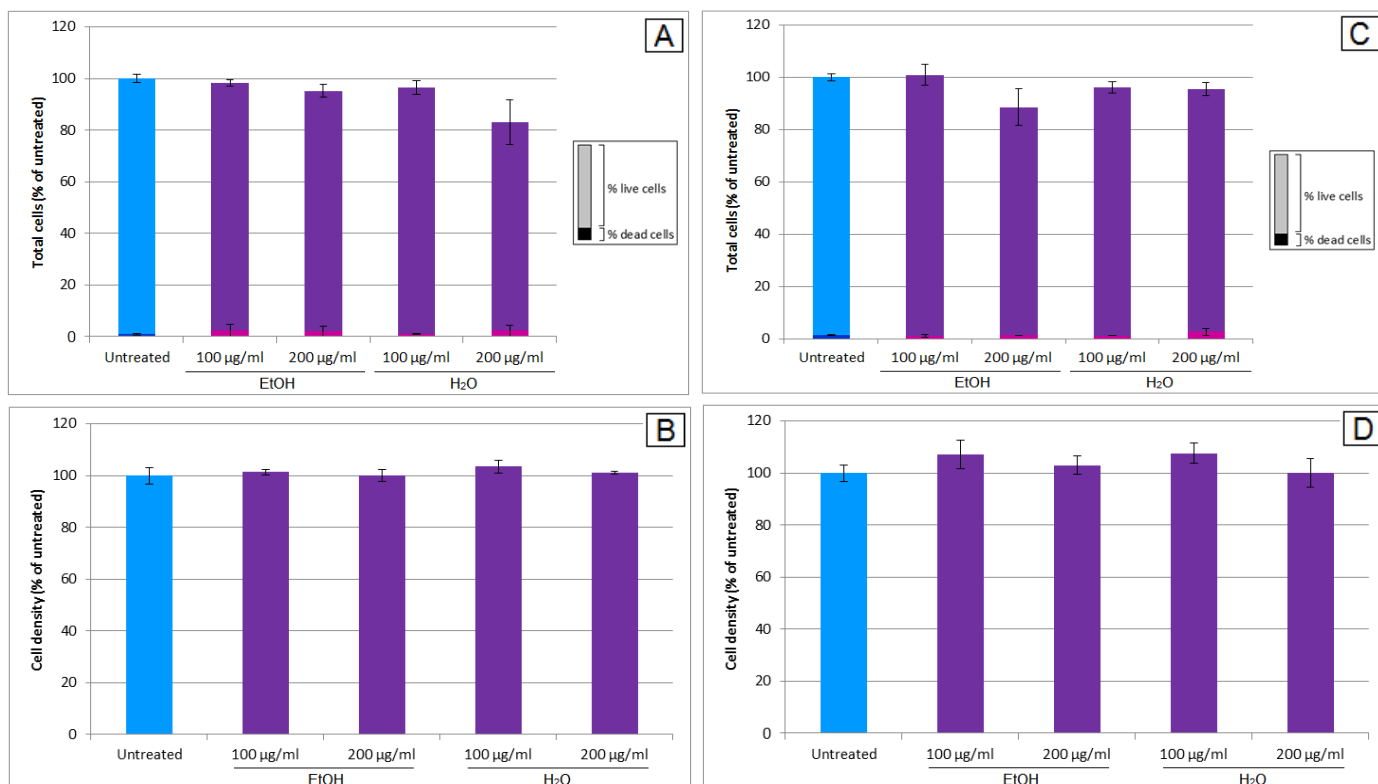
Figure 4.20: Cytotoxicity screening of *P. ostreatus* comparing (A) cell number with (B) cell density for RAW 264.7 cells and (C) cell number with (D) cell density for MRHF cells; live- and dead cell numbers were obtained from Hoechst 33342 and PI staining, respectively and cell density from crystal violet staining. Results are reported as means ± SD where each experiment was performed three times, each in triplicate (*$p<0.05$; **$p<0.01$; ***$p<0.005$ compared to untreated sample).

According to figure 4.20, no significant alterations in cell number, cell death or cell density were reported for the water or ethanol extracts of *P. ostreatus* for both RAW 264.7 cells and MRHF cells. This mushroom species thus did not show any cytotoxicity.
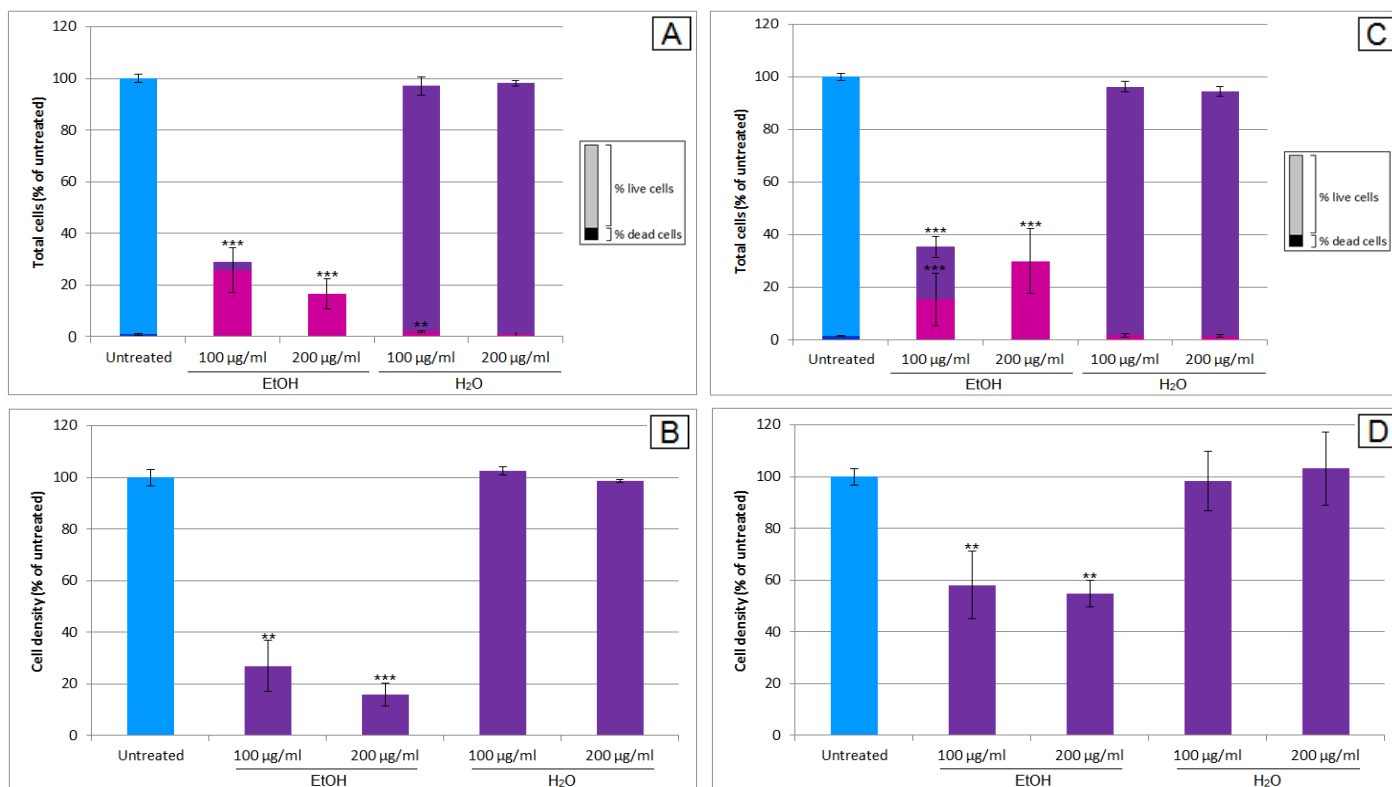
Figure 4.21: Cytotoxicity screening of *G. lucidum* comparing (A) cell number with (B) cell density for RAW 264.7 cells and (C) cell number with (D) cell density for MRHF cells; live- and dead cell numbers were obtained from Hoechst 33342 and PI staining, respectively and cell density from crystal violet staining. Results are reported as means ± SD where each experiment was performed three times, each in triplicate (*p<0.05; **p<0.01; ***p<0.005 compared to untreated sample).

A highly significant dose-dependent decrease in cell number and cell density were observed for the ethanol extract of *G. lucidum* in figure 4.21. This was accompanied by a robust increase in cell death for both RAW 264.7 and MRHF cells. No significant cytotoxicity was observed for the water extract in either cell line during the Hoechst 33342/PI method or the crystal violet assay.

4.2.2. Anti-oxidant activity

Due to the association of oxidative stress with impaired wound healing, the anti-oxidant capacity of each mushroom extract was assessed using the FRAP, DPPH and NO scavenging assays. The selection of these assays was based on the fact that each of them have been associated with different anti-oxidant activities due to the nature of the experimental conditions and thus by choosing three methods based on different principles, one is able to gain a better understanding of the true anti-oxidant capabilities of each of the five mushroom species.
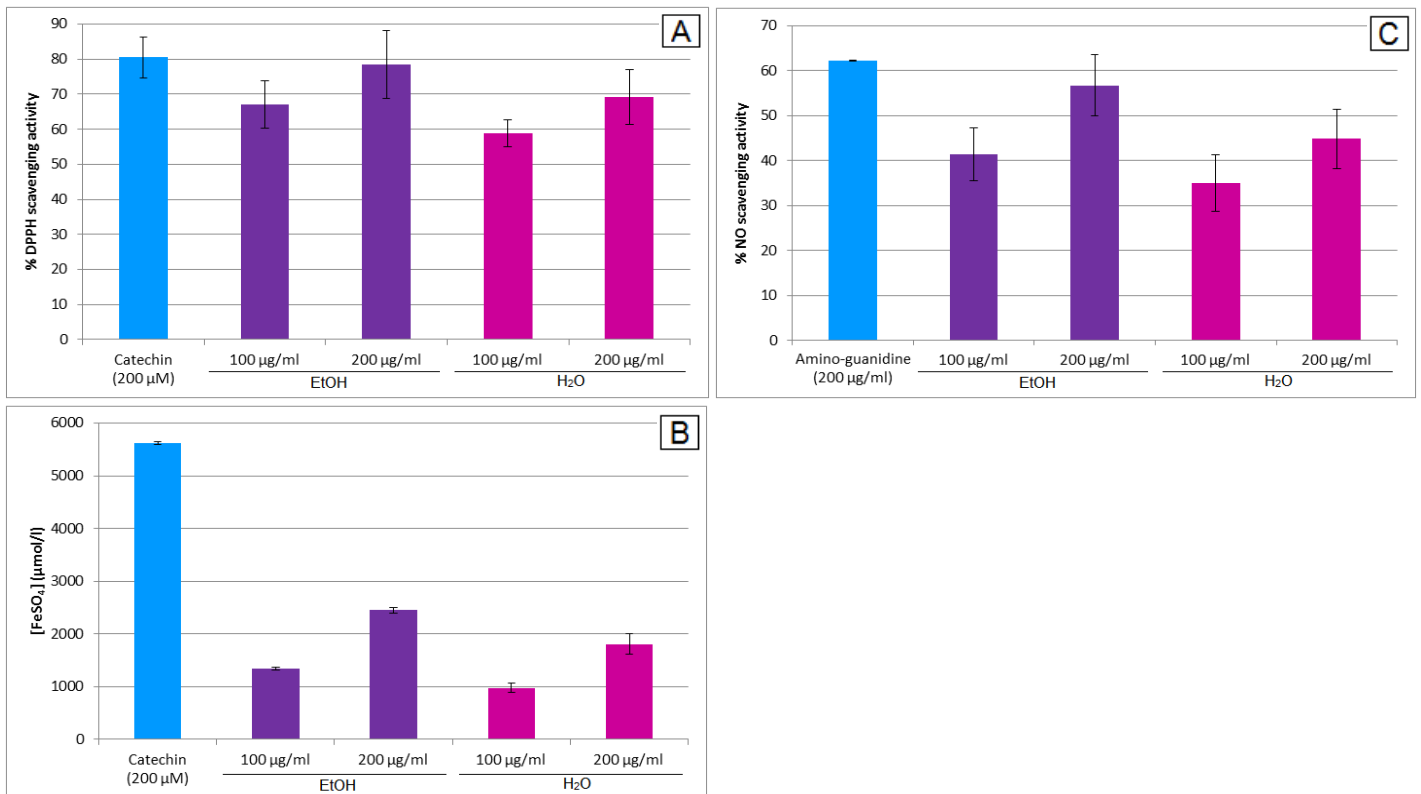
Figure 4.22: Antioxidant screening of *P. tinctorius* comparing the results from the (A) DPPH (B) FRAP and (C) NO scavenging assays; results are reported as means ± SD where each experiment was performed three times, each in triplicate.

From figure 4.22, both the water and ethanol extracts of *P. tinctorius* showed comparatively high anti-oxidant activities during the DPPH and NO scavenging assays, respectively, however, much lower anti-oxidant activities were reported during the FRAP assay in comparison to the relevant positive controls. The IC_{50} values for the DPPH and NO scavenging assays appear to be below 100 μg/ml for the DPPH assay and between 100 and 200 μg/ml for the NO scavenging assay. As these values are fairly high and consequently do not suggest much promise for significant physiological effects, the IC_{50} values were not calculated.
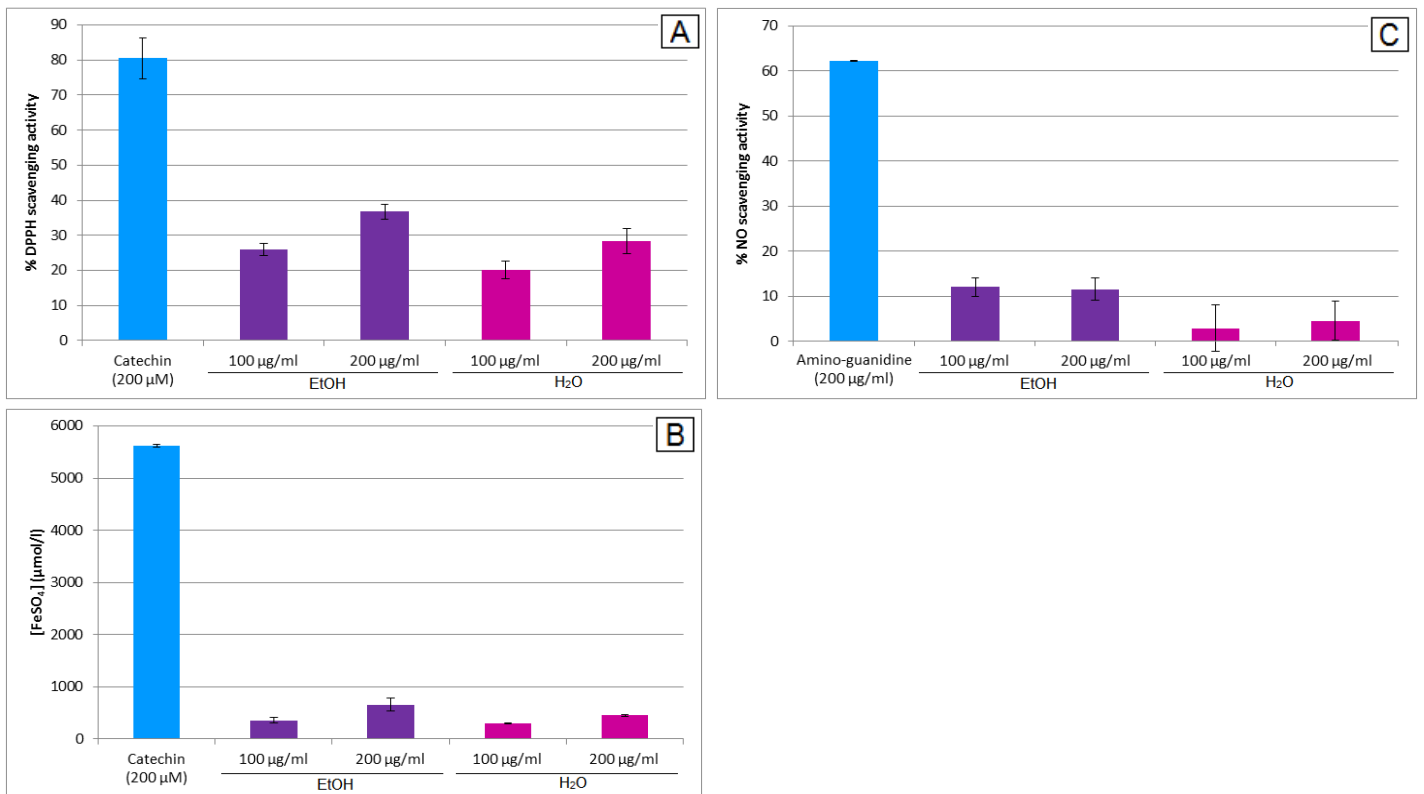
Figure 4.23: Antioxidant screening of *R. capensis* comparing the results from the (A) DPPH (B) FRAP and (C) NO scavenging assays; results are reported as means ± SD where each experiment was performed three times, each in triplicate.

Comparatively low anti-oxidant activities for both the water and ethanol extracts of *R. capensis* were reported during all three anti-oxidant screening assays (figure 4.23). The highest anti-oxidant activities of 36 % for the 200 µg/ml ethanol extract and 28 % for the 200 µg/ml water extract were reported for the DPPH assay. The IC_{50} values for the DPPH and NO scavenging assays are thus above 200 µg/ml.
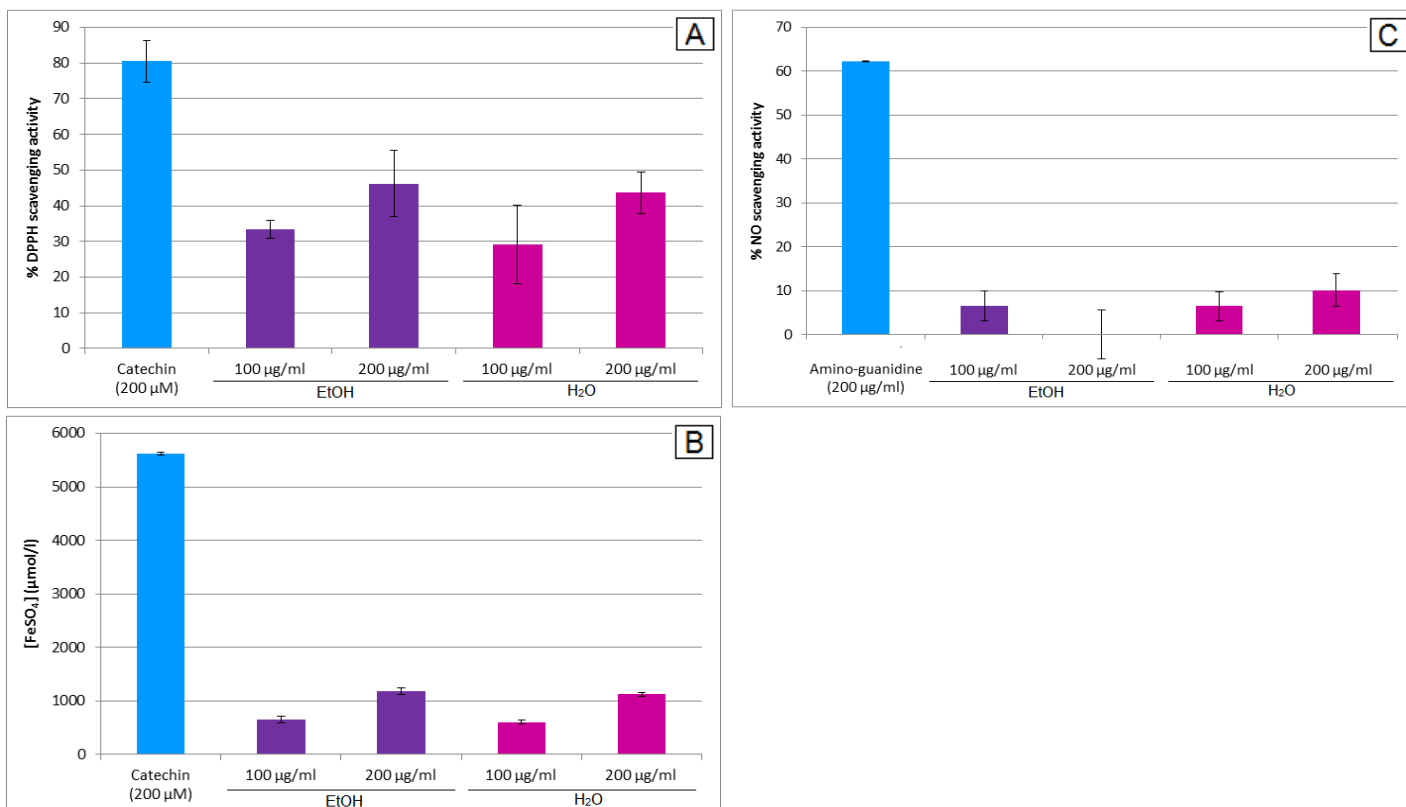
Figure 4.24: Antioxidant screening of *B. badius* comparing the results from the (A) DPPH (B) FRAP and (C) NO scavenging assays; results are reported as means ± SD where each experiment was performed three times, each in triplicate.

It is evident from figure 4.24 that the anti-oxidant capacities of the ethanol and water extracts of *B. badius* were comparatively low. While a dose-dependent increase in the anti-oxidant activity for both extracts was reported, the low values reported here do not suggest any physiological relevance. The highest activities of 46 % for the 200 µg/ml ethanol extract and 44 % for the 200 µg/ml water extract were reported for the DPPH assay.
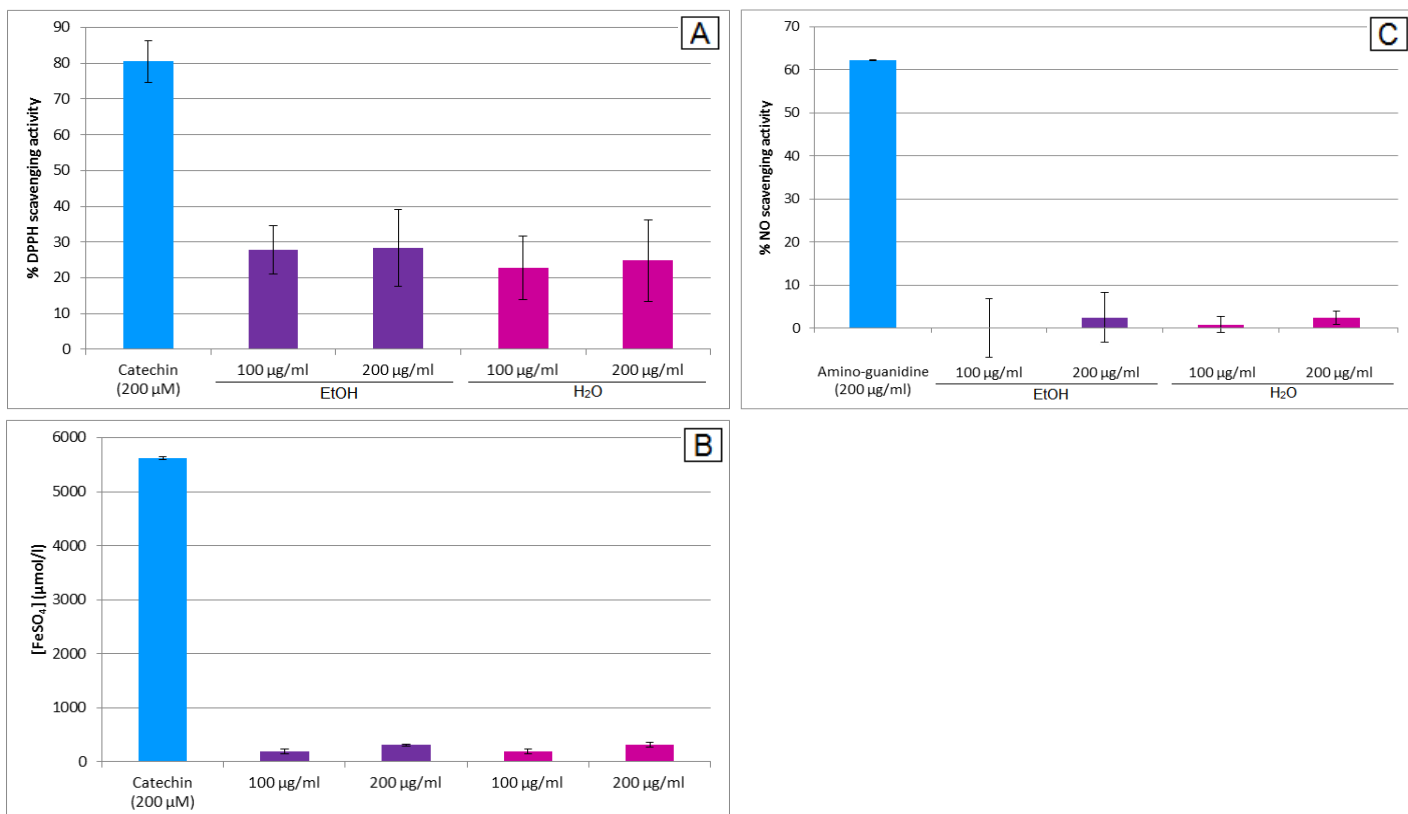
Figure 4.25: <u>Antioxidant screening of *P. ostreatus* comparing the results from the (A) DPPH (B) FRAP and (C) NO scavenging assays; results are reported as means ± SD where each experiment was performed three times.</u>

The ethanol and water extracts of *P. ostreatus* showed very low anti-oxidant activities during the DPPH assay with little to no activity during the FRAP and NO scavenging assays (figure 4.25). The highest anti-oxidant activities of 28 % for the 200 µg/ml ethanol extract and 25 % for the 200 µg/ml water extract were reported for the DPPH assay, indicating that the IC_{50} values are far above 200 µg/ml. No dose-dependent relationship between the different concentrations of either the ethanol or the water extracts for any of the assays were recorded, suggesting that *P. ostreatus* does not possess any noteworthy anti-oxidant activity.
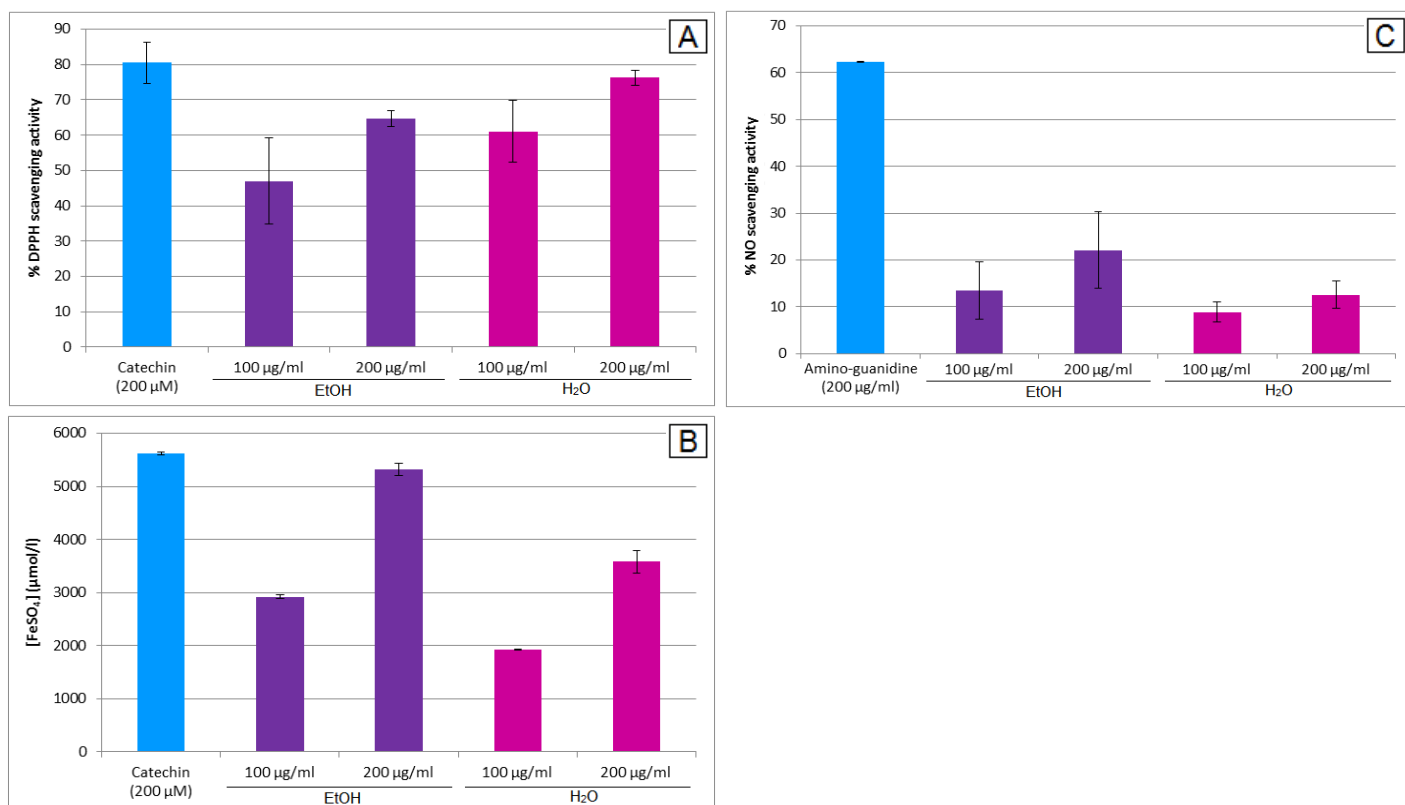
Figure 4.26: Antioxidant screening of *G. lucidum* comparing the results from the (A) DPPH (B) FRAP and (C) NO scavenging assays; results are reported as means ± SD where each experiment was performed three times.

G. lucidum showed comparatively strong anti-oxidant activities between the ethanol and water extracts during the DPPH assay with an IC_{50} value between 100 and 200 µg/ml for the ethanol extract and below 100 µg/ml for the water extract. While the 200 µg/ml ethanol extract demonstrated comparatively strong activities to the positive catechin control during the FRAP assay, the same trends were not observed during and NO scavenging assay where NO scavenging capabilities below 25 % were reported.

4.2.3. Glycation inhibition

Due to the role of AGEs in the pathogenesis of diabetes, the ability of each mushroom extract to inhibit glycation was assessed in figures 4.27 to 4.31 in order to identify a mushroom species that could serve as a potential diabetic wound healing therapy. A positive response would be demonstrated by a reduction in the relative fluorescence using the AGE excitation/emission maxima of 370/440 nm and thus false positives due to quenching were identified using pre-glycated gelatin as described in section 3.4.3. Amino-guanidine was used as a positive control for the

inhibition of the glyceraldehyde-induced glycation. The control sample consisted of unglycated gelatin (20 mg/ml) without glyceraldehyde.
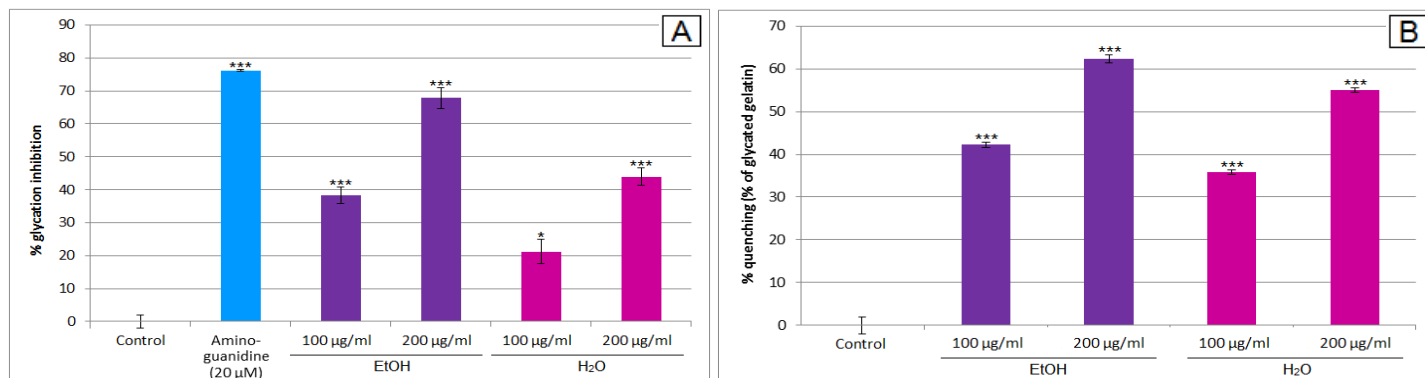
Figure 4.27: Glycation inhibition potential of *P. tinctorius* comparing (A) glycation inhibition with (B) quenching; results are reported as means ± SD where each experiment was performed three times, each in triplicate (*p<0.05; **p<0.01; ***p<0.005 compared to control sample).

Both the ethanol and water extracts of *P. tinctorius* showed significant glycation inhibitory potentials when compared to the control sample (figure 4.27). A strong dose-dependent increase in their glycation inhibition potentials was reported between the 100 and 200 µg/ml concentrations with the 200 µg/ml ethanol extract demonstrating similar capabilities for inhibiting protein glycation as the positive amino-guanidine control. Upon further investigation of potential quenching, however, significantly strong (p<0.005) quenching activities of 62 % and 55 % for the 200 µg/ml ethanol and water extracts, respectively, were reported in figure B. This suggests that most of the glycation inhibition observed in figure A was in fact due to the quenching of the intrinsic fluorescence of AGEs.
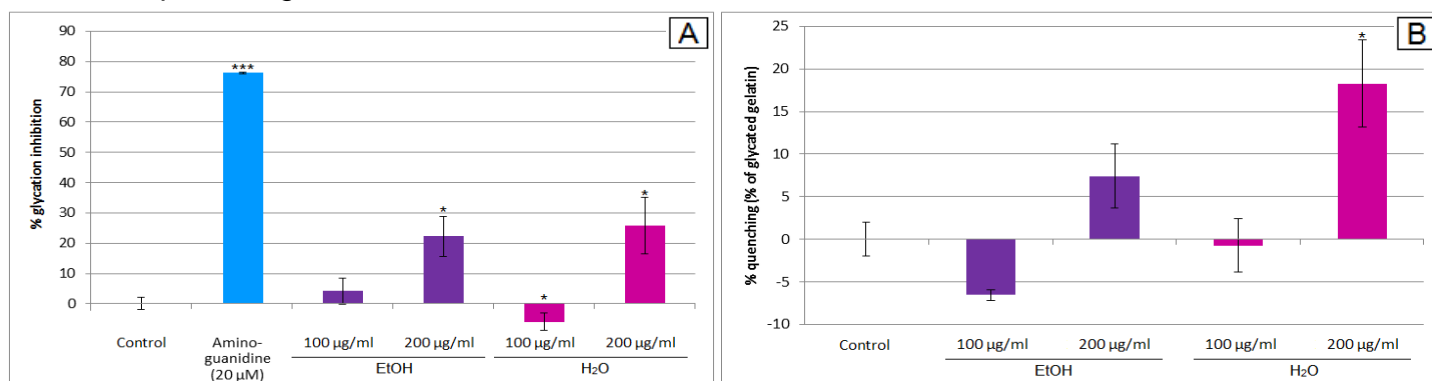
Figure 4.28: Glycation inhibition potential of *R. capensis* comparing (A) glycation inhibition with (B) quenching; results are reported as means ± SD where each experiment was performed three times, each in triplicate (*p<0.05; **p<0.01; ***p<0.005 compared to control sample).

From figure 4.28, the ethanol and water extracts of *R. capensis* showed comparatively low glycation inhibition potentials below 25 %. While the values reported for the 200 µg/ml extracts were statistically higher (p<0.05) than the control sample, significant quenching (p<0.05) of 18 % was reported for the water extract. This suggests that these results do not accurately reflect the glycation inhibition potential of *R. capensis*.
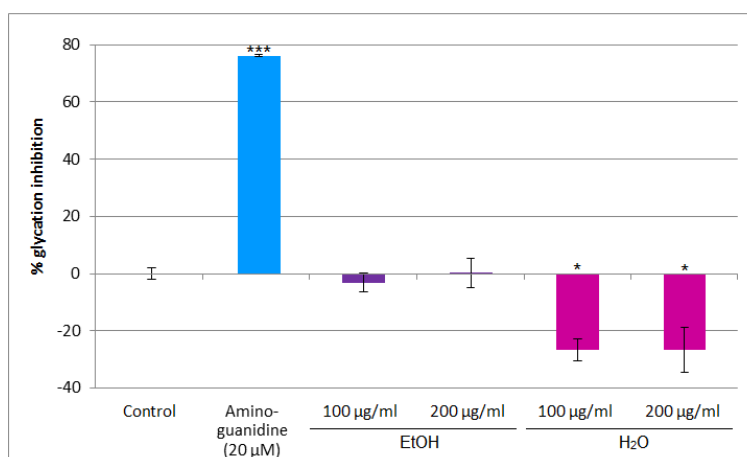
Figure 4.29: Glycation inhibition potential of *B. badius*; results are reported as means ± SD where each experiment was performed three times, each in triplicate (*p<0.05; **p<0.01; ***p<0.005 compared to control sample).

Figure 4.29 shows that *B. badius* did not show any noteworthy glycation inhibition potential with the water extract potentially acting as an inducer of glycation as evidenced by the significant increase in glycation for both the 100 and 200 µg/ml concentrations compared to the untreated sample. No significant quenching was reported (results not shown).
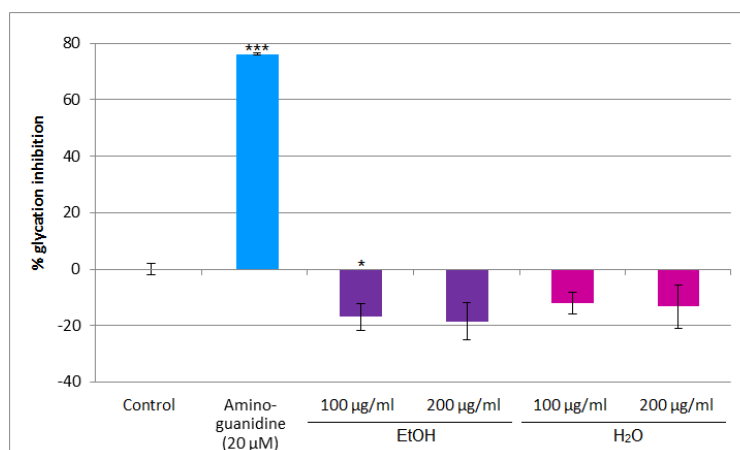
Figure 4.30: Glycation inhibition potential of *P. ostreatus*; results are reported as means ± SD where each experiment was performed three times, each in triplicate (*p<0.05; **p<0.01; ***p<0.005 compared to control sample).

Neither the ethanol nor the water extracts of *P. ostreatus* showed any significant inhibition of glycation when compared to the control sample (figure 4.30). Furthermore, no significant quenching was observed (results not shown).
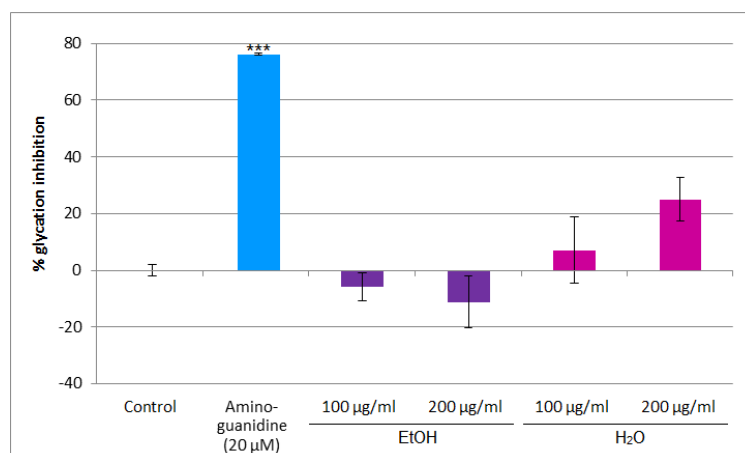
Figure 4.31: Glycation inhibition potential of *G. lucidum* comparing; results are reported as means ± SD where each experiment was performed three times, each in triplicate (*p<0.05; **p<0.01; ***p<0.005 compared to control sample).

From figure 4.31, neither the ethanol nor the water extracts of *G. lucidum* showed any statistically significant glycation inhibiton potential and no significant quenching was observed.

4.2.4. Collagenase inhibition

As diabetic wounds are characterized by the increased activity of several MMPs such as collagenase, the ability of each mushroom extract to inhibit collagenase activity in an attempt to prevent excessive ECM degradation was investigated in figure 4.33 using the collagenase enzyme isolated from *Clostridium histolyticum*. A positive inhibitory response is indicated by the formation of a protein pellet consisting of undigested gelatin which is subsequently stained with Coomassie brilliant blue. A larger pellet is associated with a darker colour, thus revealing a stronger collagenase inhibitory potential. Catechin (10 mM) was used as a positive control for collagenase inhibition and the uninhibited control sample consisted of gelatin (2 mg/ml) incubated in the absence of collagenase.
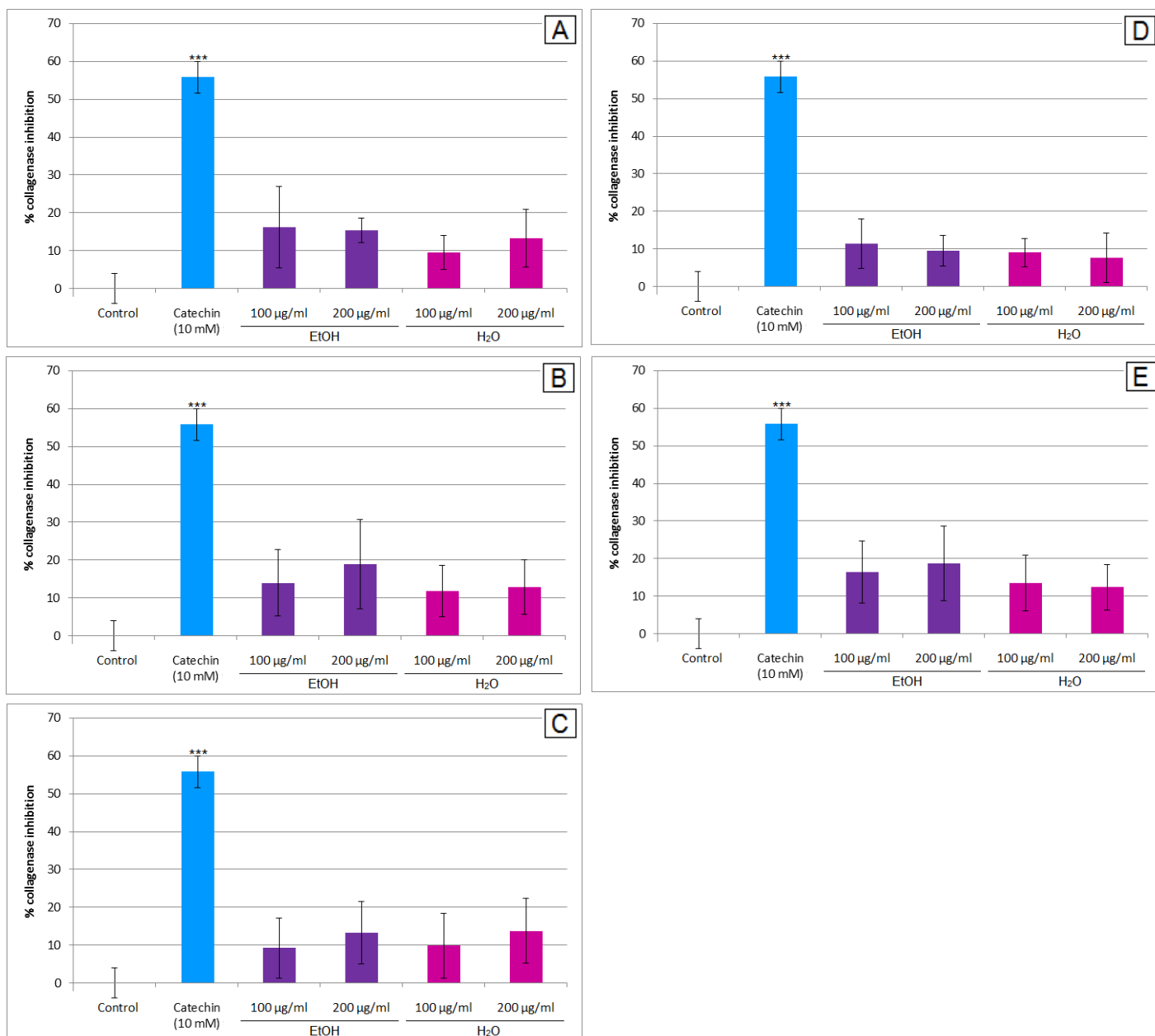
Figure 4.32: A comparison of the collagenase inhibitory potentials of (A) *P. tinctorius* (B) *R. capensis* (C) *B. badius* (D) *P. ostreatus* and (E) *G. lucidum*; results are reported as means ± SD where each experiment was performed three times, each in triplicate (*p<0.05; **p<0.01; ***p<0.005 compared to control sample).

The strong collagenase inhibition (56 %) exerted by the positive catechin control indicates that the collagenase inhibition assay was indeed functional (figure 4.32). None of the five mushroom species tested during this study resulted in any significant collagenase inhibition compared to the control sample. Consequently, none of these extracts demonstrated any promising capabilities of attenuating the increased MMP activity observed during impaired wound healing in diabetes.

4.3. THE INFLAMMATORY RESPONSE

During section 4.1, AGEs were found to reduce NO, impair macrophage phagocytosis, promote M1 macrophage activation and enhanced the nuclear translocation of NF-κB as well as the activity of COX-2 in macrophages stimulated with LPS. This reveals several potential mechanisms through which protein glycation impairs wound healing by disrupting several cellular functions during the inflammatory response. The purpose of the following section was to screen the selected mushroom samples in order to determine whether any of them were able to reverse some of the negative effects of AGEs on macrophage cell function.

4.3.1. Nitric oxide production in activated macrophages

Nitric oxide production in RAW 264.7 macrophages both in the absence and presence of LPS (200 ng/ml) was assessed using the Griess reaction (figures 4.33 to 4.37) in order to identify any pro-inflammatory or anti-inflammatory activities, respectively, in each of the selected mushroom extracts to gain a better understanding of the potential uses of these extracts during wound healing. The untreated sample consisted of high-glucose DMEM (25 mM) supplemented with 10 % FBS. LPS was used to induce NO production and thus represents the pro-inflammatory state. To assess the anti-inflammatory potential of test samples, LPS treatment alone was set to 100 % and the anti-inflammatory activity calculated as a percentage of this value. Amino-guanidine (100 μg/ml) was used as a positive control for NO inhibition.
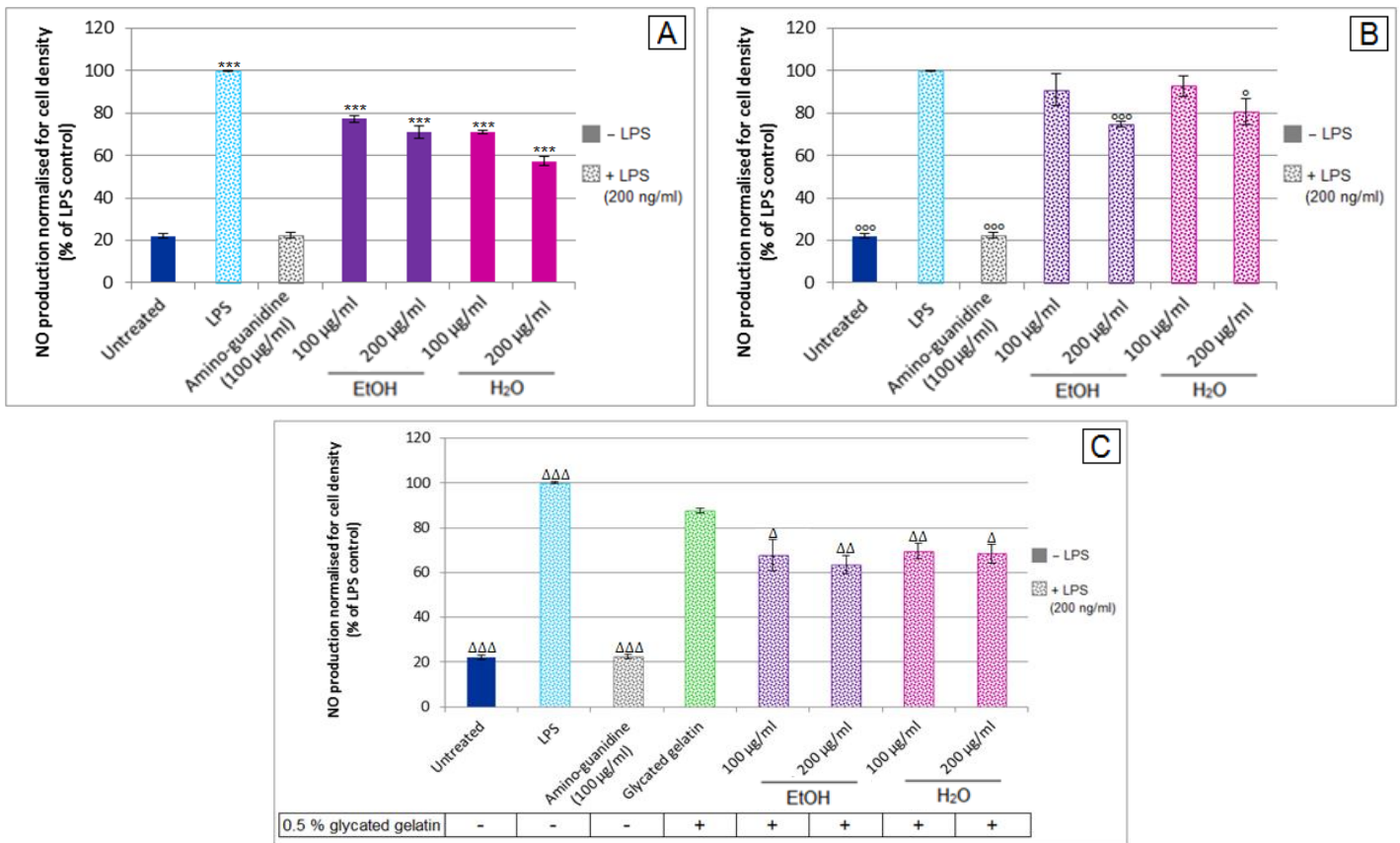
Figure 4.33: Nitric oxide production of RAW 264.7 cells treated with *P. tinctorius* (A) without LPS, (B) with LPS and (C) with glycated gelatin and LPS; results are reported as means ± SD where each experiment was performed three times, each in triplicate (*/°/Δp<0.05; **/°°/ΔΔp<0.01; ***/°°°/ΔΔΔp<0.005 where * compared to untreated sample; ° compared to LPS stimulated; Δ compared to glycated gelatin).

Figure 4.33 shows that both the ethanol and water extracts of *P. tinctorius* promoted NO production in the absence of LPS. In the presence of LPS, however, the 200 µg/ml ethanol and water extracts of *P. tinctorius* significantly inhibited NO production compared to the LPS stimulated cells, thus demonstrating both pro-inflammatory and anti-inflammatory activities. From figure C it is evident that neither the ethanol nor the water extracts of *P. tinctorius* were able to overcome the significant inhibition of NO caused by the addition of glycated gelatin despite the robust NO production observed when the cells were treated with these extracts (figure A). Furthermore, both extracts enhanced the decrease in NO observed in the presence of glycated gelatin, potentially confirming the anti-inflammatory activity reported in figure B. Due to the comparatively strong NO scavenging capabilities of *P. tinctorius* demonstrated in figure 4.22, however, it is possible that the decrease in NO observed in the presence of LPS was not due to anti-inflammatory activities but rather due to NO scavenging.
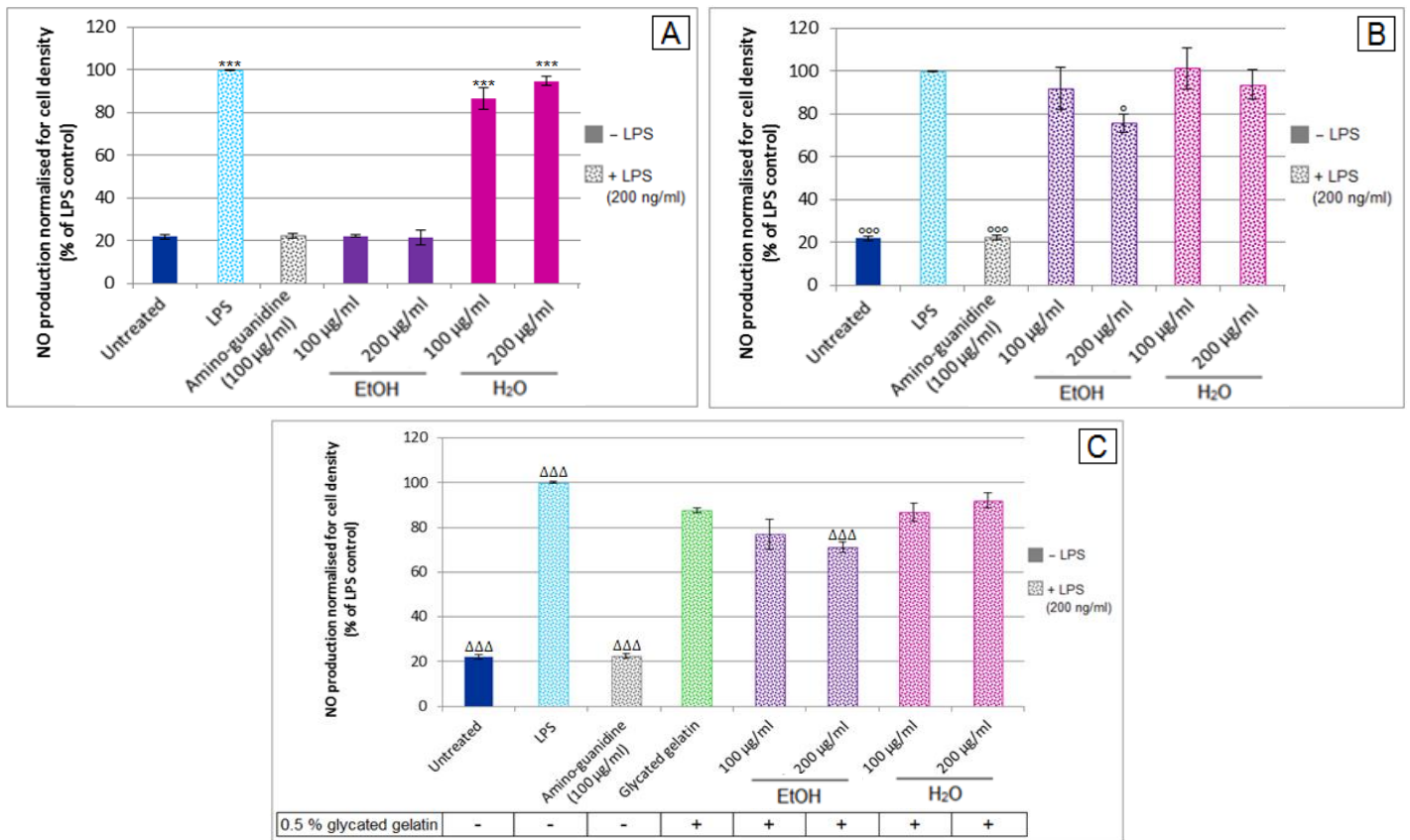
Figure 4.34: <u>Nitric oxide production of RAW 264.7 cells treated with *R. capensis* (A) without LPS, (B) with LPS and (C) with glycated gelatin and LPS; results are reported as means ± SD where each experiment was performed three times, each in triplicate (*/°/Δp<0.05; **/°°/ΔΔp<0.01; ***/°°°/ΔΔΔp<0.005 where * compared to untreated sample; ° compared to LPS stimulated; Δ compared to glycated gelatin).</u>

As seen in figure 4.34 A, no pro-inflammatory activities were reported for the ethanol extract of *R. capensis* as it did not promote NO production in the absence of LPS. Conversely, the water extract resulted in a robust dose-dependent increase in NO production (p<0.005) by the RAW 264.7 macrophages. In the presence of LPS, only the 200 µg/ml ethanol extract of *R. capensis* significantly inhibited NO production (p<0.05). Figure C demonstrates that the 200 µg/ml ethanol extract of *R. capensis* further reduced the quantity of NO measured in the presence of glycated gelatin when compared to the glycated gelatin control, confirming the potential anti-inflammatory activity observed in figure B.
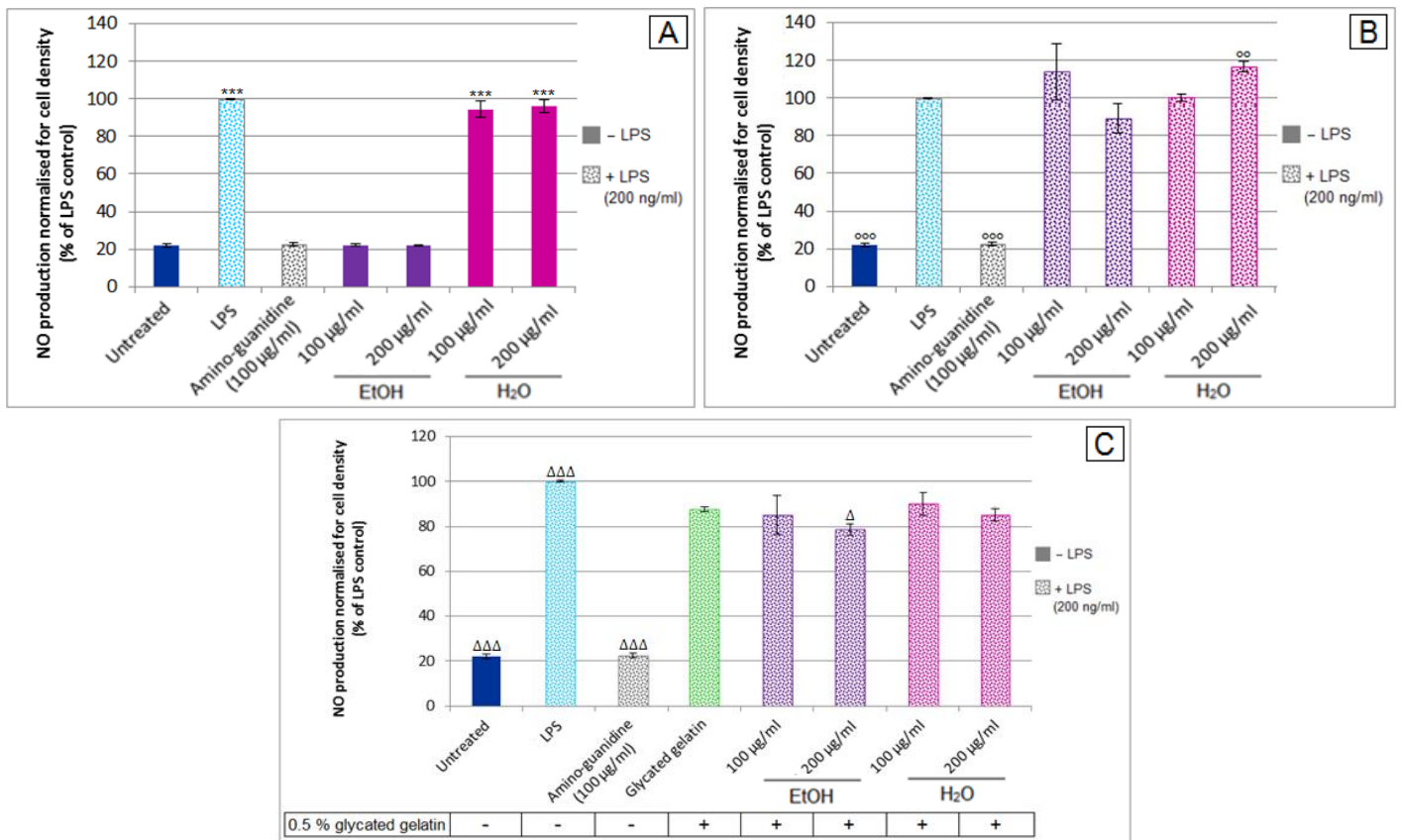
Figure 4.35: Nitric oxide production of RAW 264.7 cells treated with *B. badius* (A) without LPS, (B) with LPS and (C) with glycated gelatin and LPS; results are reported as means ± SD where each experiment was performed three times, each in triplicate ($*$/°/Δp<0.05; $**$/°°/$\Delta\Delta$p<0.01; $***$/°°°/$\Delta\Delta\Delta$p<0.005 where $*$ compared to untreated sample; ° compared to LPS stimulated; Δ compared to glycated gelatin).

No pro-inflammatory NO production was observed in figure 4.35 in the absence of LPS for the ethanol extract of *B. badius*, however, the water extract displayed strong pro-inflammatory activity (p<0.005). In the presence of LPS, no significant alterations in NO production occurred except for treatment with the 200 µg/ml water extract which increased NO production to 117 % (p<0.01). Figure C shows that the 200 µg/ml ethanol extract further reduced the quantity of NO measured in the presence of glycated gelatin when compared to treatment with glycated gelatin alone. As no measurable NO scavenging activity was reported for this particular extract (figure 4.24), the observed decrease in NO suggests potential anti-inflammatory activities for the ethanol extract of *B. badius*.

98
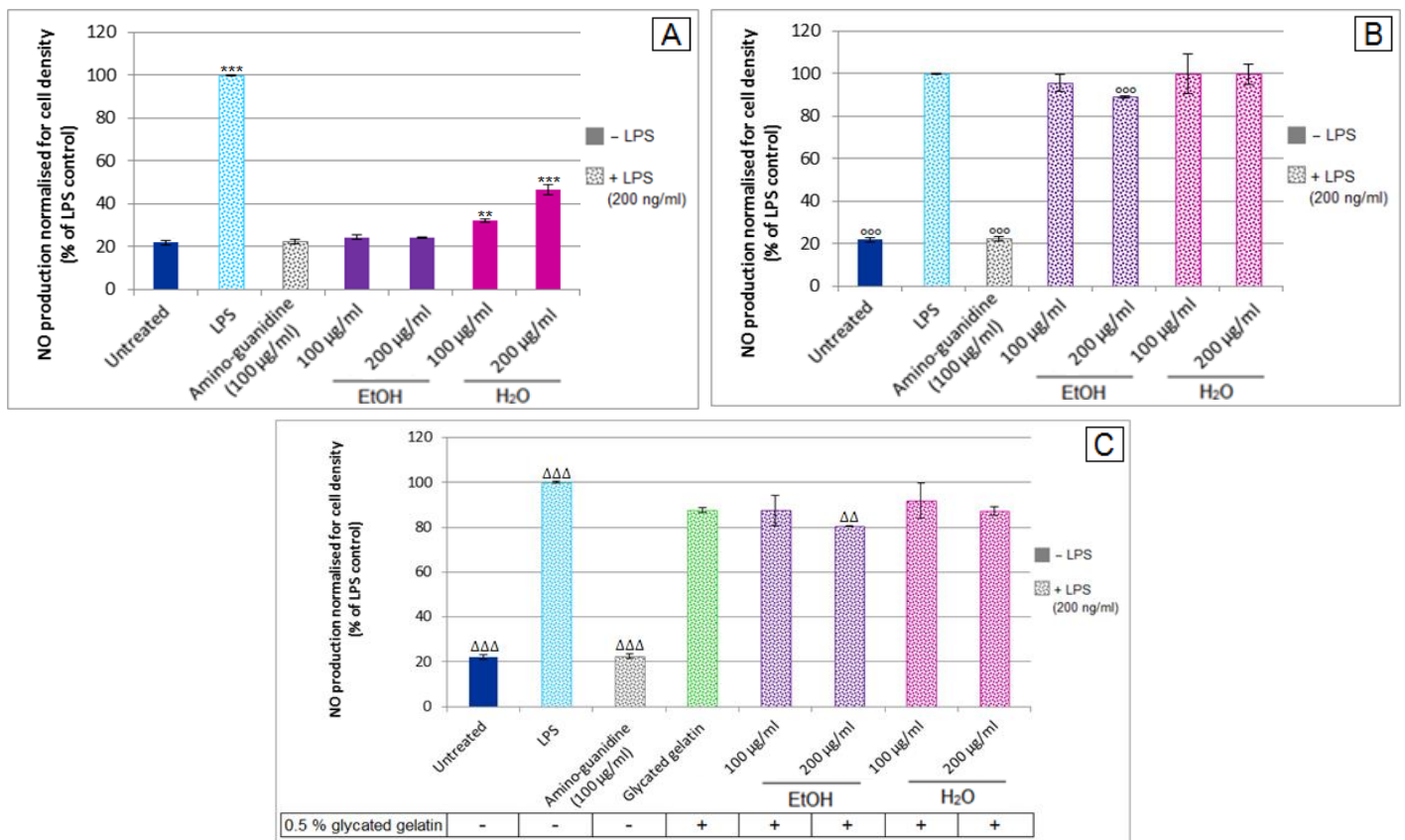
Figure 4.36: Nitric oxide production of RAW 264.7 cells treated with *P. ostreatus* (A) without LPS, (B) with LPS and (C) with glycated gelatin and LPS; results are reported as means ± SD where each experiment was performed three times, each in triplicate (*/°/Δp<0.05; **/°°/ΔΔp<0.01; ***/°°°/ΔΔΔp<0.005 where * compared to untreated sample; ° compared to LPS stimulated; Δ compared to glycated gelatin).

Figure 4.36 A shows that the ethanol extract of *P. ostreatus* did not promote NO production in the absence of LPS while a weak pro-inflammatory response was recorded for the water extract. In the presence of LPS, only the 200 µg/ml ethanol extract of *P. ostreatus* significantly reduced the quantity of NO measured, suggesting potential anti-inflammatory activity. In the presence of glycated gelatin, the 200 µg/ml ethanol extract resulted in a further decrease in NO compared to treatment with glycated gelatin alone. Since no substantial NO scavenging activity was demonstrated in figure 4.25, this confirms the presence of anti-inflammatory compounds present in the extract.
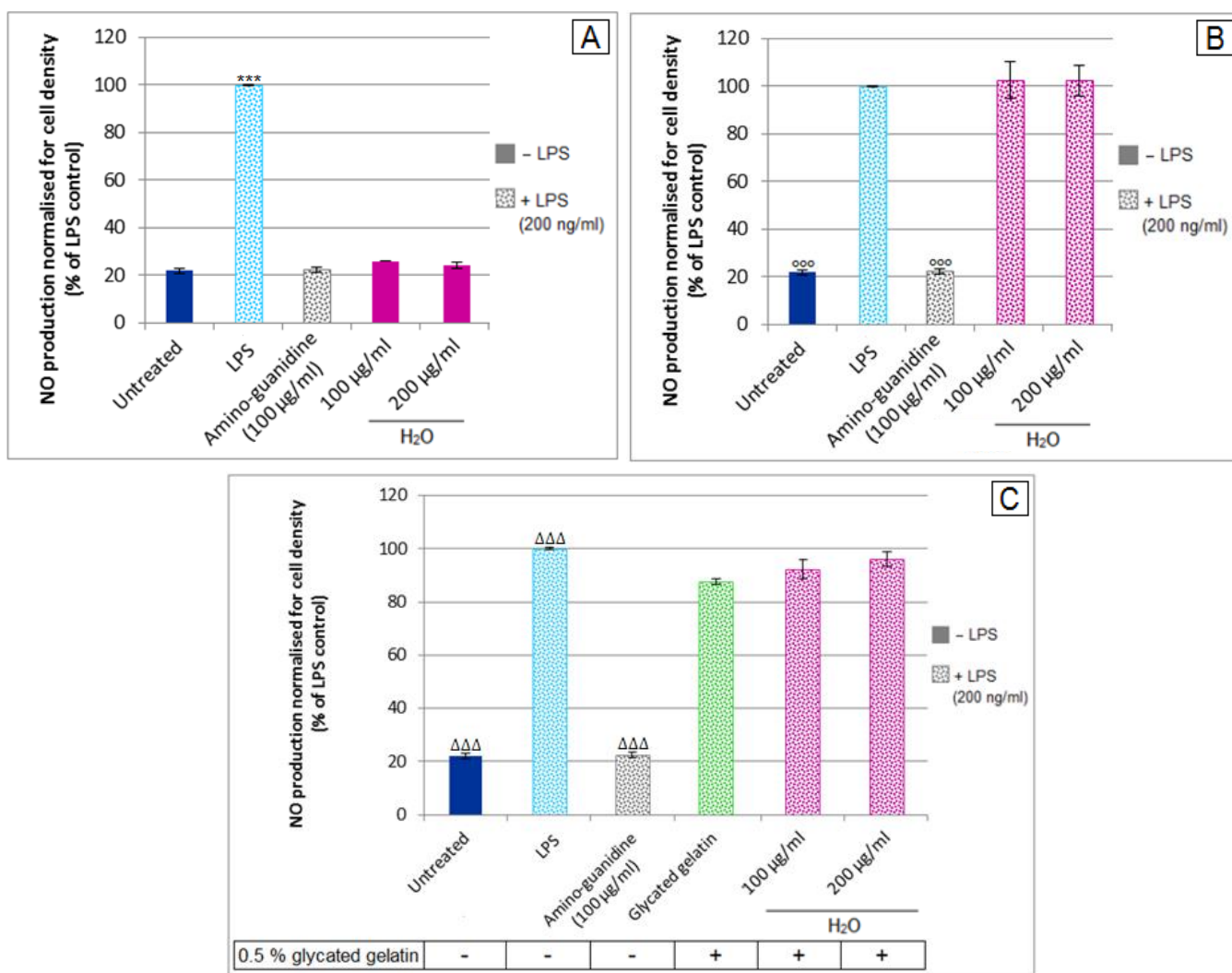
Figure 4.37: Nitric oxide production of RAW 264.7 cells treated with *G. lucidum* (A) without LPS, (B) with LPS and (C) with glycated gelatin and LPS; results are reported as means ± SD where each experiment was performed three times, each in triplicate (*/°/Δp<0.05; **/°°/ΔΔp<0.01; ***/°°°/ΔΔΔp<0.005 where * compared to untreated sample; ° compared to LPS stimulated; Δ compared to glycated gelatin).

Due to the cytotoxicity of the ethanol extract of *G. lucidum* (figure 4.21), only the water extract was subjected to further cell-based screening assays. Figure 4.37 A shows that the water extract of *G. lucidum* did not stimulate NO production in the absence of LPS nor did it result in any anti-inflammatory decreases in NO production in the presence of LPS. Furthermore, no alterations in NO production were measured in the presence of glycated gelatin, confirming that this extract does not induce any noteworthy anti-inflammatory or pro-inflammatory effects with regards to NO production.

In order to eliminate any false positives in NO production in the absence of LPS due to the presence of endotoxins in the tested mushroom extracts, NO production in

RAW 264.7 macrophages was re-assessed with the addition of Polymyxin B sulfate. The quantity of NO produced was assessed using the Griess reaction. The cytotoxic effect of Polymyxin B sulphate against RAW 264.7 cells was first established in order to select an appropriate concentration to use for further experiments. A dose-response curve for the Polymyxin B sulfate is shown in figure 4.38 while the experimental results for each of the mushroom extracts are shown in figure 4.39. All extracts, except for the ethanol extract of *G. lucidum*, were tested at concentrations of 100 and 200 µg/ml as no physiologically significant cell death was recorded during the cytotoxicity screening assay (section 4.2.1) at these concentrations. The untreated sample consisted of high-glucose DMEM supplemented with 10 % FBS where LPS (200 ng/ml) represented 100 % NO production and all treatments were thus calculated as a percentage of the LPS control. Statistical analysis was performed individually for each individual extract using the response without LPS recorded previously (figures 4.33 to 4.37 A) as a reference sample in order to establish whether any statistically relevant decreases in NO production occurred in the presence of Polymyxin B sulfate.
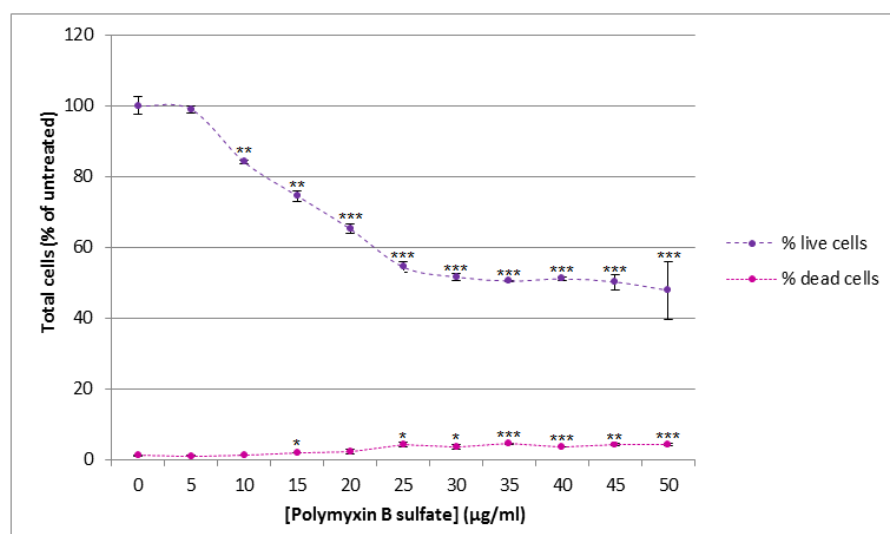
Figure 4.38: Dose-response effect of Polymyxin B sulfate on RAW 264.7 macrophage cell number after 48 hours; results are reported as means ± SD with this experiment being performed once in triplicate (*$p<0.05$; **$p<0.01$; ***$p<0.005$ compared to 0 %).

A dose-dependent decrease in the total RAW 264.7 cell number coupled to an increase in cell death can be seen in figure 4.38 as the concentration of Polymyxin B sulfate increases. In order to effectively identify potential false positives in the stimulation of NO, a non-toxic concentration of polymyxin B had to be selected. The concentration deemed most suitable for this assay was identified as 10 µg/ml as a

lower concentration might not result in any measurable effects on NO production in the presence of endotoxins while higher concentrations inhibited cell proliferation by more than 20 % and promoted substantial cell death and could thus potentially interfere with the results.
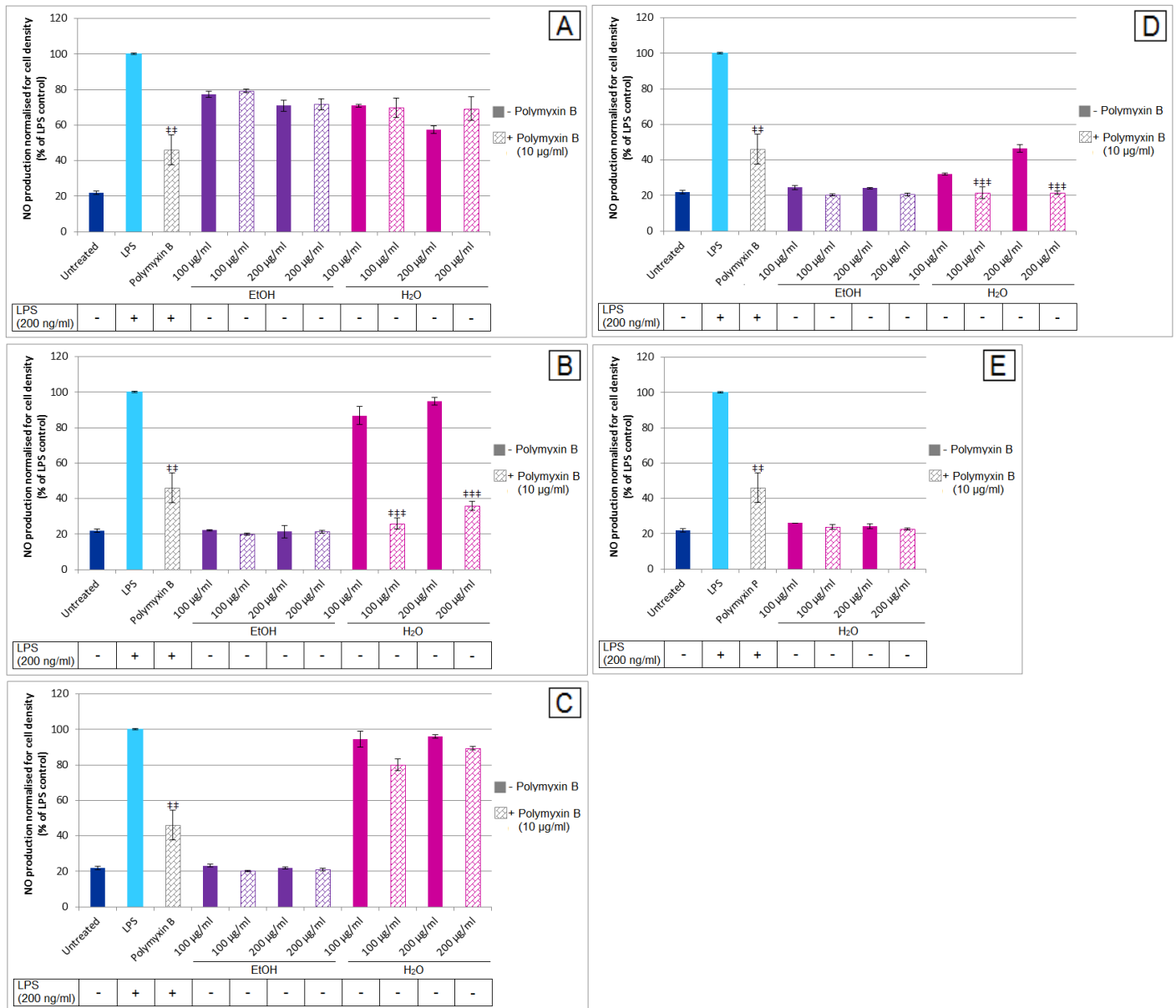
Figure 4.39: Assessment of the presence of endotoxins using RAW 264.7 macrophages with 10 µg/ml Polymyxin B sulfate for (A) *P. tinctorius* (B) *R. capensis* (C) *B. badius* (D) *P. ostreatus* and (E) *G. lucidum*; results are reported as means ± SD where each experiment was performed three times, each in triplicate (‡p<0.05; ‡‡p<0.01; ‡‡‡p<0.005 compared to LPS for polymyxin B and each extract without polymyxin B, respectively).

Figure 4.39 shows that polymyxin B resulted in a robust decrease in the NO production of RAW 264.7 cells in the presence of LPS, thus confirming the functionality of this assay. Only two extracts were found to potentially contain endotoxins, namely the water extracts of *R. capensis* and *P. ostreastus* as

102

evidenced from the attenuation of NO production ($p<0.005$) in the presence of LPS when compared to the relevant treatment without polymyxin B. Further endotoxin analysis is thus required to confirm the presence of endotoxins.

4.3.2. Phagocytosis

The phagocytic capability of RAW 264.7 macrophages was assessed in figures 4.40 to 4.44 using the pHrodo® Green *E. coli* BioParticles® Conjugate. As phagocytosis is characterized by the formation of acidic phagolysosomes, LysoTracker Red® was included in this assay in order to simultaneously monitor acidic vacuole formation. The ability of each mushroom extract to overcome the inhibition of phagocytosis observed in section 4.1.5 induced by glycated gelatin was assessed here. Extracts were tested at a concentration of 100 µg/ml in order to eliminate factors that could interfere with cell processes other than phagocytosis as some extracts exerted potential anti-proliferative effects on the RAW 264.7 cells at higher concentrations in section 4.2.1. The untreated sample consisted of high-glucose DMEM supplemented with 10 % FBS and all samples were calculated as a percentage of this control while cytochalasin B and LPS were included as a positive controls to inhibit phagocytosis and activate phagocytosis, respectively.
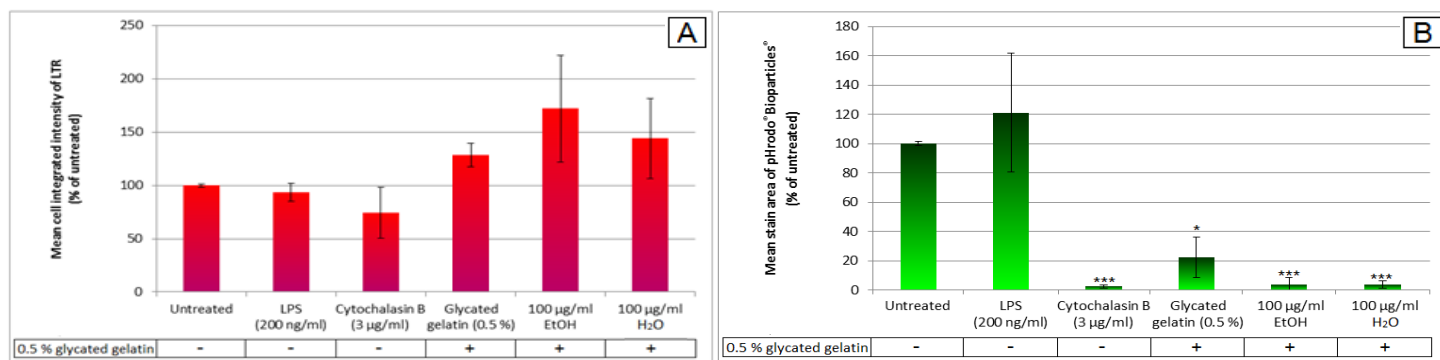
Figure 4.40: RAW 264.7 cell phagocytosis after treatment with *P. tinctorius* measuring (A) acidic vacuole formation using LysoTracker Red® and (B) phagocytosis using pHrodo® Bioparticles®; results are reported as means ± SD where each experiment was performed three times, each in triplicate (*$p<0.05$; **$p<0.01$; ***$p<0.005$ compared to untreated sample).

From figure 4.40 it is evident that neither the ethanol nor the water extracts of *P. tinctorius* resulted in any noteworthy alterations in acidic vacuole formation. Figure B shows that there was a robust decrease in phagocytosis for both the 100 µg/ml ethanol and water extracts of *P. tinctorius* when compared to the untreated sample, however, this can be attributed to the negative effect of AGEs on phagocytosis

(figure 4.7). When all three experiments were combined, the standard deviation for LTR was rather large, however, individual experiments shown in figure C.2 from appendix C show that the standard deviations were much smaller for individual experiments. In all three individual experiments the mean cell integrated intensity of LTR for the ethanol extract of *P. tinctorius* was significantly higher than the glycated gelatin sample while the water extract was significantly higher than the glycated gelatin for only two of the individual experiments. An increase in acidic vacuole formation coupled to a decrease in phagocytosis could be an indication of autophagy.
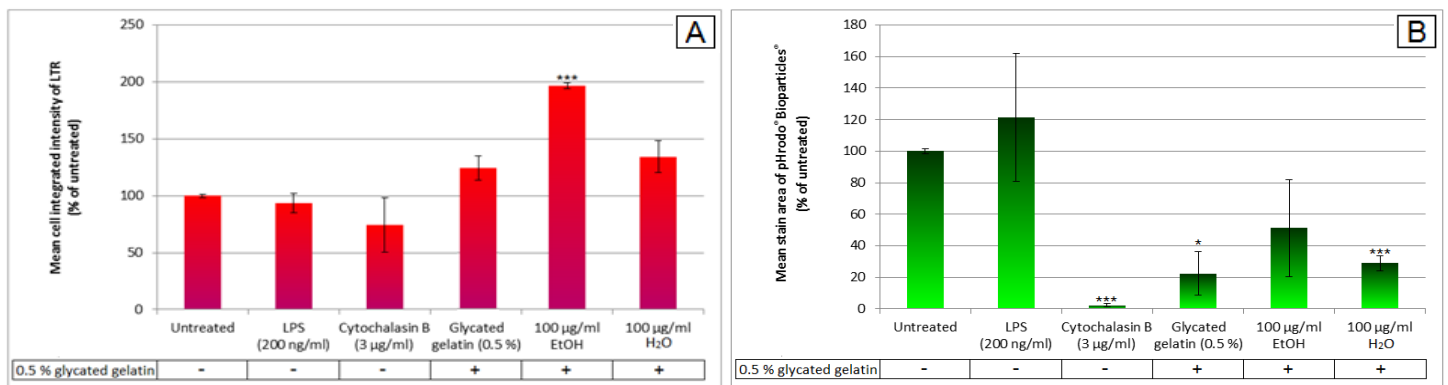
Figure 4.41: RAW 264.7 cell phagocytosis after treatment with *R. capensis* measuring (A) acidic vacuole formation using LysoTracker Red® and (B) phagocytosis using pHrodo® Bioparticles®; results are reported as means ± SD where each experiment was performed three times, each in triplicate (*p<0.05; **p<0.01; ***p<0.005 compared to untreated sample).

Figure 4.41 shows that the 100 µg/ml ethanol extract of *R. capensis* resulted in a significant increase in acidic vacuole formation. Furthermore, there was no noteworthy difference in phagocytosis between the untreated sample and the ethanol extract due to the large variation between individual experiments. Individual experiments shown in figure C.3 from appendix C show that the ethanol extract of *R. capensis* significantly increased macrophage phagocytosis when compared to the glycated gelatin for all three individual experiments while the water extract increased phagocytosis in only one of these experiments. The increase in both acidic vacuole content and phagocytosis suggests that the ethanol extract of *R. capensis* was able to reverse the negative effect of glycated protein on macrophage phagocytosis.
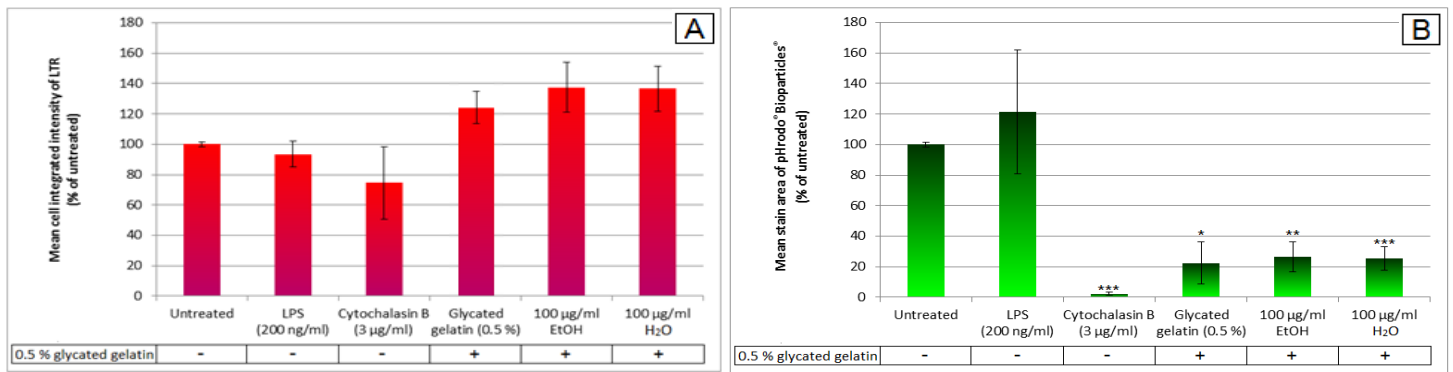
Figure 4.42: RAW 264.7 cell phagocytosis after treatment with *B. badius* measuring (A) acidic vacuole formation using LysoTracker Red® and (B) phagocytosis using pHrodo® Bioparticles®; results are reported as means ± SD where each experiment was performed three times, each in triplicate (*$p < 0.05$; **$p < 0.01$; ***$p < 0.005$ compared to untreated sample).

Figure 4.42 A shows that there was no significant increase in acidic vacuole formation for either the ethanol or water extracts of *B. badius* while figure B demonstrates that neither the ethanol nor the water extract were able to overcome the negative effect of the glycated gelatin on RAW 264.7 macrophage phagocytosis.
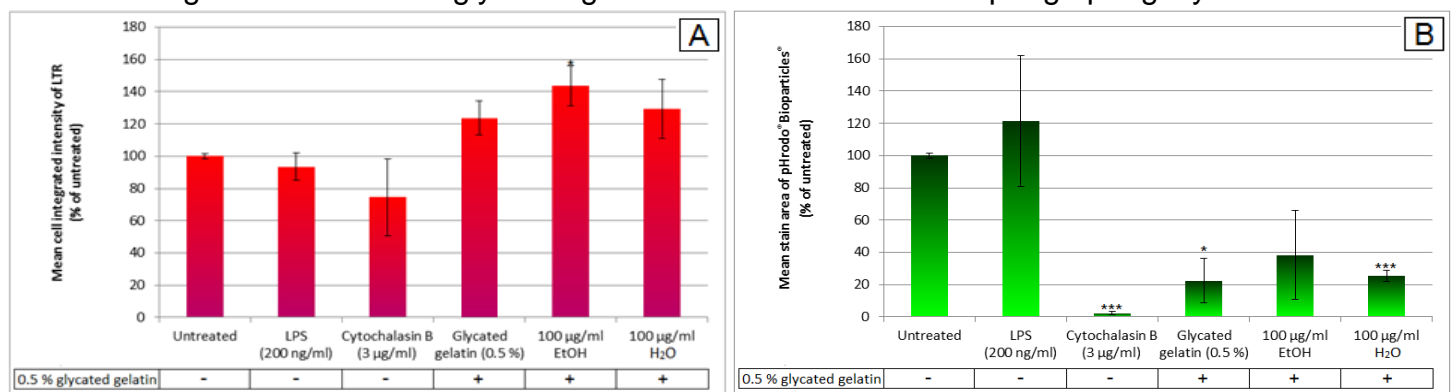
Figure 4.43: RAW 264.7 cell phagocytosis after treatment with *P. ostreatus* measuring (A) acidic vacuole formation using LysoTracker Red® and (B) phagocytosis using pHrodo® Bioparticles®; results are reported as means ± SD where each experiment was performed three times, each in triplicate (*$p < 0.05$; **$p < 0.01$; ***$p < 0.005$ compared to untreated sample).

It is evident from figure 4.43 that the 100 µg/ml ethanol extract of *P. ostreatus* resulted in a significant increase in acidic vacuole formation. No significant difference in phagocytosis was seen for either extract when compared to the untreated sample, however, individual experiments in figure C.4 from appendix C show that the water extract of *P.* ostreatus resulted in a significant increase in phagocytosis when compared to the glycated gelatin sample for all three experiments while the ethanol extract significantly promoted phagocytosis in only one of these experiments. This suggests that the ethanol extract of *P. ostreatus* could potentially overcome the impairment of phagocytosis induced by protein glycation.

105
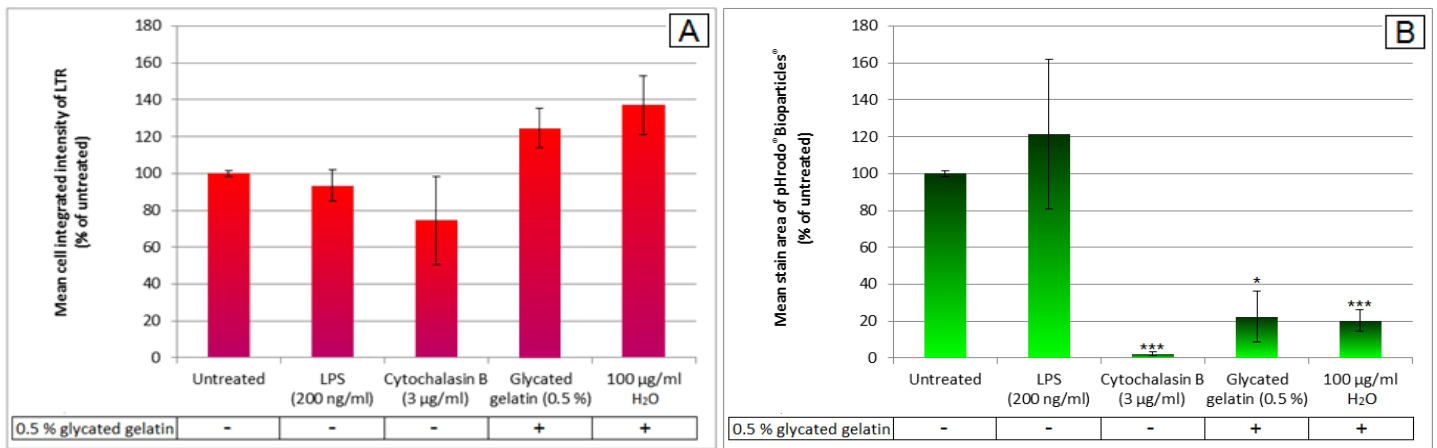
Figure 4.44: RAW 264.7 cell phagocytosis after treatment with *G. lucidum* measuring (A) acidic vacuole formation using LysoTracker Red® and (B) phagocytosis using pHrodo® Bioparticles®; results are reported as means ± SD where each experiment was performed three times, each in triplicate (*p<0.05; **p<0.01; ***p<0.005 compared to untreated sample).

Figure 4.44 shows that no significant changes in acidic vacuole formation or phagocytosis for the RAW 264.7 macrophages was observed for the 100 µg/ml water extract of *G. lucidum* and this mushroom extract was thus incapable of overcoming the negative effect of AGEs on phagocytosis.

4.3.3. M1/M2 macrophage polarization

The activation status of RAW 264.7 macrophages was further assessed using antibodies for the CD86 cell surface receptor as a measure of M1 activation (pro-inflammatory) and the CD206 cell surface receptor for M2 activation (anti-inflammatory) (figure 4.45 to 4.49). The untreated sample consisted of high-glucose DMEM (25 mM) supplemented with 10 % FBS. LPS (200 ng/ml) was used as a positive control for M1 activation while curcumin (20 µM) served as a positive control for M2 activation. A ratio of M1:M2 was calculated for each of the mushroom extracts by dividing the percentage of cells stained positive for CD86 by the percentage of cells stained positive for CD206. These results are summarised in table 4.1. As diabetic wounds are characterized by an increased population of M1 macrophages which consequently prolongs the inflammatory phase of wound healing, a favourable reaction in response to treatment with the mushroom extracts would be indicated by a reduction in the activation of M1 macrophages coupled to an increase in M2 macrophage activation.

Table 4.1: M1/M2 ratios calculated during the macrophage polarization assay.

	Glycated gelatin	P. tinctorius		R. capensis		B. badius		P. ostreatus		G. lucidum
Extract		EtOH	H$_2$O	EtOH	H$_2$O	EtOH	H$_2$O	EtOH	H$_2$O	H$_2$O
Ratio	4.5	1.24	0.51	0.94	1.24	4.06	1.55	2.4	1.59	1.41

As glycated gelatin was shown to promote M1 macrophage activation in section 4.1.6 and consequently contribute to the pathological inflammation observed during diabetic wound healing, a favourable outcome with regards to macrophage polarization would be characterized by a low M1:M2 ratio due to a decrease in M1 activation, an increase in M2 activation, or both. Table 4.1 shows several promising candidates with M1:M2 ratios below 2 which are discussed in more detail below.
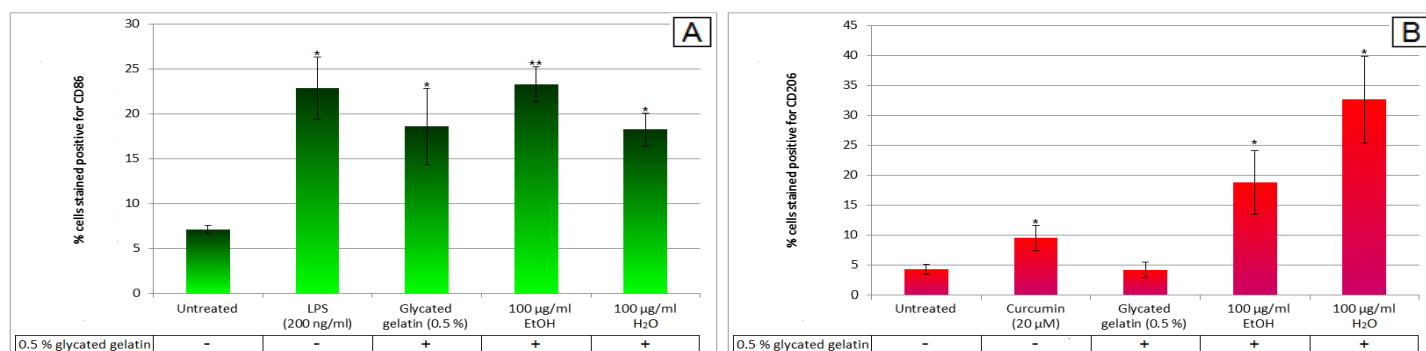
Figure 4.45: Macrophage polarization following treatment with *P. tinctorius* using (A) CD86 for M1 macrophages and (B) CD206 for M2 macrophages; results are reported as means ± SD where each experiment was performed three times, each in triplicate (*p<0.05; **p<0.01; ***p<0.005 compared to untreated sample).

Neither the ethanol nor the water extracts of *P. tinctorius* were able to lower the percentage of M1 activated cells induced by glycated gelatin, however, substantial increases (p<0.05) in M2 activation occurred in response to both extracts (figure 4.45). This suggests that both extracts of *P. tinctorius* could promote the transition from M1 to M2 macrophages required for the final tissue remodelling stage of wound healing to proceed. The results from table 4.1 and figure 4.45 provide sufficient evidence that both the ethanol and water extracts of *P. tinctorius* could promote favourable macrophage polarization during impaired wound healing with the water extract having the most potent effect of all of the tested extracts as evidenced by the lowest M1:M2 ratio of 0.51.
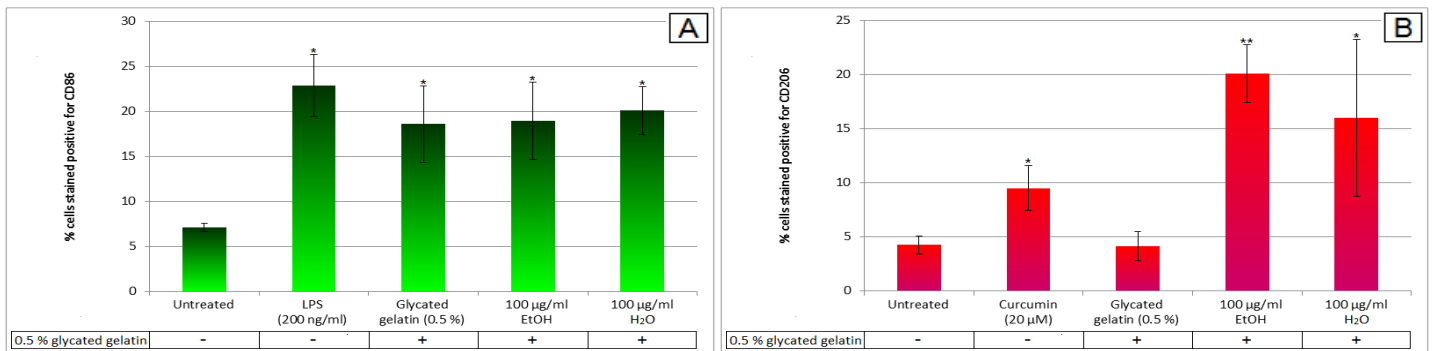
Figure 4.46: <u>Macrophage polarization following treatment with *R. capensis* using (A) CD86 for M1 macrophages and (B) CD206 for M2 macrophages; results are reported as means ± SD where each experiment was performed three times, each in triplicate (*p<0.05; **p<0.01; ***p<0.005 compared to untreated sample).</u>

From table 4.1, the M1:M2 ratios for the ethanol and water extracts of *R. capensis* were calculated to be 0.94 and 1.24, respectively. While these comparatively low ratios cannot be accounted for by a decrease in M1 macrophage activation, figure 4.46 shows that both extracts caused a robust increase in the percentage of M2 activated cells. *R. capensis* could thus prove to be very useful in attenuating the inflammatory response.
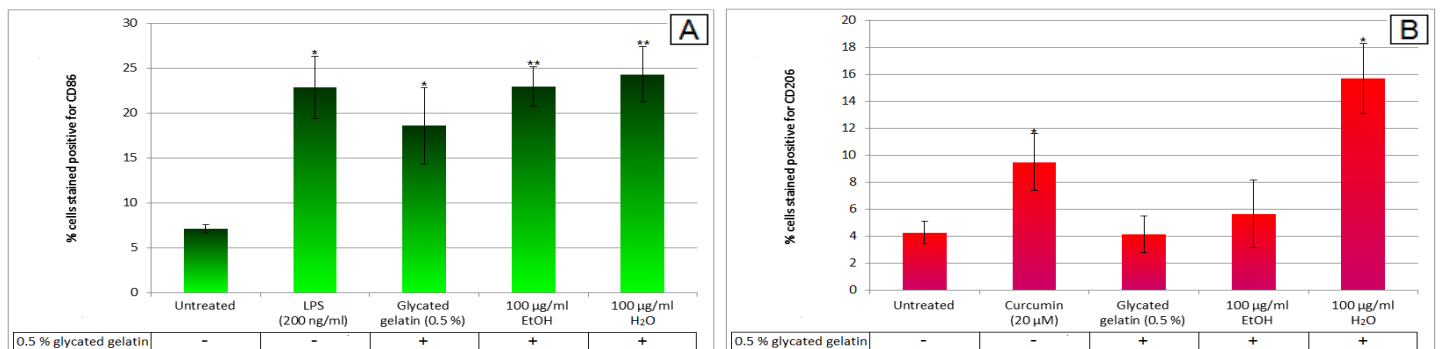
Figure 4.47: <u>Macrophage polarization following treatment with *B. badius* using (A) CD86 for M1 macrophages and (B) CD206 for M2 macrophages; results are reported as means ± SD where each experiment was performed three times, each in triplicate (*p<0.05; **p<0.01; ***p<0.005 compared to untreated sample).</u>

The 100 µg/ml ethanol and water extracts of *B. badius* were not able to reduce the percentage of M1 activated macrophages, however, the water extract appears to have successfully increased the M2 macrophage population as shown in figure 4.47. Consequently, the water extract yielded a highly promising M1:M2 ratio of 1.55 compared to 4.06 for the water extract (table 4.1).
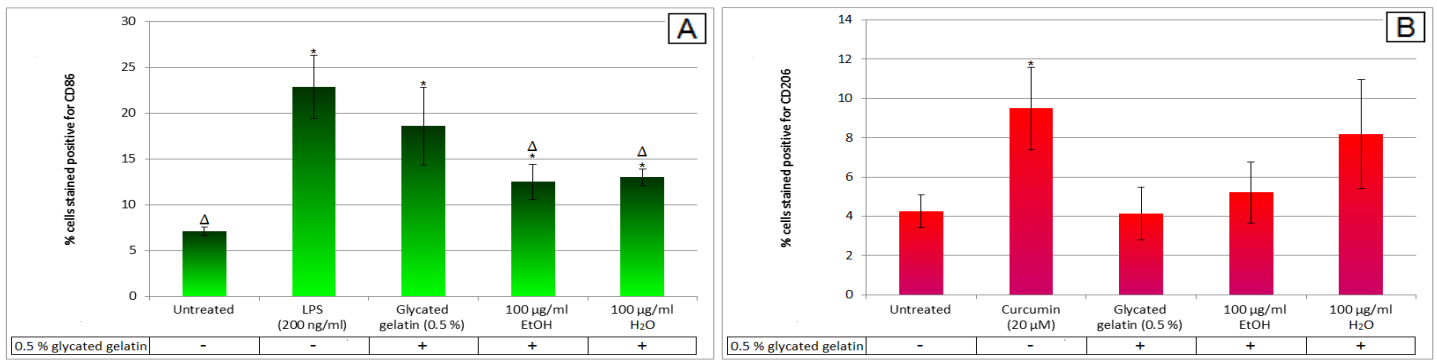
Figure 4.48: Macrophage polarization following treatment with *P. ostreatus* using (A) CD86 for M1 macrophages and (B) CD206 for M2 macrophages; results are reported as means ± SD where each experiment was performed three times, each in triplicate (*/Δp<0.05; **/ΔΔp<0.01; ***/ΔΔΔp<0.005 where *compared to untreated sample; Δ compared to glycated gelatin).

According to table 4.1, the ethanol extract yielded an M1:M2 ratio of 2.4 compared to the water extract which yielded a much more promising value of 1.55. Figure 4.48 illustrates that while both the ethanol and water extracts of *P. ostreatus* were equally capable of successfully attenuating M1 macrophage activation induced by glycated gelatin (p<0.05), only the water extract was able to promote M2 macrophage activation. Although this increase in M2 activation was not found to be statistically significant due to the variance between individual experiments, it can still account for the much reduced M1:M2 ratio recorded for the water extract which was the only extract able to affect both M1 and M2 macrophage polarization.
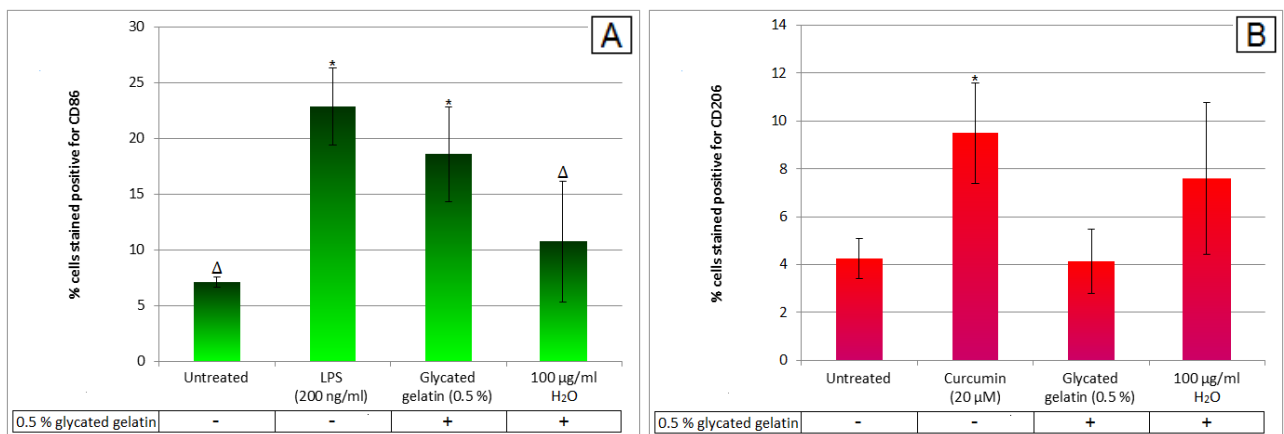
Figure 4.49: Macrophage polarization following treatment with *G. lucidum* using (A) CD86 for M1 macrophages and (B) CD206 for M2 macrophages; results are reported as means ± SD where each experiment was performed three times, each in triplicate (*/Δp<0.05; **/ΔΔp<0.01; ***/ΔΔΔp<0.005 where *compared to untreated sample; Δ compared to glycated gelatin).

Figure 4.49 shows that the 100 µg/ml water extract of *G. lucidum* significantly reduced the percentage of M1 activated cells when compared to treatment with the

glycated gelatin alone. Furthermore, no significant changes in M2 macrophage activation occurred, accounting for the comparatively favourable M1:M2 ratio of 1.41.

4.3.4. NF-κB translocation

The role of NF-κB in inflammation has been well established and this transcription factor has subsequently been identified as a favourable target during the search for useful diabetic wound healing treatment strategies. The ability of NF-κB to directly induce the expression of several pro-inflammatory markers suggests that any mushroom extract capable of attenuating the enhanced nuclear-translocation and subsequent activation of NF-κB in response to protein glycation (figure 4.1.7) could have unparalleled advantages in promoting functional wound healing in diabetic individuals. The effect of each mushroom extract on the nuclear translocation of phsopho-p65 NF-κB in RAW 264.7 macrophages in the presence of glycated gelatin was assessed in figure 4.50. The untreated sample consisted of high-glucose DMEM (25 mM) supplemented with 10 % FBS with all other treatments calculated as a percentage of this control. LPS (200 ng/ml) was used as a positive control to stimulate NF-κB translocation.
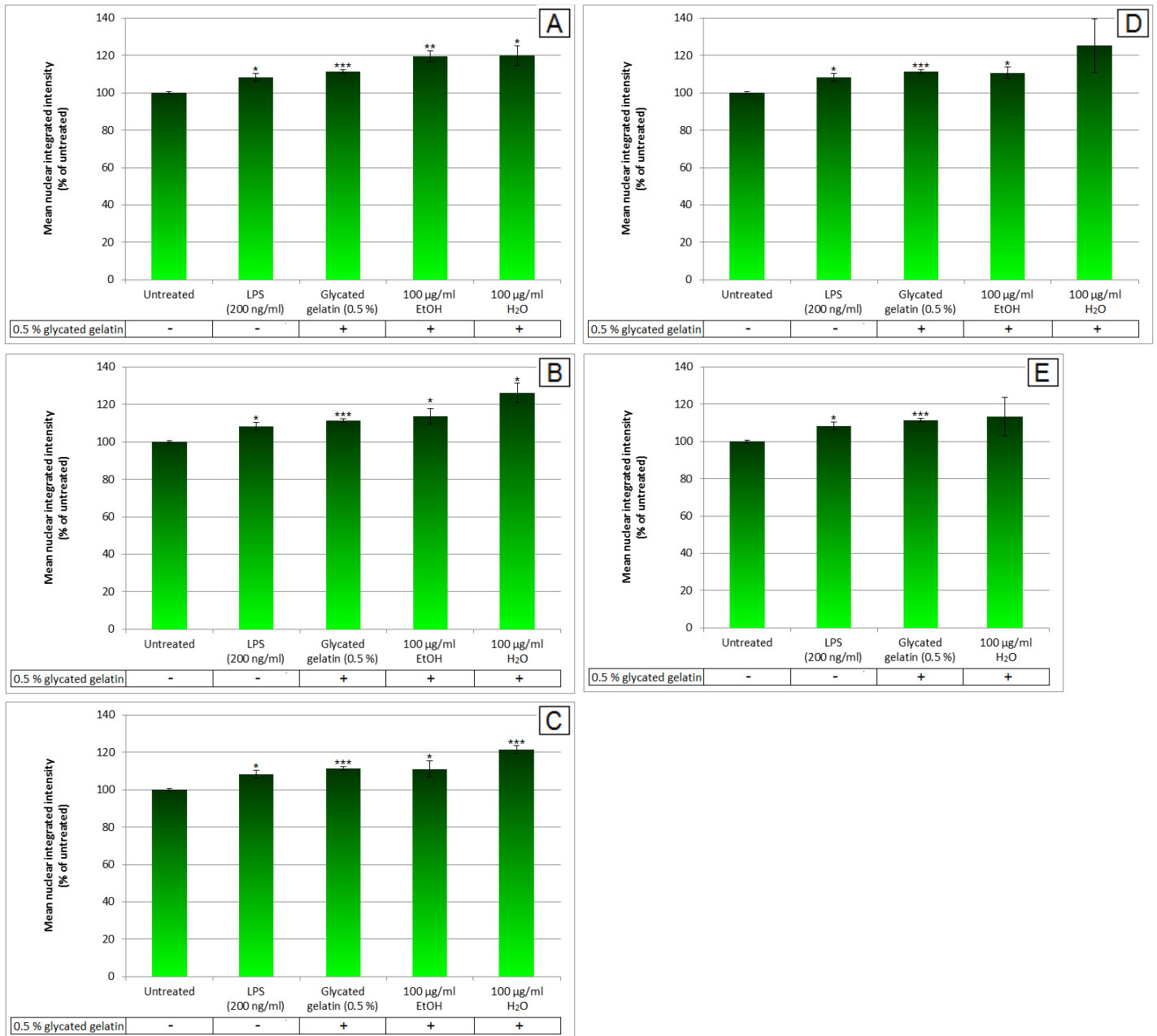
Figure 4.50: NF-κB nuclear translocation after treatment with (A) *P. tinctorius,* (B) *R. capensis*, (C) *B. badius*, (D) *P. ostreatus* and (E) *G. lucidum*; results are reported as means ± SD where each experiment was performed three times, each in triplicate (*p<0.05; **p<0.01; ***p<0.005 compared to the untreated sample).

According to figure 4.50, none of the tested mushroom extracts were able to attenuate the nuclear translocation of phospho-p65 NF-κB back to the levels observed in the untreated sample, suggesting that none of the selected mushroom species can promote normal wound healing through this pathway. While there was no significant difference in nuclear translocation between the untreated sample and the 100 µg/ml water extracts of both *P. ostreatus* and *G. lucidum*, the variation

between individual experiments resulted in no significant difference between these treatments when compared to the glycated gelatin alone. Further investigations are thus required to confirm the effects of these extracts on NF-κB nuclear translocation.

4.3.5. COX-2

One of the pro-inflammatory signalling molecules activated by NF-κB is COX-2. In section 4.1.8, glycated gelatin alone did not promote COX-2 activity, however, in the presence of LPS an additive effect on COX-2 expression was recorded. As a result, the effect of each mushroom extract on COX-2 activity in the absence and presence of LPS was analysed in figure 4.51 in order to gain a deeper understanding of the inflammatory status of RAW 264.7 macrophages in response to various treatments. The untreated sample consisted of high-glucose DMEM (25 mM) supplemented with 10 % FBS while LPS (200 ng/ml) was used as a positive control.
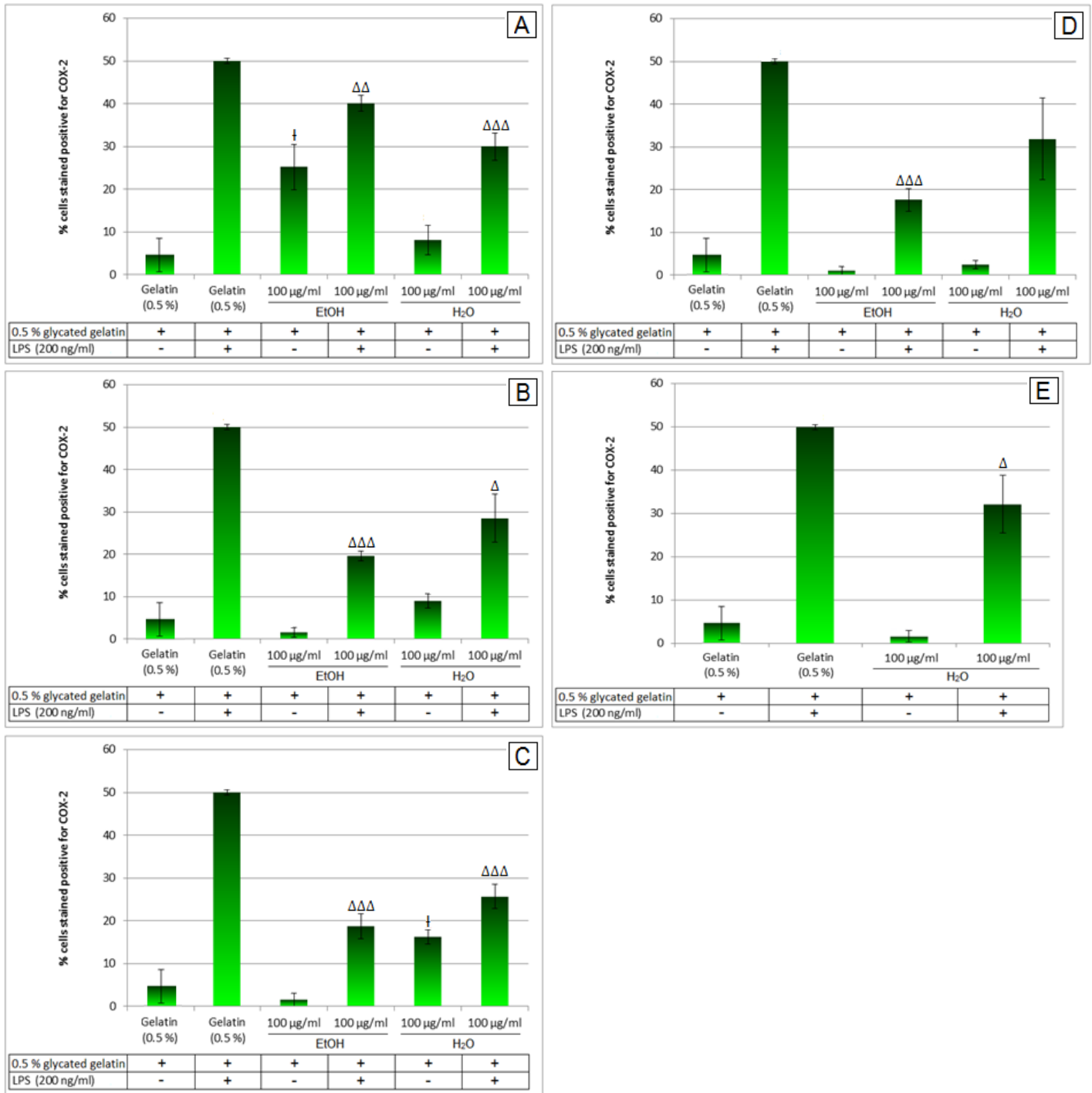
Figure 4.51: COX-2 antibody staining after treatment with (A) *P. tinctorius,* (B) *R. capensis*, (C) *B. badius*, (D) *P. ostreatus* and (E) *G. lucidum*; results are reported as means ± SD where each experiment was performed three times, each in triplicate (ł/Δp<0.05; Ⱨ /ΔΔp<0.01; ⱨ /ΔΔΔp<0.005 where ł compared to glycated gelatin without LPS; Δ compared to glycated gelatin with LPS).

Figure 4.51 shows that several of the mushroom extracts including the 100 μg/ml ethanol and water extracts of *P. tinctorius* as well as the water extracts of *R. capensis*, *B. badius* and *P. ostreatus* significantly increased COX-2 activity in the

113

absence of LPS. Four out of the five water extracts tested during this study were thus shown to contain compounds with substantial pro-inflammatory activities. In the presence of LPS, however, all the tested extracts except for the water extract of *P. ostreatus* resulted in noteworthy reductions in COX-2 activity in the presence of glycated gelatin. The presence of both pro-inflammatory and anti-inflammatory compounds in several of the selected mushroom species was thus confirmed and the overall effect of each mushroom on the inflammatory process has yet to be established.

4.4.   THE ROLE OF FIBROBLASTS IN WOUND HEALING

Fibroblasts perform import functions during the proliferation and tissue repair processes of wound healing, secreting collagen and various other factors required for the formation of a functional ECM. In section 4.1.9, glycated gelatin was found to impair both the proliferation and the migration abilities of MRHF fibroblasts thus mimicking the effects of diabetes on *in vivo* fibroblast function. The ability of the selected mushroom extracts to overcome the observed impairment in fibroblast activity was addressed in this section in order to identify any sample potentially capable of promoting the final stage of wound healing as well as to gain deeper insight with regards to the capabilities and limitations of each extract.

4.4.1. Proliferation

MRHF fibroblast proliferation was assessed using Hoechst 33342 and PI staining. An FBS-dose response curve shown in figure 4.52 was used to determine the concentration of FBS that should be used to support sub-optimal MRHF fibroblast proliferation without causing any significant cytotoxicity. In this assay a sub-optimal proliferation rate is considered advantageous as optimal conditions leave little scope for the test samples to further stimulate proliferation.
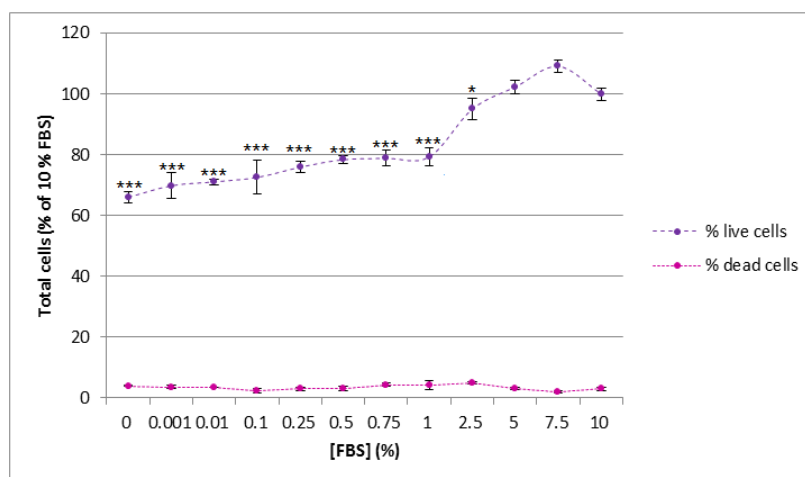
Figure 4.52: FBS dose-response effect on MRHF fibroblast cell number after 72 hours; results are reported as means ± SD with this experiment being performed once in triplicate (*p<0.05; **p<0.01; ***p<0.005 compared to 10 % FBS).

A steep dose-dependent decrease in fibroblast cell number was observed as the concentration of FBS was reduced from 10 % down to 1 %, followed by a more gradual decline between 1 % and 0 % FBS (figure 4.52). The absence of FBS was not found to exert any cytotoxic effects on the fibroblasts as no increase in cell death was reported at any of the tested concentrations. Based on these findings, 1 % FBS was selected for all further proliferation experiments as the 20 % decrease in proliferation was deemed sufficiently low to allow for a measurable effect without inducing any potentially harmful effects.

The effect of each mushroom extract on fibroblast proliferation in the absence and presence of glycated gelatin are shown in figures 4.53 to 4.57. The untreated sample consisted of low-glucose DMEM supplemented with 1 % FBS while low glucose DMEM supplemented with 10 % FBS served to define optimal cell growth. The untreated cells cultured in 1 % FBS thus represented 100 % fibroblast proliferation and all other treatments were calculated as a percentage of this control. Concurrent assessment of the cell viability was used to confirm that proliferation is not influenced by cell death.

115
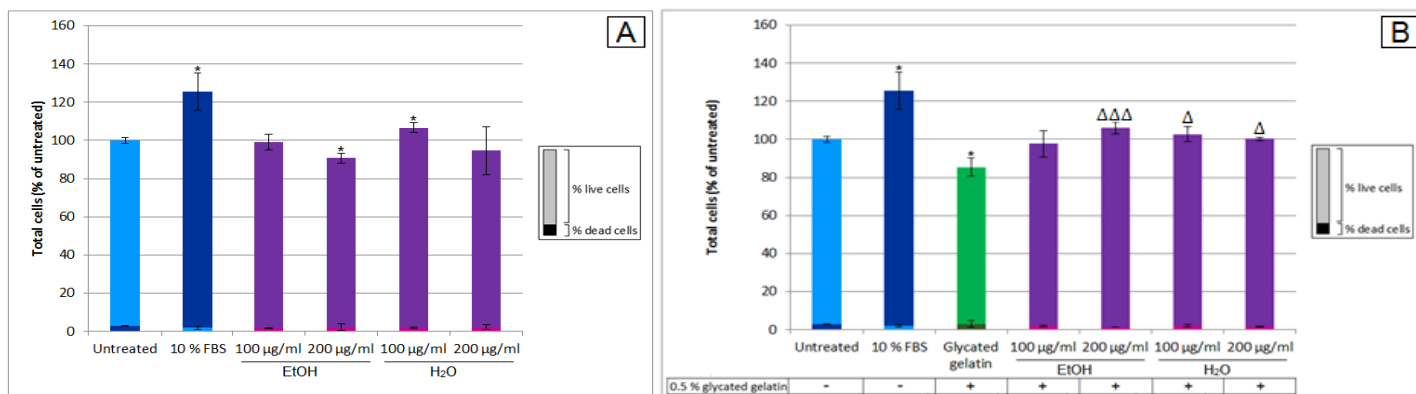
Figure 4.53: MRHF fibroblast proliferation in response to treatment with *P. tinctorius* (A) without glycated gelatin and (B) with glycated gelatin; results are reported as means ± SD where each experiment was performed three times, each in triplicate (*/Δp<0.05; **/ΔΔp<0.01; ***/ΔΔΔp<0.005 where *compared to untreated control containing 1 % FBS; Δ compared to glycated gelatin).

From figure 4.53 A it is evident that the 100 µg/ml water extract of *P. tinctorius* was the only extract that significantly increased fibroblast proliferation in the presence of 1 % FBS while the 200 µg/ml ethanol extract significantly impaired fibroblast proliferation when compared to the untreated sample. The 200 µg/ml ethanol extract and both concentrations of the water extracts were able to restore fibroblast proliferation back to the levels observed for the 1 % FBS control sample and were thus shown to overcome the negative effect observed in response to the AGEs (figure B).
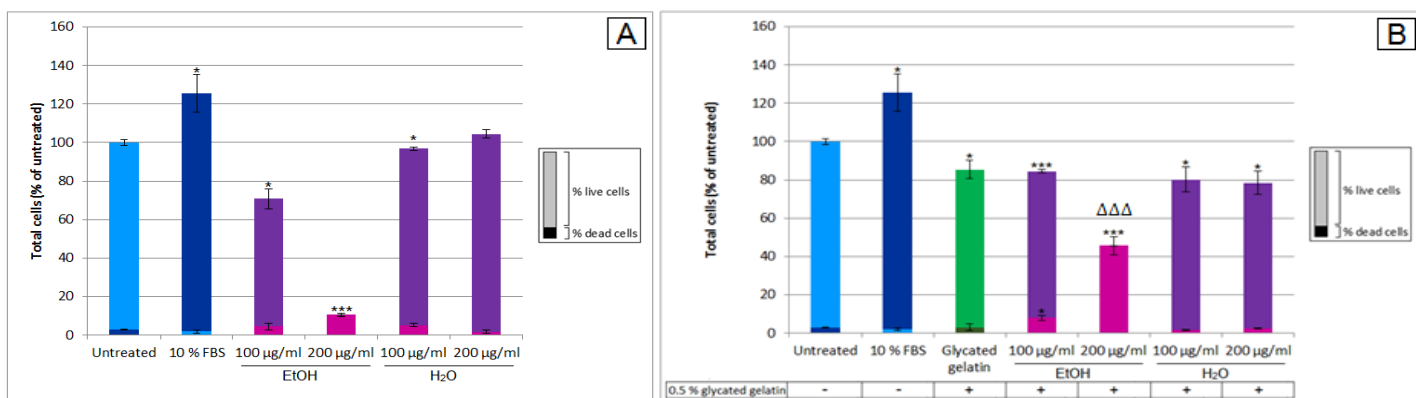
Figure 4.54: MRHF fibroblast proliferation in response to treatment with *R. capensis* (A) without glycated gelatin and (B) with glycated gelatin; results are reported as means ± SD where each experiment was performed three times, each in triplicate (*/Δp<0.05; **/ΔΔp<0.01; ***/ΔΔΔp<0.005 where *compared to untreated control containing 1 % FBS; Δ compared to glycated gelatin).

The 100 µg/ml ethanol extract of *R. capensis* significantly impaired fibroblast proliferation in (figure 4.54 A) in the presence of 1 % FBS while the 200 µg/ml ethanol extract appears to have killed all the fibroblast cells. The same cytotoxicity was not reported in section 4.2.1 in the presence of 10 % FBS, thus demonstrating the importance of assessing both parameters. The 100 µg/ml water extract also

appears to have impaired fibroblast proliferation, however, the same was not observed for the fibroblasts treated with the 200 µg/ml water extract. From figure B, neither the ethanol nor the water extracts were able to overcome the impairment in fibroblast proliferation caused by the glycated gelatin with the ethanol extract causing more damage than the glycated gelatin alone.
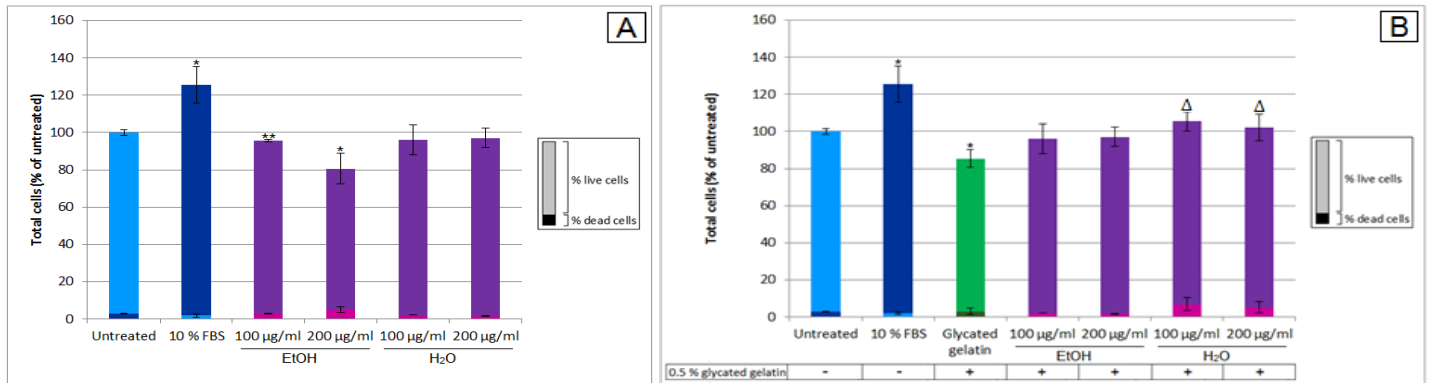
Figure 4.55: MRHF fibroblast proliferation in response to treatment with *B. badius* (A) without glycated gelatin and (B) with glycated gelatin; results are reported as means ± SD where each experiment was performed three times, each in triplicate (*/Δp<0.05; **/ΔΔp<0.01; ***/ΔΔΔp<0.005 where *compared to untreated control containing 1 % FBS; Δ compared to glycated gelatin).

The ethanol extract of *B. badius* was found to significantly impair fibroblast proliferation in a dose-dependent manner in the presence of 1 % FBS while the water extract did not cause any measurable alterations when compared to the untreated sample (figure 4.55 A). Consequently, figure B shows that only the water extract of *B. badius* was able to overcome the impairment in MRHF fibroblast proliferation caused by the glycated gelatin ($p<0.05$), suggesting that it might prove useful in restoring the correct fibroblast function.
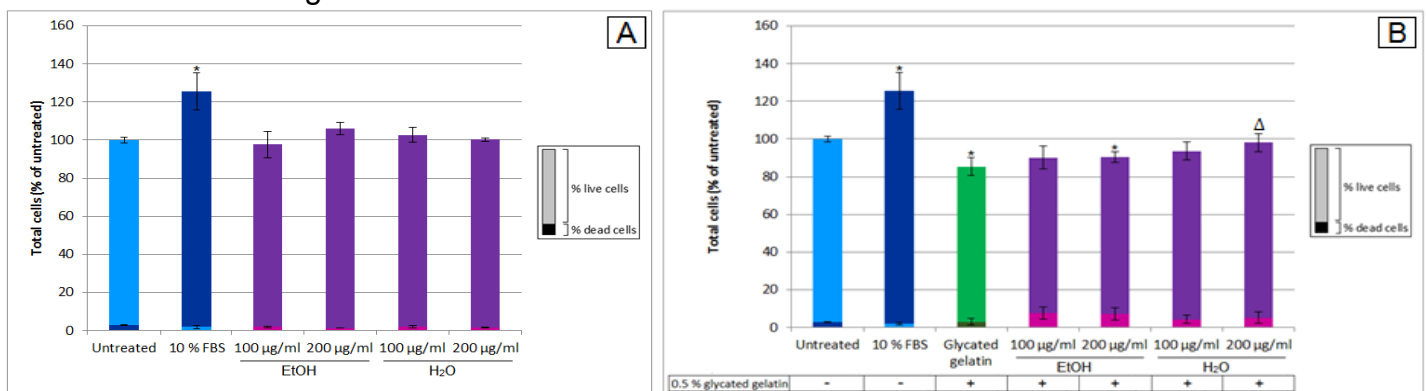
Figure 4.56: MRHF fibroblast proliferation in response to treatment with *P. ostreatus* (A) without glycated gelatin and (B) with glycated gelatin; results are reported as means ± SD where each experiment was performed three times, each in triplicate (*/Δp<0.05; **/ΔΔp<0.01; ***/ΔΔΔp<0.005 where *compared to untreated control containing 1 % FBS; Δ compared to glycated gelatin).

Figure 4.56 A shows that the ethanol and water extracts of *P. ostreatus* did not have any significant effects on the proliferative capability of MRHF fibroblasts in the presence of 1 % FBS in comparison to the untreated sample. Furthermore, only the 200 µg/ml water extract significantly enhanced fibroblast proliferation in the presence of glycated gelatin, suggesting very limited potential for this extract to overcome the impairment in fibroblast proliferation caused by the glycated gelatin in figure B.
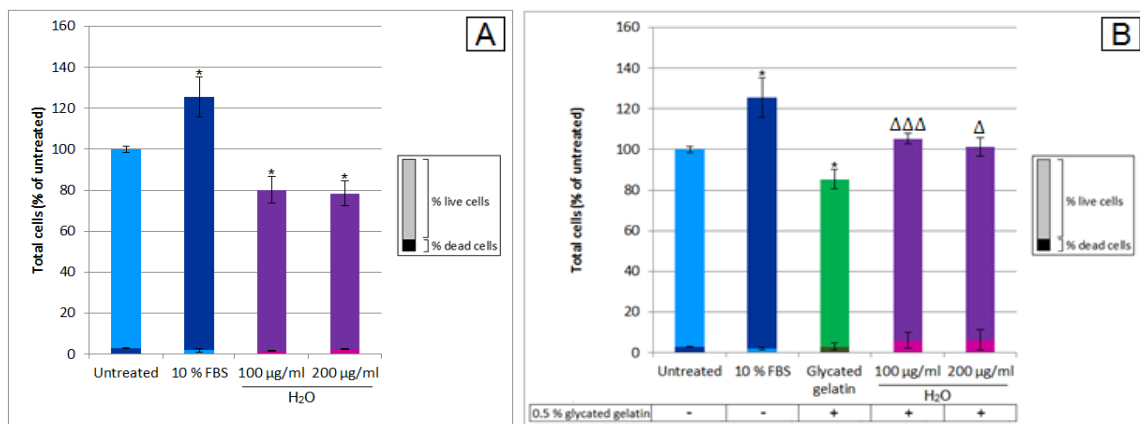
Figure 4.57: MRHF fibroblast proliferation in response to treatment with *G. lucidum* (A) without glycated gelatin and (B) with glycated gelatin; results are reported as means ± SD where each experiment was performed three times, each in triplicate (*/Δp<0.05; **/ΔΔp<0.01; ***/ΔΔΔp<0.005 where *compared to untreated control containing 1 % FBS; Δ compared to glycated gelatin).

From figure 4.57 A, the 100 and 200 µg/ml concentrations of the water extract of *G. lucidum* both significantly impaired fibroblast proliferation in the presence of 1 % FBS when compared to the untreated sample, however, figure B shows that the water extract was indeed able to overcome the impairment in proliferation caused by the glycated gelatin. Several of the tested mushroom extracts were thus able to promote fibroblast proliferation in the presence of glycated gelatin and could potentially overcome the impairment in the proliferative capacity of fibroblasts demonstrated by fibroblasts isolated from diabetic wounds.

4.4.2. Migration

Considering the variable effects of the mushroom extracts on fibroblast proliferation, MRHF fibroblast migration was assessed in the presence of the proliferation inhibitor mitomycin C (from *Streptomyces caespitosus*) using the Enzo® Cell Migration Assay kit. A mitomycin C dose-response toxicity curve was established (figure 4.58) and used to select an appropriate concentration for the migration experiments (figure 4.59). The untreated sample consisted of low-glucose DMEM supplemented with 10

% FBS. The micrographs captured after 48 hours were analysed using T-Scratch software in order to calculate the percentage wound closure. The scratch assay was performed prior to this migration assay in an attempt to identify suitable candidates for promoting fibroblast migration in the presence of glycated gelatin (results not shown) and consequently, only the most promising extracts were selected for this assay.
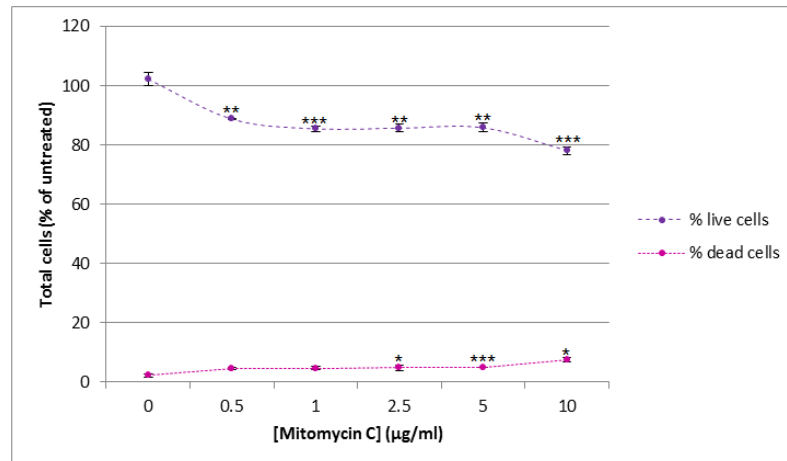
Figure 4.58: Mitomycin C dose-response curve for MRHF fibroblast proliferation after 72 hours where live and dead cell numbers were obtained using Hoechst 33342 and PI staining, respectively; results are reported as means ± SD with this experiment being performed once in triplicate (*p<0.05; **p<0.01; ***p<0.005 compared to 0 % sample).

Figure 4.58 shows that mitomcyin C resulted in a significant decrease in MRHF fibroblast proliferation in comparison to the untreated sample. A statistically significant dose-dependent increase in cell death was observed at concentrations of 2.5 μg/ml and above, however, these values were not considered physiologically relevant as the difference in cell death between the untreated sample (0 %) and the 10 μg/ml treatment was only 4 %. Consequently, a mitomycin C concentration of 10 μg/ml was selected for further experimentation.
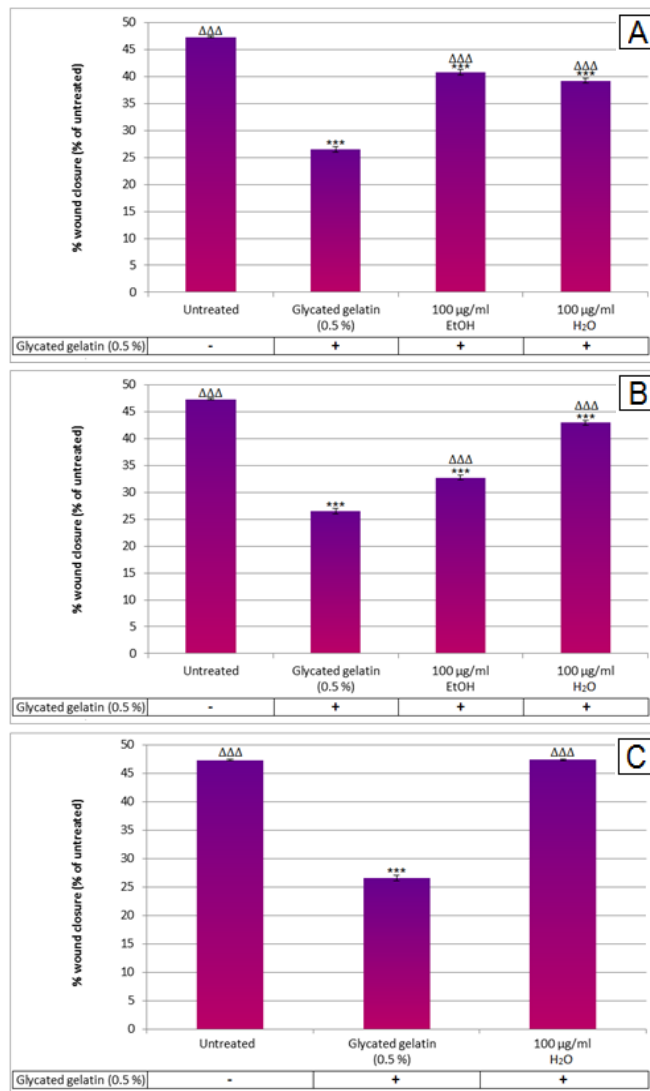
Figure 4.59: MRHF fibroblast migration using the Enzo® Cell Migration Assay kit in response to treatment with (A) *R. capensis*, (B) *B. badius* and (C) *G. lucidum*; results are reported as means ± SD where each experiment was performed three times, each in triplicate (*/Δp<0.05; **/ΔΔp<0.01; ***/ΔΔΔp<0.005 where *compared to untreated sample; Δ compared to glycated gelatin).

According to figure 4.59, the 100 µg/ml ethanol and water extracts of *R. capensis* and *B. badius* as well as the water extract of *G. lucidum* all resulted in significant increases in MRHF fibroblast migration when compared to treatment with glycated gelatin alone (p<0.005). The water extract of *G. lucidum*, however, was able to restore the migratory potential of the fibroblasts back to that seen in the untreated sample and was subsequently identified as the most promising extract for promoting normal fibroblast migration in diabetes.

Increasing evidence suggests that the dermal accumulation of AGEs remains the underlying cause of impaired wound healing in diabetic individuals (Liao *et al.*, 2009). While several models have been used to study diabetic wound healing, many of these do not suitably mimic the diabetic state while the high cost associated with purified proteins such as collagen and albumin poses a limitation to many laboratories (Mendes *et al.*, 2012; Boonkaew *et al.*, 2014). Furthermore, the process during which glycated proteins are produced in sufficient quantities for screening purposes is extremely challenging as the glycation of native proteins is very time consuming, taking several weeks to months, with a consequently large risk of microbial contamination. For these reasons, this study aimed to develop and characterize a more convenient and cost effective *in vitro* model to study diabetic wound healing using glycated gelatin as a surrogate protein.

5.1. CHARACTERIZATION OF THE GLYCATED GELATIN MODEL

Collagen is a major constituent of dermal tissue making up approximately 70 to 80 % of the dry weight of skin. Collagen consequently performs several important functions during the wound healing process including the provision of a structural scaffold and the regulation of cellular functions such as differentiation, migration and protein synthesis (Brett, 2008). Gelatin is a denatured form of collagen and was consequently identified as a suitable, more cost-effective, abundantly available alternative to collagen. Gelatin has been classified as a useful hydrocolloid with low toxicity and comprises all the amino acids except tryptophan. Furthermore, only very few tyrosine, methionine and cysteine residues are present as most of them are degraded during the hydrolysis of collagen to produce gelatin (Raja Mohd Hafidz *et al.*, 2011; Duconseille *et al.*, 2015).

Collagen consists of three α-chains which interact together to form a triple helix. The presence of the Gly-Pro-Hyp motif in the α-chain causes it to adopt an unstable left-handed helical conformation. Consequently, three α-chains will interact to form a highly stable right-handed triple helix stabilised by both intra and inter-chain hydrogen bonds where the glycine residues are buried within the centre of the helix and the side chains containing the X and Y residues remain exposed to the solvent (Duconseille *et al.*, 2015). While the amino acid composition and sequence of gelatin

differs according to its source and method of extraction and purification, the primary sequence consists of the same repetitive Gly-X-Y unit found in collagen where glycine is the most abundant amino acid and X and Y can be any amino acid but are usually proline and hydroxyproline, respectively (Raja Mohd Hafidz *et al.*, 2011).

During the denaturation process to form gelatin, the native triple-helical conformation of collagen is lost. The hydrolytic cleavage of collagen yields several fragments and gelatin thus consists of a mixture of fragments that are joined by peptide bonds to form polymers of varying mass. Upon cooling, the individual fibres are able to only partially recover their helical structure as water becomes trapped in the mesh of chains. Gelatin thus consists of junction zones composed of individual triple-helixes or triple-helix aggregates where the quantity of helix structures is directly proportional to the concentration of the gelatin (Pena *et al.*, 2010; Duconseille *et al.*, 2015).

The structure of gelatin is influenced by several factors including pH, temperature and concentration. An important characteristic of gelatin is its ability to form thermo-reversible gels in water. When aqueous solutions containing gelatin concentrations greater than 0.5 % are cooled to between 35 and 40 °C, an increase in viscosity followed by the formation of a gel occurs. The helical structures formed in gelatin gels are stabilised by several interactions including hydrogen bonds, hydrophobic interactions, electrostatic interactions and cross-links (Gelatin Manufacturers Institute of America, 2012; Duconseille *et al.*, 2015).

There has been much controversy with regards to the three-dimensional structure of gelatin. The "fringed-micelle" model describes the presence of microcrystallites interconnected with amorphous segments of randomly coiled fragments. In another model, however, local regions of protein quaternary structure have been proposed. These structures are deemed to be self-limiting in terms of their size and can exist as either a triple-helix or a partial triple-helix and may include β-turn as well as β-sheet motifs (Pena *et al.*, 2010).

5.1.1. The autofluorescence of advanced glycation end products

While gelatin naturally contains several cross-links which help to stabilise its structure, certain environmental conditions such as temperature and UV light have been shown to increase the formation of these cross-links. No specification with

regards to the time or rate of exposure required to produce the cross-links have been defined, however, it has been suggested that high temperatures above 105 °C should lead to an increase in cross-link formation. Furthermore, little knowledge with regards to which cross-links are formed in response to environmental factors as well as their mechanism of action is available (Duconseille *et al.*, 2015).

As previously explained, chronically elevated blood glucose levels witnessed in diabetic individuals leads to the formation of AGEs through the glycation process. During glycation, glucose forms covalent adducts with collagen, haemoglobin and several plasma proteins including albumin and fibrinogen (Singh *et al.*, 2014). Various sugars have been successfully used as cross-linking agents of gelatin, however, at physiological temperatures this process requires several days to weeks (Masutani *et al.*, 2014). Due to the previously mentioned ability of gelatin to form thermo-reversible gels, the glycation process can be carried out within minutes under the correct conditions without disrupting the structure of the protein. This is in contrast to most other proteins which denature at high temperature and subsequently form insoluble precipitates, and are thus not suitable for high temperature glycation.

According to a study conducted by Münch *et al.* (1999), sugars were shown to preferentially react with cysteine or tryptophan residues in peptides where the α-amino group as well as the side chains are free. In peptides containing a blocked N-terminus but free side chains the amino acids preferred for glycation were cysteine, lysine and histidine. Lastly, arginine and tryptophan were the preferred amino acids for the crosslinking of protein-AGEs to dipeptides containing free side chains but blocked N-termini. It has further been suggested that similar glycation products may be formed in proteins with lateral chains of serine, threonine and tyrosine residues and glycation reactions are thus not highly dependent on sequence specificity (Xue *et al.*, 2011; Oliveira *et al.*, 2013).

According to this knowledge, the absence of tryptophan residues and the presence of very few cysteine residues in gelatin suggests that it is mostly the arginine and lysine residues that are glycated, however, due to the incomplete knowledge with regards to the three-dimensional structure of gelatin, the exact glycation residues have not been established. Glucose-derived AGEs that have been identified in

collagen and gelatin include pentosidine and glucosepane (Oliveira *et al.*, 2013; Duconseille *et al.*, 2015).

In order to confirm that the glycation method used during this investigation was successful, the intrinsic autofluorescence of AGEs was exploited. Several AGEs such as pentosidine are fluorescent and autofluorescence is thus a commonly used and simple method employed to evaluate AGE formation in solution. During this study, glucose was selected as the carbohydrate of choice to promote the glycation process as high blood glucose levels have been identified as the main culprit responsible for AGE formation *in vivo*. Several studies have chosen to use more reactive carbohydrates such as ribose, methylglyoxal or glucose 6-phosphate to facilitate the glycation reaction due to the apparent low reactivity of glucose in solution as a result of its stable chair conformation (Boonkaew *et al.*, 2014). During this study, however, the high temperature (120 °C) employed during the glycation process provided enough energy to overcome the activation barrier needed to open the hemiacetal ring structure of glucose thus allowing it to easily participate in the glycation reaction (Nelson & Cox, 2008).

In figure 4.1 from the results section, the relative fluorescence of various stocks of unglycated gelatin, glucose and glycated gelatin were compared. The glycated gelatin showed a 5-fold increase in fluorescence when compared to the unglycated gelatin thus confirming that the glycation process was indeed successful. Minimal increase in the fluorescence was observed when the glycated gelatin was subjected to a second round in the autoclave (results not shown), suggesting that the glycation process is essentially completed after a single round in the autoclave. Furthermore, the addition of the glycation inhibitor, amino-guanidine, was found to attenuate the increase in fluorescence and consequent glycation (results not shown).

5.1.2. Cytotoxicity screening

Microscopy-based HCS is emerging as a popular tool to measure multiple cell parameters simultaneously with subcellular spatial resolution, thus providing much deeper insights into various biological processes (Boutros *et al.*, 2015). Due to the high cost associated with the required equipment and the complexity to analyse such interrelated data, very little has been published to date using HCS, particularly on the African continent. For this reason it was decided to compare the accuracy of the

cytotoxicity screening results obtained using HCS with the more traditional method of measuring cell density using the crystal violet assay. Due to the fact that the MetaXpress® software used during this study calculated the total cells by counting the number of nuclei in each well, the term 'cell number' is used throughout this discussion when referring to the data obtained using HCS. Conversely, crystal violet stains cellular DNA and proteins and the term 'cell density' thus refers to the data obtained using the crystal violet assay as it does not give a measure of cell numbers.

Hoechst 33342 and PI dual staining showed a dose-dependent decrease in RAW 264.7 macrophage and MRHF fibroblast cell number coupled to a dose-dependent increase in cell death in the presence of glycated gelatin (figure 4.3 A and C). No significant decrease in cell number was observed for either cell line in response to the unglycated gelatin with the only increase in cell death occurring at 2 % for the RAW 264.7 cells. This suggests that the AGEs present in the glycated gelatin rather than the gelatin itself are responsible for the observed toxicity. The increase in cell numbers observed for the RAW 264.7 cells in response to the unglycated gelatin may be attributed to the presence of additional adherence factors in the gelatin.

The same dose-dependent decrease in cell density for both the RAW 264.7 macrophages and the MRHF fibroblasts was observed during the crystal violet assay in response to treatment with glycated gelatin. Upon comparison of the individual values obtained here with those of the Hoechst 33342/PI staining, however, it is evident that higher values were obtained during the crystal violet assay. Using the 1 % glycated gelatin as an example, a 20 % decrease ($p < 0.05$ %) in cell number was observed in the RAW 264.7 macrophages during the nuclear staining method compared to an 8 % decrease (not statistically significant) in cell density during the crystal violet assay. The same observation was made for the MRHF fibroblasts. This suggests that the crystal violet assay was not as sensitive in detecting reductions in cell density as the nuclear staining method.

Upon comparison of the results obtained during the nuclear staining method with those from the crystal violet assay, some discrepancies with regards to the macrophage and fibroblast responses to treatment with unglycated gelatin were observed. While significant increases in cell number of up to 40 % were reported for the macrophages treated with 0.75, 1 and 1.5 % unglycated gelatin, no significant

125

changes in cell density were observed during the crystal violet assay when compared to the untreated sample. Similarly for the MRHF fibroblasts, no significant alterations in cell number or cell death were observed during the nuclear staining method while significant decreases in cell density occurred in the cells treated with 1.5 and 2% unglycated gelatin. Due to the fact that there are several washing steps that must be carried out during the crystal violet assay before and after the cells have been fixed, a plausible explanation for this phenomenon is that these discrepancies have arisen due to the fact that cells were washed away during the crystal violet assay thus leading to inaccurate results. HCS also uses a more direct method of analysis by counting the number of nuclei present, whereas crystal violet relies on an absorbance reading to determine cell density.

From the above results, the advantages of using HCS to quantify cell numbers over more traditional methods such as the crystal violet assay used during this study are obvious. The multiplexing of Hoechst 33342 with PI allows one to accurately determine whether a particular treatment is stimulating cell proliferation or whether it is anti-proliferative or cytotoxic in one single experiment. Determining cell numbers and the percentage of dead cells are the simplest measurements that can be obtained from the MetaXpress® software utilised during this assay with much more complex data relating to the stain area, cytoplasmic and nuclear fluorescence intensities etc. being available should one require it. Further practical advantages of HCS include using fewer reagents, the absence of washing steps and much shorter incubation periods. Furthermore, the data obtained during HCS takes into account the events occurring in every cell that is imaged and the quality of data obtained from the imaging software is thus unparalleled to that obtained from experiments such as the crystal violet assay where only one absorbance reading is obtained per well. The major drawback of HCS is related to the initial cost of the instrumentation and the software required.

5.1.3. The inflammatory response

Proteins that have been modified by AGEs undergo alterations in their structure and consequent function while simultaneously undergoing accelerated degradation to free AGEs. Most AGE-induced tissue dysfunction involves receptor-mediated mechanisms which stimulate various signalling pathways in several cell types. While

multiple receptors that are able to recognise AGEs have been identified, the RAGE receptor is the best studied example and is believed to be responsible for the pathogenesis associated with AGE formation. The interaction of AGEs with the RAGE receptor has indeed been linked to the pathogenesis of complications observed in diabetic patients including impaired wound healing (Xue *et al.*, 2011; Singh *et al.*, 2014).

Activation of the RAGE receptor results in its upregulation and this has been shown to stimulate the inflammatory response and oxidative stress. Some of the signalling cascades involved in RAGE activation include various members of the MAPK, JAK/STAT and Rho GTPase families. Studies have also shown that RAGE activation and its resultant up-regulation activates transcription factors such as NF-κB and early growth response protein 1 (Erg-1) which have been implicated in inflammation. The activation of these signalling pathways ultimately leads to the activation of several pro-inflammatory genes as well as phenotypic changes in cells relating to their migration, proliferation and apoptosis (Oliveira *et al.*, 2013).

5.1.3.1.   *Nitric oxide production in activated macrophages*

The addition of LPS resulted in a several-fold increase in RAW 264.7 macrophage NO production, confirming that the inflammatory potential of these cells has been activated (figure 4.4). Treatment with the glycated gelatin resulted in a significant dose-dependent decrease in NO production by the macrophages as the concentration of the glycated gelatin was increased from 0.5 % to 2 % when compared to the LPS control. No significant differences in NO production were observed in the cells treated with unglycated gelatin thus suggesting that the effect observed in response to treatment with glycated gelatin was due to the presence of AGEs.

These results are not in agreement with literature which states that hyperglycaemia and the resultant formation of AGEs leads to the activation of the RAGE receptor whose presence has been confirmed in RAW 264.7 macrophages (Sumi & Ignarro, 2004). Consequent NF-κB activation leads to the induction of several pro-inflammatory genes including iNOS which ultimately causes an increase in the production of NO. Further studies have shown that AGEs induce iNOS expression in RAW 264.7 cells through the action of tyrosine kinase, PI3K, P38MAPK as well as

PKC (Chang *et al.*, 2004; Sumi & Ignarro, 2004). According to deFronzo *et al.* (2015), a plausible explanation for the observed decrease in NO in the presence of AGEs could be attributed to NOS uncoupling from its essential cofactor in response to a restriction in the availability of L-arginine. L-arginine is an important source for the production of superoxide at sites that have been compromised by diabetes and thus superoxide production will be preferred over that of NO. There appears to be much controversy with regards to this explanation as temporal changes in NO production are observed throughout the progression of diabetic complications. Early on in the development of diabetes, for example, an increase in NO production within affected tissues is thought to occur in response to changes in NOS activity such as described above with regards to RAGE activation. As the disease progresses, however, a decline in the function of organs prone to diabetic complications together with a state of progressive NO deficiency is observed. This decrease in NO could be due to NO scavenging and inhibition by AGEs as well as post-translational modifications of NOS. A study conducted by Bucala *et al.* (1991) confirms that AGEs are able to scavenge NO activity both *in vitro* and *in vivo.*

Based on the results from the cytotoxicity screening assay for both RAW 264.7 macrophages and MRHF fibroblasts as well as those from the Griess reaction, the most suitable concentration of glycated gelatin selected to mimic the diabetic state was identified as 0.5 %. This model displayed the lowest cytotoxicity while simultaneously inducing changes with regards to the functioning of the relevant cells under investigation.

5.1.3.2.   *Nitric oxide scavenging activity*

NO has been implicated in various pathophysiological alterations during the inflammatory response. Due to the observed decrease in the LPS-activated production of NO in RAW 264.7 macrophages treated with gycated gelatin in combination with the explanation provided regarding the ability of AGEs to uncouple NOS from its essential cofactor (BH4) and consequently quench NO production, the NO scavenging capability of glycated and unglycated gelatin was assessed (figure 4.5). Amino-guanidine was selected as the positive control as it is a well-known inhibitor of iNOS and consequently displays various anti-inflammatory properties (Szabo *et al.*, 1997). The NO scavenging activity of unglycated gelatin was

calculated to be 7 % while that of glycated gelatin was 12 %. While these values seem relatively low in comparison to the positive amino-guanidine control which scavenged 62 % of the NO, it confirms that the decrease in NO observed in figure 4.4 in response to the treatment of RAW 264.7 macrophages with glycated gelatin was indeed as a result of the quenching of NO and not due to a decrease in NO production. Furthermore, other markers indicative of macrophage activation measured in this study supports a classical pro-inflammatory response upon treatment with glycated gelatin.

5.1.3.3. *Phagocytosis*

As previously described, phagocytosis is essential for the removal of dead and damaged cells, cell debris as well as pathogens during wound healing. Macrophages thus play an important role in preventing wound infection and producing the necessary signalling molecules that will enable the wound healing process to transition from the inflammatory phase to the tissue repair process. During diabetes, the function of macrophages is compromised due to impaired chemotaxis to the wound area accompanied by impaired phagocytic and killing capabilities (McCulloch & Kloth, 2010). Due to the fact that plasma from healthy non-diabetic patients does not improve the phagocytic function of diabetic phagocytic cells it stands to reason that the impairment due to diabetes is brought about by intrinsic defects, however, the pathogenic mechanisms behind impaired macrophage function in diabetes remains unclear (Geerlings & Hoepelman, 1999). An *ex vivo* study investigating the effects of hyperglycaemia on the function of alveolar macrophages revealed a decreased respiratory burst, an impairment in the secretion of cytokines including TNF-α and IL-6 as well as a decreased responsiveness to several TLR ligands as a result of alterations to the normal intracellular signalling pathways of the macrophages (Xiu *et al.*, 2014). The AGEs associated with hyperglycaemia have also been shown to directly suppress the phagocytic capability of macrophages; however, no further information with regards to their mechanism of action could be found (Khanna *et al.*, 2010).

Phagocytosis in macrophages involves the formation of phagolysosomes which tend to be fairly large, depending on the content of the ingested material. As a result, an increase in phagocytosis is generally associated with an increase in acidic vacuole

formation (Cooper, 2000). Cytochalasin B was used to inhibit phagocytosis and has been classified as a cell membrane permeable mycotoxin that has been shown to inhibit the rate of actin polymerisation as well as the interaction of actin filaments in solution by binding to the barbed end of the actin filaments (MacLean Fletcher & Pollard, 1980). LPS was used as a positive control to promote phagocytosis as it is one of the PAMPs that are recognised by macrophages during phagocytosis (Aderem, 2003).

A decrease in acidic vacuole formation by RAW 264.7 macrophages was observed in response to treatment with cytochalasin B, however, a large standard deviation resulted in no significant differences compared to the untreated sample (figure 4.7). Upon closer investigation of the individual experiments in appendix C, a significant decrease in acidic vacuole formation in response to cytochalasin B was observed for two of the three experiments. The overall trend thus suggests that cytochalasin B did indeed result in a decrease in acidic vacuole formation. Furthermore, cytochalasin B resulted in a highly significant decrease ($p<0.005$) in phagocytosis when compared to the untreated sample as was expected based on its mechanism of action. It is important to note that phagocytosis is a highly dynamic process involving several steps. In the early stages of phagocytosis an increase in the formation of phagosomes will occur, however, they do not become acidic until they fuse with lysosomes during the later stages of the phagocytic process. Furthermore, LTR does not only quantify phagolysosomes, but also lysosomes and other acidic compartments within the cell (Aderem, 2003). As cytochalasin B inhibits the microtubule system within cells, it prevents the uptake of the pHrodo™ Bioparticles® which would result in less phagolysosomes, however, it does not have any effect on the lysosomes and consequently one would not necessarily expect any significant decreases in LTR staining.

As LPS is an inducer of the inflammatory response, it was expected that LPS would stimulate macrophage phagocytosis. Treatment of RAW 264.7 macrophages with LPS (200 ng/ml) did not produce any significant alterations in acidic vacuole formation, however, a 20 % increase in the phagocytosis of the pHrodo® Bioparticles® was reported when compared to the untreated sample. This increase, however, was not significant due to the variation between individual experiments. As

the cells were only treated with LPS for one hour before the pHrodo® Bioparticles® were added to the medium, it is possible that the treatment period was not long enough for LPS to properly exert any measurable effects.

Treatment with 0.5 % glycated gelatin resulted in a significant decrease in phagocytosis as expected from literature accompanied by an increase in acidic vacuole formation. Although this increase was not significant when the results from all three experiments were combined, all individual experiments suggest that this increase was indeed significant when compared to the untreated sample. As the unglycated gelatin did not affect acidic vacuole formation or phagocytosis in RAW 264.7 macrophages, the response to glycated gelatin can be attributed to the presence of AGEs. While it is possible that the lysosomal compartment remained unaffected by treatment with the glycated gelatin and that glycation thus only affects the early stages of phagocytosis upstream of phagolysosome formation, a study conducted by Guo *et al.* (2016) showed that wound macrophages exposed to AGEs were found to undergo autophagy with an increase in autophagy inducing M1 macrophage polarization. During autophagy, autophagosomes are formed which fuse with lysosomes to form autolysosomes, thus explaining the link between autophagy and acidic vacuole formation. Furthermore, an increase in macrophage autophagy was shown to have a negative effect on the normal wound healing process and was shown to play a role in chronic wound healing.

5.1.3.4. *M1/M2 macrophage polarization*

As previously mentioned, impaired diabetic wound healing is characterized by a prolonged inflammatory state defined by an increase in pro-inflammatory M1 macrophages and a decrease in anti-inflammatory M2 macrophages. A study conducted by Jin *et al.* (2015) showed that AGEs were able to promote pro-inflammatory M1 macrophage activation and while the mechanisms behind this phenomenon are not well known, their results suggested that the AGE-RAGE interaction is important in this activation process. Furthermore, evidence exists that AGEs are capable of mediating NF-κB activation through the action of the TLR4 signalling pathway where TLR4 signalling has also been implicated in M1 macrophage polarization. Several other possibilities exist and there is consequently

much that remains to be explored with regards to the signalling pathways involved in M1 macrophage activation through AGEs.

LPS has been shown to stimulate M1 macrophage polarization and was consequently selected as a positive control for the up-regulation of CD86. Treatment of RAW 264.7 macrophages with LPS resulted in a substantial increase ($p<0.05$) in CD86 implying M1 macrophage activation as expected (figure 4.9). The 0.5 % unglycated gelatin sample did not have any effect on the M1 activation status of the RAW 264.7 macrophages, however, the glycated gelatin resulted in a significant 11.5 % ($p<0.05$) increase when compared to the untreated sample. Treatment with both glycated gelatin and LPS resulted in the same level of activation as treatment with LPS alone.

Using CD206 as a marker for M2 macrophage activation, curcumin (20 µM) was used as a positive control and resulted in a 5 % increase in the expression of CD206 when compared to the untreated sample. Neither the unglycated nor the glycated gelatin resulted in any alterations in M2 activation when compared to the untreated sample while a insignificant decrease in M2 activation was observed in the sample treated with both glycated gelatin and curcumin when compared to cells treated with curcumin alone.

There is much controversy with regards to investigating M1 and M2 macrophage polarization as there are multiple different aspects of macrophage function that must be assessed before any final conclusions can be arrived at. It would appear that the most reliable data can be obtained from studies related to the analysis of certain cell surface markers known to be specific to each macrophage phenotype (Jin *et al*., 2015). It should be noted again, however, that M1 and M2 macrophages represent two extremes in a range of possible macrophage phenotypes *in vivo* and thus it is the ratio of M1 to M2 macrophages that is important as both phenotypes will always be present. The M1:M2 ratio for the unglycated gelatin was 2.3 while that of the glycated gelatin was 4.5 compared to the untreated sample which gave a ratio of 1.67. The results obtained here thus concur with those of Jin *et al.* (2015) who found that AGEs up-regulated the expression of CD86 and consequent M1 activation but did not have any effect on the expression of CD206 and resultant M2 activation.

5.1.3.5.   NF-κB

Several reports have shown that AGEs are able to activate transcription factors such as NF-κB through various inflammatory signalling pathways. It was previously found that treatment with the anti-RAGE antibody only partly suppressed the activation of NF-κB confirming that the AGE-RAGE pathway was at least partly responsible for the observed effect of AGEs on NF-κB activation, however, it is believed that several other signalling pathways including TLR4 signalling could be involved (Jin *et al.*, 2015).

The nuclear translocation of phospho-p65 NF-κB and consequent NF-κB activation was significantly increased in cells treated with LPS as well as 0.5 % glycated gelatin (figure 4.11). The unglycated gelatin did not have any significant influence on NF-κB nuclear translocation and thus the effect observed for the glycated gelatin can again be attributed to the presence of AGEs. The glycated gelatin had a slightly higher NF-κB activating potential (111 %) than the positive LPS control (108 %), however, the samples treated with both LPS and glycated gelatin had the greatest NF-κB activating activity of 115 %.

5.1.3.6.   COX-2

As COX-2 expression is directly regulated by NF-κB activation, it was expected that AGEs would also promote COX-2 expression. This, however, was not the case. While LPS resulted in a predictably large increase in COX-2 expression of 32 % ($p<0.01$) in comparison to 1.2 % in the untreated sample (figure 4.13), no significant increase in response to treatment with the glycated gelatin alone was observed. While COX-2 expression was slightly higher in the RAW 264.7 macrophages treated with glycated gelatin compared to the unglycated gelatin, this increase was statistically insignificant. Interestingly, it was found that cells treated with both LPS and glycated gelatin resulted in the largest increase in COX-2 expression of 50 % ($p<0.005$), a value 18 % higher than treatment with LPS alone.

According to Ramsay *et al.* (2003), there are three levels of transcriptional regulation of the COX enzymes. These include initiation, alternative splicing as well as mRNA stability. COX-2 expression has been shown to be highly inducible by low levels of several transcription factors and it is well known that there is a very strong

correlation between NF-κB activation and COX-2 expression. While NF-κB may be required in most macrophage cell-lines during inflammation, it has been suggested that NF-κB activation alone may be insufficient to induce maximal COX-2 expression. It is thus plausible that additional signalling pathways required for COX-2 expression were not activated by the AGEs present in the glycated gelatin alone, however, in the presence of LPS the activation of these additional signalling pathways could potentially account for the 18 % increase in COX-2 expression described above.

5.1.4. Fibroblast function

Fibroblasts are important during the proliferation and tissue remodelling phases of the wound healing process, particularly during ECM synthesis and remodelling. In diabetes, however, fibroblasts have demonstrated impaired proliferation and migration abilities during as discussed in chapter one. RAGE receptors have been identified not only in macrophages but also in skin fibroblasts and the AGE-RAGE interaction has consequently been implicated in fibroblast dysfunction during wound healing including impaired proliferation, migration, collagen synthesis and ECM producing abilities. Furthermore, AGEs have been shown to promote fibroblast apoptosis, however, the associated mechanisms are still under current investigation (Tracy *et al.*, 2016).

5.1.4.1. Fibroblast proliferation

MRHF proliferation was not significantly altered by treatment with unglycated gelatin when compared to the untreated sample (1 % FBS), however, a significant decrease ($p<0.05$) was observed in response to the 0.5 % glycated gelatin (figure 4.14). As no changes in cell death occurred, it can be confirmed that AGEs do indeed impair fibroblast proliferation.

5.1.4.2. Fibroblast migration

Similar to the results observed during fibroblast proliferation, no changes to MRHF fibroblast migration after treatment with 0.5 % unglycated gelatin were reported (figure 4.15). Conversely, treatment with 0.5 % glycated gelatin impaired fibroblast migration by 20 % ($p<0.005$) when compared to the untreated control.

5.1.5. Summary of the glycated gelatin model

Table 5.1 provides a summary of the findings observed during the characterization of the glycated gelatin model in order to better understand the strengths and weaknesses of the model developed during this study. This table does not include the different phases of wound healing and provides a brief summary of the overall responses observed during diabetic wound healing. Individual responses may thus vary between different phases of the wound healing process. This table shows that the selected glycated gelatin model suitably mimics many aspects associated with the diabetic state and can consequently serve as an *in vitro* diabetic wound healing model as it was able to simulate the major cellular dysfunctions in macrophages and fibroblasts documented during diabetic wound healing.

Table 5.1: <u>A summary of the effects of the glycated gelatin model on macrophage and fibroblast function during wound healing</u>

Cell type	Assay	Effect of diabetes on wound healing	Effect of 0.5 % glycated gelatin*
RAW 264.7 macrophages	NO production	↓ (Witte *et al.*, 2002)	↓ (possibly due to quenching)
	Phagocytosis	↓ (Khanna *et al.*, 2010; Xu *et al.*, 2013)	↑ in acidic vacuole formation; ↓ in phagocytosis
	M1/M2	↑ in M1 activation (Khanna *et al.*, 2010; Xu *et al.*, 2013)	↑ in M1 activation, - on M2 activation
	NF-κB	↑ (Patel & Santani, 2009)	↑
	COX-2	↑ (Kämpfer *et al.*, 2005)	- without LPS; ↑ with LPS
MRHF fibroblasts	Proliferation	↓ (McKulloch & Kloth, 2010; Xu *et al.*, 2013)	↓
	Migration	↓ (McKulloch & Kloth, 2010; Xu *et al.*, 2013)	↓

*(↑) indicates a positive effect, (↓) indicates a negative effect and (-) indicates no effect

5.2. SCREENING OF EXTRACTS FOR POTENTIAL WOUND HEALING PROPERTIES

Diabetic wounds have been characterized by several abnormalities including increased oxidative stress, increased glycation with a concomitant increase in the formation of AGEs as well as an imbalance in the activation of certain MMPs and TIMPs (Xu *et al.*, 2013). While the traditional uses of several mushroom species as wound dressings have been reported, very limited research is available with regards to macrofungi and their associated wound healing properties, particularly on the African continent (Burk, 1983; Jaengklang *et al.*, 2015). Consequently, five mushroom species collected from the Eastern Cape and Western Cape of South Africa were selected based on previous reports of anti-inflammatory, antidiabetic or anti-oxidant activities. The cytotoxicity, anti-oxidant capacity, glycation inhibitory and collagenase inhibitory potentials of each of the selected mushroom species was assessed in order to probe their potential diabetic wound healing properties.

5.2.1. Cytotoxicity screening

Basal cytotoxicity screening was carried out using RAW 264.7 macrophages and MRHF fibroblasts. The same protocol using Hoechst 33342 together with PI staining was used as in the previous section and these results were again compared to the crystal violet assay. Each mushroom extract was tested at a concentration of 100 and 200 µg/ml. While some might argue that these concentrations are not physiologically relevant, the intended use of the tested mushroom extracts would be as a topical ointment rather than an oral treatment and thus fairly high concentrations were used in order to observe their maximal effects.

The ethanol extract of *P. tinctorius* did not result in any significant cytotoxicity or increases in cell death in the RAW 264.7 macrophages at the tested concentrations during the nuclear staining method (figure 4.17), however, significant cytotoxicity was observed for both the 100 and 200 µg/ml concentrations of the water extract. Interestingly, a significant increase in cell death was observed for only the 100 µg/ml water extract but not at the 200 µg/ml concentration. Due to the small standard deviations, very small differences in cell death resulted in highly significant statistical data ($p < 0.005$); however, the percentage of cell death for the 100 µg/ml water extract of *P. tinctorius* was only 2 %. Considering that the percentage of cell death for the

untreated sample was only 1 %, this difference does not seem very physiologically significant as cell death is a natural part of the cell cycle and there will thus always be a small population of cells that die due to natural causes such as apoptosis or autophagy (Thornburn, 2008; Gewirtz, 2013). For this reason, the cell death was only considered relevant in cases where it exceeded 5 %. According to the results from the crystal violet assay, no RAW 264.7 macrophage cytotoxicity was observed for either of the extracts.

The MRHF fibroblasts displayed significant cytotoxic effects in response to treatment with the 200 µg/ml ethanol and water extracts of *P. tinctorius* with the only significant increase in cell death observed for the 200 µg/ml water extract (4 %). No significant changes in fibroblast cell density in response to treatment with *P. tinctorius* were observed during the crystal violet assay. The cytotoxicity results obtained here again emphasise the higher sensitivity of the nuclear staining protocol using HCS when compared to the crystal violet assay.

No significant cytotoxicity in RAW 264.7 cells were observed during either the nuclear staining method or the crystal violet assay in response to treatment with *R. capensis* for either the ethanol or the water extracts (figure 4.18). A significant decrease in MRHF fibroblast cell number (9 %) was evident for the 200 µg/ml water extract, however, this was not accompanied by an increase in cell death. Furthermore, no decrease in cell density was recorded during the crystal violet assay at this concentration, probably due to the decreased sensitivity of this assay compared to the nuclear staining method.

A significant decrease in RAW 264.7 cell number was reported for the 200 µg/ml ethanol extract of *B. badius* (figure 4.19). This was not accompanied by any increase in cell death during the Hoechst 33342/PI method or cell density as determined by the crystal violet assay. No changes to MRHF fibroblast cell number, cell death or cell density were reported. Furthermore, no significant changes in cell number, cell death or cell density were observed for the RAW 264.7 macrophages or the MRHF fibroblasts in response to treatment with *P. ostreatus* either (figure 4.20).

A robust decrease (p<0.005) in both RAW 264.7 macrophage and MRHF fibroblast cell number was reported for the 100 and 200 µg/ml ethanol extract of *G. lucidum*

(figure 4.21). This was accompanied by a highly significant increase in cell death (26 and 17 %, respectively, for the RAW 264.7 cells and 15 and 30 %, respectively, for the MRHF cells). It is evident that the RAW 264.7 and MRHF cells present in the samples treated with 200 µg/ml of the ethanol extract were dead and the decrease in cell death observed from the 100 µg/ml to the 200 µg/ml ethanol extract in the RAW 264.7 macrophages indicates that most of the cells had already apoptosed into cell fragments thus leading to a decrease in the number of intact nuclei. The same trends in cell density were observed during the crystal violet assay; however, higher cell density values were obtained for the MRHF cells thus indicating a reduced sensitivity. No significant cytotoxicity was observed in either cell line after treatment with the water extract of *G. lucidum*. A literature search revealed that the anti-cancer activity of the ethanol extracts of *G. lucidum* against several cancer cell lines are well documented (Jang *et al.*, 2010; Mohan *et al.*, 2016).

Due to the severe cytotoxicity of the ethanol extract of *G. lucidum* observed in both the RAW 264.7 macrophages and the MRHF fibroblasts, it was decided that no further cell-based assays would be performed using this extract. Several of the tested mushroom extracts resulted in significant decreases in cell number with no increase in cell death and these extracts are thus more than likely exerting an anti-proliferative effect rather than a cytotoxic one and consequently were not excluded from further investigations. The cytotoxicity results obtained in this section concur with those obtained in the previous section with regards to the sensitivity of the nuclear staining protocol using HCS and the crystal violet assay. Many examples were provided where decreases in cell number were not accompanied by a decrease in cell density and thus it would appear that the crystal violet assay frequently provides an over-estimation of the cell number and consequently does not provide a true reflection of the cytotoxic nature of a tested extract.

5.2.2. Anti-oxidant activity

Increased oxidative stress has been observed in chronic diabetic wounds in response to hyperglycaemia as well as AGE formation. Hyperglycaemia promotes increased mitochondrial activity and consequent ROS formation (Kolluru *et al.*, 2012) while AGEs stimulate ROS production through different mechanisms including the stimulation of NADPH-oxidase (NOX) which induces the formation of the superoxide

anion. AGEs have also been shown to compromise various cellular anti-oxidant defence mechanisms such as the cross-linking of copper-zinc superoxide dismutase (Cu-Zn-SOD) which results in its inactivation and subsequent site-specific fragmentation. Furthermore, AGEs are highly reactive molecules and can thus act as electron donors during the cross-linking reaction, resulting in the formation of superoxide anions while the cross-linking of cation radical sites during protein glycation enables proteins to catalyse single-electron redox reactions through the formation of active enzyme-like centres and consequently stimulates ROS production. These redox reactions do not require oxygen or co-factors such as copper or iron that are usually required during redox reactions (Gkogkolou & Böhm, 2012).

Any mushroom extract that displays strong anti-oxidative properties might be able to counter-act the increased production of ROS in response to hyperglycaemia and AGEs at the wound area, potentially promoting normal wound healing by preventing further tissue damage caused by the ROS. To assess the anti-oxidative capacity of each mushroom species, the DPPH, FRAP and NO scavenging assays were performed. The choice to compare three different methods stems from the fact that different anti-oxidants are detected by each method, for example, the FRAP assay detects mostly water-soluble anti-oxidants while the DPPH assay will detect mostly lipophilic anti-oxidants. Perhaps the most relevant of the three assays is the NO scavenging assay as the non-specificity of the FRAP assay and the physiological irrelevance of the DPPH assay tend to raise questions with regards to the relevance of these methods to *in vivo* anti-oxidant capacities (Liang & Kitts, 2014).

Comparatively strong anti-oxidant activities were reported for the ethanol and water extracts of *P. tinctorius* during the DPPH assay with IC_{50} values below 100 µg/ml (figure 4.22). Similar activity was reported during the NO scavenging assay with an IC_{50} value between 100 and 200 µg/ml for the ethanol extract and above 200 µg/ml for the water extract. Comparatively lower values were obtained during the FRAP assay which suggests that *P. tinctorius* contains more lipophilic anti-oxidants than hydrophilic ones. Overall, *P. tinctorius* displayed comparatively high anti-oxidant activities with the ethanol extract exhibiting the strongest activity, however, the IC_{50} values are too high for the compounds in this mushroom species to be considered

potent anti-oxidants and further work with regards to determining the IC_{50} values was thus not justified. A literature search revealed that no published work exists on the anti-oxidant potential of *P. tinctorius* and this study thus presents the first report of such activities.

During the DPPH, NO scavenging and FRAP assays, comparatively low anti-oxidant activities were reported for the ethanol and water extracts of *R. capensis* with IC_{50} values above 200 µg/ml for the DPPH and NO scavenging assays (figure 4.23). Overall, the anti-oxidant activity of *R. capensis* appears to be relatively low with the ethanol extract being richer in anti-oxidants than the water extract. The anti-oxidant capacities of *B. badius* and *P. ostreatus* were comparatively low with the highest values obtained from the DPPH assay (figures 4.24 and 4.25). Both the ethanol and the water extracts exhibited equal anti-oxidant capacities. No published data was found on the anti-oxidant capacity of *R. capensis* while only one journal article reporting the anti-oxidant activities for *B. badius* could be found. Using an 80 % methanol extract prepared with heat treatment, Jaworska *et al*. (2015) reported for the first time the anti-oxidant activity of *B. badius*. Here they reported anti-oxidant activities of 25.2 mmol Trollox Equivalents (TE) during the DPPH assay and 36.4 mmol Fe^{2+} during the FRAP assay per 100 g dry weight of fresh mushrooms while Taofiq *et al*. (2016) reported an IC_{50} value of 7.69 mg/ml for an ethanol extract of *P. ostreatus* during the DPPH assay. This highlights the difficulties associated with comparing anti-oxidant activities by different authors as there is no consistency or standardisation in the way that these results are expressed. Further complicating this matter is the fact that mushrooms are known to have slightly different compositions depending on where they are cultivated and the same species of mushroom collected from different sources might thus reveal different quantities of individual anti-oxidant compounds (Taofiq *et al*., 2016).

The results from the DPPH scavenging assay show that the 200 µg/ml ethanol extract (65 %) and both concentrations of the water extract (61 % and 76 %, respectively) of *G. lucidum* had comparatively high anti-oxidant activities with IC_{50} values between 100 and 200 µg/ml for the ethanol extract and below 100 µg/ml for the water extract (figure 4.26). The FRAP assay revealed comparatively high anti-oxidant activities for the 200 µg/ml ethanol extract. The lowest anti-oxidant activities

were reported during the NO scavenging assay. A study conducted by Rajasekaran and Kalaimagal (2011) found that the ethanol extract of *G. lucidum* was able to scavenge 72.4 % of the DPPH radicals at a concentration of 250 mg/ml and calculated the IC-50 value to be 172.52 mg/ml for the ethanol extract and 5.28 mg/ml for a hot water extract. Rajasekaran and Kalaimagal (2011) further reported that the ethanol extract of *G. lucidum* resulted in 65.87 % NO scavenging at 200 mg/ml. While the percentage DPPH scavenging activity obtained for the ethanol extract is comparable to the results obtained by Rajasekaran and Kalaimagal (2011), the difference in NO scavenging activity can be attributed to the much lower concentrations used during this study. Overall, the anti-oxidant capacity of *P. tinctorius* and *G. lucidum* appear to be the highest of all the tested mushroom species.

5.2.3. Glycation inhibition

As AGEs have been identified to be largely responsible for the dysregulation of wounds in impaired diabetic wound healing, a mushroom species displaying strong anti-glycation activities could serve as a very useful treatment approach. The ethanol extract of *P. tinctorius* showed a very strong anti-glycation potential (figure 4.27) with the highest activity recorded for the 200 µg/ml ethanol extract (68 % with $p<0.005$). Upon further investigation, however, both the ethanol and water extracts resulted in significant quenching of the fluorescence signal and thus the results obtained for *P. tinctorius* were deemed to be unreliable. In order to assess the true glycation inhibitory potential of *P. tinctorius*, an alternative assay during which the proteins are precipitated in order to remove any interfering substances will have to be utilised.

The remaining four mushroom samples did not show any promising glycation inhibitory activities with both the ethanol and water extracts of *B. badius* and *P. ostreatus* as well as the ethanol extract of *G. lucidum* seemingly promoting glycation (figures 4.28 to 4.31). No published information with regards to the glycation inhibitory potential of any of the mushroom species used during this study except for *G. lucidum* could be found. A study conducted by De Silva *et al.* (2012) showed that in diabetic rats, the polysaccharides isolated from *G. lucidum* were able to ameliorate collagen cross-linking of the myocardium of diabetic rats and consequently decreased the levels of AGEs. It is thus possible that the active compounds

responsible for the observed decrease in AGEs by De Silva *et al.* (2012) were not present in the extracts prepared during this study as polysaccharides, for example, precipitate out of solution in the presence of ethanol.

5.2.4. Collagenase inhibition

Chronic wounds have been characterized by enhanced levels of the collagenase enzymes MMP-1 and MMP-8 coupled to abnormally low levels of TIMPs. As a result, these wounds experience increased ECM degradation, an altered cytokine profile as well as the destruction of growth factors (Sabino & auf dem Keller, 2015). Furthermore, collagen that is modified by glycation has been shown to be resistant to degradation by various collagenase enzymes. Consequently, wound healing becomes impaired as the collagen turnover required to ensure that the collagen remains functional is prevented (Gkogkolou & Böhm, 2012). In diabetes, increased MMP activity has been attributed to oxidative stress and/ or the presence of AGEs (Ayuk *et al.*, 2016). Any mushroom species which is thus able to inhibit collagenase activity could prove useful in the treatment of diabetic wounds, however, none of the mushroom extracts tested during this study showed any promising collagenase inhibitory activities with all the recorded activities being below 20 % (figure 4.32).

5.3. THE INFLAMMATORY RESPONSE

The wound healing process in diabetes becomes impaired due to different regions of diabetic wounds becoming stuck in different phases and consequently, the wound is unable to progress to the final phase of tissue remodelling due to the loss of synchronisation of several cellular events. Furthermore, diabetic wounds tend to enter a state of pathological inflammation as a result of persistent hyperglycaemia, chronically elevated levels of various pro-inflammatory cytokines and microbial infections (Tellechea *et al.*, 2010). The inflammatory phase thus provides a very attractive therapeutic target for encouraging normal wound healing in diabetic individuals with several possible mechanisms and signalling pathways that can be exploited. Due to the complex nature of the inflammatory response and the close relationship between multiple different signalling molecules, the results from each experiment are described individually and the findings from different assays are integrated later on in this section.

5.3.1. Nitric oxide production in activated macrophages

An important way of distinguishing classically activated and alternatively activated macrophages from one another is through their metabolism of arginine. M1 macrophages express iNOS which promotes the metabolism of arginine to NO in an attempt to kill invading microbes. M2 macrophages, however, do not express iNOS and consequently convert arginine to ornithine, a precursor molecule to various polyamines and collagen. NO production is one of the simplest measures used to assess the activation status of macrophages. Diabetic wounds are characterized by an increased burden of M1 macrophages which have been shown to be responsible for producing several inflammatory cytokines and mediators, consequently prolonging the inflammatory phase of wound healing. Theoretically then, an increase in M1 activation would be demonstrated by an increase in NO production while an increase in M2 activation would correlate to lower levels of NO being produced (Mosser & Zhang, 2008). Given the important role of NO in wound healing and the complex nature of diabetic wounds, both the anti-inflammatory and pro-inflammatory potentials of each mushroom extract were assessed.

Given the relevance of microbial infections in promoting chronic wound healing in diabetes, LPS was identified as a suitable inducer of the inflammatory response in RAW 264.7 macrophages by activating signalling pathways that are also activated *in vivo* in response to bacterial infections. In the absence of LPS, both the ethanol and water extracts of *P. tinctorius* resulted in significant increases in the measured NO with the ethanol extract having a stronger effect (figure 4.33 A). This suggests then that this mushroom species displays strong pro-inflammatory properties and consequently promotes M1 activation. In the presence of LPS, however, both the ethanol and water extracts demonstrated seemingly anti-inflammatory activities resulting in a robust decrease in the quantity of NO measured as the concentration of each extract increased. This leads one to believe that this mushroom species displayed both pro-inflammatory and anti-inflammatory activities with the pro-inflammatory activity being more dominant. It is thus possible that *P. tinctorius* contains different compounds that display different activities which would suggest that the current experimental setup is not suitable to assess the true potential of this particular mushroom species. Before such statements can be made, however, it is necessary to consider the NO scavenging potential of *P. tinctorius*. In the previous

section (figure 4.22 C) it was shown that both the ethanol and water extracts of *P. tinctorius* displayed fairly strong NO scavenging activities with the 200 µg/ml ethanol extract demonstrating a similar NO scavenging ability as the positive amino-guanidine control. The ethanol extract resulted in a larger decrease in NO in the presence of LPS than the water extract. As this same trend was observed in figure 4.22 C, it stands to reason that the observed decrease in the presence of LPS was not due to a decrease in the NO produced by the RAW 264.7 macrophages but rather as a result of the NO scavenging capability of *P. tinctorius*. As NO scavenging is also considered to be an anti-inflammatory mechanism, the ethanol and water extracts of *P. tinctorius* were shown to display both pro-inflammatory and anti-inflammatory activities with the anti-inflammatory activity being attributed to strong NO scavenging capabilities. Due to the complex nature of the extracts investigated, these findings emphasise the importance of using more than one assay to gain an accurate perspective of the capabilities and limitations of each extract in terms of their effects on macrophage activation.

Based on the results discussed in section 5.1 and the findings from literature it was established that the decrease in NO in the presence of glycated gelatin was due to scavenging rather than a decrease in the production of NO. Both the ethanol and water extracts of *P. tinctorius* resulted in significantly lower quantities of NO in the presence of glycated gelatin when compared to the sample treated with glycated gelatin alone (figure 4.33 C). As *P. tinctorius* was shown to demonstrate significantly pro-inflammatory activities with a strong NO scavenging potential, it appears that the combined effect of the NO scavenging capability of each extract as well as that of glycated gelatin acted in an additive manner. Consequently, the lowest levels of NO were recorded during this experiment.

From these results it is tempting to state that because NO is a marker for inflammation, a decrease in NO should surely be coupled to a decrease in inflammation. The process of wound healing is, however, extremely complex and involves several signalling pathways and mechanisms. This frequently makes the interpretation of results obtained from *in vitro* experiments very difficult. While NO has been shown to perform several important functions during wound healing and diabetic wounds have been characterized by decreased levels of NO in the wound

milieu (Witte *et al.*, 2002), diabetic wounds have also been characterized by pathological inflammation. NO is frequently used as a marker for inflammation and M1 macrophage activation, however, in diabetes it would appear that NO production is not a suitable measure of M1 activation as the situation is further compounded by the ability of AGEs to quench NO. The results obtained here must thus be interpreted with great caution, highlighting the importance of using a combination of different methods to measure a specific response before arriving at any definitive conclusions during *in vitro* investigations.

The ethanol extract of *R. capensis* did not promote NO production in the absence of LPS, however, a dose-dependent decrease in NO was observed in LPS stimulated cells (figure 4.34). These results indicate that the ethanol extract of *R. capensis* demonstrates anti-inflammatory activities; however, the results from the NO scavenging assay suggest that the observed decrease in NO could be due to scavenging rather than a reduction in NO production. In the presence of glycated gelatin a further decrease in NO was observed with the 200 µg/ml ethanol extract resulting in a robust decrease ($p<0.005$) in NO compared to treatment with glycated gelatin alone. Further studies involving the quantification of iNOS are needed to establish whether the reduction in NO was due to quenching or a decrease in the production of NO. In the absence of LPS, the water extract of *R. capensis* resulted in a noteworthy increase (<0.005) in NO production and consequently displays strong pro-inflammatory activities. In the presence of glycated gelatin, however, no significant alterations in NO levels were reported when compared to the samples treated with glycated gelatin alone and the pro-inflammatory activity of the water extract was thus not strong enough to overcome the NO scavenging activities of the glycated gelatin.

No significant alterations in NO production in the absence and presence of LPS were recorded for the ethanol extract of *B. badius* (figure 4.35). The ethanol extract thus did not demonstrate any pro-inflammatory or anti-inflammatory activities. In the absence of LPS, however, the water extract of *B. badius* was shown to be as potent an inducer of NO production as LPS. Treatment of the RAW 264.7 macrophages with 200 µg/ml of the water extract together with LPS appears to have produced an additive effect and consequently resulted in a significant increase in NO production

compared to the sample treated with LPS alone. In the presence of glycated gelatin, a significant decrease in the quantity of NO was recorded for the 200 µg/ml ethanol extract of *B. badius* compared to treatment with glycated gelatin alone. As negligible NO scavenging was reported for this extract, it would appear that the ethanol extract does indeed possess anti-inflammatory activities. No significant alterations in the quantity of NO were observed for the water extract when compared to glycated gelatin alone.

The ethanol extract of *P. ostreatus* did not show any pro-inflammatory activities in the absence of LPS, however, a dose-dependent decrease in NO was recorded in LPS stimulated cells (figure 4.36 B). Negligible levels of NO scavenging were reported for this particular extract in section 5.2 and thus the ethanol extract of *P. ostreatus* showed anti-inflammatory activities with a consequent decrease ($p < 0.01$) in NO production in the presence of glycated gelatin. A weak pro-inflammatory response was reported for the water extract of *P. ostreatus* in the absence of LPS while no significant anti-inflammatory activities were observed in LPS stimulated cells. Furthermore, treatment of the RAW 264.7 macrophages with the water extract of *B. badius* as well as glycated gelatin did not result in any significant changes in the quantity of NO measured when compared to treatment with glycated gelatin alone.

The water extract of *G. lucidum* did not result in any significant pro-inflammatory or anti-inflammatory activities (figure 4.38 A and B). Consequently, no significant changes in NO production were recorded in the presence of glycated gelatin when compared to treatment with glycated gelatin alone.

In order to ensure that the seemingly pro-inflammatory activities of the tested mushroom extracts were not due to the presence of endotoxins, the possibility of false positives was assessed using polymyxin B sulfate. A dose response curve was constructed in order to define the toxicity of polymyxin B and to select a tolerable concentration for further cell based assays (figure 4.38). A dose-dependent decrease in cell number was recorded up to a concentration of 25 µg/ml after which the cell number appears to have stabilised around 50 %. While a statistically significant ($p < 0.05$) increase in cell death (1.9 %) was recorded at 15 µg/ml due to minor deviations between individual replicates, this was not considered to be

146

physiologically relevant and thus an increase in cell death was only observed at concentrations of 25 µg/ml and above. This suggests that polymyxin B exerted an anti-proliferative effect typical for cytostatic agents up to a concentration of 20 µg/ml after which polymyxin B became cytotoxic. A concentration of 10 µg/ml was selected for further studies as higher concentrations resulted in an unacceptably large decline in cell number (> 20 %).

As a result of the ability of endotoxins to induce NO synthesis, the addition of polymyxin B to the culture medium should dampen NO production due to its endotoxin scavenging ability and may thus be seen as an indication of possible endotoxin contamination. In the presence of polymyxin B, a decrease in NO production in response to treatment with a particular extract compared to the response observed for that same extract in the absence of polymyxin B would consequently suggest the presence of endotoxins. The water extract of *R. capensis* showed a strong pro-inflammatory response in the absence of LPS, however, in the presence of polymyxin B the production of NO was greatly reduced (p<0.005) (figure 4.39 B). This suggests that the pro-inflammatory activity observed for the water extract of *R. capensis* could possibly be due to the presence of endotoxins and further investigations thus need to be carried out in order to confirm this. Similarly, a weak pro-inflammatory increase in NO production was observed in response to treatment of RAW 264.7 macrophages with the water extract of *P. ostreatus*, however, no such increases in NO production were observed in the presence of polymyxin B (figure 4.39 D). As the pro-inflammatory response observed for the water extract of *P. ostreatus* in the absence of LPS was very weak, the fact that the concentration of polymyxin B chosen resulted in a 15 % decrease in cell number suggests that it was this decrease in cell number and not necessarily the presence of endotoxins that affected the NO production of the macrophages treated with the water extract of *P. ostreatus* in the presence of polymyxin B. Again, a more specific endotoxin analysis assay would be required to confirm this.

Due to the saprophytic nature of mushrooms, they are known to absorb various substances from their surroundings (including nutrients and various toxins) and the composition of a particular mushroom species can thus differ as a result of varying surroundings (Taofiq *et al.*, 2016). The presence of endotoxins in mushrooms is thus

a very real possibility. The polysaccharide component of LPS is known to perform an important function during the recognition of endotoxins by TLRs, for example, and it is thus plausible that this same component is involved in the recognition of endotoxins by polymyxin B. Since it should then be possible for compounds sharing similar structural characteristics to endotoxins to be bound by polymyxin B, no final conclusions with regards to the potential presence of endotoxins in the water extracts of *R. capensis* and *P. ostreatus* could be made due to the possibility of false positives. Consequently, the results from this assay alone do not provide sufficient evidence for the presence of endotoxins.

5.3.2. Phagocytosis

The process of phagocytosis is crucial during the inflammatory response as it ensures the removal of infectious agents as well as cell debris. Furthermore, the process of efferocytosis is vital in protecting surrounding cells and tissues from the harmful substances present in apoptotic cells (Khanna *et al.*, 2010). As diabetic wounds are characterized by bacterial infections and impaired macrophage function including phagocytosis, any mushroom species capable of promoting phagocytosis could provide great benefits to diabetic patients suffering from non-healing wounds. The 0.5 % glycated gelatin model was used to impair phagocytosis and thus a favourable response would be indicated by an increase in the phagocytic capability of RAW 264.7 macrophages treated with a certain mushroom extract. All extracts were tested at a concentration of 100 µg/ml as some extracts showed anti-proliferative effects at higher concentrations which could potentially affect the phagocytic capability of the macrophages.

Treatment of RAW 264.7 macrophages with the ethanol and water extracts of *P. tinctorius* appears to have had no significant effects on acidic vacuole formation or phagocytosis when compared to the sample treated with glycated gelatin only (figure 4.40). According to the results from the individual experiments shown in appendix C, a significant increase in acidic vacuole formation was observed during all three experiments for the ethanol extract when compared to treatment with glycated gelatin alone. A similar response was recorded for the water extract for two of the three experiments. This suggests that both extracts of *P. tinctorius* enhanced the autophagic response observed in the RAW 264.7 cells induced by the glycated

gelatin, however, the magnitude of this response appears to be low in comparison to the effect of glycated gelatin on phagocytosis.

A significant increase in acidic vacuole formation was observed in RAW 264.7 cells treated with the ethanol extract of *R. capensis*. Conversely, no significant differences in phagocytosis between the untreated sample and the sample treated with both glycated gelatin and the ethanol extract were observed (figure 4.41). The individual experiments in appendix C show that a significant increase in phagocytosis was recorded in all three individual experiments in RAW 264.7 cells treated with the ethanol extract of *R. capensis* when compared to the glycated gelatin alone. The same observation was recorded for only one of the three individual experiments for the water extract. Considering the results from both the acidic vacuole formation and the individual experiments for the phagocytosis assay, it would appear that the ethanol extract of *R. capensis* substantially increased the phagocytic capability of the RAW 264.7 cells when compared to treatment with the glycated gelatin alone. This is an important finding as it provides evidence that the suppressive effects of protein glycation on the phagocytic function of macrophages is reversible, thus providing an attractive therapeutic target for future studies.

Similar to what was observed for the ethanol extract of *R. capensis*, the ethanol extract of *P. ostreatus* resulted in a significant increase in acidic vacuole formation (figure 4.43). Furthermore, no significant difference in phagocytosis between the macrophages treated with the ethanol extract and the untreated sample were recorded. Upon examination of the results from the individual experiments shown in appendix C, it is evident that the phagocytosis of the RAW 264.7 macrophages was consistently higher for cells treated with the ethanol extract of *P. ostreatus* compared to the glycated gelatin alone; however, these results were only significantly higher for one of the three experiments. When considering the results from the acidic vacuole formation as well as those from the individual phagocytosis experiments, it would appear that the ethanol extract of *P. ostreatus* does indeed promote RAW 264.7 macrophage phagocytosis in the presence of glycated gelatin. No significant differences in acidic vacuole formation or phagocytosis were reported for the water extract.

Treatment of RAW 264.7 macrophages with the ethanol and water extracts of *B. badius* (figure 4.42) as well as treatment with the water extract of *G. lucidum* (figure 4.44) did not result in any significant changes in acidic vacuole formation or phagocytosis and were thus not found to have any advantages in promoting or restoring the phagocytic function of the macrophages in the presence of glycated gelatin.

5.3.3. M1/M2 macrophage polarization

While impaired macrophage function has been associated with the chronic inflammation observed in diabetic wounds, much remains to be revealed about the exact mechanisms involved in macrophage dysfunction during diabetes. The activation status of macrophages is largely determined by the wound environment and thus early on in the wound healing process, pro-inflammatory M1 macrophages are required while the anti-inflammatory M2 macrophages are required during the final stage of tissue repair. Diabetic wounds have been characterized by an unrestrained M1 macrophage population which demonstrate an impaired ability to transition to the M2 phenotype required for the completion of the wound healing process (Jetten *et al.*, 2014). Consequently, a favourable outcome would be indicated by a decrease in M1 macrophage polarization coupled to an increase in M2 activation resulting in a lower M1:M2 ratio. Any extract that is capable of promoting M2 macrophage polarization could have significant advantages in promoting the completion of the wound healing process in diabetic individuals. Due to the complexity of macrophage polarization, more than one *in vitro* assay is required to confirm the activation status of macrophages with the most accurate data being obtained from studies incorporating cell-surface marker expression (Jin *et al.*, 2015).

Neither the ethanol nor the water extracts of *P. tinctorius* were able to overcome the increase in M1 activation in response to the glycated gelatin, however, both extracts significantly promoted M2 activation (figure 4.45). The M1:M2 ratios were consequently calculated to be 1.24 and 0.51, respectively. When compared to the M1:M2 ratio calculated for glycated gelatin (4.5), both extracts appear to have promoted favourable macrophage activation statuses with the water extract having the strongest effect. During the analysis of NO production (figure 4.33), both the ethanol and water extracts displayed strong pro-inflammatory activities in the

absence of LPS together with possible anti-inflammatory activities that were attributed to NO scavenging. The results from this section thus confirm that the water and ethanol extracts of *P. tinctorius* could indeed possess anti-inflammatory activities which would explain the decreased NO production observed previously due to an increase in M2 macrophage activation in the presence of glycated gelatin.

Similar to what was observed for *P. tinctorius*, neither the ethanol nor the water extracts of *R. capensis* were able to lower the enhanced M1 activation of RAW 264.7 macrophages in response to glycated gelatin; however, both extracts significantly increased M2 activation (figure 4.46). The M1:M2 ratios were calculated to be 0.94 and 1.24 for the ethanol and water extracts, respectively, and both extracts were thus able to promote favourable macrophage activation statuses. From the results in section 4.3.1 (figure 4.34), the ethanol extract of *R. capensis* showed potential anti-inflammatory activities in LPS stimulated cells treated with glycated gelatin which was confirmed during this section by an increase in M2 macrophage activation. While an increase in M2 macrophage activation was also observed for the water extract, the strong pro-inflammatory activity recorded in figure 4.34 B appears to have dominated and thus no decrease in NO production was observed.

The 100 µg/ml ethanol and water extracts of *B. badius* did not reverse the increased M1 activation of the RAW 264.7 macrophages in response to glycated gelatin (figure 4.47). Furthermore, the ethanol extract did not enhance M2 activation, however, a significant increase in M2 activation in response to treatment with the water extract was observed. The M1:M2 ratios were subsequently calculated to be 4.06 for the ethanol extract and 1.55 for the water extract. Only the water extract was thus able to promote favourable macrophage polarization in the presence of glycated gelatin. Despite the fact that no significant anti-inflammatory or pro-inflammatory activities were observed for the ethanol extract of *B. badius* during section 4.3.1, a significant decrease in the available NO was recorded for the 200 µg/ml extract in the presence of glycated gelatin (figure 4.35 C). As this cannot be explained by a decrease in M1 activation or an increase in M2 activation, the possibility of NO scavenging should not be ruled out. Furthermore, the strong pro-inflammatory activities observed for the water extract in the absence of LPS could explain why no significant decreases in NO production were observed in response to an increase in M2 activation.

Both the ethanol and water extracts of *P. ostreatus* resulted in significant decreases in M1 macrophage activation when compared to the treatment with glycated gelatin alone (figure 4.48). Neither of the two extracts promoted M2 macrophage activation and the M1:M2 ratios were calculated as 2.4 and 1.59 for the ethanol and water extracts, respectively. Both extracts thus promoted favourable macrophage polarization with the water extract showing greater potential. Substantial anti-inflammatory properties in the presence of LPS and glycated gelatin were reported for the 200 µg/ml ethanol extract of *P. ostreatus* during section 4.3.1. This was probably due to the decrease in M1 macrophage activation reported during this section. The same decrease in NO production was not observed for the water extract and this can potentially be attributed to the slight pro-inflammatory activity that was reported in the absence of LPS (figure 4.36 A).

The water extract of *G. lucidum* resulted in a significant decrease in M1 macrophage activation with no significant effect on M2 activation (figure 4.49). The M1:M2 ratio was calculated to be 1.41 and the water extract thus showed great potential in correcting the imbalance in M1/M2 macrophage activation caused by the glycated gelatin. The results from section 4.3.1., however, did not reveal any significant anti-inflammatory or pro-inflammatory properties with regards to NO production.

5.3.4. NF-κB translocation

It has long been known that NF-κB is an important transcription factor responsible for the expression of several pro-inflammatory signalling molecules and it thus forms an important function during inflammation (Wullaert *et al.*, 2011). In section 5.1 it was shown that glycated gelatin promotes the nuclear translocation of phospho-p65 NF-κB. As NF-κB nuclear translocation and consequent activation has been identified as one of the potential causes of impaired wound healing, any mushroom extract that is able to return the levels of nuclear phospho-p65 NF-κB back to those observed in the untreated sample could potentially serve as a useful therapy in promoting normal wound healing in diabetic individuals.

While none of the extracts tested appear to have been able to reduce the levels of nuclear phospho-p65 NF-κB back to those recorded for the untreated sample, no significant difference between the untreated sample and the water extracts of *P. ostreatus* and *G. lucidum* was observed (figure 4.50). This, however, was due to an

increase in the variation between individual experiments and further investigations would thus be required to confirm whether these extracts successfully overcame the pro-inflammatory effects exerted by the glycated gelatin or not. While no significant anti-inflammatory properties were reported for either of these extracts during section 5.3.1, both extracts were shown to significantly reduce M1 macrophage activation and the possibility of inhibiting NF-κB activation in the presence of glycated gelatin should thus not be ruled out at this stage.

The results from this section suggest that none of the extracts displayed any significant anti-inflammatory properties, however, the same findings were not observed in sections 5.3.1 and 5.3.3. According to Poligone and Baldwin (2001), dual controls exist for NF-κB activation and inactivation where some NF-κB inhibitors have been shown to carry out their functions without influencing the induced nuclear accumulation of phospho-p65. Conversley, the opposite can also be true where an increase in nuclear accumulation is not accompanied by gene expression due to the ability of certain compounds to bind directly to DNA and subsequently prevent transcription. This then could explain why some extracts demonstrated anti-inflammatory activities in previous sections but did not affect NF-κB translocation in the presence of glycated gelatin. As COX-2 is frequently used as a marker for NF-κB activation, the conflicting nature of these results prompted the further investigation of COX-2 levels.

5.3.5. COX-2

While inflammation is a crucial phase of the wound healing process, an augmented and uncontrolled response has been associated with the chronicity of impaired wound healing in both humans and mice. Studies have found that COX-2 is directly associated with inflammation and that COX-2 dysregulation can be associated with cutaneous wound healing in diabetic mice. While an increase in the expression of COX-2 can be expected during the early stages of the wound healing process, it was found that COX-2 expression remained drastically augmented during the late repair stage in diabetic mice, thus contributing to chronic inflammation (Kämpfer *et al.*, 2005).

As both pro-inflammatory and anti-inflammatory activities were reported for the various mushroom extracts tested during this study, COX-2 was measured both in

the presence and the absence of LPS (figure 4.51). Furthermore, in section 5.1 it was shown that glycated gelatin alone did not enhance the levels of COX-2 in RAW 264.7 macrophages, however, in LPS stimulated cells a significant increase in COX-2 was observed. As COX-2 is pro-inflammatory in nature and is responsible for promoting the synthesis of various pro-inflammatory signalling molecules, a decrease in the presence of COX-2 could be beneficial in attenuating the inflammatory response enough to promote the normal wound healing process in diabetic individuals.

The levels of COX-2 were significantly increased in RAW 264.7 cells treated with 100 µg/ml ethanol extract of *P. tinctorius* in the absence of LPS when compared to glycated gelatin without LPS. The pro-inflammatory activity observed for the ethanol extract during the assessment of NO production without LPS thus explains the observed increase in COX-2 expression. Upon the addition of LPS, however, a significant decrease ($p<0.01$) in COX-2 levels were recorded when compared to treatment with both glycated gelatin and LPS. These findings agree with those from section 4.3.1 and confirm that the ethanol extract of *P. tinctorius* contains compounds that display both pro-inflammatory and anti-inflammatory activities. When compared to the sample treated with glycated gelatin but not LPS, the water extract of *P. tinctorius* did not promote any significant increases in COX-2 expression. When LPS was added, however, a robust decrease ($p<0.005$) in COX-2 activity was observed in comparison to the glycated gelatin sample with LPS. While the pro-inflammatory activity seen in section 4.3.1 in the absence of LPS was not observed here, the same anti-inflammatory activity in the presence of both glycated gelatin and LPS was reported.

In the absence of LPS, no significant increase in the percentage of cells stained positive for COX-2 was seen during treatment with the ethanol extract of *R. capensis*, confirming the results obtained in section 4.3.1 where no pro-inflammatory activity was observed. In the presence of LPS, a significant decrease in COX-2 was recorded when compared to treatment with both glycated gelatin and LPS. This again confirms the same anti-inflammatory trend recorded in section 4.3.1. Similar to the ethanol extract, no significant increase in COX-2 was recorded in the absence of LPS; however, a significant decrease in COX-2 expression was reported for the

water extract of *R. capensis* when compared to treatment with both glycated gelatin and LPS. These trends do not agree with those obtained in section 4.3.1 where significant increases in NO production were reported in the absence of LPS and consequently no NO inhibition occurred in the presence of glycated gelatin. These results again emphasise the importance of measuring multiple different parameters, particularly if inflammatory pathways are under investigation, as several possible signalling pathways can lead to a wide array of unexpected and often unexplainable responses.

Confirming the results obtained in section 4.3.1, no significant changes in COX-2 expression were observed in response to treatment with the ethanol extract of *B. badius* in the absence of LPS while a significant increase in COX-2 was recorded for the water extract. Furthermore, both the ethanol and the water extracts significantly reduced the number of cells stained positive for COX-2 in the presence of both glycated gelatin and LPS when compared to relevant control. While a similar trend was observed for the ethanol extract in section 4.3.1, the same cannot be said for the water extract.

Neither the ethanol nor the water extracts of *P. ostreatus* resulted in any significant increases in COX-2 in the absence of LPS when compared to treatment with glycated gelatin alone. The same trend was observed for the ethanol extract in section 4.3.1; however, the water extract did not demonstrate the same weak pro-inflammatory response during the COX-2 assay. In the presence of LPS, only the ethanol extract significantly decreased the percentage of cells stained positive for COX-2, confirming the trends observed in section 4.3.1.

No significant alterations in COX-2 were observed in response to treatment with the water extract of *G. lucidum* in the absence of LPS; however, a significant decrease was recorded in the presence of LPS when compared to the relevant controls. While no pro-inflammatory activity for this extract was reported in section 4.3.1, the same anti-inflammatory activities were not observed.

In order to gain a better understanding of the overall effect of each extract on the inflammatory phase of the wound healing process in diabetic wounds, the results from this section are summarised in table 5.2 to 5.6 below.

Table 5.2: A summary of the effects of *P. tinctorius* on RAW 264.7 macrophage function and inflammation during diabetic wound healing.

Experiment	Assay conditions	Ethanol extract*	Water extract*	Putative relevance to therapeutic potential
NO production	without LPS	↑	↑	May be beneficial during the early stages of wound healing where diabetic wounds display reduced NO levels.
	with LPS	- at 100 µg/ml; ↓ at 200 µg/ml	- at 100 µg/ml; ↓ at 200 µg/ml	May be beneficial in attenuating the inflammatory response during later stages of chronic wound healing. [‡]
	with glycated gelatin, with LPS	↓	↓	Potential anti-inflammatory activity which may be beneficial in attenuating the chronic inflammation in diabetes caused by AGEs. [‡]
Phagocytosis	with glycated gelatin, without LPS	-	-	-
M1/M2	with glycated gelatin, without LPS	- on M1; ↑ in M2	- on M1; ↑ in M2	May be beneficial in attenuating chronic inflammation and promoting the transition from inflammation to the final tissue repair stage.
NF-κB	with glycated gelatin, without LPS	-	-	-
COX-2	with glycated gelatin; without LPS	↑	-	May be beneficial in promoting inflammation during the early stages of normal wound healing.
	with glycated gelatin; with LPS	↓	↓	May be beneficial in attenuating chronic inflammation due to AGEs.

*(↑) indicates a positive effect, (↓) indicates a negative effect and (-) indicates no effect

[‡] Potentially due to quenching; further tests needed to confirm this

The same activities were reported for both the ethanol and water extracts of *P. tinctorius* with the only exception occurring during the COX-2 assay in the absence of LPS. Both extracts displayed pro-inflammatory activities during the measurement of NO production as well as anti-inflammatory activities, however, the anti-inflammatory activities appear to dominate in the presence of glycated gelatin. No improvements in the phagocytic capability of RAW 264.7 cells were reported while significant increases in M2 macrophage activation were observed. Furthermore, neither extract was able to attenuate NF-κB translocation; however, both extracts

significantly reduced the percentage of cells stained positive for COX-2. These results suggest that both the ethanol and water extracts could be useful in attenuating the inflammatory response in diabetic wound healing through pathways promoting an increase in M2 macrophage activation. No published data on the effects of *P. tinctorius* on inflammation has been reported to date.

Table 5.3: A summary of the effects of *R. capensis* on RAW 264.7 macrophage function and inflammation during diabetic wound healing.

Experiment	Assay conditions	Ethanol extract*	Water extract*	Putative relevance to therapeutic potential
NO production	without LPS	-	↑	May be beneficial during the early stages of wound healing where diabetic wounds display reduced NO levels.
	with LPS	- at 100 µg/ml; ↓ at 200 µg/ml	-	May be beneficial in attenuating the inflammatory response during later stages of chronic wound healing.
	with glycated gelatin, with LPS	↓	-	Potential anti-inflammatory activity which may be beneficial in attenuating the chronic inflammation in diabetes caused by AGEs.
Phagocytosis	with glycated gelatin, without LPS	↑	-	May be beneficial in promoting macrophage phagocytosis of microbes in infected diabetic wounds.
M1/M2	with glycated gelatin, without LPS	- on M1; ↑ in M2	- on M1; ↑ in M2	May be beneficial in attenuating chronic inflammation and promoting the transition from inflammation to the final tissue repair stage.
NF-κB	with glycated gelatin, without LPS	-	-	-
COX-2	without LPS, with glycated gelatin	-	-	-
	with LPS, with glycated gelatin	↓	↓	May be beneficial in attenuating chronic inflammation due to AGEs.

*(↑) indicates a positive effect, (↓) indicates a negative effect and (-) indicates no effect

The ethanol extract of *R. capensis* showed anti-inflammatory activities during the NO, macrophage polarization and COX-2 assays. Furthermore, an increase in phagocytosis was observed. These results suggest that the ethanol extract of *R. capensis* could thus prove to be very useful in promoting macrophage phagocytosis

while simultaneously attenuating the inflammatory response and promoting M2 macrophage polarization during diabetic wound healing. The results for the water extract of *R. capensis* show that this extract was capable of promoting M2 macrophage polarization and reducing the percentage of cells stained positive for COX-2, however, it did not affect NO production or phagocytosis in the presence of glycated gelatin. A literature search revealed that no data on the effects of *R. capensis* on inflammation could be found.

Table 5.4: <u>A summary of the effects of *B. badius* on RAW 264.7 macrophage function and inflammation during diabetic wound healing.</u>

Experiment	Assay conditions	Ethanol extract*	Water extract*	Putative relevance to therapeutic potential
NO production	without LPS	-	↑	May be beneficial during the early stages of wound healing where diabetic wounds display reduced NO levels.
	with LPS	-	- at 100 µg/ml; ↑ at 200 µg/ml	May be beneficial in promoting the inflammatory response during normal wound healing.
	with glycated gelatin, with LPS	- at 100 µg/ml; ↓ at 200 µg/ml	-	Potential anti-inflammatory activity which may be beneficial in attenuating the chronic inflammation in diabetes caused by AGEs.
Phagocytosis	with glycated gelatin, without LPS	-	-	-
M1/M2	with glycated gelatin, without LPS	-	- on M1; ↑ in M2	May be beneficial in attenuating chronic inflammation and promoting the transition from inflammation to the final tissue repair stage.
NF-κB	with glycated gelatin, without LPS	-	-	-
COX-2	without LPS, with glycated gelatin	-	↑	May be beneficial in promoting inflammation during the early stages of normal wound healing.
	with LPS, with glycated gelatin	↓	↓	May be beneficial in attenuating chronic inflammation due to AGEs.

*(↑) indicates a positive effect, (↓) indicates a negative effect and (-) indicates no effect

The ethanol extract of *B. badius* displayed weak anti-inflammatory activities in the presence of glycated gelatin with regards to NO production and COX-2 activity. No

improvements in macrophage phagocytosis, M2 macrophage polarization or NF-κB activation were observed and this extract thus does not show much potential in promoting normal wound healing in diabetic individuals. The water extract does not seem very promising either as it demonstrated strong pro-inflammatory properties during the NO assay as well as the COX-2 assay in the absence of LPS. While it was able to promote M2 macrophage activation and reduce COX-2 activity (in the presence of LPS), it did not promote phagocytosis or NF-κB inactivation. No documented reports on the effects of *B. badius* on the inflammatory process could be found.

Table 5.5: A summary of the effects of *P. ostreatus* on RAW 264.7 macrophage function and inflammation during diabetic wound healing.

Experiment	Assay conditions	Ethanol extract*	Water extract*	Putative relevance to therapeutic potential
NO production	without LPS	-	↑	May be beneficial during the early stages of wound healing where diabetic wounds display reduced NO levels.
	with LPS	- at 100 µg/ml; ↓ at 200 µg/ml	-	May be beneficial in attenuating the inflammatory response during later stages of chronic wound healing.
	with glycated gelatin, with LPS	- at 100 µg/ml; ↓ at 200 µg/ml	-	Potential anti-inflammatory activity which may be beneficial in attenuating the chronic inflammation in diabetes caused by AGEs.
Phagocytosis	with glycated gelatin, without LPS	↑	-	May be beneficial in promoting macrophage phagocytosis of microbes in infected diabetic wounds.
M1/M2	with glycated gelatin, without LPS	↓ in M1; - on M2	↓ in M1; - on M2	May be beneficial in attenuating chronic inflammation due to AGEs.
NF-κB	with glycated gelatin, without LPS	-	-	-
COX-2	without LPS, with glycated gelatin	-	-	-
	with LPS, with glycated gelatin	↓	-	May be beneficial in attenuating chronic inflammation due to AGEs.

*(↑) indicates a positive effect, (↓) indicates a negative effect and (-) indicates no effect

The ethanol extract of *P. ostreatus* showed promising anti-inflammatory activity in the presence of glycated gelatin and LPS for both the NO and COX-2 assays. Furthermore, it was found to promote phagocytosis and reduce M1 macrophage activation; however, the water extract did not show any promising activities other than reducing M1 macrophage polarization. A study conducted by Jedinak *et al.* (2011) found similar anti-oxidant activities in RAW 264.7 macrophages where *P. ostreatus* was found to inhibit the LPS-induced NO production and COX-2 through mechanisms involving the down-regulation of iNOS and NF-κB. Furthermore, this mushroom species was found to inhibit inflammation in mice.

Table 5.6: A summary of the effects of *G. lucidum* on RAW 264.7 macrophage function and inflammation during diabetic wound healing.

Experiment	Assay conditions	Water extract*	Putative relevance to therapeutic potential
NO production	without LPS	-	-
	with LPS	-	-
	with glycated gelatin, with LPS	-	-
Phagocytosis	with glycated gelatin, without LPS	-	-
M1/M2	with glycated gelatin, without LPS	↓ in M1; - on M2	May be beneficial in attenuating chronic inflammation due to AGEs.
NF-κB	with glycated gelatin, without LPS	-	-
COX-2	without LPS, with glycated gelatin	-	-
	with LPS, with glycated gelatin	↓	May be beneficial in attenuating chronic inflammation due to AGEs.

*(↑) indicates a positive effect, (↓) indicates a negative effect and (-) indicates no effect

The water extract of *G. lucidum* showed anti-inflammatory activities during the COX-2 assay and was able to reduce M1 macrophage activation; however, no effects on phagocytosis, NO production or NF-κB activation were reported. This extract thus shows very limited potential in promoting the correct macrophage function during diabetes.

Overall, the ethanol extracts displayed the most promising abilities to attenuate inflammation and promote normal macrophage function in the presence of protein glycation. In general, more lipophilic compounds are isolated in polar solvents such as ethanol. These results thus concur with those of Vaskovsky *et al.* (1998) who reported that mushrooms possess larger quantities of polar compounds such as phenolic compounds including flavonoids and polyphenols. Information with regards to the bioactive compounds present in *B. badius*, *P. tinctorius* and *R. capensis* are severely lacking and remain poorly characterized for *P. ostreatus* and *G. lucidum*. The principle bioactive compounds isolated from *G. lucidum* include mostly polysaccharides, sterols, triterpenes and various proteins such as lectin whereas most of the bioactivities of *P. ostreatus* have been attributed to the presence of B-glucans and lectin (Patel *et al.*, 2012; Saltarelli *et al.*, 2015).

5.4.   THE ROLE OF FIBROBLASTS IN WOUND HEALING

Fibroblasts perform important functions during the proliferative stage of the wound healing process as they are responsible for fibroplasia. In diabetes, however, fibroblasts have been shown to demonstrate premature senescence (Menke *et al.*, 2007). Consequently fibroblast function is altered such that their proliferation and migration abilities become impaired. The mechanisms responsible for the observed effects of diabetes on fibroblast function are still under current investigation.

Using a glycated collagen model, Liao *et al.* (2010) showed that the glycation process observed during diabetes negatively influenced the mechanical strength and properties of collagen. Furthermore, it was found to influence several cell-collagen interactions such as cell attachment, migration and proliferation while simultaneously impairing fibroblast facilitated ECM remodelling and collagen contraction. As a result of the greatly reduced fibroblast population, a decrease in the volume of granulation tissue was observed. According to Li *et al.* (2007), fibroblasts isolated from diabetic ulcers showed a reduced proliferative responsiveness to TGF-β1 as well as PDGF and various other growth factors and cytokines necessary for regulating normal fibroblast function. Additionally, a decrease in the expression of TGF-β receptors was observed which greatly impaired signal transduction.

It was recently shown that AGEs induce autophagy in dermal fibroblasts and diabetic skin tissues through a mechanism that at least partly involves the regulation of the

transcriptional activity of FOXO1. Excessive autophagy and resultant cell death could thus also explain the impairments in fibroblast function observed during diabetes. The signalling pathways responsible for FOXO1 mediated autophagy in diabetic fibroblasts have not yet been elucidated. Two possible mechanisms through which AGEs can induce fibroblast autophagy include suppression of the PI3K-AKT pathway thus promoting FOXO1 transcriptional activation and nuclear translocation or the inhibition of the transcriptional activity of p53 by AGEs and resultant mRNA suppression which would lead to a decrease in p53 dependent exclusion of FOXO1 from the nucleus and a resultant increase in FOXO1 transcription (Sun *et al.*, 2016).

5.4.1. Proliferation

A dose-response curve was carried out in order to determine the optimal concentration of FBS that should be used to support sub-optimal proliferation in MRHF fibroblasts (figure 4.52). A sharp decline in fibroblast proliferation was recorded when the concentration of FBS was decreased from 10 % to 1 % followed by a more gradual decline as the FBS concentration approached 0 %. While none of the concentrations of FBS tested resulted in any significant increases in cell death, 1 % FBS was chosen as lower concentrations could potentially induce autophagy and subsequently interfere with the results.

In the presence of 10 % FBS, the 200 µg/ml concentrations of the ethanol and water extracts of *P. tinctorius* were found to exert an anti-proliferative effect on MRHF fibroblasts (figure 4.17 C). When the serum concentration was reduced to 1 %, the same trend was observed for the ethanol extract whereas no negative effects of the water extract on MRHF proliferation were reported (figure 4.53). The anti-proliferative effect of the sub-optimal serum concentration thus superseded the anti-proliferative effect of the water extract.

No noteworthy alterations in fibroblast proliferation were reported for the ethanol extract of *R. capensis* in the presence of 10 % FBS (figure 4.18 C). At sub-optimal serum concentrations, however, a robust cytotoxic effect was reported (figure 4.54), suggesting that the 10 % serum was able to protect the fibroblasts from the damaging effects of this extract. Similar activities were reported for the water extract at both serum concentrations. Similarly, the ethanol extract of *B. badius* did not affect MRHF cell numbers in the presence of 10 % FBS (figure 4.19 C) whereas a 20 %

decrease in the proliferation activity of fibroblasts at sub-optimal serum concentrations was reported (figure 4.55 A). The same activities were reported for the water extract of *B. badius* at both serum concentrations.

The ethanol and water extracts of *P. ostreatus* did not affect the proliferation of the MRHF fibroblasts at both serum concentrations tested during this study. Conversely, the water extract of *G. lucidum* resulted in a significant decrease ($p<0.05$) in MRHF proliferation that was not observed in section 4.2.1. In the presence of glycated gelatin, several of the mushroom extracts including the ethanol and water extracts of *P. ostreatus* and the water extracts of *B. badius, P. ostreatus* and *G. lucidum* were capable of restoring the proliferative capacity of MRHF fibroblasts back to the levels observed in the 1 % FBS control. None of the tested mushroom samples were, however, able to promote fibroblast proliferation to levels higher than those observed for the 1 % FBS control.

Overall, the water extracts displayed the strongest abilities to promote fibroblast migration in the presence of glycated gelatin, suggesting that the compounds responsible for this effect were not present in the ethanol extracts. According to a study conducted by Cheng *et al.* (2013) a hot aqueous extract of *G. lucidum* was also found to promote fibroblast proliferation in diabetic rats, however, no mechanism for the observed activity was provided. No published literature on the effects of the remaining four mushroom species on dermal fibroblast proliferation in diabetes has been reported to date.

5.4.2. Migration

A mitomycin C dose-response curve was performed in order to determine the concentration of mitomycin-C that should be used to inhibit fibroblast proliferation. Mitomycin C concentrations as low as 0.5 µg/ml significantly reduced fibroblast cell numbers with the greatest effect observed at 10 µg/ml. Ideally the highest non-toxic concentration should be selected in order to ensure maximum inhibition of proliferation. While statistically significant increases in cell death were observed at concentrations of 2.5 µg/ml and above, the difference in cell death between the untreated sample (0 %) and the sample treated with 10 µg/ml mitomycin C was only 4 % and was thus not considered physiologically relevant. For this reason, 10 µg/ml was selected as the optimal concentration for further experimentation.

Based on preliminary studies performed using the scratch assay (results not reported), the most promising mushroom extracts were identified for further investigation. The 100 µg/ml ethanol and water extracts of *R. capensis* and *B. badius* as well as the water extract of *G. lucidum* were all found to significantly promote MRHF fibroblast migration in the presence of glycated gelatin. The water extract of *G. lucidum* showed the strongest response as it was able to restore MRHF fibroblast migration back to the levels observed in the untreated sample. The effects of each of the tested mushroom extracts of fibroblast proliferation and migration are summarised in table 5.7.

Table 5.7: <u>A summary of the effects of each mushroom extract on fibroblast proliferation and migration.</u>

Mushroom species	Experiment	Assay conditions	Ethanol extract*	Water extract*
P. tinctorius	Proliferation	Without glycated gelatin	- at 100 µg/ml; ↓ at 200 µg/ml	↑ at 100 µg/ml; - at 200 µg/ml
		With glycated gelatin	- at 100 µg/ml; ↑ at 200 µg/ml	↑at 100 µg/ml; ↑ at 200 µg/ml
	Migration	With glycated gelatin	n/d	n/d
R. capensis	Proliferation	Without glycated gelatin	↓	↓ at 100 µg/ml; - at 200 µg/ml
		With glycated gelatin	- at 100 µg/ml; ↓ at 200 µg/ml	-
	Migration	With glycated gelatin	↑	↑
B. badius	Proliferation	Without glycated gelatin	↓	-
		With glycated gelatin	-	↑
	Migration	With glycated gelatin	↑	↑
P. ostreatus	Proliferation	Without glycated gelatin	-	-
		With glycated gelatin	-	- at 100 µg/ml; ↑ at 200 µg/ml
	Migration	With glycated gelatin	n/d	n/d
G. lucidum	Proliferation	Without glycated gelatin	n/d	↓
		With glycated gelatin	n/d	↑
	Migration	With glycated gelatin	n/d	↑

*(↑) indicates a positive effect, (↓) indicates a negative effect, (-) indicates no effect and (n/d) indicates no data

While several of the tested mushroom extracts were seemingly capable of promoting normal fibroblast proliferation in the presence of glycated gelatin, only the water extracts of *B. badius* and *G. lucidum* were found to promote both fibroblast proliferation and migration and were thus identified as the most promising candidates for promoting the proliferative phase of wound healing in diabetes.

5.5. LIMITATIONS OF THIS STUDY AND SUGGESTIONS FOR FUTURE STUDIES

In diabetes, several factors including neuropathic, microvascular, macrovascular, biochemical, immune function and hormonal irregularities contribute to the impairment of wound healing. Consequently, diabetic individuals pose a unique challenge with the impact of diabetes affecting protein synthesis, leukocyte function, oxygen transportation and utilisation systems as well as the availability of a multitude of growth factors (McCulloch & Kloth, 2010).

Due to the moral and ethical dilemmas with regards to animal testing, *in vitro* screening models are an essential tool for the initial screening phase of a research study as they can provide both proof of concept as well as justification for further research using animal models (Scherer *et al.*, 2008; Stacey, 2012). While every effort is made to duplicate the *in vivo* environment, *in vitro* modelling remains unable to capture the complexity behind the pathology of diabetes and the results must thus be interpreted accordingly. The fact that single cell types are used means that the cell-cell interactions are different *in vitro* compared to *in vivo* and thus cellular signalling could be affected. Furthermore, culture conditions are continuously altered by the depletion of nutrients, accumulation of waste products and sudden media changes. While certain responses can be imitated *in vitro* with confidence, the fact remains that isolated cells that do not form part of a tissue or organ are cultured as monolayers and thus whole tissue or systemic responses that occur *in vivo* could cause completely different responses to those observed *in vitro* (Hartung & Daston, 2009). The various end-point assays utilised during this study may be physiologically relevant, however, they are incapable of measuring the fluctuations that might occur throughout the incubation period, possibly resulting in a skewed interpretation of an event as it occurs *in vivo*. Furthermore, by measuring only the concentration of a given signalling molecule such as NO or COX-2, one is not able to determine

whether the expression and consequent synthesis of that particular molecule is being altered or whether it is simply the activity of that molecule that is affected.

Future studies should be directed at incorporating dermal keratinocytes in the glycated gelatin model as these cells also perform important functions during the proliferation and tissue remodelling phases of wound healing. Co-cultures of macrophages and fibroblasts could be used to produce an environment that is more suitable in mimicking the physiological response as it occurs *in* vivo and could also provide deeper insight into the effect of different cell products on certain cell types. The effect of AGEs on collagen synthesis in fibroblasts as well as the cytoskeletal arrangement of the various skin cells should also be explored. Further investigations related to characterising the inflammatory response should include macrophage infiltration as well as the measurement of iNOS and various signalling molecules such as ROS, ERK1/2 and phosphorylated JNK in order to establish other inflammatory pathways that may be activated. The effect of the different mushroom species on each of the above-mentioned parameters should be assessed. Anti-microbial studies should also be included as diabetic wounds are often characterized by infection. Once the most promising extracts have been selected, further *in vivo* investigations should follow. Should the *in vivo* studies reveal any real advantages of these mushrooms in diabetic wound healing, these species should be characterized and the active compounds should be isolated in order to gain a deeper understanding of the possibilities and limitations of each compound.

5.6. CONCLUSION

The aim of the present study was to develop and characterize a low-cost *in vitro* glycated gelatin model that reflects the cellular dysfunction observed during diabetic wound healing and to evaluate its use as a screening tool to identify potential therapeutic agents. Characterization of the glycated gelatin model revealed a remarkable correlation to known features defining diabetic wound healing, thus providing confidence as a screening assay. This model was then used to assess the potential of five wild mushroom species to overcome the cellular impairments observed in diabetes, thus promoting normal wound healing under diabetic conditions. In addition, other in vitro assays with relevance to wound healing were

also investigated in order to build a more comprehensive screening platform relating to diabetic wound healing.

The glycated gelatin model presented several advantages with regards to cost and convenience over other commonly used purified proteins, however, the two greatest advantages of using gelatin as a surrogate protein are related to the heat stability and resistance to thermal denaturation of gelatin during autoclaving thus allowing the glycation process to be carried out within one hour as well as the certified absence of endotoxins which allows one to accurately characterize the inflammatory response in macrophages treated with AGEs. This model was found to accurately reproduce several cellular dysfunctions observed in macrophages and fibroblasts during diabetic wound healing both *in vivo* and *in vitro*; however, as with all *in vitro* studies it should be noted that this model was not able to replicate the complexity of *in vivo* diabetic wound healing and the results should thus be interpreted accordingly.

The ethanol and water extracts of *P. tinctorius* displayed comparatively strong anti-oxidant activities and could thus provide several advantages during diabetic wound healing in combating oxidative stress, however, no significant glycation inhibition or collagenase inhibition activities were demonstrated. The ethanol extract displayed strong pro-inflammatory activity coupled to a weaker anti-inflammatory activity during the measurement of both NO and COX-2. The same phenomenon was observed for the water extract, however, no pro-inflammatory activity was observed during the measurement of COX-2. Furthermore, both extracts showed strong NO scavenging capabilities and thus further studies measuring iNOS activity are required to confirm the effects of these extracts on NO production. While neither extract was able to overcome the effect of AGEs on phagocytosis or NF-κB activation, they significantly increased M2 macrophage activation and significantly promoted fibroblast proliferation in the presence of AGEs which could be highly beneficial in promoting the transition from inflammation to tissue remodelling during impaired wound healing.

R. capensis did not demonstrate particularly strong anti-oxidant, glycation inhibition or collagenase inhibition activities, however, the ethanol extract showed a strong potential for promoting the resolution of inflammation due to its anti-inflammatory activities recorded during the measurement of both NO and COX-2 as well as its ability to promote phagocytosis, M2 macrophage activation and fibroblast migration

167

in the presence of AGEs. The water extract was also capable of promoting M2 macrophage activation, reducing COX-2 and promoting fibroblast migration, however, it did not show the same potential in promoting phagocytosis and demonstrated strong pro-inflammatory activity by promoting NO production. The potential presence of endotoxins in the water extract warrants further investigation.

The ethanol and water extracts of *B. badius* did not show promising anti-oxidant, glycation inhibition or collagenase inhibition activities with the water extract seemingly promoting glycation. The water extract showed strong pro-inflammatory activities during the measurement of NO and COX-2, however, it significantly promoted M2 macrophage activation, reduced COX-2, and promoted fibroblast proliferation and migration in the presence of AGEs. The ethanol extract did not demonstrate the same potential as the water extract as it was only capable of reducing COX-2 and promoting migration in the presence of AGEs.

P. ostreatus did not demonstrate any anti-oxidant or collagenase inhibition activities and was found to potentially promote glycation. In the presence of AGEs, however, it showed great promise in attenuating the inflammatory response due to its anti-inflammatory properties during both NO and COX-2 measurement as well as its ability to promote phagocytosis and reduce M1 macrophage activation. The water extract showed a weak pro-inflammatory response with regards to NO production, however, it was found to reduce M1 macrophage activation and promoted fibroblast proliferation in the presence of AGEs.

The ethanol extract of *G. lucidum* was highly cytotoxic and was thus excluded from this study. The water extract displayed strong anti-oxidant activity with an IC_{50} below 100 µg/ml for the DPPH assay. While no promising glycation inhibition or collagenase inhibition potential was demonstrated, the water extract was able to reduce M1 macrophage activation and COX-2 in the presence of AGEs while simultaneously promoting fibroblast proliferation and migration.

The ethanol extracts of *R. capensis* and *P. ostreatus* showed the most promising ability to restore the correct macrophage function; however, their abilities to restore the correct fibroblast function were limited. Conversely, the water extract of *G. lucidum* showed the greatest potential to promote normal fibroblast function;

however, it demonstrated very limited capabilities in restoring the correct macrophage function. Different mushroom species were thus found to promote different macrophage and fibroblast functions and could thus provide different therapeutic advantages during diabetic wound healing. The results from this study consequently provide strong evidence to support further *in vitro* and *in vivo* studies related to the use of macrofungi in the treatment of diabetic wound healing.

The findings from the present study have contributed to the understanding of the role of AGEs in cellular dysfunction by confirming discoveries made by other researchers as well as providing some unexpected and novel results. The dramatic effect of AGEs on macrophage phagocytosis coupled to the knowledge that this process may be fully reversible, for example, provides a potential therapeutic target for diabetic wound healing that has yet to be explored. This model can thus be used as a simple tool to explore the mechanisms behind the pathology of diabetic wound healing that have yet to be elucidated and in doing so reveal novel therapeutic targets. The relevance of protein glycation in skin aging and the effects of cigarette smoke on the skin suggest that the glycated gelatin model developed during this study could be relevant to the cosmetic industry during the search for novel anti-aging compounds and this model could thus be adapted for research in areas that are not related to diabetic wound healing.

REFERENCES

Abbas, A. K., Lichtman, A. H. and Pillai, S. (2012) Cellular and Molecular Immunology, 7th edition. Elsevier Saunders, Philadelphia.

Abdel-Naser, M. B., M. Abdallah, H. L. J. De Almeida and U. Wollina. (2005) Human Skin Cell Culture and its Impact on Dermatology. Egyptian Dermatology Online Journal; **1(2)**: 1 - 25. [Online]. Available: http://www.edoj.org.eg/vol001/00102/01/cellculture.html [Accessed 20 October 2016].

Aderem, A. (2003) Phagocytosis and the inflammatory response. The Journal of Infectious Diseases; **187(2)**:S340-S350. [Online]. Available: http://jid.oxfordjournals.org/content/187/Supplement_2/S340.full [Accessed 31 December 2016].

Aderem, A. and Underhill, D. M. (1999) Mechanisms of phagocytosis in macrophages. Annual Review of Immunology; **17**:593-623. [Online]. Available: https://www.ncbi.nlm.nih.gov/pubmed/10358769 [Accessed 31 December 2016].

Aktan, F. (2004) iNOS-mediated nitric oxide production and its regulation. Life Sciences; **75(6)**:639-653. [Online]. Available: https://www.ncbi.nlm.nih.gov/pubmed/15172174 [Accessed 31 December 2016].

Alam, M. N., N. J. Bristi and M. Rafiquzzaman. (2013) Review on in vivo and in vitro methods evaluation of antioxidant activity. Saudi Pharm J; **21(2)**: 143-152. [Online]. Available: http://www.ncbi.nlm.nih.gov/pubmed/24936134 [Accessed 24 December 2016].

Alexandrescu, V. L. (2016) *Wound Healing - New insights into Ancient Challenges*. Intech, Croatia.

Amura, C.R., T. Kamei, N. Ito, M.J. Soares and D.C. Morrison. (1998) Differential regulation of lipopolysaccharide (LPS) activation pathways in mouse macrophages by LPS-binding proteins. *The Journal of Immunology*; **161(5)**:2552-2560. [Online]. Available: http://www.jimmunol.org/content/161/5/2552.long [Accessed 15 March 2015].

Ansell, D. M., K. A. Holden and M. J. Hardman. (2012) Animal models of wound repair: Are they cutting it? Exp Dermatol; **21(8)**: 581-585. [Online]. Available: http://www.ncbi.nlm.nih.gov/pubmed/22775993 [Accessed 21 October 2016].

Appusamy, A., I. John, K. Ponnusamy and A. Ramalaingam. (2014) Removal of crystal violet dye from aqueous solution using triton X-114 surfactant via cloud point extraction. *Engineering Science and Technology, an International Journal*; **17(3)**:137-144. [Online]. Available: http://www.sciencedirect.com/science/article/pii/S2215098614000305 [Accessed 16 March 2015].

Ayuk, S. M., Abrahamse, H. and Houreld, N. N. (2016) The Role of Matrix Metalloproteinases in Diabetic Wound Healing in relation to Photobiomodulation. *Journal of Diabetes Research*;

2016(2016):2897656. [Online]. Available:
https://www.ncbi.nlm.nih.gov/pmc/articles/PMC4893587/ [Accessed 28 January 2017].

Beldon, P. (2010) Basic science of wound healing. *Surgery;* **28(9)**: 409-412. [Online]. Available:
http://www.sciencedirect.com/science/article/pii/S0263931910001195 [Accessed 4 March
2015].

Boonkaew, B., K. Tompkins, J. Manokawinchoke, P. Pavasant and P. Supaphol. (2014)
Characterization and cytological effects of a novel glycated gelatine substrate. Biomed Mater;
9(2): 025001. [Online]. Available: http://www.ncbi.nlm.nih.gov/pubmed/24486986 [Accessed 3
November 2016].

Borena, B. M., A. Martens, S. Y. Broeckx, E. Meyer, K. Chiers, L. Duchateau and J. H. Spaas.
(2015) Regenerative Skin Wound Healing in Mammals: State-of-the-Art on Growth Factor and
Stem Cell Based Treatments. Cell Physiol Biochem; **36(1)**: 1-23. [Online]. Available:
http://www.ncbi.nlm.nih.gov/pubmed/25924569. [Accessed 20 October 2016].

Boutros, M., F. Heigwer and C. Laufer. (2015) Microscopy-Based High-Content Screening. Cell;
163(6): 1314-1325. [Online]. Available: http://www.ncbi.nlm.nih.gov/pubmed/26638068
[Accessed 29 December 2016].

Branch, M. (2001) *First Field Guide to Mushrooms of Southern Africa*. Struik Nature, South Africa

Brem, H. and M. Tomic-Canic. (2007) Cellular and molecular basis of wound healing in diabetes.
The Journal of Clinical Investigation; **117(5)**: 1219-1222. [Online]. Available:
http://www.ncbi.nlm.nih.gov/pubmed/17476353 [Accessed 4 March 2015].

Brett, D. (2008) A Review of Collagen and Collagen-based Wound Dressings. *Wounds: A
Compendium of Clinical Research and Practice*; **20(12)**:347-356. [Online]. Available:
http://www.ncbi.nlm.nih.gov/pubmed/25941895 [Accessed 28 October 2015].

Brodell, L. A. and K. S. Rosenthal. (2008) Skin Structure and Function: The Body's Primary
Defense Against Infection. Infectious Diseases in Clinical Practice; **16(2)**: 113-117. [Online].
Available:
http://journals.lww.com/infectdis/Fulltext/2008/03000/Skin_Structure_and_Function__The_Bo
dy_s_Primary.8.aspx [Accessed 19 October 2016].

Bryan, N.S. and M.B. Grisham. (2007) Methods to detect nitric oxide and its metabolites in biological
samples. *Free Radical Biology and Medicine*; **43(5)**:645-657. [Online]. Available:
http://www.sciencedirect.com/science/article/pii/S0891584907002936 [Accessed 15 March
2015].

Bucala, R., K.J. Tracey and A. Cerami. (1991) Advanced Glycosylation Products Quench Nitric
Oxide and Mediate Defective Endothelium-dependent Vasodilatation in Experimental
Diabetes. *The Journal of Clinical Investigation*; **87(2)**:432-438. [Online]. Available:
http://www.ncbi.nlm.nih.gov/pubmed/1991829 [Accessed 19 August 2015].

Burk, W. R. (1983) Puffball usages among North American Indians. *Journal of Ethnobiology*; **3(1)**: 55-62. [Online]. Available: https://ethnobiology.org/sites/default/files/pdfs/JoE/3-1/Burk1983.pdf [Accessed 5 February 2016].

Chang, P., Chen, T., Chang, C., Hou, C. Chan, P. and Lee, H. (2004) Advanced glycosylation end products induce inducible nitric oxide synthase (iNOS) expression via a p38 MAPK-dependent pathway. *Kidney International*; **65(5)**:1664-1675. [Online]. Available: http://www.sciencedirect.com/science/article/pii/S0085253815498977 [Accessed 20 January 2017].

Chawla, A. (2010) Control of Macrophage Activation and Function by PPARs. Circulation Research; **106(10)**:1559-1569. [Online]. Available: https://www.ncbi.nlm.nih.gov/pubmed/20508200 [Accessed 30 December 2016].

Chazaud, B. (2013) Macrophages: Supportive cells for tissue repair and regeneration. Immunobiology; **219(3)**:172-180. [Online]. Available: https://www.ncbi.nlm.nih.gov/pubmed/24080029 [Accessed 24 December 2016].

Chen, F., Bower, J., Demers, L. M. and Shi, X. (2002) Upstream Signal Transduction of NF-kB Activation. Atlas of Genetics and Cytogenetics in Oncology and Haematology; **6(2)**:156-170. [Online]. Available: https://www.ncbi.nlm.nih.gov/pubmed/14561196 [Accessed 28 December 2016].

Chen, J. and K. Raymond. (2008) Beta-glucans in the treatment of diabetes and associated cardiovascular risks. *Vascular Health and Risk Management*; **4(6)**: 1265-1272. [Online]. Available: http://www.ncbi.nlm.nih.gov/pmc/articles/PMC2663451/ [Accessed 11 February 2016].

Cheng, P. G., C. W. Phan, V. Sabaratnam, N. Abdullah, M. A. Abdulla and U. R. Kuppusamy. (2013) Polysaccharides-Rich Extract of Ganoderma lucidum (M.A. Curtis:Fr.) P. Karst Accelerates Wound Healing in Streptozotocin-Induced Diabetic Rats. *Evidence Based Complementary and Alternative Medicine*; **2013(2013)**: 1-9. [Online]. Available: http://www.ncbi.nlm.nih.gov/pubmed/24348715 [Accessed 21 January 2016].

Cooper, G. M. (2000) *The Cell: A Molecular Approach*, 2nd edition. ASM Press, Washington.

Cory, G. (2011) Scratch-wound assay. *Methods in Molecular Biology*; **769**: 25-30. [Online]. Available: http://www.ncbi.nlm.nih.gov/pubmed/21748666 [Accessed 24 October 2015].

Crous, P. W., I. H. Rong, A. Wood, S. Lee, H. Glen, W. Botha, B. Slippers, W. Z. De Beer, M. J. Wingfield and D. L. Hawksworth. (2006) How many species of fungi are there at the tip of Africa? Studies in Mycology; **55**: 13-33. [Online]. Available: https://www.ncbi.nlm.nih.gov/pmc/articles/PMC2104731/ [Accessed 31 October 2016].

De Mendonca, R. J. and J. Coutinho-Netto. (2009) Cellular aspects of wound healing. *Anais Brasileiros de Dermatologia*; **84(3)**: 257-262. [Online]. Available: http://www.ncbi.nlm.nih.gov/pubmed/19668939 [Accessed 4 March 2015].

De Silva, D. D., S. Rapior, K. D. Hyde and A. H. Bahkali. (2012) Medicinal mushrooms in prevention and control of diabetes mellitus. *Fungal Diversity*; **56(1)**: 1-29. [Online]. Available: http://link.springer.com/article/10.1007%2Fs13225-012-0187-4 [Accessed 21 July 2015].

DeFronzo, R. A., Ferrannini, E., Zimmet, P. and Alberti, K. G. M. M. (2015) *International Textbook of Diabetes Mellitus*, 4th edition. Wiley & Sons, Chichester.

Desta, T., J. Li, T. Chino and D. T. Graves. (2010) Altered fibroblast proliferation and apoptosis in diabetic gingival wounds. *Journal of Dental Research*; **89(6)**: 609-614. [Online]. Available: http://www.ncbi.nlm.nih.gov/pubmed/20354230 [Accessed 25 October 2015].

Dhamodharan, G. and S. Mirunalini. (2010) A Novel Medicinal Characterization of Agaricus Bisporus. *Pharmacologyonline*; **2**: 456-463. [Online]. Available: http://pharmacologyonline.silae.it/files/newsletter/2010/vol2/55.Mirunalini.pdf [Accessed 5 February 2016].

Duconseille, A., T. Astruc, N. Quintana, F. Meersman and V. Sante-Lhoutellier. (2015) Gelatin structure and composition linked to hard capsule dissolution: A review. Food Hydrocolloids; **43**: 360-376. [Online]. Available: http://www.sciencedirect.com/science/article/pii/S0268005X1400232X [Accessed 23 November 2016].

Dumitriu, S. and Popa, V.I. (2013) *Polymeric Biomaterials: Structure and function*, volume 1. CRC Press, USA.

Elengoe, A. and S. Hamdan. (2014) Evaluation of hyperthermia effect on cell viability using crystal violet staining, LDH and trypan blue assays. *Advances in Environmental Biology*; **8(3)**: 744-747. [Online]. Available: http://www.aensiweb.com/aeb.html [Accessed 12 March 2015].

Enoch, S. and D. J. Leaper. (2005) Basic science of wound healing. *Surgery (Oxford)*; **23(2)**: 37-42. [Online]. Available: http://www.sciencedirect.com/science/article/pii/S0263931906700679 [Accessed 4 March 2015].

Enzo. (2016) Cell migration assay, Tri-Coat. [Online]. Available: http://www.enzolifesciences.com/ENZ-KIT116/cell-migration-assay-tri-coat/ [Accessed 23 September 2016].

Erjavec, J., J. Kos, M. Ravnikar, T. Dreo and J. Sabotic. (2012) Proteins of higher fungi - from forest to application. Trends Biotechnol; **30(5)**:259-273. [Online]. Available: http://www.ncbi.nlm.nih.gov/pubmed/22341093 [Accessed 31 October 2016].

Falanga, V. (2005) Wound healing and its impairment in the diabetic foot. *The Lancet*; **366(9498)**: 1736-1743. [Online]. Available: http://www.sciencedirect.com/science/article/pii/S0140673605677008 [Accessed 4 March 2015].

Ferreira, I. C. F. R., L. Barros and R. M. V. Abreu. (2009) Antioxidants in Wild Mushrooms. *Current Medicinal Chemistry*; **16(12)**: 1543-1560. [Online]. Available: http://www.ncbi.nlm.nih.gov/pubmed/19355906 [Accessed 21 January 2016].

Finimundy, T. C., A. J. P. Dillon, J. a. P. Henriques and M. R. Ely. (2014) A Review on General Nutritional Compounds and Pharmacological Properties of the Lentinula edodes Mushroom. *Food and Nutrition Sciences*; **5(12)**: 1095-1105. [Online]. Available: http://www.scirp.org/journal/PaperInformation.aspx?PaperID=47339 [Accessed 11 February 2016].

Freshney, R. I. (1986) Animal Cell Culture: A Practical Approach, edition. IRL Press, Oxford.

Freshney, R. I. (2005) *Culture of Animal Cells: A Manual of Basic Techniques*, 5th edition. Wiley, New York.

Frykberg, R. G. and J. Banks. (2015) Challenges in the Treatment of Chronic Wounds. Adv Wound Care (New Rochelle); **4(9)**: 560-582. [Online]. Available: http://www.ncbi.nlm.nih.gov/pubmed/26339534. [Accessed 25 October 2016].

Gao, S., Zhou, J., Liu, N., Wang, L., Gao, Q., Wu, Y., Zhao, Q., Liu, P., Wang, S., Liu, Y., Guo, N., Shen, Y., Wu, Y. and Yuan, Z. (2015) Curcumin induces M2 macrophage polarization by secretion IL-4 and/or IL-13. *Journal of Molecular and Cellular Cardiology*; **85**:131-139. [Online]. Available: https://www.ncbi.nlm.nih.gov/pubmed/25944087 [Accessed 20 January 2017].

Gebäck, T., M.M. Schultz, P. Koumoutsakos and M. Detmar. (2009) TScratch: a novel and simple software tool for automated analysis of monolayer wound healing assays. *Biotechniques*; **46(4)**:265-274. [Online]. Available: http://www.ncbi.nlm.nih.gov/pubmed/19450233 [Accessed 24 October 2015].

Geerlings, S. E. and Hoepelman, A. I. M. (1999) Immune dysfunction in patients with diabetes mellitus (DM). *FEMS Immunology and Medical Microbiology*; **26(3-4)**:259-265. [Online]. Available: https://www.researchgate.net/publication/12726382_Immune_dysfunction_in_patients_with_diabetes_mellitus_DM [Accessed 18 January 2017].

Gelatin Manufacturers Institute of America (2012) Gelatin Handbook. [Online]. Available: http://www.gelatin-gmia.com/images/GMIA_Gelatin_Manual_2012.pdf. [Accessed 26 November 2016].

Gewirtz, D. A. (2013) Autophagy and senescence. *Autophagy*; **9(5)**:808-812. [Online]. Available: http://www.tandfonline.com/doi/pdf/10.4161/auto.23922 [Accessed 19 January 2017].

Gill, M. and Watling, R. (1986) The Relationships of Pisolithus (Sclerodermataceae) to other Fleshy Fungi with Particular Reference to the Occurrence and Taxonomic Significance of Hydroxylated Pulvinic Acids. *Plant Systematic and Evolution*; **154(3/4)**:225-236. [Online].

Available: https://www.jstor.org/stable/pdf/23673772.pdf?seq=1#page_scan_tab_contents [Accessed 28 Jaunary 2017].

Gill, S. E. and W. C. Parks. (2008) Metalloproteinases and their inhibitors: regulators of wound healing. *The International Journal of Biochemistry and Cell Biology*; **40(6-7)**: 1334-1347. [Online]. Available: http://www.ncbi.nlm.nih.gov/pubmed/18083622 [Accessed 5 February 2016].

Gkogkolou, P. and Böhm, M. (2012) Advanced glycation end products: Key players in skin aging? *Dermato-endocrinology*; **4(3)**:259-270. [Online]. Available: https://www.ncbi.nlm.nih.gov/pubmed/23467327 [Accessed 10 March 2016].

Gould, A., C. Naidoo, D. Kruger and G. Candy. (2011) The role of advanced glycation end products in the hyperinflammatory response of diabetic wounds. *Wound Healing Southern Africa*; **4(1)**: 25-28. [Online]. Available: http://www.woundhealingsa.co.za/index.php/WHSA/article/viewFile/102/174 [Accessed 10 March 2015].

Gryzenhout, M. (2010) *Mushrooms of South Africa*. Struik Nature, South Africa.

Guix, F. X., Uribesalgo, I., Coma, M. and Munoz, F. J. (2005) The physiology and pathophysiology of nitric oxide in the brain. Progress in Neurobiology; **76(2)**:126-152. [Online]. Available: https://www.ncbi.nlm.nih.gov/pubmed/16115721 [Accessed 31 December 2016].

Guo, S. and L. A. Dipietro. (2010) Factors affecting wound healing. *Journal of Dental Research*; **89(3)**: 219-229. [Online]. Available: http://www.ncbi.nlm.nih.gov/pubmed/20139336 [Accessed 20 February 2015].

Guyton, A.C. and J.E. Hall. (2006) Textbook of Medical Physiology, 11th edition. Elsevier Saunders, China.

Hartung, T. and Daston, G. (2009) Are *In Vitro* Tests Suitable for Regulatory Use? *Toxicological Sciences*; **111(2)**:233-237. [Online]. Available: https://academic.oup.com/toxsci/article/111/2/233/1641269/Are-In-Vitro-Tests-Suitable-for-Regulatory-Use#24067793 [Accessed 20 January 2017].

Hulkower, K.I. and R.L. Herber. (2011) Cell migration and invasion assays as tools for drug discovery. *Pharmaceutics*; **3(1)**:107-124. [Online]. Available: http://www.ncbi.nlm.nih.gov/pmc/articles/PMC3857040/ [Accessed 13 March 2015].

Hurd, T. (2013) Understanding the financial benefits of optimising wellbeing in patients living with a wound. Wounds International; **4(2)**: 13-17. [Online]. Available: http://www.woundsinternational.com/journal-content/view/understanding-the-financial-benefits-of-optimising-wellbeing-in-patients-living-with-a-wound [Accessed 20 October 2016].

International Diabetes Federation. (2013) *IDF Diabetes Atlas*, 6th edition. [Online]. Available: http://www.idf.org/sites/default/files/EN_6E_Atlas_Full_0.pdf [Accessed 7 March 2015].

Jaengklang, C., S. Jarikasem, P. Sithisarn and P. Klungsupya. (2015) Determination on Antioxidant Capacity and TLC Analysis of Ten Thai Russula Mushroom Extracts. *The International Conference on Herbal and Traditional Medicine*; 241-250. [Online]. Available: http://www.tci-thaijo.org/index.php/IJPS/article/view/39682 [Accessed 11 February 2016].

Jang, K., Han, M., Lee, B., Kim, B., Kim, C., Yoon, H. and Choi, Y. (2010) Induction of Apoptosis by Ethanol Extracts of *Ganoderma lucidum* in Human Gastric Carcinoma Cells. *Journal of Acupuncture and Meridian Studies*; **3(1)**:24-31. [Online]. Available: http://www.jams-kpi.com/article/S2005-2901(10)60004-0/abstract [Accessed 19 January 2017].

Jaworska, G., Pogoń, K., Skrzypezak, A. and Bernaś, E. (2015) Composition and antioxidant properties of wild mushrooms *Boletus edulis* and *Xerocomus badius* prepared for consumption. *Journal of Food Science and Technology*; **52(12)**:7944-7953. [Online]. Available: https://www.ncbi.nlm.nih.gov/pubmed/26604366 [Accessed 28 January 2017].

Jedinak, A., Dudhgaonkar, S., Wu, Q., Simon, J. and Sliva, D. (2011) Anti-inflammatory activity of edible oyster mushroom is mediated through the inhibition of NF-κB and AP-1 signaling. *Nutrition Journal*; **10**:52. [Online]. Available: https://www.ncbi.nlm.nih.gov/pmc/articles/PMC3120742/ [Accessed 25 January 2017].

Jetten, N., Roumans, N., Gijbels, M. J., Romano, A., Post, M. J., de Winther, M. P. J., van der Hulst, R. R. W. J. and Xanthoulea, S. (2014) Wound Administration of M2-Polarized Macrophages Does Not Improve Murine Cutaneous Healing Responses. *PLoS One*; **9(7)**:e102994. [Online]. Available: http://journals.plos.org/plosone/article?id=10.1371/journal.pone.0102994 [Accessed 22 January 2017].

Jin, X., Yao, T., Zhou, Z., Zhu, J., Zhang, S., Hu. W. and Shen, C. (2015) Advanced Glycation End Products Enhance Macrophages Polarization into M1 Phenotype through Activating RAGE/NF-κB Pathway. *BioMed Research International*; **2015**:732450. [Online]. Available: https://www.ncbi.nlm.nih.gov/pmc/articles/PMC4465680/ [Accessed 22 November 2016].

Kämpfer, H., Schmidt, R., Geisslinger, G., Pfeilschifter, J. and Frank, S. (2005) Wound Inflammation in Diabetic ob/ob Mice: Functional Coupling of Prostaglandin Biosynthesis to Cyclooxygenase-1 Activity in Diabetes-Impaired Wound Healing. *Diabetes*; **53(5)**:1543-1551. [Online]. Available: http://diabetes.diabetesjournals.org/content/54/5/1543 [Accessed 20 January 2017].

Khan, M. A., M. Tania, R. Liu and M. M. Rahman. (2013) Hericium erinaceus: an edible mushroom with medicinal values. *Journal of Complementary and Integrative Medicine*; **10(1)**: 253-258. [Online]. Available: http://www.ncbi.nlm.nih.gov/pubmed/23735479 [Accessed 11 February 2016].

Khanna, S., S. Biswas, Y. Shang, E. Collard, A. Azad, C. Kauh, V. Bhasker, G. M. Gordillo, C. K. Sen and S. Roy. (2010) Macrophage Dysfunction Impairs Resolution of Inflammation in the

Wounds of Diabetic Mice. *PLoS One*; **5(3)**: 1-12. [Online]. Available: http://www.ncbi.nlm.nih.gov/pmc/articles/PMC2832020/ [Accessed 15 March 2015].

Kolluru, G. K., S. C. Bir and C. G. Kevil. (2012) Endothelial dysfunction and diabetes: effects on angiogenesis, vascular remodeling, and wound healing. *International Journal of Vascular Medicine*; **2012(2012)**: 1-30. [Online]. Available: http://www.ncbi.nlm.nih.gov/pubmed/22611498.

Kurahashi, T. and J. Fujii. (2015) Roles of Antioxidative Enzymes in Wound Healing. *Journal of Developmental Biology*; **3(2)**: 57-70. [Online]. Available: http://www.mdpi.com/2221-3759/3/2/57/htm [Accessed 1 February 2016].

Kwon, A. H., Z. Qiu, M. Hashimoto, K. Yamamoto and T. Kimura. (2009) Effects of medicinal mushroom (Sparassis crispa) on wound healing in streptozotocin-induced diabetic rats. *American Journal of Surgery*; **197(4)**: 503-509. [Online]. Available: http://www.ncbi.nlm.nih.gov/pubmed/18585672 [Accessed 20 July 2015].

Laessoe, T. (2013) *Mushrooms & Toadstools: The Difinitive Guide to Fungi*. Dorling Kindersley Limited, London.

Landén, N. X., Li, D. and Stahle, M. (2016) Transition from inflammation to proliferation: a critical step during wound healing. *Cellular and Molecular Life Sciences*; **73(20)**:3861-3885. [Online]. Available: http://link.springer.com/article/10.1007/s00018-016-2268-0 [Accessed 20 January 2017].

Lawrence, T. (2009) The Nuclear Factor NF-kB Pathway in Inflammation. Cold Spring Harbor Perspectives in Biology; **1(6)**:a001651. [Online]. Available: https://www.ncbi.nlm.nih.gov/pubmed/20457564 [Accessed 26 December 2016].

Lerman, O.Z., R.D. Galiano, M. Armour, J.P. Levine and G.C. Gurtner. (2003) Cellular dysfunction in the diabetic fibroblast. American Journal of Pathophysiology; **162(1)**:303-312. [Online]. Available: http://www.ncbi.nlm.nih.gov/pmc/articles/PMC1851127/ [Accessed 4 March 2015].

Li, J., J. Chen and R. Kirsner. (2007) Pathophysiology of acute wound healing. *Clinics in Dermatology*; **25**:(9-18). [Online]. Available: http://www.ncbi.nlm.nih.gov/pubmed/17276196 [Accessed 4 March 2015].

Liang, C., A. Y. Park and J. Guan. (2007) In vitro scratch assay: a convenient and inexpensive method for analysis of cell migration in vitro. *Nature Protocols*; **2(2)**: 329-333. [Online]. Available: http://www.nature.com/nprot/journal/v2/n2/full/nprot.2007.30.html [Accessed 23 October 2015].

Liang, N. and D. D. Kitts. (2014) Antioxidant property of coffee components: assessment of methods that define mechanisms of action. Molecules; **19(11)**: 19180-19208. [Online]. Available: http://www.ncbi.nlm.nih.gov/pubmed/25415479 [Accessed 26 December 2016].

Liao, H., J. Zakhaleva and W. Chen. (2009) Cells and tissue interactions with glycated collagen and their relevance to delayed diabetic wound healing. *Biomaterials*; **30(9)**:1689-1696. [Online]. Available: http://www.sciencedirect.com/science/article/pii/S0142961208009113 [Accessed 4 March 2015].

Life Technologies (2013a) pHrodo™ Red and Green BioParticles® Conjugates for Phagocytosis. [Online]. Available: https://www.thermofisher.com/order/catalog/product/P35366 [Accessed 26 December 2016].

Life Technologies (2013b) LysoTracker® and LysoSensor™ Probes. [Online]. Available: https://www.thermofisher.com/order/catalog/product/L7528 [Accessed 26 December 2016].

Luo, J. and Chen, A. F. (2005) Nitric oxide: a newly discovered function on wound healing. Acta Pharmacologica Sinica: **26(3)**:259-264. [Online]. Available: https://www.ncbi.nlm.nih.gov/pubmed/15715920 [Accessed 31 December 2016].

Macdonald-Wicks, L. K., L. G. Wood and M. L. Garg. (2006) Methodology for the determination of biological antioxidant capacityin vitro: a review. Journal of the Science of Food and Agriculture; **86(13)**: 2046-2056. [Online]. Available: http://onlinelibrary.wiley.com/doi/10.1002/jsfa.2603/abstract [Accessed 24 December 2016].

MacLean-Fletcher, S. and Pollard, T. D. (1980) Mechanism of action of cytachalasin B on actin. *Cell*; **20(2)**:329-341. [Online]. Available: https://www.ncbi.nlm.nih.gov/pubmed/6893016 [Accessed 18 January 2017].

Masutani, E. M., C. K. Kinoshita, T. T. Tanaka, A. K. Ellison and B. A. Yoza. (2014) Increasing Thermal Stability of Gelatin by UV-Induced Cross-Linking with Glucose. Int J Biomater; **2014**: 979636. [Online]. Available: http://www.ncbi.nlm.nih.gov/pubmed/24963297 [Accessed 23 November 2016].

May, R. C. and Machesky, L. M. (2001) Phagocytosis and the actin cytoskeleton. Journal of Cell Science; **114**:1061-1077. [Online]. Available: https://www.ncbi.nlm.nih.gov/pubmed/11228151 [Accessed 31 December 2016].

McCarty, S. M. and S. L. Percival. (2013) Proteases and Delayed Wound Healing. Adv Wound Care (New Rochelle); **2(8)**: 438-447. [Online]. Available: http://www.ncbi.nlm.nih.gov/pubmed/24688830 [Accessed 26 December 2016].

McCulloch, J. M. and L. C. Kloth. (2010) *Wound Healing: Evidence-Based Management,* 4th edition. F. A. Davis, USA.

McKillup, S. (2012) *Statistics explained: An introductory Guide for Life Scientists,* 2nd edition. Cambridge University Press, United Kingdom.

McLennan, S., D. K. Yue and S. M. Twigg. (2006) Molecular aspects of wound healing in diabetes. *Primary Intention*; **14(1)**: 8-13. [Online]. Available: http://www.awma.com.au/journal/1401_01.pdf [Accessed 7 March 2015].

Melzer, S., C. S. Nunes, D. C. Endringer, T. U. De Andrade, A. Tarnok and D. Lenz. (2016) Trypan blue as an affordable marker for automated live-dead cell analysis in image cytometry. Scanning. [Online]. Available: http://www.ncbi.nlm.nih.gov/pubmed/27353800 [Accessed 22 November 2016].

Mendes, J. J., C. I. Leandro, D. P. Bonaparte and A. L. Pinto. (2012) A Rat Model of Diabetic Wound Infection for the Evaluation of Topical Antimicrobial Therapies. Comparative Medicine; **62(1)**: 37-48. [Online]. Available: https://www.ncbi.nlm.nih.gov/pmc/articles/PMC3276391/pdf/cm2012000037.pdf [Accessed 7 March 2015].

Menke, N. B., K. R. Ward, T. M. Witten, D. G. Bonchev and R. F. Diegelmann. (2007) Impaired wound healing. *Clinics in Dermatology*; **25(1)**: 19-25. [Online]. Available: http://www.ncbi.nlm.nih.gov/pubmed/17276197 [Accessed 4 March 2015].

Mohan, K., Padmanaban, M., Uthayakumar, V., Chandrasekhar, R. and Muralisamkar, T. (2016) Cytotoxic activities of *Ganoderma lucidum* ethanol extract against HepG2 cell line. *Bangladesh Journal of Pharmacology*; **11**(3):632-633. [Online]. Available: https://www.researchgate.net/publication/304038310_Cytotoxic_activities_of_Ganoderma_lucidum_ethanol_extract_against_HepG2_cell_line [Accessed 18 January 2017].

Molecular Devices. (2017) MetaXpress Software Multi-Wavelength Cell Scoring Application Module. [Online]. Available: https://www.moleculardevices.com/resources/data-sheets/metaxpress-software-multi-wavelength-cell-scoring-application-module [Accessed 25 January 2017].

Moon, J.-K. and T. Shibamoto. (2009) Antioxidant Assays for Plant and Food Components. Journal of Agricultural and Food Chemistry; **57(5)**: 1655-1666. [Online]. Available: http://pubs.acs.org/doi/abs/10.1021/jf803537k [Accessed 24 December 2016].

Mosser, D. M. (2003) The many faces of macrophage activation. *Journal of Leukocyte Biology*; **73(2)**: 209-212. [Online]. Available: http://www.ncbi.nlm.nih.gov/pubmed/12554797 [Accessed 23 October 2015].

Mosser, D.M. and X. Zhang. (2008) Activation of Murine Macrophages. *Current Protocols in Immunology*; **83(14.2)**:14.2.1-14.2.8. [Online]. Available: http://www.ncbi.nlm.nih.gov/pmc/articles/PMC2822273/ [Accessed 8 November 2015].

Münch, G., Schicktanz, D., Behme, A., Gerlach, M., Riederer, P., Palm, D. and Schinzel, R. (1999) Amino acid specificity of glycation and protein–AGE crosslinking reactivities determined with a dipeptide SPOT library. *Nature Biotechnology*; **17**:1006-1010. [Online]. Available: http://www.nature.com/nbt/journal/v17/n10/full/nbt1099_1006.html [Accessed 18 Jauary 2017].

Murray, P. J. and Wynn, T. A. (2011) Protective and pathogenic functions of macrophage subsets. Nature Reviews: Immunology; **11(11)**:723-737. [Online]. Available: https://www.ncbi.nlm.nih.gov/pubmed/21997792 [Accessed 29 December 2016].

Na, Y. R., Y. N. Yoon, D. Son, D. Jung, G. J. Gu and S. H. Seok. (2015) Consistent inhibition of cyclooxygenase drives macrophages towards the inflammatory phenotype. PLoS One; **10(2)**: e0118203. [Online]. Available: http://www.ncbi.nlm.nih.gov/pubmed/25680189 [Accessed 27 December 2016].

Natarajan, M., S. Mohan, B. R. Martinez, M. L. Meltz and H. T.S. (2000) Antioxidant compounds interfere with the 3. Cancer Detection and Prevention; **24(5)**: 405-414. [Online]. Available: https://www.ncbi.nlm.nih.gov/pubmed/11129982 [Accessed 23 December 2016].

Nelson, D.L. and M.M. Cox. (2008) *Lehninger Principles of Biochemistry*, 5th edition. W. H. Freeman, New York.

Nestle, F. O., P. Di Meglio, J. Z. Qin and B. J. Nickoloff. (2009) Skin Immune Sentinels in Health and Disease. Nature Reviews Immunology; **9(10)**: 679-691. [Online]. Available: http://www.ncbi.nlm.nih.gov/pubmed/19763149 [Accessed 19 October 2016].

Nomoto, K., M. Yagi, U. Hamada, J. Naito and Y. Yonei. (2013) Identification of Advanced Glycation Endproducts derived fluorescence spectrum in vitro and human skin. Anti-Aging Medicine; **10(5)**: 92-100. [Online]. Available: http://www.anti-aging.gr.jp/english/pdf/2013/10(5)92100.pdf [Accessed 23 November 2016].

Nunan, R., K. G. Harding and P. Martin. (2014) Clinical challenges of chronic wounds: searching for an optimal animal model to recapitulate their complexity. Disease Models & Mechanisms; **7(11)**: 1205-1213. [Online]. Available: https://www.ncbi.nlm.nih.gov/pubmed/25359790 [Accessed 21 Otober 2016].

Oliveira. M. I. A., de Souza, E. M., de Oliveira Pedrosa. F., Rea, R. R., da Silva Couto Alves, A., Picheth, G. and de Moraes Rego, F. G. (2013) RAGE receptor and its soluble isoforms in diabetes mellitus complications. *Jornal Brasileiro de Patologia e Medicina Laboratoria;* **49(2)**:97-108. [Online]. Available: http://www.scielo.br/scielo.php?script=sci_abstract&pid=S1676-24442013000200004&lng=en&nrm=iso&tlng=en [Accessed 22 November 2016].

Opletal, L. (1993) Phytotherapeutic aspects of diseases of the circulatory system. 2. The oyster mushroom and its potential use. *Ceskoslovenska Farmacie*; **42(4)**:160-166. [Online]. Available: https://www.ncbi.nlm.nih.gov/pubmed/8402971 [Accessed 28 January 2017].

Papich, M. G. 2016. Saunders Handbook of Veterinary Drugs: Small and Large Animal. 4th ed. Philadelphia: Elsevier.

Patel, S. and Santani, D. (2009) Role of NF-κB in the pathogenesis of diabetes and its associated complications. Pharmacological Reports; **61(4)**:595-603. [Online]. Available: https://www.ncbi.nlm.nih.gov/pubmed/19815941 [Accessed 26 December 2016].

Patel, Y., R. Naraian and V. K. Singh. (2012) Medicinal Properties of Pleurotus Species (Oyster Mushroom): A Review. *World Journal of Fungal and Plant Biology*; **3(1)**: 1-12. [Online]. Available: https://www.researchgate.net/publication/259867820 [Accessed 5 February 2016].

Pena, C., K. De La Caba, A. Eceiza, R. Ruseckaite and I. Mondragon. (2010) Enhancing water repellence and mechanical properties of gelatin films by tannin addition. Bioresource Technololgy; **101(17)**: 6836-6842. [Online]. Available: http://www.ncbi.nlm.nih.gov/pubmed/20400296 [Accessed 16 January 2017].

Perez, R. and S. Davis. (2008) Relevance of Animal Models for Wound healing. Wounds; **20(1)**. [Online]. Available: http://www.woundsresearch.com/article/8200 [Accessed 21 October 2016].

Poligone, B. and Baldwin, A. S. (2001) Positive and Negative Regulation of NF-κB by COX-2. The Journal of Biological Chemistry; **274(42)**:38658-38664. [Online]. Available: http://www.jbc.org/content/276/42/38658.full [Accessed 30 December 2016].

Preeti, A., S. Pushpa, S. Sakshi and A. Jyoti. (2012) Antioxidant Mushrooms: A review. International Research Journal of Pharmacy; **3(6)**: 65-70. [Online]. Available: http://www.irjponline.com/admin/php/uploads/1167_pdf.pdf [Accessed 24 December 2016].

Prior, R., W. Wu and K. Schaich. (2005) Standardized Methods for the Determination of Antioxidant Capacity and Phenolics in Foods and Dietary Supplements. **53(10)**: 4290-4302. [Online]. Available: https://faculty.missouri.edu/~glaserr/3700s14/Antioxidant-Capacity_jf0502698.pdf [Accessed 24 December 2016].

Promega (2009) Griess Reagent System. [Online]. Available: https://worldwide.promega.com/resources/protocols/technical-bulletins/0/griess-reagent-system-protocol/ [Accessed 26 December 2016].

Raja Mohd Hafidz, R. N., Yakoob, C. M., Amin, I. and Noorfaizan, A. (2011) Chemical and functional properties of bovine and porcine skin gelatin. *International Food Research Journal*; **18**:813-817. [Online]. Available: http://www.ifrj.upm.edu.my/18%20(02)%202011/(48)%20IFRJ-2010-159.pdf. [Accessed 23 November 2016].

Rajasekaran, M. and Kalaimagal, C. (2011) In Vitro Antioxidant Activity of Ethanolic Extract of a Medicinal Mushroom, Ganoderma Lucidum. *Journal of Pharmaceutical Sciences and Research*; **3(9)**:1427-1433. [Online]. Available: http://www.jpsr.pharmainfo.in/Documents/Volumes/Vol3Issue09/jpsr%2003110901.pdf [Accessed 20 October 2016].

Ramsay, R. G., Ciznadija, D., Vanevski, M. and Mantamadiotis, T. (2003) Transcriptional regulation of cyclo-oxygenase expression: Three pillars of control. International Journal of Immunopathology and Pharmacology; **16(2)**:59-67. [Online]. Available: https://www.ncbi.nlm.nih.gov/pubmed/14552705 [Accessed 20 September 2016].

Rath, M., Müller, I., Kropf, P., Closs, E. I. and Munder, M. (2014) Metabolism via arginase or nitric oxide synthase: two competing arginine pathways in macrophages. Frontiers in Immunology;

5(2014):532. [Online]. Available: https://www.ncbi.nlm.nih.gov/pmc/articles/PMC4209874/ [Accessed 30 December 2016].

Rathee, S., R. Rathee, D. Rathee, V. Kumar and P. Rathee. (2011) Mushrooms as therapeutic agents. *Brazilian Journal of Pharmacognosy*; **22(2)**: 459-474. [Online]. Available: http://www.scielo.br/scielo.php?script=sci_arttext&pid=S0102-695X2012000200030 [Accessed 5 Febraury 2016].

Reczynski, W., B. Muszynska, W. Opoka, A. Smalec, K. Sulkowska-Ziaja and M. Malec. (2013) Comparative study of metals accumulation in cultured in vitro mycelium and naturally grown fruiting bodies of Boletus badius and Cantharellus cibarius. *Biological Trace Element Research*; **153(1-3)**: 355-362. [Online]. Available: http://www.ncbi.nlm.nih.gov/pubmed/23613150 [Accessed 6 Febraury 2016].

Ricciotti, E. and FitzGerald, G. A. (2011) Prostaglandins and Inflammation. Arteriosclerosis, Thrombosis, and Vascular Biology; **31(5)**:986-1000. [Online]. Available: https://www.ncbi.nlm.nih.gov/pmc/articles/PMC3081099/ [Accessed 30 December 2016].

Sabino, F. and U. Auf Dem Keller. (2015) Matrix metalloproteinases in impaired wound healing. *Metalloproteinases In Medicine*: **1**. [Online]. Available: https://www.dovepress.com/matrix-metalloproteinases-in-impaired-wound-healing-peer-reviewed-article-MNM [Accessed 5 February 2016].

Saltarelli, R., Ceccaroli, P., Buffalini, M., Vallorani, L., Casadei, L., Zambonelli, A., Iotti, M., Badalyan, S. and Tocchi, V. (2015) Biochemical Characterization and Antioxidant and Antiproliferative Activities of Different *Ganoderma* Collections. *Journal of Molecular Microbiology and Biotechnology*; **25(1)**:16-25. [Online]. Available: https://www.ncbi.nlm.nih.gov/pubmed/25662590 [Accessed 28 January 2017].

Santa Cruz Biotechnology (2016) *Trypan Blue*. [Online]. Available: https://www.scbt.com/scbt/product/trypan-blue-72-57-1 [Accessed 22 November 2016].

Schafer, M. and S. Werner. (2008) Oxidative stress in normal and impaired wound repair. *Pharmacological Research*; **58(2)**: 165-171. [Online]. Available: http://www.ncbi.nlm.nih.gov/pubmed/18617006 [Accessed 6 Febraury 2016].

Schalkwijk, C. G., C. D. Stehouwer and V. W. Van Hinsbergh. (2004) Fructose-mediated non-enzymatic glycation: sweet coupling or bad modification. Diabetes/ Metabolism Research and Reviews; **20(5)**: 369-382. [Online]. Available: http://www.ncbi.nlm.nih.gov/pubmed/15343583 [Accessed 26 December 2016].

Scherer, S.S., G. Pietramoggiori, J.C. Matthews., R. Chan., P. Fiorina and D.P. Orgill. (2008) Wound healing kinetics of the genetically diabetic mouse. *Wounds;* **20(1)**:18-28. [Online]. Available: http://www.woundsresearch.com/article/8207 [Accessed 4 March 2015].

Scientific, T.-F. (2016) Propidium Iodide. [Online]. Available: https://www.thermofisher.com/za/en/home/life-science/cell-analysis/fluorophores/propidium-iodide.html [Accessed 23 December 2016].

Sen, C. K. (2009) Wound healing essentials: let there be oxygen. *Wound Repair and Regeneration*; **17(1)**: 1-18. [Online]. Available: http://www.ncbi.nlm.nih.gov/pubmed/19152646 [Accessed 7 February 2016].

Sen, C. K., G. M. Gordillo, S. Roy, R. Kirsner, L. Lambert, T. K. Hunt, F. Gottrup, G. C. Gurtner and M. T. Longaker. (2009) Human skin wounds: a major and snowballing threat to public health and the economy. *Wound Repair and Regeneration*; **17(6)**: 763-771. [Online]. Available: http://www.ncbi.nlm.nih.gov/pubmed/19903300 [Accessed 1 February 2016].

Sigma-Aldrich. (2016a) bisBenzimide H 33342. [Online]. Available: http://www.sigmaaldrich.com/catalog/product/sial/b2261?lang=en&region=ZA [Accessed 23 December 2016].

Sigma-Aldrich. (2016b) Propidium iodide. [Online]. Available: http://www.sigmaaldrich.com/catalog/product/sigma/p4170?lang=en&region=ZA [Accessed 23 December 2016].

Sigma-Aldrich. (2016c) Collagenase from Clostridium histolyticum. [Online]. Available: http://www.sigmaaldrich.com/catalog/product/sigma/c0130?lang=en&region=ZA [Accessed 29 December 2016].

Sigma-Aldrich. (2016d) Polymmyxin B sulfate salt. [Online]. Available: http://www.sigmaaldrich.com/catalog/product/sigma/p4932?lang=en&region=ZA [Accessed 24 December 2016].

Sigma-Aldrich. (2016e) Mitomycin C from Streptomyces caespitosus. [Online]. Available: http://www.sigmaaldrich.com/catalog/product/sigma/m4287?lang=en&region=ZA [Accessed 20 December 2016].

Silverthorn, D.U. (2014) Human Physiology: An Integrated Approach. Pearson, England.

Singh, V. P., A. Bali, N. Singh and A. S. Jaggi. (2014) Advanced glycation end products and diabetic complications. *The Korean Journal of Physiology & Pharmacology*; **18(1)**: 1-14. [Online]. Available: http://www.ncbi.nlm.nih.gov/pubmed/24634591 [Accessed 21 February 2015].

Sinno, H. and Prakash, S. (2013) Complements and the Wound Healing Cascade: An Updated Review. *Plastic Surgery International*; **2013**:146764. [Online]. Available: https://www.ncbi.nlm.nih.gov/pmc/articles/PMC3741993/ [Accessed 28 December 2016].

Sorci, G., F. Riuzzi, I. Giambanco and R. Donato. (2013) RAGE in tissue homeostasis, repair and regeneration. *Biochimica et Biophysica Acta*; **1833(1)**: 101-109. [Online]. Available: http://www.ncbi.nlm.nih.gov/pubmed/23103427 [Accessed 5 February 2016].

Stacey, G. (2012) Current developments in cell culture technology. *Advances in Experimental Medicine and Biology*; **745(1)**:1-13. [Online]. Available: http://www.ncbi.nlm.nih.gov/pubmed/22437809 [Accessed 7 March 2015].

Sumi, D. and Ignarro, L. J. (2004) Regulation of Inducible Nitric Oxide Synthase Expression in Advanced Glycation End Product–Stimulated RAW 264.7 Cells: The Role of Heme Oxygenase-1 and Endogenous Nitric Oxide. *Diabetes*; **53(3)**:1841-1850. [Online]. Available: http://diabetes.diabetesjournals.org/content/diabetes/53/7/1841.full.pdf [Accessed 18 January 2016].

Sun, K., Wang, W., Wang, C., Lao, G., Liu, D., Mai, L., Yan, L., Yang, C. and Ren, M. (2016) AGEs trigger autophagy in diabetic skin tissues and fibroblasts. *Biochemical and Biophysical Research Communications*; **471(3)**:355-360. [Online]. Available: https://www.ncbi.nlm.nih.gov/pubmed/26872427 [Accessed 3 November 2016].

Szabo, C., Ferrer-Sueta, G., Zingarelli, B., Southan, G. J., Salzman, A. L. and Radi, R. (1997) Mercaptoethylguanidine and Guanidine Inhibitors of Nitric-oxide Synthase React with Peroxynitrite and Protect against Peroxynitrite-induced Oxidative Damage. *The Journal of Biological Chemistry*; **274(14)**:9030-9036. [Online]. Available: http://www.jbc.org/content/272/14/9030.full [Accessed 18 January 2016].

Taofiq, O., Heleno, S. A., Calhelha, R. C., Alves, M. J., Barros, L., Barreiro, M. F., Gonzalez-Paramas, A. M. and Ferreira, I. C. F. R. (2016) Development of Mushroom-Based Cosmeceutical Formulations with Anti-Inflammatory, Anti-Tyrosinase, Antioxidant, and Antibacterial Properties. *Molecules*; **21(10)**:1372. [Online]. Available: http://www.mdpi.com/1420-3049/21/10/1372/htm [Accessed 20 January 2017].

Tellechea, A., Leal, E., Veves, A. and Carvalho, E. (2010) Inflammatory and Angiogenic Abnormalities in Diabetic Wound Healing: Role of Neuropeptides and Therapeutic Perspectives. *The Open Circulation and Vascular Journal*; **3(1)**:43-55. [Online]. Available: https://www.researchgate.net/publication/270098123_Inflammatory_and_Angiogenic_Abnormalities_in_Diabetic_Wound_Healing_Role_of_Neuropeptides_and_Therapeutic_Perspectives [Accessed 22 November 2016].

Thaipong, K., U. Boonprakob, K. Crosby, L. Cisneros-Zevallos and D. H. Byrne. (2006) Comparison of ABTS, DPPH, FRAP, and ORAC assays for estimating antioxidant activity from guava fruit extracts. Journal of Food Composition and Analysis; **19(2006)**: 669-675. [Online]. Available: http://www.sciencedirect.com/science/article/pii/S0889157506000081 [Accessed 1 March 2016].

The Great Encyclopedia of Mushrooms. (1998) Könemann, Germany.

Thermo Fischer Scientific. (2017) Protein glycosylation. [Online]. Available: https://www.thermofisher.com/za/en/home/life-science/protein-biology/protein-biology-learning-center/protein-biology-resource-library/pierce-protein-methods/protein-glycosylation.html [Accessed 20 January 2017].

Thornburn. A. (2008) Apoptosis and Autophagy: regulatory connections between two supposedly different processes. *Apoptosis*; **13(1)**:1-9. [Online]. Available: https://www.ncbi.nlm.nih.gov/pmc/articles/PMC2601595/ [Accessed 19 January 2017].

Tortora, G.J. and B. Derrickson. (2012) Principles of Anatomy and Physiology, 13th edition. Wiley and Sons, USA.

Tracy, L. E., Minasian, R. A. and Caterson, E. J. (2016) Extracellular Matrix and Dermal Fibroblast Function in the Healing Wound. *Advances in Wound Care*; **5(3)**:119.136. [Online]. Available: https://www.ncbi.nlm.nih.gov/pmc/articles/PMC4779293/ [Accessed 18 January 2017].

Tricco, A. C., E. Cogo, W. Isaranuwatchai, P. A. Khan, G. Sanmugalingham, J. Antony, J. S. Hoch and S. E. Straus. (2015) A systematic review of cost-effectiveness analyses of complex wound interventions reveals optimal treatments for specific wound types. BMC Medicine; **13**: 90-106. [Online]. Available: http://bmcmedicine.biomedcentral.com/articles/10.1186/s12916-015-0326-3 [Accessed 20 October 2016].

Tullberg-Reinert, H. and G. Jundt. (1999) In situ measurement of collagen synthesis by human bone cells with a Sirius Red-based colorimetric microassay: effects of transforming growth factor β2 and ascorbic acid 2-phosphate. *Histochemistry and Cell Biology*; **112(4)**: 271–276. [Online]. Available: http://www.ncbi.nlm.nih.gov/pubmed/10550611 [Accessed 23 July 2015].

Vaskovsky, V. E., Khotimchenko, S. V. and Boolugh, E. M. (1998) Distribution of diacylglycerotrimethylhomoserine and phosphatidylcholine in mushrooms. *Phytochemostry*; **47(5)**:755-760.

Vekshin, N. (2011) Binding of Hoechst with nucleic acids using fluorescence spectroscopy. *Journal of Biophysical Chemistry*; **2(4)**: 443-447. [Online]. Available: http://www.scirp.org/journal/PaperInformation.aspx?PaperID=8433 [Accessed 6 February 2016].

Venter, G., M. Wijiers, F. Oerlemans, G. Manjeri, J. Fransen and B. Wieringa. (2015) Glycolytic Metabolism is Differentially Coupled to Proliferative Potential and Morphodynamic Capacity in RAW 264.7 and Mafb/C-Maf Deficient Macrophage Lineages. Journal of Clinical & Cellular Immunology; 06(01). [Online]. Available: http://www.omicsonline.org/open-access/glycolytic-metabolism-is-differentially-coupled-to-proliferative-potential-and-morphodynamic-capacity-2155-9899-1000292.pdf [Accessed 21 Noverber 2016].

Wijetunge, D. C. R. and H. K. I. Perera. (2014) A novel in vitro method to identify protein glycation inhibitors. Asian Journal of Medical Sciences; **4(3)**: 15-21. [Online]. Available: http://www.nepjol.info/index.php/AJMS/article/view/8670 [Accessed 26 December 2016].

Williamson, D. and Harding, K. (2004) Wound healing. Medicine; **32(12)**:4-7. [Online]. Available: http://www.sciencedirect.com/science/article/pii/S135730390670696X [Accessed 4 March 2015].

Witte, M. B., Kiyama, T. and Barbul, A. (2002) Nitric oxide enhances experimental wound healing in diabetes. *The British Journal of Surgery*; **89(12)**:1594-1601. [Online]. Available: https://www.ncbi.nlm.nih.gov/pubmed/12445072 [Accessed 20 January 2017].

Wu, S. C., W. Marston and D. G. Armstrong. (2010) Wound care: the role of advanced wound healing technologies. Journal of Vascular Surgery; **52(3)**: 59S-66S. [Online]. Available: http://www.ncbi.nlm.nih.gov/pubmed/20804934.

Wullaert, A., Bonnet, M. C. and Pasparakis, M. (2011) NF-κB in the regulation of epithelial homeostasis and inflammation. *Cell Research*; **21(1)**:146-158. [Online]. Available: https://www.ncbi.nlm.nih.gov/pubmed/21151201 [Accessed 26 December 2016].

Xiu, F., Stanojcic, M., Diao, L. and Jeschke, M. G. (2014) Stress Hyperglycemia, Insulin Treatment, and Innate Immune Cells. *International Journal of Endocrinology*; **2014**. [Online]. Available: https://www.hindawi.com/journals/ije/2014/486403/cta/ [Accessed 18 January 2017].

Xu, F., C. Zhang and D. T. Graves. (2013) Abnormal cell responses and role of TNF-alpha in impaired diabetic wound healing. *BioMed Research International*; **2013(2013)**: 1-9. [Online]. Available: http://www.ncbi.nlm.nih.gov/pubmed/23484152 [Accessed 6 February 2016].

Xue, J., V. Rai, D. Singer, S. Chabierski, J. Xie, S. Reverdatto, D. S. Burz, A. M. Schmidt, R. Hoffmann and A. Shekhtman. (2011) Advanced glycation end product recognition by the receptor for AGEs. Structure; **19(5)**: 722-732. [Online]. Available: http://www.ncbi.nlm.nih.gov/pubmed/21565706 [Accessed 22 November 2016].

Young, A. and C-E. McNaught. (2011) The physiology of wound healing. *Surgery*; **29(10)**:475-479. [Online]. Available: http://www.sciencedirect.com/science/article/pii/S0263931911001323 [Accessed 4 March 2015].

APPENDICES

APPENDIX A: Materials and consumables list

The following table lists the materials and consumables that were utilised during this study, listed according to manufacturer.

Product	Product code	Manufacturer
Alexa Fluor® 488 anti-mouse CD86	105018	BioLegend (USA)
Alexa Fluor® 488 IgG2a, κ Isotype Ctrl	400525	
APC anti-mouse CD206 (MMR)	141708	
APC Rat IgG2a, κ Isotype Ctrl	400512	
Anti-rabbit IgG (H+L), F(ab')2 Fragment (Alexa Fluor® 488 Conjugate)	4408S	Cell Signaling Technology (USA)
Cox2 (D5H5) XP® Rabbit mAb (Alexa Fluor® 488 Conjugate)	13596	
Phospho-NF-κB p65 (Ser536) (93H1) Rabbit mAb	3033S	
Cell Migration Assay, Tri-Coat	ENZ-KIT116-0001	Enzo (USA)
HyClone™ DMEM (High glucose, with L-glutamine and sodium pyruvate)	SH30243	GE Healthcare Life Sciences (USA)
HyClone™ DMEM (Low glucose with L-glutamine, sodium pyruvate)	SH30021	
HyClone™ Foetal Bovine Serum	SV30160	
BioWhittaker® Dulbecco's phosphate buffered saline (DPBS) with Ca2+ and Mg2+	17-513F	Lonza (USA)
BioWhittaker® Dulbecco's phosphate buffered saline (DPBS) without Ca2+ and Mg2+	17-512F	
Trypsin-EDTA	CC-5012	
Aminoguanidine hemisulfate salt	A7009	Sigma-Aldrich (USA)
Collagenase	C0130	
Curcumin	28260	
Cytochalasin B	C2743	
D-(+)-Glucose	G7021	
Dulbecco's Modified Eagle's Medium (low glucose, with glucose and sodium bicarbonate; without L-glutamine and phenol red)	D5921	
Griess' Reagent for nitrite	03553	
Mitomycin C	M4287	
Polymyxin B sulfate salt	P4932	
Propidium iodide	81845	
Tripyridyltriazine	93285	

2,2-Diphenyl-1-picrylhydrazyl	D9132	
Hoechst® 33342	B2261	Thermo Fisher Scientific (USA)
LysoTracker® Red		
pHrodo™ Green BioParticles®	P35366	
Acrodisc® 25 mm syringe filters with 0.2 µm Supor® membrane	103484D	Pall Corporation (USA)

APPENDIX B: Reagent preparation

The reagents required for the FRAP assay were prepared as follows:

- Acetate buffer (300 mM)

  Dissolve 3.1 g sodium acetate in 800 ml distilled water; add 16 ml glacial acetic acid and fill to 1 L with distilled water. Store at 4 °C.

- Dilute HCl (40 mM)

  Add 1.5 ml HCl to 500 ml distilled water.

- TPTZ (10 mM)

  Dissolve 0.031 g TPTZ in 10 ml dilute HCl in a water bath at 50 °C; freshly prepared.

- Ferric chloride (20 mM)

  Dissolve 0.108 g $FeCl_3 \cdot 6H_2O$ to 20 ml distilled water; freshly prepared.

- FRAP reagent

  The FRAP reagent should be prepared fresh on the day. Add 20 ml sodium acetate buffer (300 mM), 2 ml TPTZ (10 mM), 2 ml $FeCl_3$ (20 mM in distilled water; freshly prepared) and 2.4 ml distilled water.

The reagents required for the DPPH assay were prepared as follows:

- Tris-HCl buffer (50 mM)

  Dissolve 0.606 g Tris in 80 ml distilled water; adjust the pH to 7.4 using HCl then fill to 100 ml with distilled water.

- DPPH (0.1 mM)

  Dissolve 0.002 g DPPH in 50 ml ethanol; prepare freshly and protect from light.

The reagents required for the glycation inhibition assay were prepared as follows:

- Glyceraldehyde solution (500 mM)

  Dissolve 0.225 g of glyceraldehyde in 5 ml distilled water in a boiling water bath; store in working aliquots at -20 °C.

- Protein solution (20 mg/ml)

  Dissolve 0.1 g gelatin in 5 ml distilled water in a 37 °C water bath.

The reagents required for the collagenase inhibition assay were prepared as follows:

- Assay buffer (200 mM)

  Dissolve 2.4 g Tris, 0.44 g $CaCl_2$ and 3.51 g NaCl in 80 ml distilled water; adjust the pH to 7.4 using HCl then fill to 100 ml with distilled water.

- Protein solution (2 mg/ml)

  Dissolve 0.006 g gelatin in 3 ml distilled water in a 37 °C water bath.

- Enzyme (40 μg/ml)

  Dissolve 0.08 mg collagenase in 0.5 ml assay buffer and 1.5 ml distilled water.

- Coomassie Brilliant Blue (0.25 % in 40 % methanol/10 % acetic acid)

  Dissolve 25 g of Coomassie Brilliant Blue in 100 ml of a solution containing 40 ml methanol, 10 ml acetic acid and 50 ml distilled water. Filter through Whatman™ filter paper (no. 1) and heat three times for three minutes in a microwave.

APPENDIX C: Phagocytosis and acidic vacuole content in RAW 264.7 cells

Experiment 1:
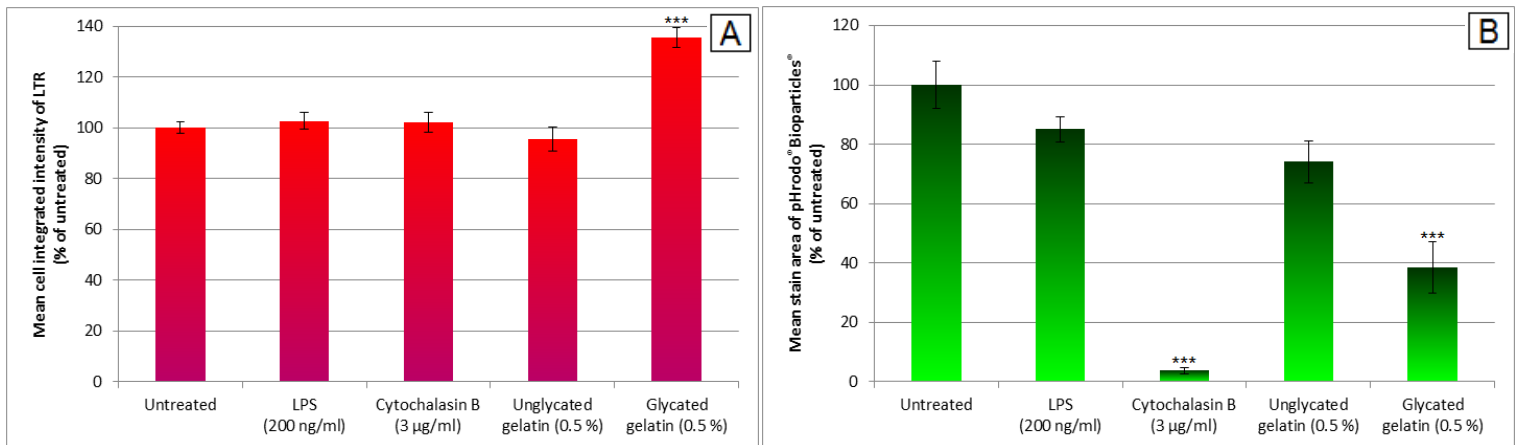
Experiment 2:
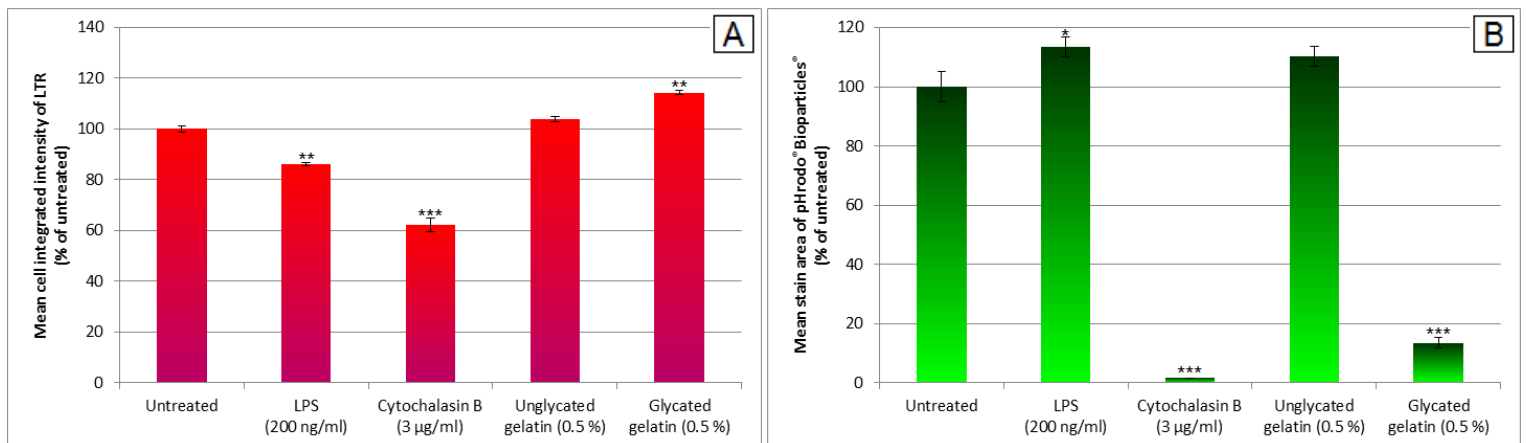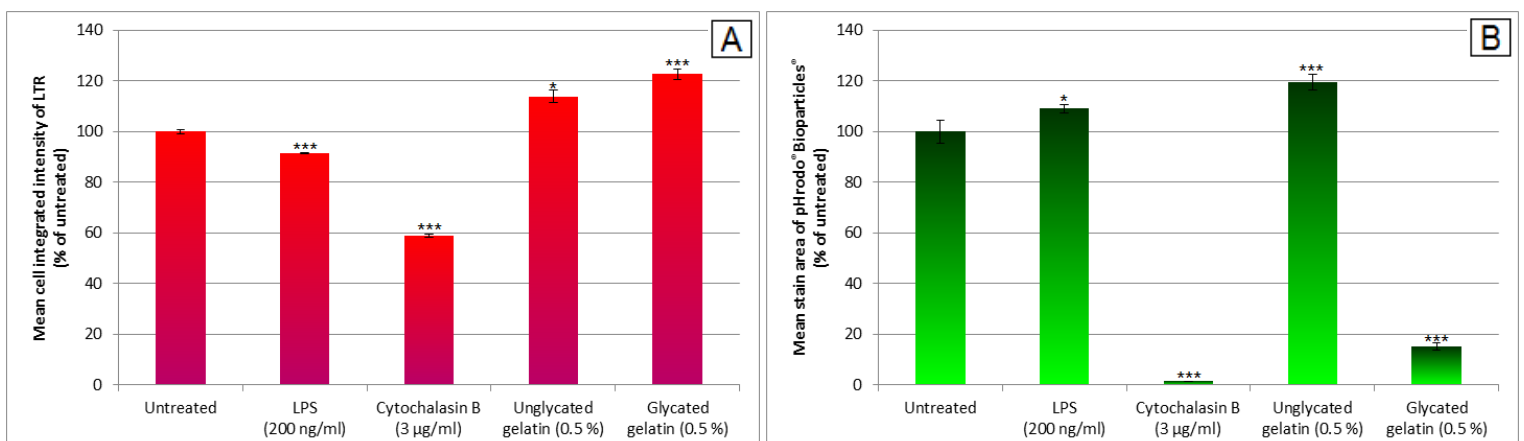
Experiment 3:

Figure C.1: Effect of gelatin on RAW 264.7 cell phagocytosis measuring (A) acidic vacuole formation using LysoTracker Red® and (B) phagocytosis using pHrodo® Bioparticles®; results are reported as means ± SD where each experiment was performed once in triplicate (*p<0.05; **p<0.01; ***p<0.005 compared to untreated sample).

Experiment 1:
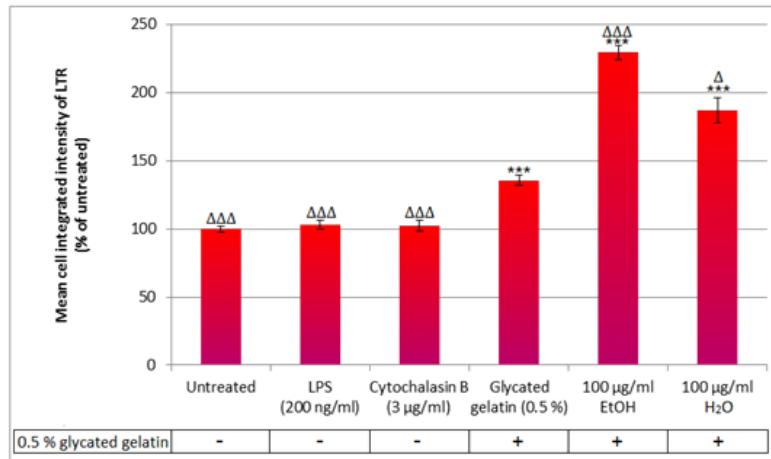
Experiment 2:
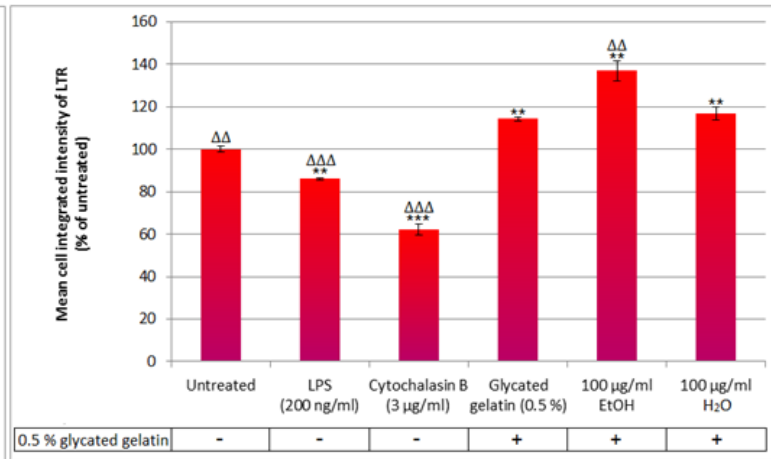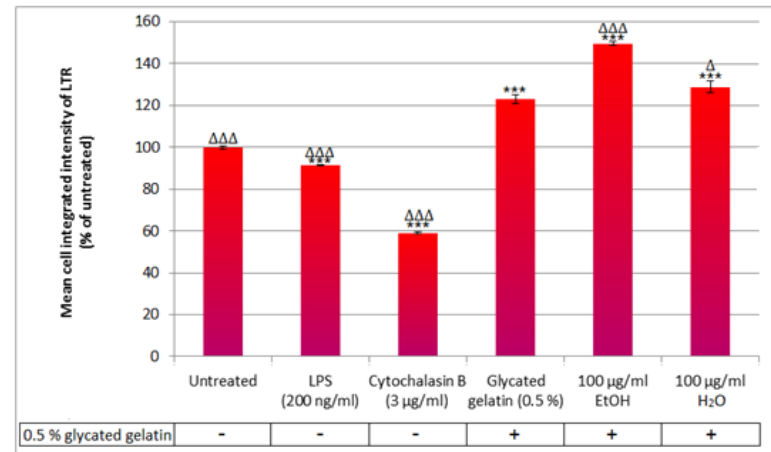
Experiment 3:

Figure C.2: Effect of *P. tinctorius* on RAW 264.7 cell phagocytosis measuring acidic vacuole formation using LysoTracker Red®; results are reported as means ± SD where the experiment was performed once in triplicate (*/Δp<0.05; **/ΔΔp<0.01; ***/ΔΔΔp<0.005 where *compared to untreated sample; Δ compard to glycated gelatin).
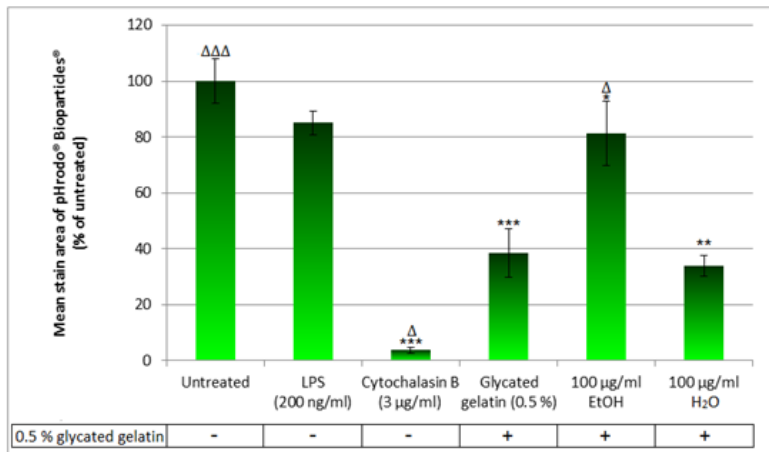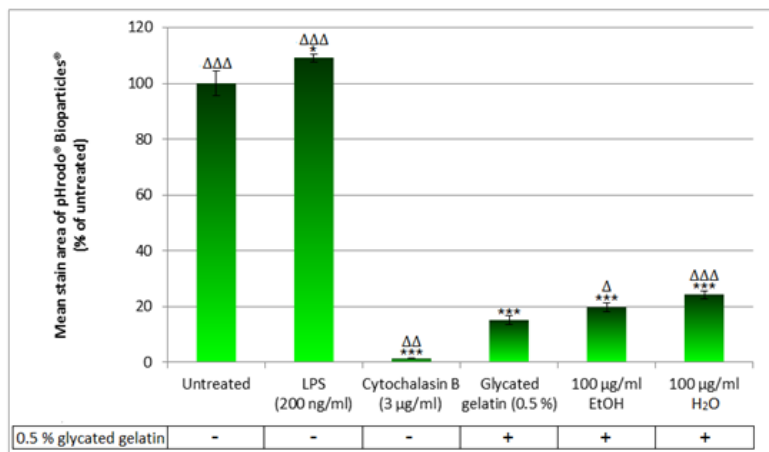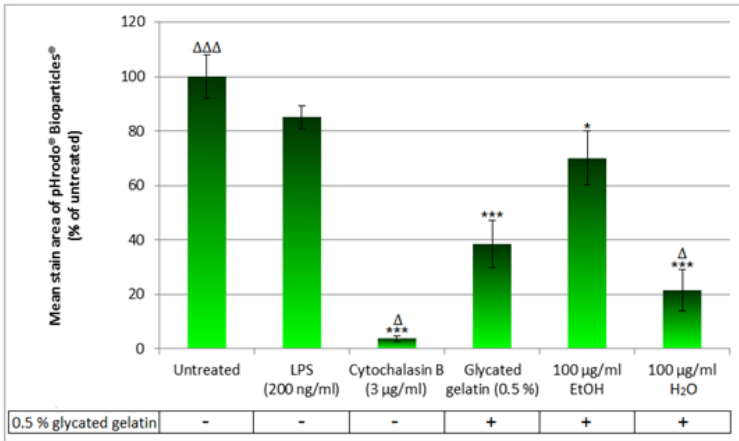
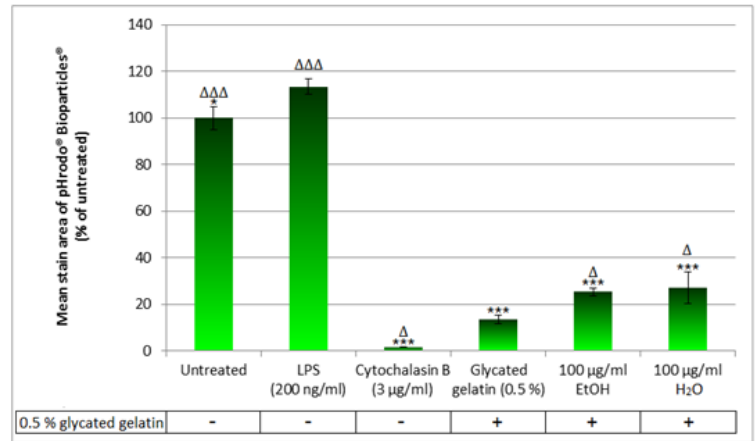Experiment 1:
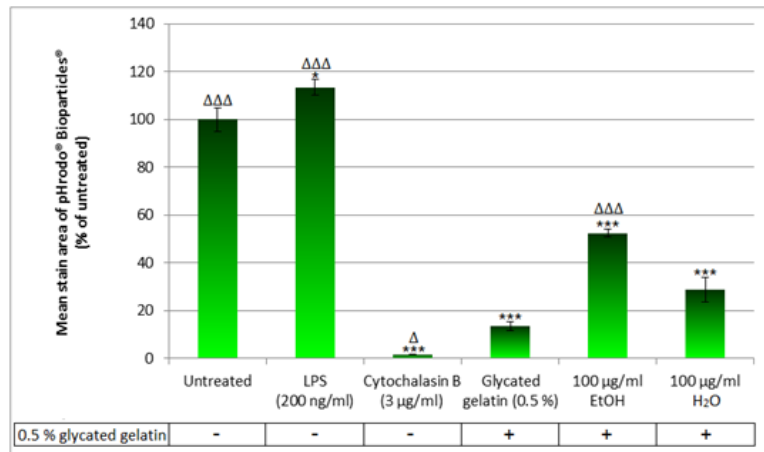
Experiment 2:

Experiment 3:

Figure C.3: Effect of *R. capensis* on RAW 264.7 cell phagocytosis using pHrodo[®] Bioparticles[®]; results are reported as means ± SD where the experiment was performed once in triplicate (*/Δp<0.05; **/ΔΔp<0.01; ***/ΔΔΔp<0.005 where *compared to untreated sample; Δ compard to glycated gelatin).

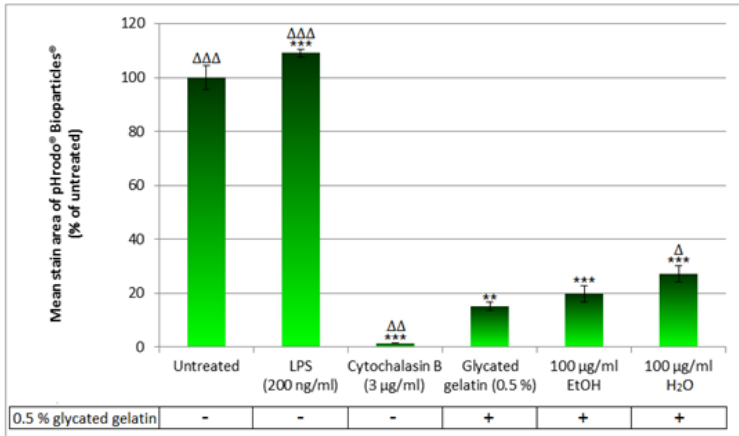Experiment 1:

Experiment 2:

Experiment 3:

Figure C.4: Effect of *P. ostreatus* on RAW 264.7 cell phagocytosis using pHrodo® Bioparticles®; results are reported as means ± SD where the experiment was performed once in triplicate (*/Δp<0.05; **/ΔΔp<0.01; ***/ΔΔΔp<0.005 where *compared to untreated sample; Δ compard to glycated gelatin).